Universidade de Aveiro Departamento de Física
2007

Nuno Alexandre Firmino Vaz

Estudo dos processos de transporte de calor e de sal no Canal do Espinheiro (Ria de Aveiro)

Study of heat and salt transport processes in the Espinheiro Channel (Ria de Aveiro)

Universidade de Aveiro Departamento de Física
2007

Nuno Alexandre Firmino Vaz

Estudo dos processos de transporte de calor e de sal no Canal do Espinheiro (Ria de Aveiro)

Study of heat and salt transport processes in the Espinheiro Channel (Ria de Aveiro)

Tese apresentada à Universidade de Aveiro para cumprimento dos requisitos necessários à obtenção do grau de Doutor em Física, realizada sob a orientação científica do Prof. Doutor João Miguel Dias, Professor Auxiliar do Departamento de Física da Universidade de Aveiro, e do Doutor Paulo Chambel Leitão, Consultor da empresa de consultoria Hidromod, Modelação em Engenharia, Lda.

o júri

presidente

Prof. Dr. Carlos Fernandes da Silva
Professor Catedrático do Departamento de Ciências da Educação da Universidade de Aveiro

Prof. Dr. Jesús Manuel Pedreira Dubert
Professor auxiliar do Departamento de Física da Universidade de Aveiro

Prof. Dr. João Miguel Sequeira Silva Dias
Professor auxiliar do Departamento de Física da Universidade de Aveiro

Prof. Dr. José Fortes do Nascimento Lopes
Professor auxiliar do Departamento de Física da Universidade de Aveiro

Prof. Dra. Maria Inés Álvarez Fenández
Professora associada da Departamento de Física Aplicada, Facultad de Ciências de Ourense, Universidade de Vigo (Grupo de Física Oceanográfica y de Costas)

Doutor Paulo Miguel Chambel Filipe Lopes Teles Leitão
Consultor, Hidromod, Modelação em Engenharia, Lda.

Prof. Dr. Ramiro Joaquim de Jesus Neves
Professor associado do Departamento de Engenharia Mecânica do Instituto Superior Técnico (MARETEC – Marine Environmental and Technology Centre

acknowledgments

I would like to thank the funding institution that has made my work possible. The University of Aveiro provided me support through a Ph.D. grant.

A special thanks to my supervisor, João Miguel Dias, for giving me the first impulse toward the physics of estuaries. A special thanks for setting me off on an interesting research topic and for sharing his ideas at every step. He provided mentorship and advice at critical moments, following closely and with enthusiasm the development of this work. Thanks for your constant presence.

I wish to thank to my “Lisbon supervisor”, Paulo Chambel Leitão, for the trust, enthusiasm, advices and patience during my “modelling adventure” with Mohid. Thank you.

I also wish to thank to Inês Martins for all the help gave during the field experiments. Thanks for your enthusiasm!

To Sr. Mário from Associação Náutica da Gafanha da Encarnação thanks for your nautical experience and advices.

Special thanks to the Mohid developers at MARETEC for acting like real “Mohid Gurus”.

Thank you to all my friends and colleagues at the Physics Department and especially at the “Laboratório de Atmosfera” for providing me a good work environment.

Thanks also are due to my family and all my friends, who supported me throughout this work in ways less scientific but even more essential.

There was a special and particular forcing driving the last two years of the thesis, a storm wind flowing from the south which motivated me more than anything… *Obrigado Susana*!

palavras-chave

Salinidade, temperatura da água, maré, caudal fluvial, modelos numéricos
Canal do Espinheiro

resumo

O principal objectivo deste trabalho consistiu no estudo da dinâmica termohalina do Canal do Espinheiro em função de dois forçamentos principais: maré e caudal fluvial, usando duas abordagens distintas: trabalho experimental e modelação numérica.

A propagação da maré e o caudal fluvial do Rio Vouga são determinantes no estabelecimento da estrutura horizontal da salinidade ao longo do canal. A estrutura térmica horizontal ao longo do canal é, em grande parte, determinada pela variação sazonal da temperatura da água do Rio Vouga, bem como, pela variação sazonal das condições meteorológicas devido à reduzida profundidade.

Foi observada a formação de fortes gradientes de salinidade (relacionados com a formação de frentes estuarinas) numa região a cerca de 7-8 km da embocadura do canal, observando-se a sua migração numa região de aproximadamente 1 km, dependendo do regime de maré.

O balanço entre o transporte de sal de natureza advectiva e difusiva foi calculado, revelando que junto à embocadura os processos físicos que mais contribuem para o transporte de sal são a circulação residual e o aprisionamento da água em canais secundários. Junto à foz do Rio Vouga os termos devidos à descarga fluvial e à circulação gravitacional dominam o transporte de sal.

Foi calibrado e validado um modelo numérico (Mohid, em modo 2D e 3D), sendo posteriormente utilizado para estudar a hidrologia do canal. Foi concedida particular atenção ao estudo da hidrologia em condições extremas de caudal fluvial e de maré. Os resultados da modelação numérica permitiram numa primeira fase avaliar o bom desempenho do Mohid na reprodução dos escoamentos barotrópicos na Ria de Aveiro, bem como na evolução temporal das propriedades termohalinas da água.

Sob condições de caudal fluvial reduzido, a dinâmica do canal é essencialmente dominada pela maré. Com o aumento do caudal fluvial, a influência da água doce estende-se para jusante, estratificando a coluna de água.

As simulações 3D do Canal do Espinheiro foram efectuadas para períodos marcadamente diferentes de caudal fluvial e de maré. O modelo reproduziu qualitativamente/quantitativamente as observações de alturas de água, velocidade e distribuições longitudinais de salinidade e temperatura sob um regime fraco a médio de caudal fluvial. Sob condições de caudal fluvial elevado, os resultados mostram que o modelo subestima a estratificação.

Este estudo contribuiu para o aumento do conhecimento da dinâmica do Canal do Espinheiro, bem como para o desenvolvimento de um sistema numérico capaz de reproduzir e prever os processos de transporte de sal e calor.

keywords Salinity, water temperature, tides, river inflow, numerical model, Canal do Espinheiro

abstract

The main objective of this work was to study the Espinheiro channel's thermohaline dynamics as a function of two major forcings: tides and river inflow using field experiments and numerical modelling simulations.

The salinity distribution along the channel was found closely related to the incoming river flow and tidal propagation. The water temperature distribution is related to the freshwater temperature seasonal variation and, due to the shallowness of the study area, it is also related to the seasonal variation of meteorological conditions.

The formation of strong salinity gradients (commonly related to estuarine fronts) has been found in a region between 7 and 8 km from the lagoon's mouth. These gradients migrate within a region of about 1 km, depending on the tidal regime (spring or neap).

The balance between the advective and diffusive salt transport was assessed. Near the channel's mouth, the main contributions to the salt transport are due to the residual circulation (or freshwater discharge) and tidal correlation. Near the channel's head, this last term is not as important as the gravitational circulation.

The Mohid numerical model was calibrated and validated (both in 2D depth integrated and 3D modes), and then used to study the channel's hydrography. The channel's hydrography was studied under extreme conditions of tides and river inflow. The model results allow the evaluation of Mohid in reproducing the barotropic flows and the time evolution of salinity and water temperature within Ria de Aveiro.

Under low river inflow regimes, the channel's dynamics is tidally dominated. Under high river inflow, the freshwater from Vouga extends its influence downstream until the channel's mouth, increasing the water column stratification.

The three-dimensional simulations of the Espinheiro Channel were performed under markedly different tides and river runoff. Under low-to-medium river inflow, the model reproduces qualitatively/quantitatively sea level height, current velocity and longitudinal distributions of salinity and water temperature, underestimating salinity stratification when the river inflow is high.

The residual circulation was calculated revealing an ebb-dominated channel. When the river inflow is high, the channel is nearly laterally homogeneous in terms of salinity and current residual velocity, presenting a two-layer structure with flood currents close to the bottom and ebb currents close to the surface.

This study has contributed for the characterization and understanding of the dynamical behaviour of the Espinheiro Channel, as well as to develop a numerical system of 2D and 3D numerical models able to reproduce and predict transport processes there occurring.

Contents

List of Figures

List of Tables

Chapter 1

Introduction

"...An estuary is a semi-enclosed body of water which has a free connection to the open sea and within which sea water is measurably diluted with fresh water derived from land drainage..." [Cameron and Pritchard, 1963]

1.1 Motivation

Derived from the latin word *aestuarium*, which means tide or very high wave, estuaries are highly dynamic systems with constant responses to natural and anthropogenic forcing factors. The definition by Cameron and Pritchard [1963] is the most used by the scientific community, but more commonly, for oceanographers, engineers and natural scientist, estuaries are regions of interaction between fresh and salt water. However, there are over than 40 definitions of estuaries [Perillo, 1995]. In spite all these definitions, Dyer [1997] refer that the most satisfactory overall definition would be an adaptation of the Pritchard definition [Pritchard, 1967]: "An estuary is a semi-enclosed coastal body of water which has a free connection to the open sea, extending into the river as far as the limit of tidal influence, and within which sea water is measurably diluted with freshwater derived from land drainage".

The importance of the estuarine environments has been recognized a long time ago not only by the scientific community but also by the populations who live around these areas. As an interface area these ecosystems are highly variable and rich, supporting important economical and social activities. Factors like sewage effluents and industrial waste reduces the water quality affecting people's health and other activities like fisheries. Studying the thermohaline behavior within these ecosystems, and how estuarine waters interact with the adjacent ocean provides an important insight of the behavior of conservative particles since salinity is considered a natural tracer. To fully characterize these systems, it is necessary to have an extensive data set with high spatial and temporal resolution. Due to human and material limitations it is difficult to describe a coastal system using only field measurements. A way to overleap this difficulty is to use numerical models which provide spatial and temporal information about the study area, filling the gaps existent in the field data.

Besides scientific motivations, estuaries have an enormous historical importance, being fundamental for the human development. Almost 60% of the most important cities in the world are located near or around estuaries [Geophysics Study Commitee, 1997]. The scientific knowledge about these systems can be used to develop solutions to several problems as the hydrographic basin's changes, the identification of sedimentation areas that can affect navigation, the computation of the residence time of substances within these areas (conservative and non-conservative substances), study water properties patterns to support aquaculture projects and so on.

Ria de Aveiro is a shallow mesotidal temperate coastal lagoon, located in the north coast of Portugal (Figure 1.1), with an adjacent surface of about 250 km^2 [Dias, 2001]. It is highly dynamic in terms of physical and biogeochemical processes and affects the life of more than 300 000 people who live around the lagoon and its channels [Ré et al., 1991]. The human concentration around the lagoon bring up several environmental and pollution problems. Ria de Aveiro has a very complex and irregular geometry characterized by a high number of narrow and shallow channels and the existence of significant intertidal areas. The lagoon has four main channels: Mira and Ílhavo channels in its southern region, S. Jacinto channel in its northern region and the Espinheiro channel in the central area of the lagoon. The lagoon is connected to the Atlantic Ocean by a single inlet and the freshwater contributions are from five rivers: Vouga, Antuã, Caster, Gonde and Boco River. The major contributor is Vouga River which discharges more than 66% of the incoming freshwater [Dias, 2001] and is connected to the Atlantic Ocean by the Espinheiro Channel. Due to their individual characteristics, these main channels behave like independent estuaries connected to a common inlet. The human intervention is fundamental in the lagoon's evolution, due to frequent works near its inlet which are necessary due to the intense ship traffic and harbour activities.

In a coastal system like Ria de Aveiro, the salinity and water temperature dynamics are influenced, in a very complex interaction, by tides, freshwater coming from terrestrial drainage and by exchange processes with the adjacent atmosphere. The water movements and the turbulent mixing due to the action of the different driving forces constitute an interesting and challenging issue in the hydrodynamic domain. The study of these problems is very important as a basis for the full biogeochemical characterization of the ecosystem as well as for the comprehension of how such complex systems really work.

In the physical oceanography area, estuarine studies are usually performed using two different but interconnected approaches: field measurements and modelling work (physical and numerical models).

The main goal of this work is the study of heat and salt transport processes along the Espinheiro Channel, and through its boundaries with the Atlantic Ocean and the Vouga River. This is a very dynamic channel and was chosen because it connects the major freshwater contributor of Ria de Aveiro (Vouga River) and the Atlantic Ocean. The thermohaline dynamics within the channel is examined evaluating how tides and river inflow interact within this natural system. In order to achieve this purpose two complementary and interconnected approaches are proposed: *in situ* measurements of water temperature, salinity, current velocity, river flow and water flux between the lagoon and

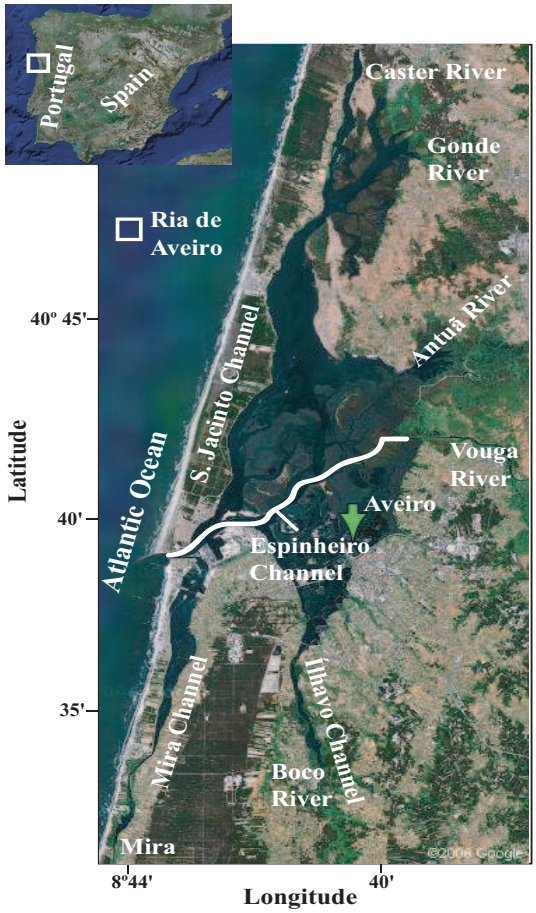

Figure 1.1: The Ria de Aveiro lagoon. The study area is marked (white thick line).

the ocean and numerical results obtained through the use of a finite volume model that combines hydrodynamic and transport modules: Mohid - Water Modelling System.

The study region brought to our attention here is located in the central area of the Ria de Aveiro lagoon, and extends itself from the the mouth of the lagoon to the Vouga River mouth, including the Espinheiro Channel itself. For simplicity, and throughout this dissertation, the study area will be named as Espinheiro channel.

Synoptic campaigns were performed along the Espinheiro channel in order to examine horizontal and vertical thermohaline structures and their dependence on tidal regime and freshwater inflow. For that purpose, ten cross-section were defined along the channel in which salinity and water temperature measurements were taken. These synoptic surveys were performed at maximum spring and neap tide - twice a month - during a full year. Concurrent to this campaigns, the Vouga River inflow was measured. Fixed station surveys of thermohaline and water velocity were also performed in order to characterize the main mechanisms driving the tidally-averaged salt transport at two different and critical locations: the channel's mouth and head.

The irregular geometry of the Ria de Aveiro (and its main channels) and the complexity of the

system equations which describe the water mass characteristics within the lagoon, require the use of an accurate numerical model which, conjugated with the field measurements, provide detailed information about spatial and temporal variations of the system.

In order to study mixing processes within Espinheiro Channel, it was used Mohid [Martins et al., 2001], a three-dimensional baroclinic model with the ability to simulate flooding and drying of tidal flats. The model was first implemented for the entire lagoon, in a two-dimensional mode (depth-integrated), with a closer look to the central area (where Espinheiro Channel is located), in order to study the dependence of the thermohaline horizontal structure with the tidal regime and freshwater inflow. Although these kind of applications reveal some of the main features of the horizontal thermohaline structure, mixing processes within the lagoon are driven not only by freshwater discharge and the barotropic component of the pressure gradient due to tides, but also by its baroclinic component due to salinity gradients (horizontal and vertical). Due to the shallowness of the lagoon and the existence of large intertidal areas, it is virtually impossible to study the whole system in a three-dimensional mode. In order to overleap this difficulty, a high resolution three-dimensional application for the Espinheiro Channel was developed.

The narrow and complex morphology of the channel with its several contributors make this area a challenging place to develop, for the first time, a predictive three-dimensional model. The water exchange between Espinheiro and the adjacent areas is critical, rendering necessary the simulation of the inflow/outflow between the channel and the rest of the lagoon. In order to simulate water exchange between the channel and the rest of the lagoon, the three-dimensional model uses as landward boundary conditions water flow values computed using the two-dimensional model. This is a complex kind of nesting, in which a more general model provides boundary conditions for a more specific model.

1.2 Literature survey

As previously referred, the importance of estuarine environments (classic shape estuaries, tidal channels or coastal lagoons) is recognized all around the world. These ecosystems are subject to an enormous human and natural stress. In order to perform estuarine studies from the physical point of view, research programs in which are developed numerical models and in which the numerical results are conjugated with field measurements are being implemented world wide. The estuarine dynamics, regarding water temperature and salinity, has been studied since, at least, 1960, exploring topics like the hydrographic characterization and the salt fluxes calculation. The main driving forces of the estuarine circulation are sea level changes at the mouth, the river inflow near the head of these systems and meteorological conditions of the adjacent atmosphere. These driving forces interacting with the estuarine topography determine the thermohaline distribution.

During the last decades, thermohaline dynamics has been studied in many estuarine systems world wide. Among others, the pioneer studies by Cameron and Pritchard [1963], Hansen and Rattray [1966] and Pritchard [1967] have provided definitions and classification modes (qualitative and

quantitative) of the estuarine areas using criteria like stratification, characteristics of the salinity distributions and circulation, and salinity structure. Topics like salinity intrusion were studied under the scope of estuarine circulation and salt transport research works.

The classical main core of these studies is the analytic solution by Hansen and Rattray [1965] and the closely related diagnostic scheme of Hansen and Rattray [1966] where estuaries are described through a steady-state balance of three salt fluxes: down-estuary advection of salt by the mean flow, up estuary salt return by the vertical gravitational circulation and up-estuary diffusive flux, representing all other exchange, which closes the balance. MacCready [1999] generalized this theory in order to include time dependence. Studies of the estuarine response to changes in the river flow input in terms of both their time scale [Kranenburg, 1986; MacCready, 1999] and magnitude [Officer and Kester, 1991; Gibson and Najjar, 2000; Monismith et al., 2002] occupy much of the literature.

Estuarine salt dynamics studies are ecologically significant at regional levels, since salt is a natural tracer, and can be used to provide insight about other conservative substances behaviour. Several authors examined the net salt fluxes and computed the salt balance using different approaches. Fischer [1972] and Dyer [1974] began to described a number of mechanisms and methods by which the salt balance and dispersion are analyzed for partially and stratified estuaries. The main driving forces of the non-tidal circulation and the calculation of the advective and dispersive contributions to the salt transport were examined by Hunkins [1981]; Miranda and Castro Filho [1996]; Bérgamo [2000] in their studies for the Hudson and Cananéia Sea estuaries. The cross-sectional salt balance in a tropical estuary was studied by Dyer et al. [1992] illustrating the dynamic coupling between the transverse and vertical contributions on a tidal and tidally averaged basis. More recently, several observational studies have provided a description of the salt transport and exchange processes: Simpson et al. [2001] and Banas et al. [2004] in their studies in the Conwy Estuary (UK) and Willapa Bay (USA) explore the hydrographic features of two macrotidal highly energetic estuaries and compute the salt balance in those systems due to tidal motion and river flow. Miranda et al. [2005] examined the interaction of river discharge and tidal modulation in a tropical estuary using observations of thermohaline properties and currents revealing salt transport features both during neap and spring tidal cycles. Bowen and Geyer [2003] examined the mechanisms and variability of salt transport at a relatively uniform section of the Hudson estuary using a 70-day moored time series. MacCready and Geyer [2001]; MacCready et al. [2002] explored the approach proposed by Dronkers and van de Kreeke [1986], in which the concept of looking at the salt flux through a vertical cross section which moves up and down the estuary with the tidal velocity was developed, and took a step forward, by using an actual isohaline as the surface through which salt and fluxes are computed, including long time scales and the case in which isohalines are ejected from the ocean's end.

In the north of the Iberian Peninsula, the Galician Rias have been exhaustively studied in terms of their hydrologic features. These studies turn important because the Rias Baixas (local name of the Galician Rias) support a very important national industry: the mussel industry. This aquaculture industry can be affected by the hydrographic characteristics of the local waters rendering important this kind of studies. In the following it will be presented some recent studies in this area. Thus, the

salinity and water temperature behavior have been studied in order to characterize its intra and inter-annual evolution in the boundary between the Rias and the adjacent ocean [Alvarez et al., 2005], and Prego et al. [2001] provided an assessment of the physical-hydrodynamical characteristics of the Pontevedra Ria, studying its hydrography during Spring upwelling events; the hydrography of the Ria of Pontevedra has also been investigated under Winter-upwelling conditions [Álvarez et al., 2003], and the effect of the Rio Minho's intrusion in the hydrographic behaviour of the Rias Baixas was assessed using thermohaline observations [Alvarez et al., 2006]; deCastro et al. [2004] studied the along estuary negative circulation in the Ria of Pontevedra, revealing a two-layered circulation pattern generated by the existence of two different water masses at intermediate depths.

During the last years, an enormous effort was placed in the implementation of numerical models that resolve the main physical processes occurring in estuarine systems. The main scope of these studies has been the characterization of the estuarine salinity structure (in the literature, there are few examples of the estuarine water temperature structure characterization). As Warner et al. [2005] describe in their study of the Hudson estuary: "The estuarine salinity structure is a result of a complex interplay between the buoyancy flux from the river inflow, advection by tides and the estuarine circulation, and mixing". Thus, model predictions of the time-dependent salinity field depend on the model representation of tidal and subtidal motions as well as the turbulence parameterizations for mixing of momentum and salt. This complex interaction makes the implementation of estuarine numerical models particularly challenging.

Recently, several estuarine modelling studies have considered one-dimensional (vertical) representations of the velocity and salinity fields [Nunes Vaz et al., 1989; Simpson et al., 1990, 1991; Simpson and Sharples, 1991; Nunes Vaz and Simpson, 1994; Monismith and Fong, 1996; Zhou, 1998] with the objectives of evaluating turbulence closure models and assessing the interaction between tidal shear, mixing and stratification. However, the comparison between one-dimensional model results and observations often presents some discrepancies that may be due to unresolved variations of the salinity gradient [Simpson and Sharples, 1991], or inadequacy of the turbulence closure [Simpson and Sharples, 1991; Nunes Vaz and Simpson, 1994]. One common failure in these one-dimensional models with second-order closure [Mellor and Yamada, 1982] is the so called "runaway stratification" in which stratification tends to increase when the tidal amplitude drops below some threshold value.

The classic estuarine theory found in Hansen and Rattray [1965] demonstrate that the longitudinal salinity gradient ($\partial s/\partial x$) is not an independent variable, but it is part of the solution of the momentum and salinity conservation equations for a specified freshwater flow. Theoretical studies by MacCready [1999] and Kranenburg [1986] reveal the large temporal variability of $\partial s/\partial x$ indicating its variation with tidal amplitude. These studies suggest that the salinity gradient should be included as a dependent variable, limiting this way the prognostic abilities of one-dimensional (vertically resolving) models.

One way to overcome the problem of specifying the salinity gradients is the use of three-dimensional models (where the salinity gradient is a dependent variable). Lately, there has been

multiple applications in which the variability of stratification, tidal and mean shear, and longitudinal salinity gradient have been evaluated. All these model applications used measured data in order to validate their results. In the following paragraphs a few recent three-dimensional model applications will be referred. Cugier and Le Hir [2002] developed a 3D hydrodynamical model to study the Seine river plume. Prandle [2004] presents a model which studies the salinity intrusion in partially stratified estuaries, extending earlier studies which relate tidally averaged linearized theories relating to the vertical structure of salinity and velocities, to include tidal straining and associated convective overturning. The applicability of the model was evaluated by the simulation of measurements by Rippeth et al. [2001]. Warner et al. [2005] have used ROMS [Haidvogel et al., 2000] in order to evaluate the estuarine dynamics of the Hudson estuary, providing a skill assessment of the model by comparison of model results and observed data. The dynamics of Chesapeake Bay has been studied using ROMS [Li et al., 2005]. In this last work, a new three-dimensional model for the bay was developed. Model results and observations were compared in order to validate the model, and several tests using different turbulence closure models were carried out in order to evaluate the model sensitivity to the mixing parameterizations. The same model was used by Zhong and Li [2006] to compute tidal energy fluxes and dissipation in Chesapeake bay. The numerical model GETM [Burchard and Bolding, 2002; Burchard et al., 2004] was used to analyze transport pathways and residence time in Willapa bay, Washington [Banas and Hickey, 2005], examining the mechanisms and timescales of exchange between the estuary and the near-ocean. This model has previously been used to model tidal dynamics in the East Frisian Wadden Sea [Stanev et al., 2003], the baroclinic dynamics estuarine turbidity maximum in the Elbe estuary [Burchard et al., 2004], and seasonal hydrographic patterns in the North Sea [Stips et al., 2004]. In Tomales Bay (California), the DELFT3D-Flow has been used to understand the Summer circulation under differing conditions where cold water density currents intrusion events were qualitatively simulated and the sensitivity of the density driven circulation to different parameters and processes were assessed [Harcourt-Baldwin and Diedericks, 2006].

Regarding Ria de Aveiro, there are not many studies exploiting the hydrography or the physical characteristics of the lagoon. In fact, during the last 20/30 years, the lagoon has been studied mainly from a biological and chemical point of view. These studies gave origin to several publications like Almeida et al. [2001]; Cunha et al. [2001] (bacterioplancton) or Morgado et al. [2003] (zooplankton). Other authors like Moreira et al. [1993]; Queiroga et al. [1994]; Cunha [1999] performed some localized measurements of water temperature, salinity and currents as backup to their studies. More recently, Saraiva [2005] and Trancoso et al. [2005] used a three-dimensional numerical model to study macroalgae dynamics within the lagoon, revealing its importance in the primary production. Lopes et al. [2005] present a characterization of the lagoon's water quality using a physical, chemical and biological data set and the implementation of a numerical model for the water quality within the lagoon. Coelho et al. [26] and Ramalhosa et al. [2006] in their recent papers have studied mercury bioaccumulation and mercury cycle within the Ria de Aveiro. Rocha et al. [2005] have studied the sediments within the lagoon in terms of their chemical and mineralogical characterization, and Bobos and Rocha [2006] have studied sediment dispersion in several locations within the lagoon.

From the physical point of view, several studies were performed in order to investigate topics such as the tidal propagation in the lagoon [Dias et al., 2000], the lagrangian transport of particles [Dias et al., 2001] and sediment transport [Abrantes et al., 2005; Dias et al., 2003; Lopes et al., 2001, 2006]. Dias [2001] present a complete two-dimensional hydrodynamic study of the lagoon, revealing its main features; Dias and Lopes [2006] present the implementation and assessment of a two-dimensional hydrodynamic and transport model for the entire area of the lagoon, and the sea level variability inside the lagoon was studied by Araújo [2005] using field data and modelling work. Abrantes [2005] has used fine fractions as tracer on sediment dynamics within the lagoon. Dias and Fernandes [2006] examined the propagation of tidal and subtidal oscillation within the lagoon and Dias et al. [1999] reveal the lagoon's Summer hydrologic characteristics. More recently, Vaz et al. [2005a] used numerical modelling and field measurements to study the salinity and water temperature distributions, in the central area of the lagoon, using extreme tidal and river flow forcing conditions, and the fluvial estuary of the Vouga River was characterized by means of the salinity, temperature and current structure [Vaz et al., 2005b]. The water exchange between the lagoon and the near ocean was studied using the motionally induced voltage (MIV) method [Nolasco et al., 2006], showing that it is possible to indirectly measure the water transport, by tidal and residual flows, through the lagoon's inlet using differences of electrical potential measurements.

1.3 Structure of this work

The aim of this dissertation is the study of salinity and water temperature dynamics in the Espinheiro channel, one of the four main branches of the Ria de Aveiro lagoon. A detailed description of the channel is given in sections like Section 2.2 and 3.2. This channel connects the major source of freshwater of the lagoon - Vouga river - [Dias et al., 1999] and the Atlantic Ocean, being ideal to perform these studies. As previously referred, knowing the salinity and water temperature behavior provide insight not only for a better comprehension of the study area's dynamics but also for subsequent biogeochemical studies. In order to study the thermohaline dynamics, this work uses results from field measurements of salinity, water temperature and current velocity performed in the Espinheiro channel and results provided by a numerical model.

This dissertation contains several articles originally prepared for independent publication in international journals together with non-published or non-submitted texts. Chapter 1 describes the motivation, structure of the work and presents a general literature survey. Chapter 2 describes the hydrographic characterization of the Espinheiro channel based on the field measurements, consisting in the submitted paper "Hydrographic characterization of an estuarine tidal channel" by N. Vaz and J. M. Dias (2006). Chapter 3 is the submitted paper by N. Vaz and J. M. Dias (2006), "Salt fluxes in a complex river mouth system of POrtugal". In Chapter 4 are described the equations resolved by the model as well as the parameterizations used. Chapter 5 describes the two-dimensional application of the hydrodynamic model to the Ria de Aveiro lagoon, resulting in the submitted paper: "Application of the MohidD-2D model to a mesotidal temperate coastal lagoon" by N. Vaz, J. M. Dias, P. C. Leitão

and R. Nolasco. Chapter 7 consists on the published paper by Vaz et al. (2005), "Horizontal patterns of water temperature and salinity in an estuarine tidal channel: Ria de Aveiro". The next chapter is a non-submitted text describing the calibration and validation of the salt and heat transport models and, Chapter 8 is a paper under preparation which presents the three-dimensional application of the numerical model to the Espinheiro channel. The last chapter is reserved for general conclusions and future work.

Due to these different origins, there are some repetitions among the introductions, study area and numerical model description along the chapters of this dissertation. These repetitions have been retained because the papers are considered sequential, providing a synthesis of the physical observations and modelling work on Ria de Aveiro and Espinheiro Channel.

1.4 Papers

- Chapter 2 is the submitted paper: Nuno Vaz, João Miguel Dias (2006). "Hydrographic characterization of an estuarine tidal channel". Submitted to *Journal of Marine Systems*.

  The following paper was excerpted from Chapter 2

- N. Vaz, J. M. Dias, I. Martins (2005). "Dynamics of a temperate fluvial estuary in early winter". *Global Nest Journal*, Vol 7, N^{o} 3: pp 237-243.

- Chapter 3 is the submitted paper: Nuno Vaz, João Miguel Dias (2006). "Salt fluxes in a complex river mouth system of Portugal". Submitted to *Environmental Fluid Mechanics*.

- Chapter 5 is the submitted paper: Nuno Vaz, João Miguel Dias, Paulo Chambel Leitão, Rita Nolasco (2006). "Application of the Mohid-2D model to a mesotidal temperate coastal lagoon". Accepted, *Computers & Geosciences*.

- Chapter 7 is the paper: Nuno Vaz, João Miguel Dias, Paulo Leitão, Inês Martins (2005). "Horizontal patterns of water temperature and salinity in an estuarine tidal channel". *Ocean Dynamics*, 55:416-429. doi: 10.1007/s10236-005-0015-4.

  The following papers were excerpted from Chapter 8

- N. Vaz, P.C. Leitão, Dias, J.M. (2006). "Channel-ocean Exchange driven by tides and river flow: Espinheiro Channel (Portugal)". Accepted, *Journal of Coastal Research*, SI50, ICS2007.

- Nuno Vaz, João Miguel Dias, Paulo Chambel Leitão (2006). "Three-dimensional modelling of a tidal channel: The Espinheiro Channel (Portugal)". Submitted to *Continental Shelf Research*.

Chapter 2

Hydrographic characterization of an estuarine tidal channel

The hydrography of the Espinheiro channel, an estuarine tidal channel located within Ria de Aveiro (Portuguese northwest coast), is investigated through the analysis of a thermohaline variables data set as function of two main forcing factors: incoming river flow and tide. Salinity and water temperature vertical profiles were measured twice a month from September 2003 to September 2004 at ten stations along the channel. Furthermore, in order to characterize the upper fluvial region of the channel in terms of these variables, thermohaline properties and current speed were also measured during two tidal cycles at an anchor station near the channel's head. The salinity distribution along the channel has been found to be closely related to the incoming river flow and tidal propagation. The water temperature distribution is related to the freshwater temperature seasonal variations and, due to the shallowness of the study area, is also related to the meteorological conditions. Formation of strong salinity gradients (commonly related to estuarine fronts) have been found in a region between 7 and 8 km from the lagoon's mouth. These gradients migrate within a region of about 1 km depending on the tidal regime: neaps or springs and its formation is related to changes in the channel's morphology (depth and width).

2.1 Introduction

According to Barnes [1980] coastal lagoons are saline water bodies separated or partially-isolated from the sea. They may be enclosed by several barrier islands, like Ria Formosa (in southern Portugal), as well as sand spits, or linked to the sea by one or more channels, which are small relative to the lagoon [Barnes, 1980], like Ria de Aveiro (in northern Portugal). The main driving forces of circulation in a large number of coastal lagoons and estuaries are river flow at the head of the estuary and sea level changes at its mouth. These driving forces determine the thermohaline distribution, as well as the distribution of any other tracer. In fact, MacCready [1999] have shown that the estuarine behavior adjusts dynamically to changes in river flow and tidal mixing. In coastal lagoons, forcing

due to the precipitation to evaporation balance, wind stress and surface heat balance are, according to Kjerfve [1994], also important. Newton and Mudge [2003] found these features in the study of the water temperature and salinity regimes in Ria Formosa (Southern Portugal).

This paper examines the hydrographic characteristics of an estuarine tidal channel, the Espinheiro Channel, evaluating the importance of the main forcing mechanisms: incoming river flow and tides.

The Espinheiro Channel is one of the four main branches of Ria de Aveiro, a mesotidal and shallow coastal lagoon located in the northwest coast of Portugal. This channel connects the major source of freshwater of the lagoon - Vouga River - to the Atlantic Ocean (Figure 2.1), being ideal to perform studies such as the one proposed here. This lagoon is the most dynamic in terms of physical and biogeochemical processes in Portugal. It is a very important system in the region where it is situated due to the intense human activity in its waters and along its margins. In spite its importance, the lagoon and particularly this channel are not well known, in terms of its hydrographic and physical processes. In fact, in the last 20/30 years the lagoon was studied mainly from a biologic, chemical and geological point of view, conducting to several publications like Cunha et al. [2001]; Almeida et al. [2001] (bacterioplancton), Morgado et al. [2003] (zooplankton), Abrantes et al. [2005] (suspended sediments). Other authors like Moreira et al. [1993]; Queiroga et al. [1994]; Cunha [1999] performed some localized measurements of water temperature, salinity and currents. There are not many studies or publications regarding the hydrography or the physical processes of the lagoon. However, Dias et al. [1999] in a prior hydrographic study reveal some of the main features of Ria de Aveiro. Records of water level, hereinafter SSE (sea surface elevation), current velocity and thermohaline properties were performed at several stations in the lagoon during the Summer seasons of 1996 and 1997. They have determined the type of tide at the mouth of the lagoon (semi-diurnal) and have observed that the astronomical tide is the main forcing driving water circulation within the lagoon. They also have

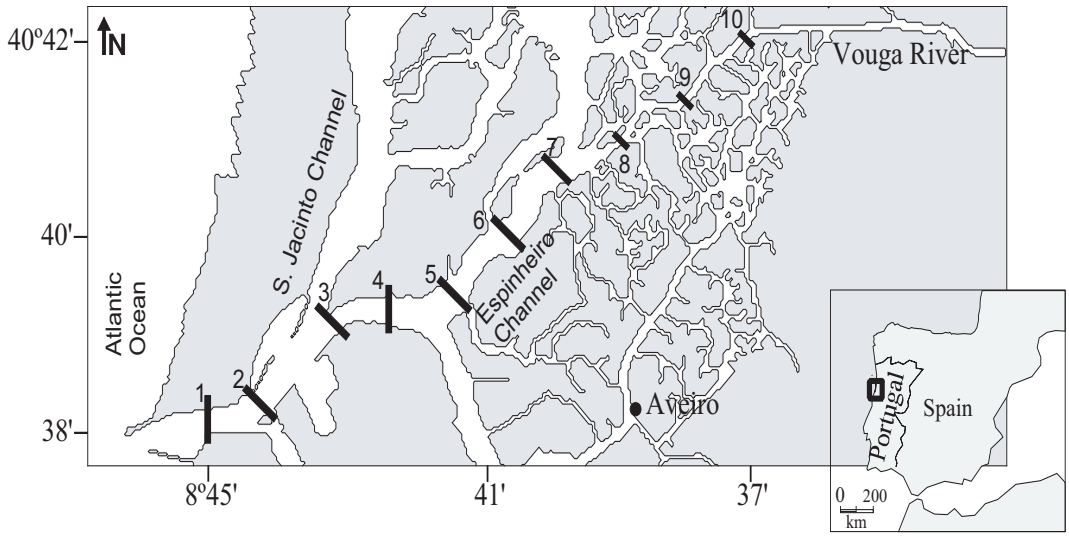

Figure 2.1: Map of the study area with the location of the sampling stations along the Espinheiro channel.

observed that the tidal wave propagation in the lagoon has the characteristics of a damped progressive wave. A more recent study [Vaz et al., 2005a], combining field measurements and modelling results, revealed the importance of the river flow in the establishment of the thermohaline horizontal patterns in the central area of the lagoon. Ria de Aveiro has been also studied through the use of numerical models. In fact, several studies were performed to investigate topics such as the tidal propagation in the lagoon [Dias et al., 2000], the lagrangian transport of particles [Dias et al., 2001] and sediment transport [Lopes et al., 2001; Dias et al., 2003].

The Ria de Aveiro constitutes a unique ecosystem in Europe. According to Barnes [1980], 5.3% of the Europe's coastline falls into the category of coastal lagoons. Most of these environments are located in the microtidal Mediterranean basin. Atlantic mesotidal lagoons include some lagoons in south-west France and some of western Iberian Peninsula. Lagoons fall into another type of wetland habitats like estuarine lagoons (Ria de Aveiro) or yet another which constitutes a coastal shape correspondent to a re-entrance, resultant from the submersion by the sea of the terminal zone of a fluvial network (like the Galician Rias) [Granja, 1996].

This study intends to be a step forward in the understanding of a coastal system that has received almost no oceanographic attention beyond the studies cited before. In the following, it will be investigated how the seawater and the freshwater interact within Espinheiro channel, evaluating the behavior of the salt and water temperature three-dimensional structure in terms of the main forcing factors: incoming river flow and astronomical tide. Studies about the estuarine response to changes in river flow in terms of the time scale [Kranenburg, 1986; MacCready, 1999] or magnitude [Monismith et al., 2002] are common in the literature. In fact, the study of the salt behavior within estuaries is an actual and extremely important issue because it provides an enormous insight to predict the behavior of other soluble tracers. Simpson et al. [2001] and Banas et al. [2004], in their studies, explore the hydrographic features of two macrotidal highly energetic estuaries and compute the salt balance in those systems due to tidal motion and river flow. This paper describes one year observations in Espinheiro channel in terms of the thermohaline properties. In Section 2 a description of the study area is presented. In Section 3 it is presented the methodology as well as the materials used during the field campaigns. The next sections contain the results and the conclusions.

2.2 Study area

A map of the Ria de Aveiro location and Espinheiro channel is shown in Figure 2.1. Espinheiro channel is located in the very complex central area of Ria de Aveiro, a mesotidal and shallow (mean depth of about 1 m relative to the local datum) coastal lagoon situated in the northwest Atlantic coast of the Iberian Peninsula, in Portugal. For simplicity, the study area from the mouth of the lagoon (near section 1) until near section 10 will be hereinafter referred as Espinheiro channel. However, it includes two distinct regions: the first extending from the mouth of the lagoon to near station 5 (see Figure 1 for reference) and the second is the Espinheiro channel itself, extending from section 5 to near section 10. The study area is approximately 11 km long, has an averaged width of about 200 m

and a mean depth, along its longitudinal axis, of about 10 m. The tides are mixed semi-diurnal, being M_2 the most important constituent, representing about 90% of the tidal energy [Dias et al., 1999].

The estimated tidal prism for the lagoon at extreme spring and extreme neap is according to Dias [2001] 136.7×10^6 and 34.9×10^6 m^3, respectively. Near section 5 is about 40×10^6 at extreme spring and 15×10^6 m^3 at extreme neap tide [Dias, 2001]. The total estimated freshwater input for the lagoon is very small (about 1.8×10^6 m^3 during a complete tidal cycle) [Moreira et al., 1993] when compared with the tidal prism both at the mouth or at the beginning of Espinheiro channel. In spite of the small contribution of the discharging rivers in terms of water input, when compared to the tidal prism, they may have a long-term influence in the residual transport [Dias et al., 2003]. Previous studies by Dias et al. [2000] and Dias [2001] revealed that the tide is strongly distorted as it progresses upstream from the mouth toward the end of the channels of the lagoon, due to changes in channel's geometry and bathymetry. The general characteristics of the tidal wave are those of a damped progressive wave. Nevertheless, in shallow areas the tidal wave assumes the main characteristics of a standing wave.

From a dynamical point of view, Espinheiro channel may be considered the most important area of the Ria de Aveiro, because the strongest currents are observed here, reaching values higher than 2 ms^{-1}. The lagoon's other channels are mainly shallow and tidal flat areas, contributing to a strong dumping of currents.

2.3 Materials and Methods

2.3.1 Sampling strategy

In order to obtain a good spatial coverage, producing a reliable synoptic view, *in situ* vertical profiles of water temperature and salinity were sampled along ten cross-sections (Figure 2.1) separated by 1000 m (see Table 2.1 for reference). The first cross-section is located near the mouth of the lagoon and the last one is located near the channel's head, close to the mouth of the Vouga River. In order to perform the measurements, it was used a SAIV A/S mini STD model SD204. Water pressure, water temperature and salinity were measured using a time step of 1 s. This instrument measures water temperature using a Thermistor in a range from -2 to 40°C with an accuracy of +/- 0.01°C. The water pressure is measured using a Piezoresistive sensor with an accuracy of +/- 0.02% of the depth (500 m) and for the conductivity the instrument uses a Inductive cell in a range of 0 to 70 mS/cm with an accuracy of +/- 0.02 mS/cm. The salinity is calculated from the conductivity, water temperature and water pressure in a range from 0 to 40 ppt with an accuracy of 0.02 ppt.

The measurements were performed twice a month at spring tide (maximum of tidal amplitude) and at the following neap (minimum of tidal amplitude). Each survey began at station 1 approximately 1h 40 min after the low tide hour predicted for the mouth of the lagoon, during the flood stream. In each cross-section, the profiles of the thermohaline variables were sampled at three points: near the margins of the channel and in its axis. The survey period lasted from September 2003 (be-

Table 2.1: Depth and location of the 10 stations located along longitudinal axis of the study area

Station	Depth [m]	Latitude [N]	Longitude [W]
1	27.5	40°38.66'	8°44.90'
2	21.5	40°38.93'	8°44.15'
3	21.6	40°39.45'	8°43.39'
4	14.5	40°39.62'	8°42.79'
5	9.6	40°39.66'	8°41.96'
6	14.6	40°40.20'	8°41.23'
7	14.8	40°40.60'	8°40.63'
8	5.7	40°40.95'	8°39.81'
9	5.8	40°41.17'	8°39.13'
10	7.5	40°41.57'	8°38.60'

ginning of Autumn) until September 2004 (end of Summer) covering extreme tidal conditions (twice a month) during one full year.

Data were collected in order to characterize the along and cross-channel distribution of water temperature and salinity during extreme tidal events. The spatial distribution of the cross-sections defined along the channel allow the coverage of at least three distinct regions: a marine or lower area of the channel, in free connection with the open sea; a middle area, subject to strong salt and freshwater mixing; and the upper fluvial area of the channel, characterized by freshwater but subject to daily tidal action.

Longitudinal (horizontal and vertical) and cross-sectional fields of water temperature and salinity were determined by spatial interpolation of the measured data using an ordinary Point-Krigging method [Cressie, 1993].

At the lagoon's mouth a moored station was installed. Water temperature, salinity and SSE were sampled every hour during 3 months, from September 23 of 2003 to January 7 of 2004 , in order to characterize the water mass characteristics at the mouth of the lagoon. Ideally, this station should be located in the middle of the channel in order to better characterize the tidal flow. However, due to the strong currents existing here and the intense boat traffic, the station was installed in a existent tidal gauge station, located in the south channel margin. The measurements were performed using the SAIV A/S mini STD model SD204 previously referred.

An anchor station, near cross-section 9, was selected for an intensive study of tidal cycles (25 h). The location of this station was chosen because it is an important and sensible area of fisheries and recreational waters, and because a paper industry is located a few km upstream. It is also ecological important due to the existence of rice (and other) cultures in the surrounding low lands of Baixo-Vouga. These cultures are affected by the saline intrusion and the knowledge of the behavior of the thermohaline variables response to tides and river flow in this area is commercially important, especially in dry years when the incoming freshwater is very low. Thus, in order to evaluate how current speed, salinity and water temperature stratification behaves under the influence of a freshwater source in this tidal domain, lunar-hourly vertical profiles of the thermohaline properties and current speed were measured during two consecutive tidal cycles (25 hours) for four sampling periods (one at each year season): January 15^{th}, June 16^{th}, August 27^{th} and December 3^{rd} corresponding to river

runoff of 58 m^3s^{-1}, 11.2 m^3s^{-1}, 3 m^3s^{-1} and 5 m^3s^{-1}, respectively. The instrumentation used was the SAIV A/S mini STD model SD204 previously referred and a Valeport current meter model 105. This current meter has a High Impact Styrene Impeller to measure the current speed in a range of 0.1 to 5 ms^{-1} with an accuracy of ±2.5% of reading above 0.5 ms^{-1} and ±0.01 ms^{-1} below 0.5 ms^{-1}. The current direction is measured using a flux gate compass with a range from 0-360° with a resolution of 0.5°.

In order to determine the incoming river flow, concurrent with each survey period, measurements of current speed were obtained several km upstream from the river mouth, 3 hours after the low tide hour predicted for the lagoon's mouth. This procedure assures that the measurements of current speed were made outside the region of tidal flood influence. The current velocity data were collected using the Valeport current meter model 105 previously referred. In order to compute the flow, the river section was divided in twenty four 2 m segments and the current velocity and the water depth measured for each segment. The current velocity was sampled at 60% of the water column following a standard procedure. The total river flow was obtained adding all individual segment results.

2.4 Results and discussion

2.4.1 Meteorological conditions and incoming river flow

A 1 year data set of daily values of precipitation, minimum and maximum air temperature and wind intensity measured at the meteorological station located at the University of Aveiro is depicted in Figure 2.2.

This data set is from September 2003 until October 2004, covering the field work period. The

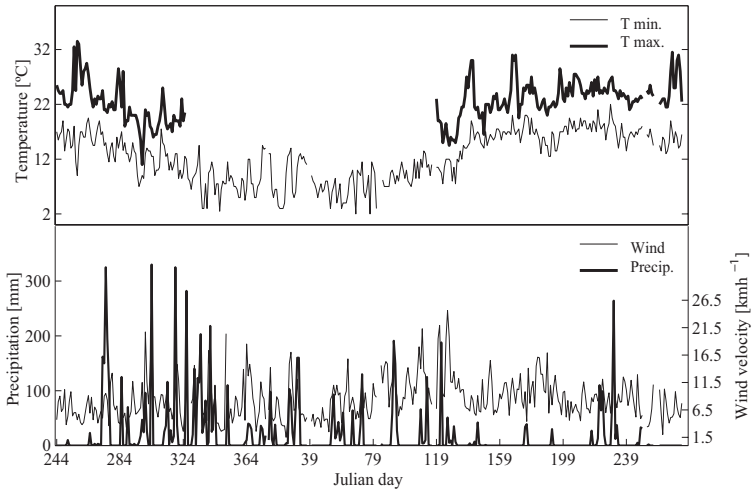

Figure 2.2: Maximum and minimum air temperature, precipitation and wind intensity measured at the University of Aveiro meteorological station during the survey period (September 2003 to September 2004).

rainy season was the Autumn of 2003 with 46 days of rainfall, reaching a daily maximum of about 330 mm. As expected, the Summer was the driest season with 22 days of rainfall and a daily maximum of about 264 mm. The maximum of the wind intensity was found in the beginning of the Spring, reaching a daily maximum of 24.6 kmh^{-1}. The mean values of wind intensity remain almost constant during all year with values around 8 kmh^{-1}. The air temperature values ranged from 2 °C in the Winter to 33.5 °C in the beginning of September 2003. A malfunction in the thermometer did not allow the measurement of temperature maximum during all Winter.

The incoming river flow concurrent with the field surveys is depicted in Figure 2.3. The highest values was reached during the Autumn of 2003 and at the beginning of the Winter season, with a maximum of 143.16 m^3s^{-1} in the end of January. During the Winter and until late Spring, the river flow values are lower than 50 m^3s^{-1} and at the end of Spring and during the Summer the river flow decreases to values lower than 10 m^3s^{-1}. The annual mean river flow is 31.5 m^3s^{-1}. The minimum values are reached in the Summer with values ranging from 2.0 to 5.0 m^3s^{-1}. The highest river flow values were reached during the Autumn when the rainfall reached a daily maximum of 330 mm (see Figure 2.2). The river flow highest value occurred during January 2004 as a result of the persistent rainy conditions during December and January (visible in Figure 2.2). In the following sections, the importance of the river flow will be discussed in terms of the salinity and water temperature seasonal cycles and in terms of the spatial distribution of these two variables.

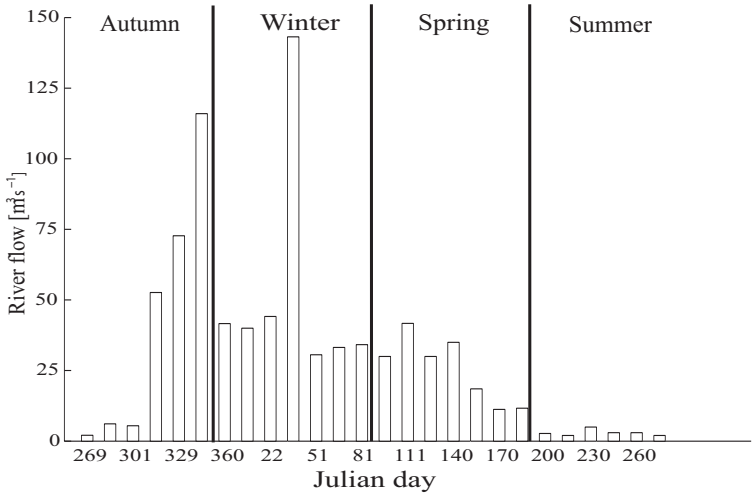

Figure 2.3: Discrete river flow values during the survey period (September 2003 to September 2004).

2.4.2 Water mass characteristics at the mouth of the lagoon

The water mass characteristics at the mouth of the lagoon are investigated through the analysis of 3 month hourly time series of SSE, salinity and water temperature obtained at the moored station referred at Section 2.3. In Figure 2.4 are depicted the first 15 days of the initial data set and the spectral energy computed using the complete data set.

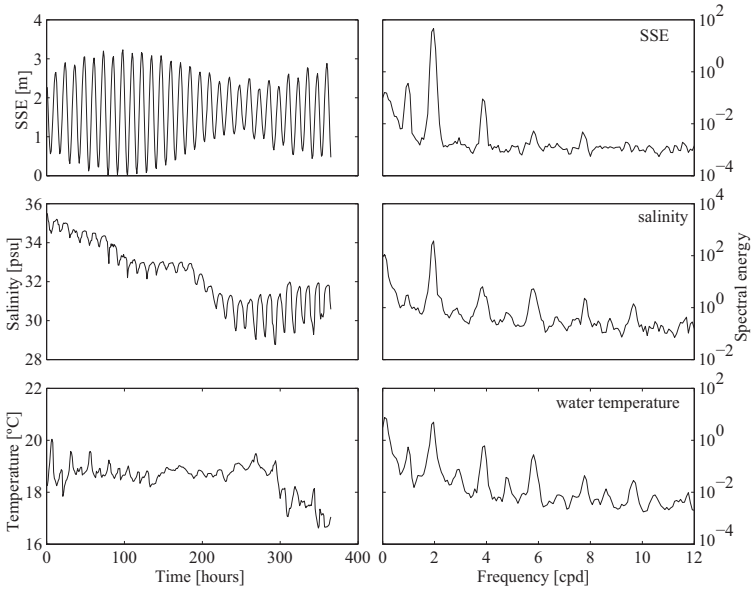

Figure 2.4: Time series and computed spectral energy of sea surface elevation [m^2/cpd], salinity and water temperature [$°C^2$/cpd] measured at a fixed station located near the lagoon's mouth.

The tide is semi-diurnal with a diurnal inequality. The minimum value of SSE is about 0.2 m and the maximum is 3.2 m, observed at spring tide. Salinity has also a strong semi-diurnal component, with a maximum value typically oceanic -36 psu- and a minimum value of 13.5 psu (in the Autumn's end). These low salinity values are due to an increase of the freshwater inflow into the lagoon and also the dilution of the salt water due to rainfall. The water temperature evolution is not so regular. The maximum and minimum values were 20 and 12.1 °C, respectively. The periodicity of the salinity and water temperature time series is forced by the SSE evolution. The higher salinity values and the lower water temperature values where observed at high tide, while the lower salinity values and the higher water temperature values were measured at low water.

The spectral energies computed for the SSE, salinity and water temperature time series are also depicted in Figure 2.4. The SSE spectrum presents a high energy peak at semi-diurnal frequency (2 cycles per day (cpd)). The energy associated with the diurnal constituent is also significant, revealing the diurnal inequality of the tide. The SSE spectrum also exhibit peaks at the frequencies correspondent to first harmonics of the semi-diurnal constituents, revealing the importance of the shallow water constituents characteristic of shallow systems like Ria de Aveiro, where there is a significative tidal wave deformation due to bottom friction. Salinity and water temperature spectra also exhibit a high peak at the same frequency, as well as smaller energy peaks at frequencies correspondent to the first harmonics of the semi-diurnal constituents. The energy of the diurnal frequency peak observed in the salinity spectrum is relatively low, revealing that the salinity cycle is mainly induced by the tide. In the case of water temperature spectrum, the energy of the diurnal frequency peak is significant, revealing the importance of the meteorological variables on the heating/cooling cycle of the water.

These results are similar to those obtained by Dias et al. [1999] in a previous work. One more aspect should be addressed: the high energy near the lower frequencies is a typical red noise behavior. This fact is due to the persistence of the SSE, salinity and water temperature data used in the spectral analysis.

2.4.3 Spatial surveys

A description of the general hydrography of Espinheiro channel is presented here. This analysis is based on measurements of water temperature and salinity obtained during the field work conducted throughout a year between September 2003 and September 2004. The seasonal cycle of water temperature and salinity will be referred here and discussed in the next subsection.

In Figure 2.5 is depicted the vertical structure of salinity and water temperature along the longitudinal axis of Espinheiro channel. Station 1 is near the mouth of the lagoon and station 10 is near the channel's head (see Figure 2.1 for reference).

These figures were obtained through spatial interpolation of salinity and water temperature vertical profiles, measured along the channel, and represent synoptic snapshots of the channel in terms

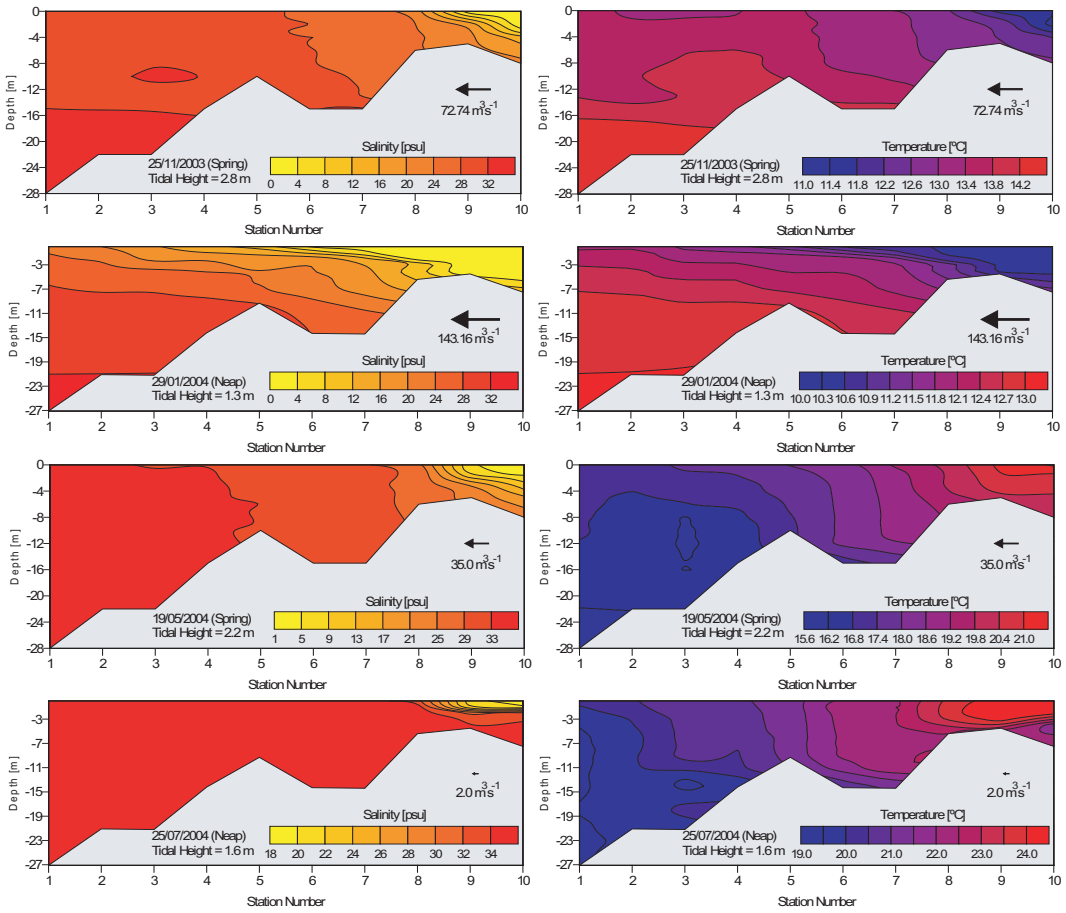

Figure 2.5: Vertical distribution of salinity and water temperature along Espinheiro channel.

of the thermohaline properties. Through the analysis of these figures it will be discussed the balance between the water column stratification/homogenisation evaluating its dependence on the freshwater inflow and tidal propagation.

The four cases represented are typical conditions of salinity and water temperature for each year season. It can be observed that near the channel's head, the fluvial region, the water temperature ranges from 10 °C during the Winter to values of 24/25 °C during the Summer. The salinity ranges from fluvial (about 0 psu) to oceanic typical values (between 32 and 35 psu) depending on the freshwater inflow. In this region the water column is always stratified, except during intense river inflow (higher than 100 m^3s^{-1}) and neap conditions when the water column is totaly filled with freshwater. During high river flow periods (72.74 m^3s^{-1}) and spring tide periods, the salinity intrusion through the channel's bed lead to the establishment of stratification. When the river flow is higher than 40 m^3s^{-1}, the entire water column is filled with freshwater during the low tide and vertical stratification is established when the high tide is reached, due to the saline intrusion through the bottom connected to the sea level rise. In the marine region, the stratification is mainly dependent on the occurrence of high river discharge events (higher than 100 m^3s^{-1}). When the river flow is weak, the water column is completely filled with oceanic water (homogeneous water column) and when the river flow is high the water column is stratified even during spring tides, presenting oceanic water in the lower layers and brackish water near the surface. In this region the difference between surface and bottom values of salinity and water temperature is never too high. Between these two sectors a transition area is evident , with strong horizontal salinity gradients. In this region, the stratification is established only when the river flow is very intense (higher than 100 m^3s^{-1}), presenting the maximum observed vertical salinity gradient.

Due to the channel's shallowness, meteorological variables like air temperature and solar radiation also play a key role in the heating/cooling cycle of the water. When the river flow is lower than 100 m^3s^{-1} the vertical water temperature difference is perceptible at the side ends of the channel (in the regions of ocean and river influence) but it is almost imperceptible in the inner region of the channel. When the river flow is higher than 100 m^3s^{-1}, vertical water temperature difference is observed from the mouth until the channel's head, with oceanic values along the bottom and fluvial values along the top layers. One more feature should be addressed, the higher salinity values are observed during the Summer season with oceanic values of about 36 psu. The presence of this highly saline water may be related to upwelling events that occurred during this season when the northwest coast of Portugal in under the influence of northwestern winds.

When the river flow is lower than 100 m^3s^{-1} it is perceptible the existence of strong salinity gradients, commonly related to estuarine fronts (more visible in the salinity results), between stations 7 and 8. This strong salinity gradient appears in this region due to changes in the channel's morphology (channel's width and depth) and the proximity of the region of freshwater influence. In fact, in an estuarine system only two facts contribute to the decrease of salinity near the head: first, the shoaling of the depth decreases the effectiveness of the exchange flow as a means for up-estuary salt flux; and second, the tidal excursion is decreased due to the tidal energy damping in an estuarine river [Jay and

Smith, 1990a,b], or due to the tides being reflected near the estuary's head [Lavelle et al., 1988]. In Espinheiro channel, depending on the type of tide (spring or neap) and the incoming river flow, these strong salinity gradients are visible within a region between station 7 (neap) to station 8 (spring). The thermal gradients are less perceptible due to the smaller horizontal gradients between the mouth and the channel's head.

2.4.4 The seasonal cycle

In Figure 2.6 are depicted the spatial-temporal variation of salinity and water temperature at three different depths: near surface (2.6a, 2.6d), mid-water (2.6b, 2.6e) and near bottom (2.6c, 2.6f). The period represented covers an entire year from September 2003 to September 2004. The annual salinity distribution is closely related to the type of tide (spring or neap) and with the Vouga River discharge variability, with salinity values increasing progressively towards the mouth of the lagoon. On the other hand, due to the channel's shallowness the water temperature distribution is less dependent on the river discharge and it is closely related to the freshwater temperature and from its dependence on the air temperature pattern (see Figure 2.2).

At the top layer (Figure 2.6a) when the river flow is weak, in the beginning of the Autumn, the saline intrusion goes further upstream (almost 1 km) during spring tide. As the river flow increases, the freshwater extends its influence downstream towards the lagoon's mouth. Under low river inflow, the channel can be divided in two distinct regions: a marine region (from station 1 to near station 8) and a fluvial region (from station 8 to station 10). This near surface pattern remains the same during Autumn and Winter except in two cases: during surveys 6 (December, 5^{th}) and 10 (January, 29^{th}) the river flow is higher than 100 m^3s^{-1} (see Figure 2.3 for reference) and the near surface water is brackish up to the lagoon's mouth. The freshwater and the oceanic water mixes and near the lagoon's mouth the salinity has values between 20 and 25 psu. During the Spring season, when the river flow presents values between 30 and 40 m^3s^{-1}, it is perceptible an intense horizontal salinity gradient which migrates back and forth for about 1 km during neap and spring tide surveys, respectively. During this period, the channel can be divided in three distinct regions: a lower marine region with salinity values between 30 and 35 psu (from stations 1 and 6), an inner brackish region with salinity values between 20 and 30 psu (between stations 6 and 8) and a upper fluvial region with salinity values ranging from 0 to 20 psu. During the Summer season, the incoming freshwater is low -less than 5 m^3s^{-1}- and the channel is filled with oceanic waters.

The mid-depth and near bottom salinity distribution presents almost the same pattern (Figures 2.6b and 2.6c). Near the channel's head (from station 8 to 10) during high river runoff events, the water column is filled with freshwater. At mid-depth and from station 8 to near the channel's mouth the salinity structure present brackish values. Near the channel's head, during the Autumn, Winter and Spring seasons, the surface water present fluvial values. Even during the Summer, the surface waters may present low salinity values. Near the channel's bed, the salinity intrusion effect is more perceptible when the river inflow decreases, presenting high salinity values during the Summer and in early

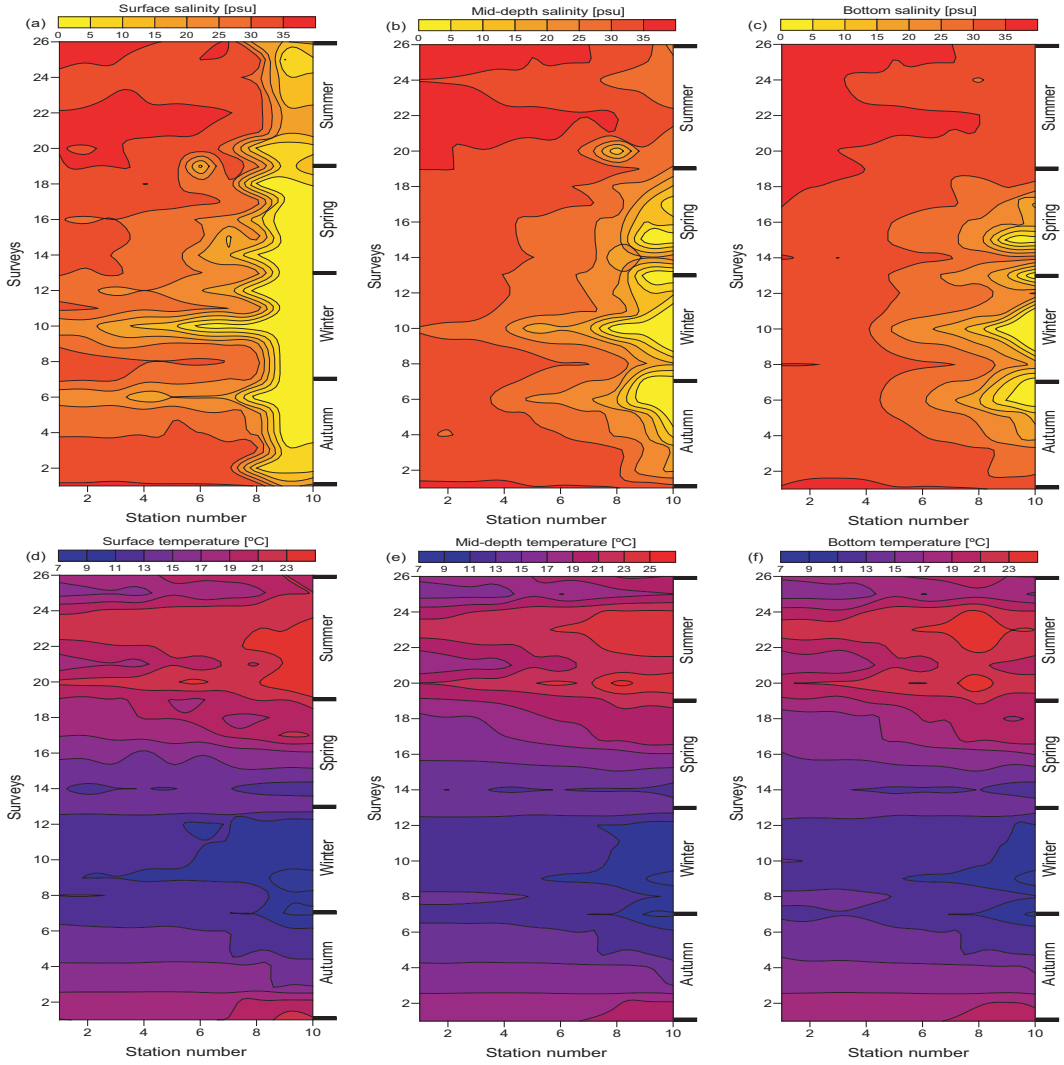

Figure 2.6: Temporal distribution of salinity and water temperature along the Espinheiro channel during the sampling period (September 2003 to September 2004).

Autumn. The salinity intrusion problem is a very important issue concerning agricultural exploration when the river inflow present values lower than 3 m^3s^{-1}. From the salinity figures is perceptible that higher salinity values are found in the Spring and Summer seasons. Not only because the river flow decreases but also because more saline waters incoming from the coastal ocean penetrates into the channel. This may be related to the upwelling season in the northwest Atlantic coast of the Iberian Peninsula.

The water temperature distribution is similar at the surface, mid-depth and near the bottom of the channel. As it can be observed, the horizontal gradients, between the mouth and the channel's head are smooth during all survey year. This feature may be due to the fact that the oceanic water temperature has low annual variability when compared to the seasonal fluvial water temperature variability, which has a higher range. The signal inversion of water temperature gradient between

the coastal and fluvial waters is perceptible in the figures. In fact, starting from the middle of the Spring season to middle of the Autumn, warmer fluvial waters enter into the channel. The opposite occurs during the colder seasons when warmer waters came into the channel from the sea. From Autumn to Winter, the water temperature in the inner part of the channel decreases almost 6 °C, from values between 17 and 19 °C to values between 11 and 13 °C. This effect is due not only to the water temperature of the ocean and river waters but also due to the decrease of the air temperature, an effect visible in Figure 2.2 where it is perceptible a decrease of the minimum air temperature of about 5 °C. From the Winter to Spring the water in the inner part of the channel becomes warmer, increasing from 11-13 °C to 19/21 °C at the end of the Spring season. The same effect is, once more, perceptible in Figure 2.2 where it is visible an increase of the minimum and maximum air temperatures. In the Summer, the water temperature within the channel increases to values higher than 23 °C. The oceanic and fluvial boundaries of the channel have similar water temperature variations. It is difficult to divide the channel in different regions when considering water temperature results. However, near the fluvial region, the water temperature values are always 1-2 °C warmer or cooler, depending on the year season, than in the rest of the channel.

The analysis of Figure 2.6 reveals the existence of strong salinity gradients (commonly related to estuarine fronts) along all of the water column, being noticeable the decreasing of the horizontal gradients intensity from surface to bottom. These strong gradients are much more perceptible in the salinity patterns. Near the surface, these estuarine gradients occur during the full year, even when the river flow is weak. During the Summer, when the river flow is very low, this strong gradients are not established at the bottom layers. Typically, these gradients exist between stations 7 and 8, but during high river inflow events (surveys 6-10) they migrate downchannel, revealing a strong salinity horizontal gradient. These strong gradients can be considered as areas of sediment retention (sediment trapping) and their existence may influence the downstream migration of the fluvial sediments from the Vouga river. Near the surface, during the Winter and Spring seasons, it is verified the effect of the spring-neap tidal cycle on the migration of the observed gradients. During neap tides they migrate downstream and during spring tide periods they migrate further upstream due to the higher tidal prism.

During survey 6 (December's beginning) and 10 (January's end), the water temperature patterns are similar to those observed for salinity. The main difference is the longer time scale, i.e. the salinity response to changes in river flow occurs more rapidly. For the water temperature, there is a slower response due to the lower difference between oceanic and fluvial water temperature values.

2.4.5 Tidal cycling

Figures 2.7, 2.8 and 2.9 show the temporal evolution of the salinity, water temperature and current velocity during two tidal cycles in the sampling periods of January (a), June (b), August (c) and December (d) 2004. These four sampling periods characterize the Winter, late Spring, Summer and Autumn conditions.

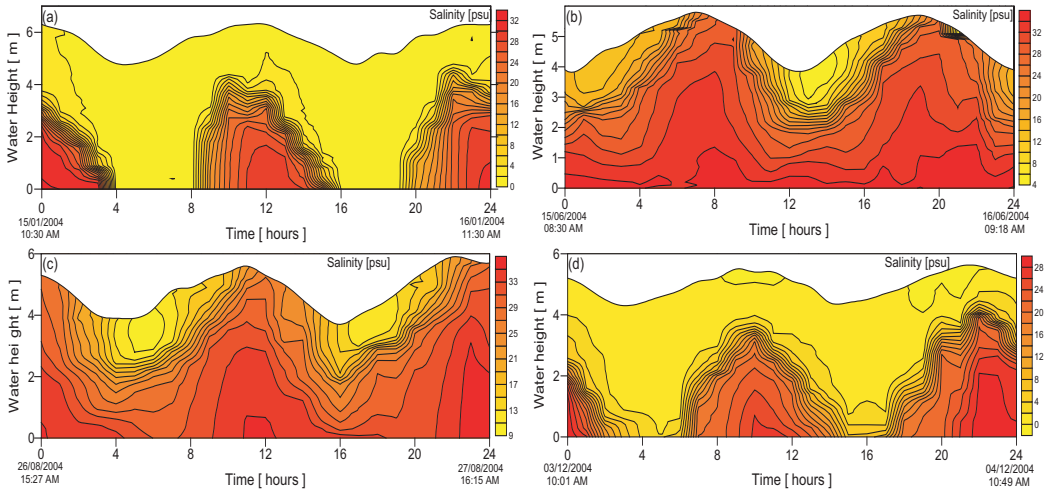

Figure 2.7: Temporal evolution of salinity, measured at an anchor station located near station 9, during the January (a), June (b), August (c) and December (d) tidal cycle sampling campaigns.

The river flow is 58, 11.2, 3 and 5 m^3s^{-1} for the sampling periods of January, June, August and December, respectively, and the tidal range is 1.7, 2.0, 1.4 and 1.2 m, respectively, corresponding to neap tide periods. Under these tidal conditions and river flow values, the upper fluvial region of the Espinheiro channel presents salt wedge (Autumn and Winter sampling periods) and partially mixed (Spring and Summer) estuary characteristics, according to the classification found in Bowden [1967] and Pritchard [1967].

The upper fluvial region of the Espinheiro channel reveals a semi-diurnal pattern (same feature is

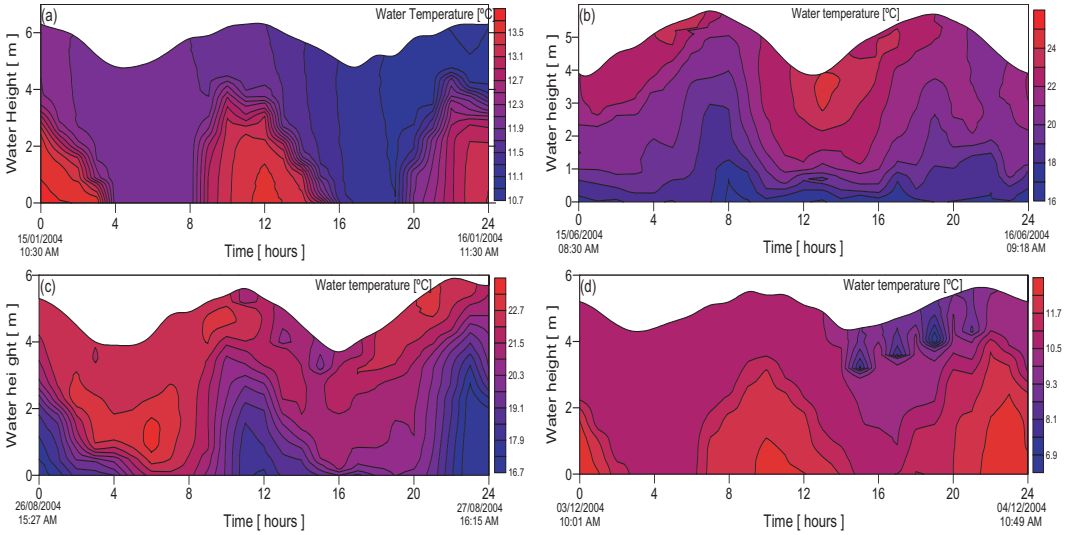

Figure 2.8: Temporal evolution of water temperature, measured at an anchor station located near station 9, during the January (a), June (b), August (c) and December (d) tidal cycle sampling campaigns.

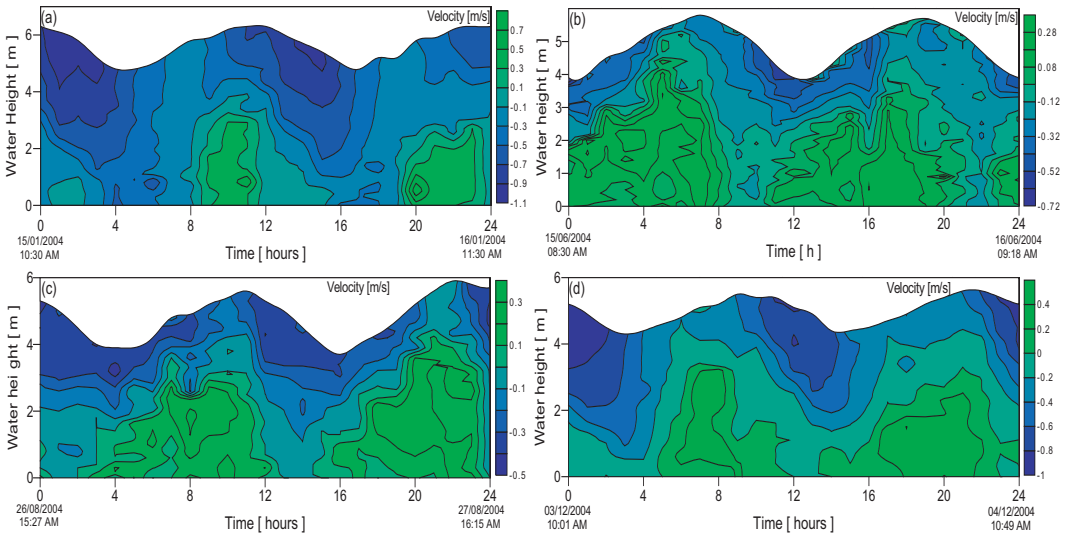

Figure 2.9: Temporal evolution of current velocity, measured at an anchor station located near station 9, during the January (a), June (b), August (c) and December (d) tidal cycle sampling campaigns.

found in the lagoon's mouth). As previously referred, the M_2 constituent has almost 90% of the total tidal energy at the lagoon's mouth, being its effect dominant even near the far end of the channel. In fact, Figures 2.7a, 2.7d and 2.8a and 2.8d show that the salinity and water temperature present typical oceanic values when the high tide reaches this location. In the Spring and Summer sampling campaigns, this periodicity is more visible during the low water hours.

The January and December results reveal that a stratification/destratification event takes place. It may be observed that the stratification increases during the flood period, reaching its maximum one hour before the high tide. The difference between the high water time at this location and at the channel's mouth is about 2 hours. Thus, the tidal wave propagated through the 9 km of this channel (from the mouth until this point) with a velocity of about 4.5 kmh^{-1}. Stratification decreases during ebb until the local low water hour. The entire water column is filled with freshwater propagating from the river, which pushes back the brackish water. Salinity and water temperature values are about 0 psu and 12 °C, respectively. The June and August results reveal the partially mixed characteristics of the upper region of the channel. In fact, the salinity results show some stratification, especially during low water and beginning of the flood period. The water column is mainly filled with the salt water coming from the coastal ocean. The salinity maximums are reached during the Spring and Summer campaigns with values higher than 33 psu. This is an expected feature since the late Spring and Summer periods are characterized, in the Aveiro region, by northern winds which induces upwelling events. In fact, the salinity maximums ranges from 28 (December campaign) to almost 36 psu (August campaign).

Near the surface, the water temperature decreases during the day in the January, June and August sampling periods, but during the December campaign the water temperature is approximately constant during the first tidal cycle, decreasing during the second one. Nevertheless, the water tem-

perature variation is strongly connected to the variation - decrease - of the air temperature along the day. In Figure 2.8 the inversion of the water temperature is perceptible between the beginning of the Winter (warmer oceanic waters) and the end of Spring (warmer fluvial waters) and between the Summer and the Winter season. During the Autumn and Winter the water temperature maximums are reached during high water near the bottom, and in opposition, in the warmer seasons sampling campaigns the maximums of water temperature are reached during low water at the surface. The water temperature minimums ranges from 6.9 (December) and 16.7 °C (August) and maximums ranges from 12.4 in December and values higher than 26 in the June sampling campaign. The water temperature minimums and maximums varies, between the Winter and the Summer, about 9.8 and 14 °C.

The vertical lunar hourly profiles of the velocity modulus during all the sampling campaigns indicate an asymmetry between flood ($\vec{V} > 0$) and ebb ($\vec{V} < 0$) currents. The ebb currents are higher than the flood currents, reaching maximum speeds, during the January survey, around -1.1 and 0.7 ms^{-1}, respectively (Figure 2.9a). The lower current velocities are observed during the August campaign (Figure 2.9c), being the maximums of -0.5 for the ebb and 0.3 for the flood current. The tidal ebb velocity is, in general, enhanced by the freshwater runoff. Near the surface and at mid-water, the current velocity is predominately downstream (in the Autumn and Winter periods), with the surface values higher than the mid-water ones. During the June and August sampling campaigns, the current velocities obtained are, in general, lower than the ones observed during the January and December campaigns with ebb velocities ranging from 0 to -0.72 (June) and 0 to -0.5 ms^{-1} (August) and flood velocities of about 0.3 ms^{-1}. A similar current velocity asymmetry was found by Miranda et al. [2004] in studying the dynamics of a tropical estuary, the Curimataú River, northeast Brazil.

2.5 Conclusions

This one year sampling campaign in the Espinheiro channel has provided the first insight into its hydrographic features. The channel's hydrodynamics is largely dependent on the freshwater inputs variability as well on the tidal wave characteristics.

At the lagoon's mouth, the salinity daily variation is strongly connected to the tidal propagation. The spectral analysis of a data set of SSE and salinity show that the most energetic peak is correspondent to the semidiurnal frequency, being the diurnal frequency peak less relevant. On the other hand, the water temperature spectral analysis reveal high energy peaks in both frequencies, semidiurnal and diurnal, demonstrating the importance of the meteorological variables in the modulation of the water temperature in shallow areas like this study area. All the spectra reveal the existence of significative energy peaks correspondent to the first harmonics of the semi-diurnal constituents, revealing the importance of the shallow water constituents in a system like Espinheiro channel. The thermohaline features found in each one of the cross-sections are closely related to the tidal characteristics found at the lagoon's mouth.

When the river flow is low - lower than 10 m^3s^{-1} - the water column until near station 8 is filled

with salt water incoming from the coastal waters. When the river flow is higher than 100 m^3s^{-1} vertical stratification is established along all the channel. The incoming freshwater from the river extends its influence, and near the surface, the water is brackish, up to the lagoon's mouth, with salinity values of about 20 psu. When the river flow is between 30 and 50 m^3s^{-1} the channel can be divided into three different regions: a lower marine region where the salinity and water temperature present oceanic values; an intermediate inner brackish region, where the incoming freshwater mixes with the coastal ocean's water and a upper fluvial region, dominated by the freshwater but still subject to semidiurnal tidal action.

During the survey period, it was observed the formation of strong salinity gradients, commonly related to estuarine fronts, in a region between stations 7 and 8. The formation of these strong gradients is strongly connected to the interaction between the salt and freshwater as well as to changes in channel's morphologic characteristics, like the width and the depth. It was observed that these gradients migrate within a region of about 1 km, between station 7 and 8, depending on the type of tide: neap and spring, respectively. The longitudinal water temperature variation in the study area is smoother than the salinity one, showing lower horizontal gradients. Besides the dependence on the water temperature variation at the channel's boundaries (ocean and river), the water temperature within the Espinheiro channel is closely related to meteorological forcing, like air temperature, incoming solar radiation or relative humidity. This feature may be explained by the shallowness of the study area.

From the four tidal cycle survey campaigns changes were observed in the classification of the upper fluvial region of the Espinheiro channel. In fact, during the January and December survey periods, that regions reveal salt wedge characteristics, with the establishment of vertical stratification during the flood period. In opposition, these region reveal partially mixed characteristics during the June and August survey periods, when the incoming freshwater is lower.

The results shown in the previous sections reveal the importance of the major forcing factors that influences the water temperature and salinity behavior within Espinheiro channel. In fact, the salinity distribution within the channel is closely related to the interaction between the tide and the river flow. The water temperature distribution is related to the tide and the river flow and, due to the small depth of the channel, is also influenced by meteorological variables as air temperature.

Chapter 3

Salt fluxes in a complex river mouth system of Portugal

Measurements of velocity and salinity near the mouth and head of the Espinheiro channel (Ria de Aveiro lagoon) are used to assess the balance, under steady conditions, between the seaward salt transport induced by river discharge and the landward dispersion induced by various mixing mechanisms. This assessment is made using data sampled during complete tidal cycles. Under the assumption that the estuarine tidal channel is laterally homogeneous and during moderate tidal periods (except for one survey), currents and salinity data were decomposed into various spatial and temporal means and their deviations. Near the channel's mouth, the main contributions to the salt transport are the terms due to freshwater discharge and the tidal correlation. Near the channel's head, this last term is not so important as the gravitational circulation, which is enhanced by the increase of the freshwater discharge. The remaining terms, which are dependent on the deviations from the mean depth have a smaller role in the salt transport results. The computed salt transport per unit width of a section perpendicular to the mean flow is in close agreement to the sum of the advective and dispersive terms (within or very close to 12%). An imbalance of the salt budget across the sections is observed for all the sampling periods.

3.1 Introduction

An estuary is defined as a semi-enclosed body of water having a free connection with the open sea and within sea water is diluted with freshwater derived from land drainage [Pritchard, 1967]. More commonly, for oceanographers, engineers and natural scientists an estuary is an important and sensible area of interaction between fresh and salt water. These systems can, generally, be divided in three areas [Kjerfve, 1989]: (a) a marine or lower estuary, (b) a middle estuary where the mixing between the fresh and salt water occurs and an (c) upper or fluvial estuary characterized by freshwater but subject to a daily tidal action. The delimitation of these areas is dynamic and can change seasonally

(or in lower time scales) due to the tide, winds or the freshwater inflow [Kjerfve, 1990; Miranda et al., 2002].

In estuaries and tidal channels, which often transverse heavy populated regions, factors like sewage effluent or industrial waste reduce water quality, affecting people's health and other activities like fisheries. The behavior of salt within this systems, its flux and transport due to advection and turbulent diffusion, provides a basis to predict the behavior of other soluble conservative substances since the salt is a natural tracer.

In a tidal channel, the main mechanisms which drive the circulation and provide the turbulent energy for mixing processes are the freshwater discharge and the barotropic and baroclinic components of the gradient pressure force due to tide and longitudinal salinity, respectively [Miranda and Castro Filho, 1996]. Under steady conditions, there is a balance between seaward advection and landward mixing. This balance is due to the mixing process between oceanic salt water and fluvial freshwater which mixes upchannel. Among the processes that causes mixing, longitudinal turbulent diffusion plays a minor role and the overall landward mixing is better termed dispersion rather than diffusion [Fischer, 1976; Hunkins, 1981; Miranda and Castro Filho, 1996]. Consequently, the advective seaward salt transport is driven by the circulation components due to the river flow and the landward salt dispersion is a consequence of the dispersion produced by the effects of tides, gravitational circulation and winds. In this paper, the effect of mixing caused by freshwater discharge and tides is investigated in a tidal channel located in the northern coast of Portugal, the Espinheiro channel.

During the last decades, the salt balance and salt transport have been studied in several estuaries and coastal systems by many authors. Fischer [1972] and Dyer [1974] described a number of mechanisms and methods by which the salt balance and dispersion are analyzed for partially and stratified estuaries. Among others, Hunkins [1981]; Miranda and Castro Filho [1996]; Bérgamo [2000] have investigated the main driving forces of the non-tidal circulation and calculated the advective and dispersive contributions to the salt transport in their studies for the Hudson and Cananéia Sea estuaries. Dyer et al. [1992] studied the cross-sectional salt balance in a tropical estuary and illustrated the dynamic coupling between the transverse and vertical contributions on a tidal and tidally averaged basis. More recently, Simpson et al. [2001] and Banas et al. [2004] in their studies explore the hydrographic features of two macrotidal highly energetic estuaries and compute the salt balance in those systems due to tidal motion and river flow. Bowen and Geyer [2003] examined the mechanisms and variability of salt transport at a relatively uniform section of the Hudson estuary using a 70-day moored time series. MacCready and Geyer [2001]; MacCready et al. [2002] have explored the approach proposed by Dronkers and van de Kreeke [1986], in which the concept of looking at the salt flux through a vertical cross section which moves up and down the estuary with the tidal velocity was developed, and took a step forward, by using an actual isohaline as the surface through which salt and fluxes are computed, including long time scales and the case in which isohalines are ejected from the ocean´s end.

This work examines the main mechanisms that commands the salt transport in the Espinheiro

channel, one of the four main branches of the Ria de Aveiro Lagoon. A brief description of the physical characteristics of the channel is presented in Section 3.2. This channel connects the major source of freshwater of the Ria de Aveiro to the Atlantic Ocean, rendering it ideal to perform these kind of studies. It crosses an important and traditional fishing area of the lagoon and has storage areas of chemical products along its margins, as well as the Aveiro fishing and comercial harbors. Despite these facts, this region has received almost no physical attention by the scientific community. The exception are a few studies, based on field measurements of thermohaline properties and current velocity, that examine the hydrologic characteristics of the lagoon in early Summer [Dias et al., 1999] and the horizontal patterns of water temperature and salinity in the central area of the lagoon [Vaz et al., 2005a].

The main objective of this work is to calculate the advective and dispersive contributions for the salt transport, with the salt transport computed per unit width of a section perpendicular to the channel passing through the fixed stations A and B, located near the mouth of the lagoon and 8 km upstream, respectively. In this paper the water column stability is investigated using the Richardson number. This work is based on the assumption that the channel can be considered laterally homogeneous, the main components of the advective salt transport are due to the freshwater discharge and density-driven currents being the surface wind stress forcing negligible on the steady-state salinity and velocity profiles. Sections 3.2 and 3.3 describe the study area and the sampling methodology used. Section 3.4 describes the salt transport calculations and the following sections present the results and conclusions.

3.2 The study area

The Espinheiro channel is one of the four main branches of Ria de Aveiro, a mesotidal and shallow coastal lagoon (mean depth of about 1 m relative to the local datum) located in the northwest coast of the Iberian Peninsula (see Figure 3.1). This channel is located in the very complex central area of the lagoon and it includes two distinct regions: the first extending from the mouth of the lagoon to near the black solid line marked in Figure 3.1 and the second is the Espinheiro channel itself, extending from the referred line to near station B (about 2 km upstream). For simplicity, the study area from the mouth of the lagoon (near station A) until station B will be hereinafter referred as Espinheiro channel. The study area is approximately 11 km long, has an averaged width of about 200 m and a mean depth, along its longitudinal axis, of about 10 m. The tides are mixed semi-diurnal, being M_2 the most important constituent, representing about 90% of the tidal energy [Dias et al., 1999].

Previous studies by Dias et al. [2000] and Dias [2001] revealed that the tide is strongly distorted as it progresses upstream from the mouth toward the end of the channels of the lagoon, due to changes in channel's geometry and bathymetry. The general characteristics of the tidal wave are those of a damped progressive wave. Nevertheless, in shallow areas the tidal wave assumes the main characteristics of a standing wave.

From a dynamical point of view, the Espinheiro channel may be considered the most important area of Ria de Aveiro, because the strongest currents are observed here, reaching values higher than

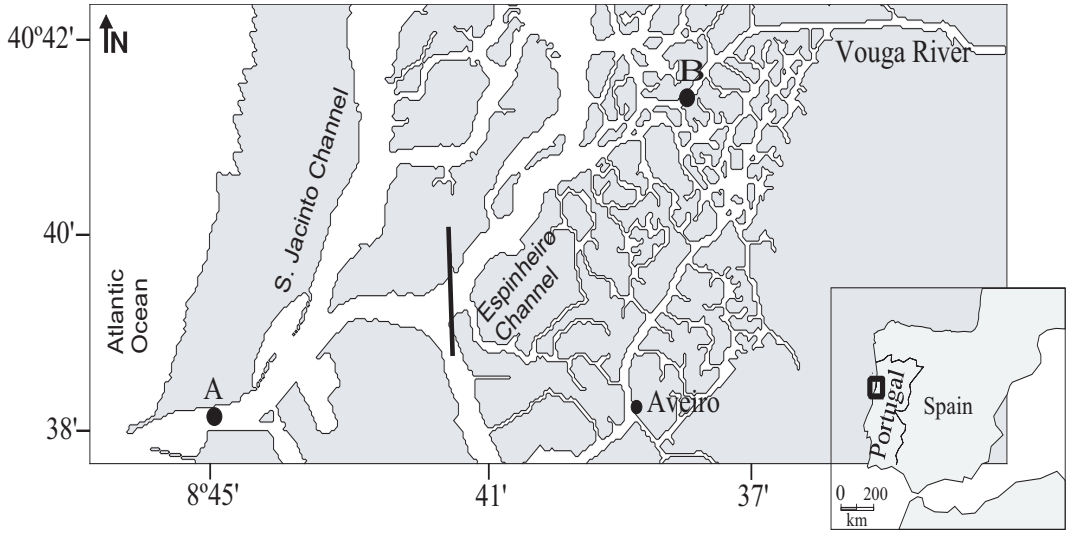

Figure 3.1: The Espinheiro channel showing the survey sites A and B.

2 ms^{-1}. The lagoon's other channels are mainly shallow and tidal flat areas, contributing to a strong dumping of currents.

The estimated tidal prism for the lagoon at extreme spring and extreme neap is according to Dias [2001] 136.7×10^6 and 34.9×10^6 m^3, respectively. Close to the black solid line it is about 40×10^6 at extreme spring and 15×10^6 m^3 at extreme neap tide [Dias, 2001]. The total estimated freshwater input for the lagoon is very small (about 1.8×10^6 m^3 during a complete tidal cycle) [Moreira et al., 1993] when compared to the tidal prism, both at the mouth and at the beginning of Espinheiro channel. In Ria de Aveiro, tidal currents are predominant, relatively to the currents induced by the rivers discharge. Nevertheless, the freshwater inputs are very important in the establishment of the salinity patterns [Dias et al., 1999]. Although, the small contribution of the discharging rivers in terms of water input, when compared to the tidal prism, they may have a long-term influence in the residual transport [Dias et al., 2003].

Several rivers discharge into Ria de Aveiro. The most important freshwater contribution is from Vouga River. Its mouth is located near the head of the study area and therefore its freshwater inflow is determinant in the establishment of the channel's physical patterns. There is a study by Vicente [1985] presenting flood freshwater values of 3400 m^3s^{-1} for a period of 25 years. The average flow for Vouga river is referred by Borrego et al. [1990] as 25 m^3s^{-1}, but according to Vicente [1985] this value is underestimated. During the period from September 2003 to September 2004, measurements of the Vouga river's incoming flow were performed by the authors under the scope of this work and the annual averaged flow value found was 31.45 m^3s^{-1}. The highest river flow values occurred during Autumn and the beginning of the Winter with a maximum of 143.16 m^3s^{-1} in January. The minimum flows occur during the hotter seasons, with values ranging from 30 m^3s^{-1} (early Spring) to 2.0 m^3s^{-1} (late Summer).

3.3 Current and salinity measurements

Vertical profiles of salinity and current velocity were sampled near the mouth of the channel (station A - 40°38.66'N, 8°44.91'W) and near the channel's head (station B - 40°41.29'N, 8°39.03'W) (see Figure 3.1). At both stations, the measurements were made in an anchor station placed in the middle of the channel. In these two locations, the cross-section has a regular geometry and the salinity differences between the two channel's sides are always less than 2 psu. Therefore, it seems to be fair the assumption of a laterally homogeneous channel. At station A, two surveys were performed during a neap and the following spring tide (February 2002). At station B, four surveys were performed, one for each year season, during neap tide periods. The depths of stations A and B (during high tide) are 25 and 6.5 m, respectively. The main tidal and river flow characteristics for the sampled periods are resumed in Table 3.1.

Table 3.1: Resume of tidal and river discharge conditions during the survey periods.

Date	River flow [m^3s^{-1}]	Tide	Tidal range [m]
21/02/2002	-	neap	1.0
28/02/2002	-	spring	3.0
15/01/2004	58.0	neap	1.7
16/06/2004	11.2	neap	2.0
27/08/2004	3.0	neap	1.8
03/12/2004	5.0	neap	1.6

The station A measurements were taken during one tidal cycle in each survey and were performed by the Hydrographic Institute of the Portuguese Navy. The instruments used were an ADCP for the current velocity measurements and a CTD for the salinity measurements. The ADCP is a Workhorse Sentinel (RD Instruments) with a frequency of 614.4 Khz. This instrument measures current velocity in a range from 0 to 5 ms^{-1} with a resolution and an accuracy of 0.001 ms^{-1} and 0.25% of the water velocity relative to the ADCP, respectively. The CTD used is an Idronaut model 316. This instrument measures water temperature in a range from -3 to 50 °C with a resolution and an accuracy of 0.005 and 0.003 °C, respectively. The conductivity is measured from 0 to 64 mS/cm with a resolution and accuracy of 0.001 and 0.003 mS/cm. The salinity is calculated from the water temperature and conductivity data using the Practical Salinity Scale 1978 (PSS78). The station B measurements were taken during two consecutive tidal cycles, being used for the salinity measurements a SAIV A/S mini STD model SD204 and for the current velocity a Valeport current meter model 105. The STD measures water temperature using a Thermistor that works in a range from -2 to 40°C with an accuracy of +/- 0.01°C. The water pressure is measured using a Piezoresistive sensor with an accuracy of +/- 0.02% of the depth (500 m) and for the conductivity the instrument uses an Inductive cell working in a range of 0 to 70 mS/cm with an accuracy of +/- 0.02 mS/cm. The salinity is calculated from the conductivity, water temperature and water pressure in a range from 0 to 40 ppt with an accuracy of 0.02 ppt. The current meter has a High Impact Styrene Impeller to measure the current speed in a range of 0.1 to 5 ms^{-1} with an accuracy of ±2.5% of reading above 0.5 ms^{-1} and

± 0.01 ms^{-1} below 0.5 ms^{-1}. The current direction is measured using a flux gate compass with a range from 0-360° with a resolution of 0.5°.

River flow values concurrent with station B surveys were estimated. Measurements of current speed were obtained several km upstream from station B, 3 hours after the low tide hour predicted for the lagoon's mouth. This procedure guarantees that the measurements of current speed were made outside the region of tidal flood influence. The current velocity data were collected using the Valeport current meter model 105 previously referred. In order to compute the flow, the river section was divided in twenty four 2 m segments and the current velocity and the water depth measured for each segment. The current velocity was sampled at 60% of the water column following a standard procedure. The total river flow was obtained adding all individual segment results.

From the current velocity intensity and the direction original data, the current velocity was calculated along the main flow direction. The measurements were performed at lunar hourly intervals, for a total of 13 (station A surveys) and 25 sampling times (station B surveys). Following a standard procedure, the main direction velocity component (V-component) and the salinity profiles were combined into a simultaneous lunar hourly measurements data set with constant depth intervals of 0.5 (station A) and 0.2 m (station B), respectively. The sampling depth of each measurement was reduced to the non-dimensional depth [$Z = z/h(t)$], taking into account the local water depth [$h(t)$], to minimize the sampling water depth variations during the tidal cycle [Kjerfve, 1975]. Down the water column, the measurements were interpolated from surface to bottom, in depth intervals of $Z/10$. The surface and the bottom values were assigned one-half of the others when averaging over depth. For the station B measurements, were considered two tidal cycles of 12.41 h (the M_2 period) in the time sequence and for the first and the last of the samples of each tidal cycle were assigned one-half the weight of the others when averaging over time.The possible errors in the computation of the salt transport were obtained using the methodology followed by Dyer [1974]; Miranda et al. [2005] by re-running the programmes using the bands of sensor precision of the equipment used.

3.4 Salt transport and vertical stability

3.4.1 Salt transport theory

The formulation used for the instantaneous advective mass transport of salt per unit width of a section, normal to the longitudinal flow of the estuarine channel, is equal to

$$M_s = \int_0^h \rho V S \, dz = \overline{\rho V S} . h \tag{3.1}$$

where ρ is the density, V and S are the longitudinal velocity component and salinity, respectively. The upper bar denote averaging over the total depth of the water column, h. In the International System of Units (SI), the salt transport is given in kgm^{-1}s^{-1}.

The non-tidal salt transport (T_s) over one or more tidal cycles (T) is given by

$$T_s = \frac{1}{T}\int_0^T M_s dt = \overline{\rho} < \overline{VSh} > \tag{3.2}$$

where the mean density $\overline{\rho}$ is assumed to be constant and the angle brackets denote averaging over one or more tidal cycles. The time interval T is a multiple integer of the tidal period.

The time-averages of depth-averages (residual values) of current velocity and salinity are given by

$$< \overline{V} >= \frac{1}{T}\int_0^T \left[\frac{1}{h}\int_0^h V(x,z,t)dz\right]dt = \frac{1}{T}\int_0^h \overline{V}dt \tag{3.3}$$

$$< \overline{S} >= \frac{1}{T}\int_0^T \left[\frac{1}{h}\int_0^h S(x,z,t)dz\right]dt = \frac{1}{T}\int_0^h \overline{S}dt \tag{3.4}$$

In the case of a tidal flow, only a part of the transport is described by the product of the tidal and depth averages of the longitudinal component of the velocity (V-velocity) and salinity. As previously shown, various correlations between the tidally fluctuating salinity and velocity can be, generally, identified with a particular physical process [Bowden, 1963; Fischer, 1976; Hunkins, 1981; Kjerfve, 1986; Miranda and Castro Filho, 1996; Dyer, 1997]. Turbulent fluctuations, which have time scales smaller than 1 minute, were not measured since only time scales of minutes or longer are of interest for estuaries [Hunkins, 1981]. The correlations between fluctuating salinity and velocity at a given point may be obtained through the decomposition of the instantaneous salinity and velocity profiles into mean, tidal, steady and deviation terms. For a laterally homogeneous estuary or when the salt transport is calculated per unit width of a section perpendicular to the mean flow at time t, these profiles may be written as,

$$V(x,z,t) = V_a(x) + V_t(x,t) + V_s(x,z) + V'(x,z,t) \tag{3.5}$$

$$S(x,z,t) = S_a(x) + S_t(x,t) + S_s(x,z) + S'(x,z,t) \tag{3.6}$$

where the mean component $V_a = < \overline{V} >$, the tidal (barotropic) component $V_t = \overline{V} - V_a$, the steady (steady-state baroclinic component of the vertical circulation) component $V_s = < V > -V_a$, and the deviation component $V' = V - V_a - V_t - V_s$. Similar expressions are valid in the S_a, S_t, S_s and S' computation.

The local depth $h(x,t)$ at the anchor station varies with the tidal height and may be decomposed into two components [Miranda and Castro Filho, 1996],

$$h(x,t) = h_a + h_t(x,t) \tag{3.7}$$

where $h_a = < h >$ is the time-average water depth and $h_t(x,t)$ is the tidal height.

Introducing Equations (3.5), (3.6) and (3.7) into Equation (3.2), the advective salt transport under steady-state conditions may be decomposed into 32 terms [Miranda and Castro Filho, 1996]. Many

of these terms vanish or may be neglected upon forming depth and time averages [Bowden, 1963; Fischer, 1976; Hunkins, 1981; Miranda and Castro Filho, 1996; Dyer, 1997] since, by definition, $< V_t > = \overline{V}_s = < \overline{V'} > = \overline{V'} = 0$, and similarly for salinity. Only the product of similar V and S components are considered. Other terms which have no physical reason, since no expected correlations between steady, tidal and deviation components exists, are neglected. This leaves seven terms and the total salt transport, per unit width, during a tidal cycle is described by,

$$\begin{aligned} T_s &= \overline{\rho}[[\underbrace{V_a h_a}_{(a)} + \underbrace{< h_t V_t >}_{(b)}]S_a + \underbrace{h_a < V_t S_t >}_{(c)} + \underbrace{h_a \overline{V_s S_s}}_{(d)} \\ &+ \underbrace{h_a < \overline{V' S'} >}_{(e)} + \underbrace{< V_t S_t h_t >}_{(f)} + \underbrace{V_a < S_t h_t >}_{(g)}] \end{aligned} \tag{3.8}$$

The first two terms of Equation 3.8 represent the seaward salt advection by the mean current and Stokes wave transport. This two terms ((a) and (b)) taken together give the transport of mean salinity by freshwater discharge. This process tends to turn the estuary clear of salt and sharpen the frontal gradient between the river and ocean [Hunkins, 1981]. The remaining terms are considered to represent landward dispersion of salt through mixing by various processes, decreasing the frontal gradient. Only term (d), the correlation of tidal salinity and current, may be either dispersive or in some cases it may act in the same direction as (a) and (b), increasing the frontal gradient [Hunkins, 1981]. Several authors related these terms to certain physical mechanisms which are listed in Table 3.2 [Bowden, 1963; Fischer, 1976; Hunkins, 1981; Kjerfve, 1986; Miranda and Castro Filho, 1996; Dyer, 1997].

Table 3.2: Physical processes related to the terms of Equation 3.8

Term	Physical processes
(a)	Freshwater discharge or residual velocity
(b)	Stokes drift or progressive tidal wave transport
(c)	Topographic trapping
(d)	Gravitational circulation, bathymetric tidal pumping and steady wind effect
(e)	Tidal shear and unsteady wind effect
(f)	Tide dispersion via triple correlation
(g)	Net advection of cross correlation between salt and tide

Under steady conditions, there is no net transport and the sum of the right hand side terms of Equation 3.8 should be zero. Equations (3.2) and (3.8) are distinct mathematical expressions of the same quantity. Therefore, in order to check the computational procedure and if the neglected terms are in fact small, a comparison of the net salt transport results computed using both equations will be used.

3.4.2 Water column stability

Here, the water column stability during a tidal cycle is investigated through the determination of the Richardson number. Due to some difficulties on measuring precisely the gradients used to compute

this number, it can be defined the layer Richardson number [Dyer, 1997]. It is given by,

$$Ri_L = \frac{gh\triangle\rho}{\overline{U^2}\overline{\rho}} \tag{3.9}$$

where, $h = h(t)$ is the local depth, $\triangle\rho$ is the difference between the seabed and surface density and $\overline{U} = \overline{U}(t)$ is the depth averaged velocity. Dyer [1982]; Dyer and New [1986] defined $Ri_L = 20$ as the limit below which the turbulent mixing occurs closer to the halocline in partially mixed estuaries.

If $Ri_L > 20$, mixing is small. When this value is smaller than 20 the bottom turbulence increases, and the stratification decreases. If $Ri_L < 2$ the turbulence becomes isotropic and the mixing is fully developed [Dyer, 1997]. Using this range ($2 < Ri_L < 20$) as a simplified mixing criterium, it is possible to evaluate the spatial and temporal variation of the vertical stability of the water column. This method was used by Bérgamo [2000] and Mantovanelli [1999] to study the gravitational stability at anchor stations.

3.5 Results and discussion

3.5.1 Currents, salinity results

Figures 3.2 and 3.3 show the temporal evolution of the salinity and longitudinal velocity profiles for the surveys performed. Figures 3.2a and 3.2b reveal almost no stratification. The lower salinity values appear near low tide. During the February 21 survey, the water column is always well mixed except in the two hours before and after the low water when the differences between the surface and bottom salinity is 2.5 psu. Near the mouth of the channel, the higher velocities are reached during ebb, with values of -1.0 and -2.0 ms^{-1} as shown in Figures 3.3a and 3.3b.

The profiles of non-tidal velocity and salinity are shown in Figures 3.4 and 3.5. Station A results reveal almost no gravitational circulation, especially during the second survey (February 28^{th}). The difference between surface and bottom salinity is lower than 1 psu (in both surveys) (figures a and b). The non-tidal velocity is seaward along almost all the water column. Near the surface, the velocity maximum is -0.24 and -0.17 ms^{-1} during the first and second survey, respectively. During the first survey, an inversion of the non-tidal velocity is visible close to the bottom (Z=-0.7). The Layer Richardson number present values lower than 2 and increasing to 20 during the time interval of 1 hour before and after low tide, revealing a well mixed water column. For the February 28 survey, the Layer Richardson number present values lower than 20 during all the tidal cycle, which mean that no stratification is observed.

From station B results several features should be addressed. This anchor station was placed closed to the mouth of the Vouga River, and therefore the circulation is strongly influenced not only by the tidal flow but also by the freshwater inflow. Furthermore, this location is narrow (approximately 60 m wide) and relatively shallow (maximum of 6.5 m depth during the high water in this location). The tidal and freshwater inflow are resumed in Table 3.1. The Spring and Summer results appear to

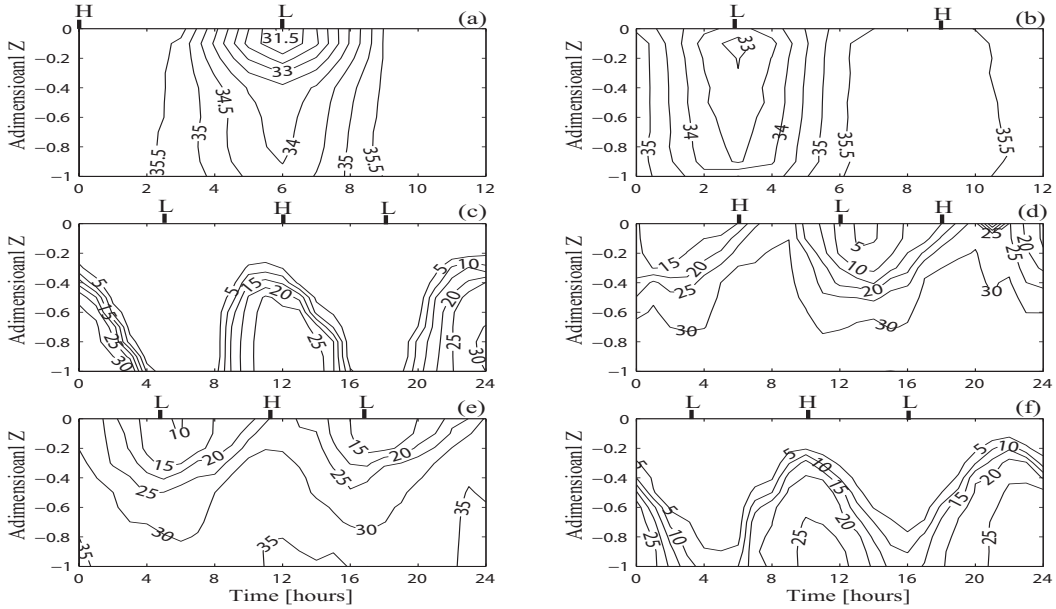

Figure 3.2: Contour figures of salinity as a function of the adimensional depth (Z) and time for all survey periods. H and L indicates the local high and low water. (a) 21/02/2002 (station A); (b) 28/02/2002 (station A); (c) 15/01/2004 (station B); (d) 16/06/2004 (station B); (e) 27/08/2004 (station B); (f) 03/12/2004 (station B).

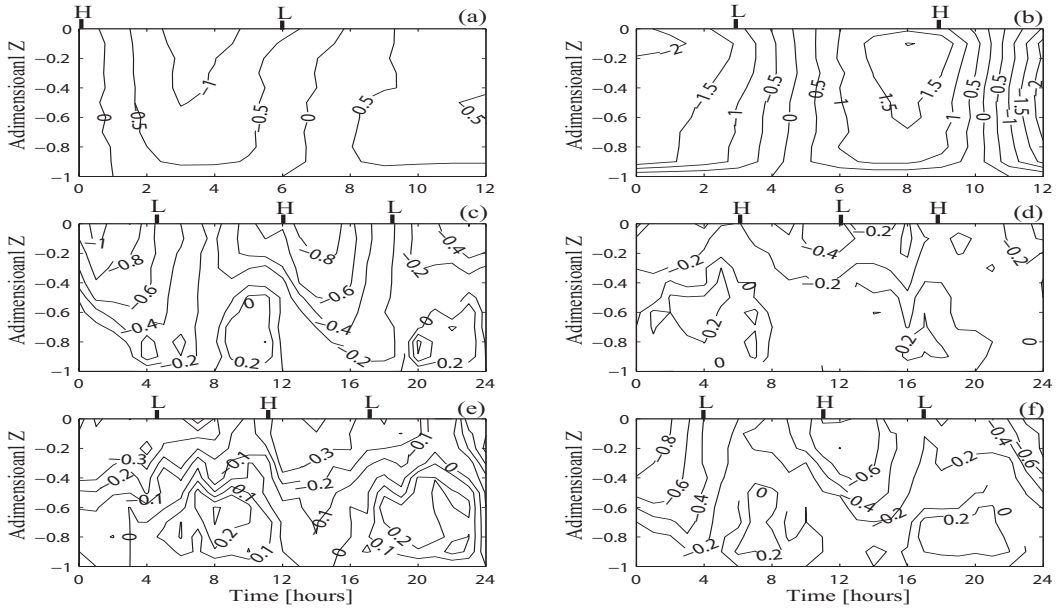

Figure 3.3: Contour figures of longitudinal velocity component as a function of the adimensional depth (Z) and time for all survey periods. H and L indicates the local high and low water. (a) 21/02/2002 (station A); (b) 28/02/2002 (station A); (c) 15/01/2004 (station B); (d) 16/06/2004 (station B); (e) 27/08/2004 (station B); (f) 03/12/2004 (station B).

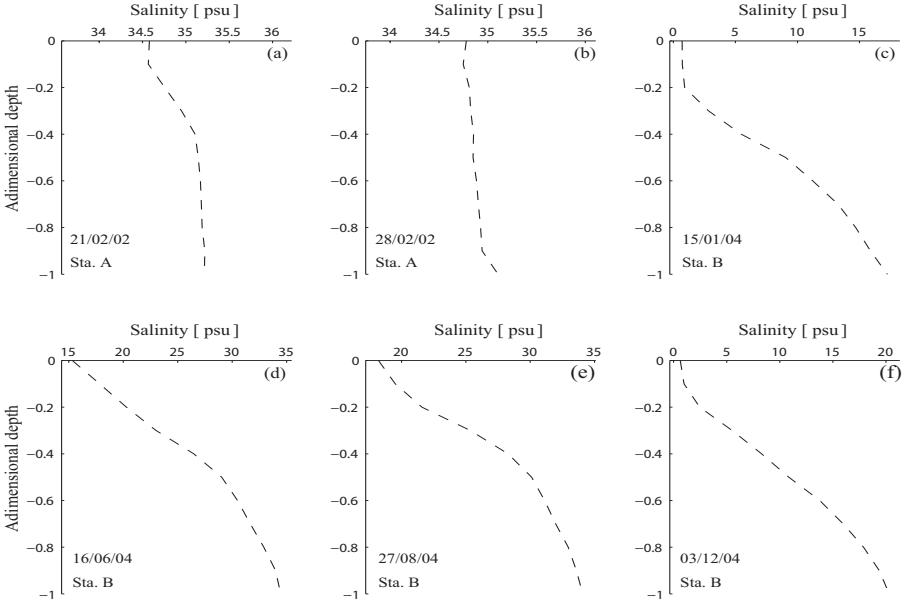

Figure 3.4: Profiles of non-tidal salinity at stations A and B.

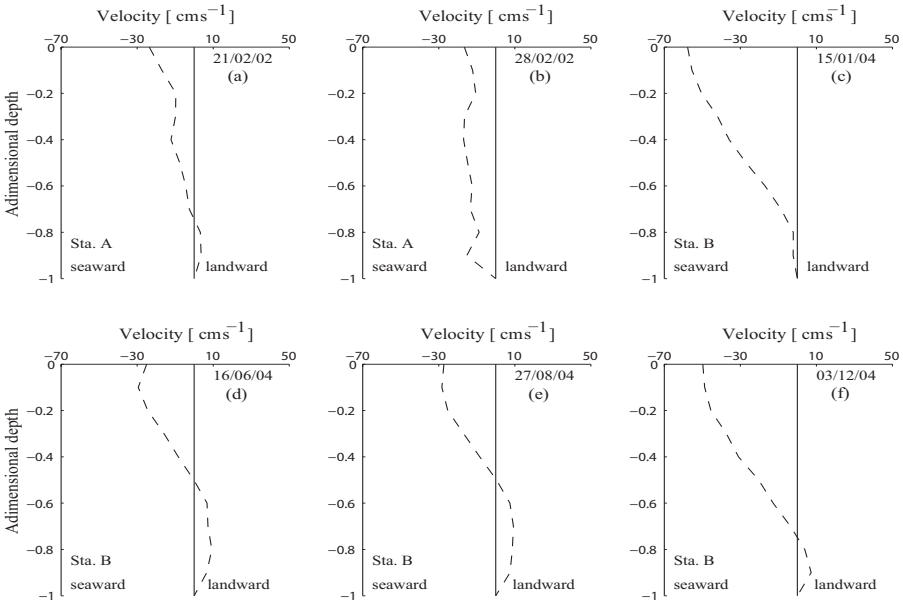

Figure 3.5: Profiles of non-tidal velocity at stations A and B.

be influenced by the existence of a small dam 2 km upstream of the station B. This dam is builded during the dryer seasons to protect the low-land of Baixo-Vouga (agricultural fields) and a paper mill residual waters station of the salinity intrusion, being opened during a short period of time when the local low tide is reached.

During the January and December surveys, the estimated freshwater inflow was 58 and 5 m^3s^{-1}, respectively. During this survey periods, the salinity and velocity evolution (Figures 3.2c, 3.2f, 3.3c

and 3.3f) reveal that a stratification/destratification event takes place. The stratification increases during the flood period, reaching its maximum one hour before the high water. Stratification decreases during the ebb until the local low water hour. The entire water column is filled with freshwater propagating from the river during the beginning of the flood period. During the December survey, when the discharge from the river is lower, the water column present values of 5 psu during the beginning of the flood. The vertical lunar hourly profiles of the longitudinal velocity indicates an asymmetry between flood ($\vec{V} > 0$) and ebb ($\vec{V} < 0$) currents. The ebb currents are higher than the flood currents, reaching maximums of -1.0 and 0.3 ms^{-1} during the January survey and -0.8 and 0.3 ms^{-1} during the December survey, respectively. A similar current velocity asymmetry was observed by Miranda et al. [2004] in studying the dynamics of a tropical estuary, the Curimataú River, NE Brazil. The non-tidal current profiles show that the current is seaward through all the water column (Figure 3.5c) being visible a inversion near the bottom (Z = -0.8) during the December survey (Figure 3.5f). The surface maximums are -0.58 and -0.5 ms^{-1} during January and December, respectively. The non-tidal salinity profiles present values close to 0 psu near the surface increasing in depth to values of 17.2 (January) and 20.3 psu (December).

The stability of the water column is evaluated using the Layer Richardson number. In January (Figure 3.6c), this adimensional number present values lower than 20 during the low tide, revealing a reduction of the stratification and consequently a mixing increase. The maximum values are reached one hour before high water when the stratification is fully developed. For December (Figure 3.6f) this number present values higher than 20, revealing the high stability of the water column, except during the low tide hours, when a stratification reduction occurs and the turbulent mixing increases.

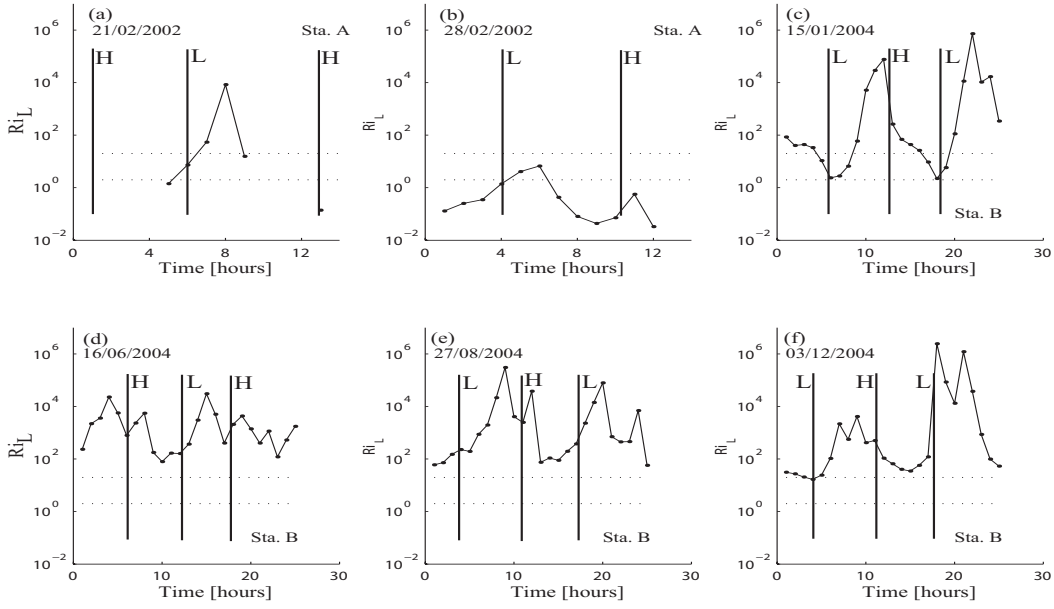

Figure 3.6: Temporal variation of the layer Richardson number. The dotted lines (Ri_L equal to 2 and 20) are the limits of weak vertical stability.

During the Spring and Summer campaigns, the temporal evolution of the salinity reveal a stratified water column during all the sampling period. Although, the estimated freshwater inflow of 11.2 and 3.0 m^3s^{-1} during the June and August campaigns be higher and of the same order than the December value, the water column is saltier than in the winter. This is due to the dam located 2 km upstream which is open only during a short period of time. In fact, the freshwater is "stored" upstream of the dam and during the local low water hour the structure is open and during a limited period of time it discharge freshwater into the channel. As it can be seen in Figure 3.2d and 3.2e is after the low water that is reached the minimum values of salinity, 5 and 10 psu, respectively. Close to the channel's bed, the salinity is always higher than 30 psu revealing the presence of ocean water. The current velocity evolution (Figures 3.3d and 3.3e) show low velocity values, ranging from -0.4 and 0.2 ms^{-1} during June and -0.3 and 0.2 ms^{-1} during the August campaign. Once more, the asymmetry between ebb and flood currents is observed. The vertical profiles of non-tidal velocity and salinity confirm the results presented before. The ebb currents are higher than the flood ones with maximums surface values of -0.29 (Figure 3.5d) and -0.27 ms^{-1} (Figure 3.5e). It is observed an inversion of the current velocity near the half water column (Z = -0.6) (ebb to flood currents) with maximums of 0.093 (Figure 3.5d) and 0.072 ms^{-1} (Figure 3.5e) for the June and August surveys, respectively. The salinity profiles show brackish surface values with maximums of 15.3 and 18.2 psu during the June and August surveys, respectively. These values increase toward the bottom to values higher than 34 psu. During these two campaigns, the Layer Richardson number present values always higher than 20, revealing a highly stable water column (see Figure 3.6d and 3.6e for reference).

3.5.2 Salt transport results

The salt transport method presented in Section 3.4.1 has been applied to compute the relative contribution of the individual terms of Equation 3.8, in systems with several degrees of stratification, and the results are reported in several studies cited previously. The variation of the relative contribution of the salt transport terms to the net upstream transport, during neap and spring tides, have been studied by Lewis and Lewis [1983] in their study in the Tees Estuary.

The net salt transport and its advective and dispersive components obtained from the application of this methodology for stations A and B are show in Table 3.3. As a check on the use of Equation 3.8, to evaluate the computational method, a calculation was made using Equation 3.2 and the results are compared. There was agreement between the two calculations within 12% for almost all the survey periods. The exception is the January results when the results are significatively different. This result may be due to the large river flow (58 m^3s^{-1}) which combined with the tidal propagation address to that location some salt wedge characteristics. This 12% value was considered acceptable by Hunkins [1981] and Miranda and Castro Filho [1996]. The agreement between both calculations confirm that the terms omitted to obtain Equation 3.8 were in fact small.

According to the results, the main contribution to the salt transport is from term (a). The sum of term (a) and (b), which represent salt transport due to the freshwater discharge, is negative for all

surveys indicating a seaward (advective) salt transport due to the non-tidal velocity induced by the river discharge. At station A, term (a) almost double (-59.33±0.51 to -105.48±0.61 $kgm^{-1}s^{-1}$) from the neap tide period of February 21 to the following spring tide. At station B, this term is higher during the January and December surveys than during the June and August surveys, presenting a maximum of -12.61±0.41 during the January survey and a minimum of -7.96±0.57 $kgm^{-1}s^{-1}$ during the August survey.

Table 3.3: Salt transport in the Espinheiro channel [$kgm^{-1}s^{-1}$].

Station	A	A	B	B	B	B
Date	21/02/2002	28/02/2002	15/01/2004	16/06/2004	27/08/2004	03/12/2004
(a)	-59.33±0.51	-105.48±0.61	-12.61±0.41	-8.08±0.52	-7.96±0.57	-11.26±0.39
(b)	2.95±0.10	23.87±0.80	0.43±0.01	0.46±0.01	0.94±0.06	0.33±0.01
(c)	5.53±0.31	14.42±0.82	1.81±0.04	-0.03±0.02	-0.12±0.01	0.27±0.01
(d)	0.35±0.01	0.04±0.01	6.78±0.14	4.00±0.20	3.48±0.17	6.85±0.18
(e)	0.34±0.01	0.44±0.01	3.97±0.05	0.54±0.03	0.22±0.02	1.51±0.02
(f)	0.00	-0.06±0.001	-0.033±0.001	0.00	0.00	-0.030±0.002
(g)	-0.02±0.001	-0.09±0.005	-0.98±0.03	-0.11±0.01	-0.12±0.01	-0.030±0.002
$\sum(a)-(g)$	-50.18±1.00	-66.86±1.21	-0.67±0.20	-3.22±0.33	-3.56±0.38	-2.82±0.20
Equation 2	-50.17±1.00	-66.88±1.21	-0.16±0.16	-3.51±0.34	-3.71±0.38	-2.58±0.20

Term (b) is positive for all the surveys. Having a positive sign it represent a landward (dispersive) tidal wave transport of salt contribution. In this channel, as in many others estuaries and tidal channels, there is a progressive wave component, which means that the high water occurs at maximum flood and low water at maximum ebb. So, the water is carried out up estuary and its mean salt content with it. This is the Stokes Drift associated with a finite-amplitude tidal wave propagating back and forth into the channel. At station A, this term is higher during the spring tide survey than in the neap survey, 23.87±0.80 and 2.95±0.10 $kgm^{-1}s^{-1}$, respectively. At station B this term is close to zero, presenting a maximum and minimum value of 0.94±0.06 and 0.43±0.01 $kgm^{-1}s^{-1}$ during the August and January survey, respectively. These values may be explained by the tidal wave characteristics in this region of the channel. Station B is located near the channel's head (close to the river's mouth) and as Dias et al. [2000] found in their work, as the tidal wave propagates from deeper toward shallow areas of the lagoon, due to the shore's reflections, the wave characteristics move from progressive to standing wave. In the case of a standing wave, tidal elevation and tidal velocity would have a phase difference of 90°, so this term, which is averaged over a tidal cycle would be zero. This does not happens, because at this point, the tidal wave has a progressive and a standing component. This feature is visible not only due to the location of the survey point, which is placed on a shallow area, but also due to the presence of a dam 2 km upstream. Therefore, the Stokes wave transport presents positive values (close to zero), which mean a tidal wave transport up the channel.

The tidal correlation term (c) switches sign from the colder to the warmer season surveys. During the January and December surveys, this term (c) is positive (dispersive) contributing to carry salt into the channel. The opposite, a seaward contribution to the salt transport, occur during the June and August surveys. At station A, this value is maximum during the February 28 survey, (14.42±0.82 $kgm^{-1}s^{-1}$). Hunkins [1981] refer that in an idealized well mixed estuary the phase difference be-

tween V_t and S_t would be 90°, since the maximum salinity is reached at the end of the flood tide, and therefore the contribution of this term to the net transport would be zero since their integral in quadrature is zero. Fischer et al. [1979] suggested that trapping of water by topographic irregularities could lead to a phase difference lower than 90°. That is, in a system like Espinheiro channel with a major channel and several side branches, the tidal elevation and velocities are not in phase in the main channel. The momentum of the flow in the main channel causes the current to continue to flow against an opposing pressure gradient. On the other hand, the side channel has less momentum and the current direction changes when the water level begins to drop. At this stage, the water in the side channel return into the main stream in a different tidal hour, leading to a phase difference between S_t and V_t lower than 90°. This can explain the positive sign of the colder seasons surveys, but not the other results. If the phase difference is higher than 90°, as observed by Miranda and Castro Filho [1996] and Hunkins [1981] term (c) will be negative. This can be observed in two-layered estuaries, where the longitudinal salinity gradients are lower in the bottom layer than in the upper layer of the estuary. So, the tidal salinity oscillation is reduced in the bottom layer. The tidal current near the bottom leads the tidal current in the upper layer on account of friction effects. Then, the tide turn from ebb to flood earlier in the bottom layer. The depth averaged velocity V_t will be advanced an amount intermediate between the surface and bottom values. In opposition, the depth averaged salinity will be little influenced by the bottom layer salinity oscillation and will follow the surface salinity values. This makes the phase difference higher than 90° with the consequent negative term (c) values.

Term (d) which represents the gravitational circulation, is positive, that is directly landward (dispersive). At station A, this term is residual, presenting values of 0.35±0.01 (February 21) and 0.04±0.01 $\mathrm{kgm^{-1}s^{-1}}$ (February 28). These values confirm the analysis made in Section 3.5.1 where the non-tidal velocity and salinity figures reveal almost no gravitational circulation. At station B, this term (d) is one of the most important in driving the salt transport. A pronounced gravitational circulation is observed in all survey periods as depicted in Figures 3.4 and 3.5. This term is higher during the January and December surveys, presenting a maximum of 6.85±0.18 $\mathrm{kgm^{-1}s^{-1}}$ reached during the December survey. The minimum value is found during the August survey with a value of 3.48±0.17 $\mathrm{kgm^{-1}s^{-1}}$. At station B, this term increases by at least one order of magnitude when compared to station A results. In a well mixed estuary, high freshwater inflow may flush out the salt almost completely, but in a partially mixed estuary when the freshwater discharge increase, the compensating bottom current also increases carrying salt up estuary, turning the circulation results more vigorous.

Term (e), which is associated with tidal shear or unsteady wind effect, is not relevant for station A salt transport results. In fact, in this station, the results reveal marginally small values for terms (e), (f) and (g) when compared to the other terms. However, at station B, the results show that this term has the same order of magnitude as the gravitational circulation term for the colder seasons surveys (January and December), presenting values of 3.79±0.05 (January) and 1.51±0.02 $\mathrm{kgm^{-1}s^{-1}}$ (December). This term is positive for all the surveys, being consequently dispersive. Terms (f) and

(g) present residual values for all the survey periods. These terms are dependent of the tidal amplitude and their small values are due to the moderate tidal amplitude of the forcing tidal wave.

In the absence of sampling errors, under steady conditions, the sum of terms (a) to (g) in Table 3.3 would be zero. In all the surveys this sum was not zero but negative. In fact, the highest disagreement between the sum of all terms and the value calculated using Equation 3.2 occur during the January survey. This disagreement may be explained but the high river runoff observed during that survey. This fact conjugated with a moderate tide address to this fixed point salt wedge characteristics, resulting in a high-stratified location. Apparently, in this case the major contribution to the salt transport is the entrainment process, i.e. the upward flux of salt with little or no horizontal diffusion. The calculation method used in this work does not capture this process, since it is not included into Equation 3.8. All the results reveal an imbalance in the net advective salt budget and during all the survey periods the channel was exporting salt. This imbalance may be due to a wrong previous assumption on the laterally characteristics (homogeneity) of the survey locations. Another fact that can influence the results is that this channel is located in the very complex central area of the Ria de Aveiro lagoon, where the study area has an enormous amount of side channels discharging into the main one, influencing the circulation characteristics. The results may be strongly influenced by the wind conditions. Local winds tend to increase the gravitational circulation, leading to positive dispersion values. As Hunkins [1981] refer in his work the loss of salt by the channel is probably influenced by large-scale wind gradients over all the lagoon and adjacent continental shelf which drives salt transport toward the ocean. Such wind-driven effect is not captured by the terms (a) and (b) and a much longer time series is needed to determined its behavior.

3.6 Conclusions

The two locations studied in this work represent sensible and important areas of the Espinheiro channel. Station A, located near the channel's mouth is important because the channel has only a connection between its interior and the adjacent ocean and the channel's dynamics is strongly influenced by the tidal flow. Station B, located near the channel's head, close to Rio Vouga's mouth, is located in a ecological important area, where the existence of a paper industry turn important the quantification of the amount of conservative particles, like salinity or others, that enters into the channel with the fluvial flow.

It is found that near the mouth of the channel, at station A, the main contributions to the transport of salt are the transport due to the freshwater discharge (terms (a) and (b)) and the tidal correlation term (c). At this location, the net salt transport accounts more than 80% of the downstream salt transport component driven by the freshwater discharge. At station B, near the channel's head, the major contributions to the salt transport are the transport due to the freshwater discharge and the gravitational circulation. The tidal shear term (e) is found to be, during the January and December surveys, of the same order of magnitude of the gravitational circulation term, but one order of magnitude lower during the other two surveys. The net salt transport accounts, on average, 31% for the salt flushed by

the river. In regions so close to the river's mouth as the one studied here (station B), the gravitational circulation plays a major contribution to the salt transport, i.e. in regions where the river inflow plays a major role, a compensating bottom current is originated near the bottom to carry salt up estuary, balancing the salt flushed out by the river.

The presence of a small dam 2 km upstream of station B, from May to October, influences the results. In fact, this dam is open just for a short period of time when the local low tide is reached and it functions as a barrier to the tidal evolution further upstream. Thus, the tidal wave, which is a progressive wave, gain in this region some standing wave characteristics and at this point, the mixing increases and the estuary becomes well mixed, turning the phase difference between V_t and S_t close to 90°. This changing in the characteristics of the tidal wave acts to reduce the tidal correlation to values close to zero.

In the absence of sampling errors and assuming a steady condition, the sum of all terms in Equation 3.8 would be zero. This does not happens and during all surveys a salt imbalance is found meaning that the estuary is in fact exporting salt. The rates are presented in Table 3.3, indicating a seaward salt transport.

In spite these kind of short term surveys, during one or two tidal cycles, are too small to give information about meteorological effect influencing salt transport, they can produce valuable results about processes on tidal and subtidal time scales. Sampling strategies like the one followed in the data acquisition, with just one station in the middle of the channel, without assessing the results against the tidal strength (neap and spring periods), changes in the bathymetry or magnitude of the longitudinal density gradient, could lead to a salt transport value that ends up as a number only meaningful for the specific conditions under which the measurements where made [Jay et al., 1997]. Nevertheless, this study must be understood as a first step in the understanding of the circulation of a barely studied area. Due to the lack of observational program, the total salt budget of the channel can only be studied using three-dimensional numerical models which allows the coverage of all channel during much higher time scales.

Chapter 4

The numerical model

4.1 Introduction

The numerical model used in this work is Mohid, a three-dimensional baroclinic model under development at the Instituto Superior Técnico (Universidade Técnica de Lisboa) [Santos, 1995; Martins et al., 2001]. In its initial versions [Santos, 1995], a finite difference approach was implemented in the discretization. In the present, a finite volume discretization approach has been implemented [Martins et al., 2001], allowing the use of a generic vertical coordinate. Mohid has been applied to several different coastal and estuarine areas and has shown its ability to simulate complex features of the flows. Along the Portuguese coast, several environment have been studied, from river mouths (Douro and Mondego) to coastal lagoons (Ria de Aveiro [Trancoso et al., 2005; Vaz et al., 2005a] and Ria Formosa) and broader estuaries (Tagus [Braunschweig et al., 2003] and Sado estuaries [Martins et al., 2001]). Moreover, the model has been implemented to simulate the Galician Rias hydrodynamics (Ria de Vigo [Taboada et al., 1998; Montero, 1999], Ria de Pontevedra [Villarreal et al., 2002]). Far from the Atlantic coast of the Iberian Peninsula, some European estuaries have been studied (Western Scheltd, Holland, and Gironde, France, [Cancino and Neves, 1999] and Hellingford [Leitão, 1996]) as well as some coastal estuaries in Brazil (Santos and Fortaleza). Regarding the open sea, Mohid has been applied to the north-east Atlantic region where some processes including the Portuguese coastal current [Coelho et al., 1994, 2001], the slope current along the shelf [Neves et al., 1999] and the generation of internal tides [Neves et al., 1998] have been studied, and also to the Mediterranean Sea to simulate the seasonal cycle [Taboada, 1999] or the circulation in the Alboran Sea [Santos, 1995].

4.2 The numerical model equations

Mohid solves the three-dimensional incompressible primitive equations. Hydrostatic equilibrium is assumed as well as the Boussinesq and Reynolds approximations. All the equations below have been derived taken into account these approximations. A detailed derivation of the model equations

was presented in several studies [Santos, 1995; Martins et al., 2001; Leitão, 2003]. The hydrostatic approximation is assumed with:

$$\frac{\partial z}{\partial p} = -\rho g \tag{4.1}$$

where g is gravity and ρ is density. If the atmospheric pressure p_{atm} is subtracted from p, and density ρ is divided into a constant reference density ρ_0 and a deviation component ρ', after integrating from the free surface η to the depth z where pressure is calculated, it is obtained:

$$p(z) = p_{atm} + g\rho(\eta - z) + g\int_z \eta\rho' dz \tag{4.2}$$

This equation relates pressure at any depth with the atmospheric pressure at the sea surface, the sea level and the anomalous pressure integrated between the level and the surface. By using the Boussinesq approximation - where the density variation are fairly small ($\sim 3\%$), to a first approximation their effect on the fluid's mass can be neglected but must be retained on the weight, and therefore the changes in the horizontal acceleration due to the fluid's mass variation resulting from the density is negligible - the horizontal pressure gradient in the x_i directions can be divided into:

$$\frac{\partial p}{\partial x_i} = \frac{\partial p_{atm}}{\partial x_i} - g\rho_0\frac{\partial \eta}{\partial x_i} - g\int_z \eta\frac{\partial \rho'}{\partial x_i} dz \tag{4.3}$$

The total pressure gradient is the sum of the gradients of the atmospheric pressure, the sea surface elevation (barotropic pressure gradient) and the density distribution (baroclinic pressure gradient). This decomposition is substituted in the 3D incompressible primitive equations and yields to the mass momentum equation:

$$\begin{aligned}\frac{\partial u_i}{\partial t} + \frac{\partial (u_i u_j)}{\partial x_j} &= -\frac{1}{\rho_0}\frac{\partial p_{atm}}{\partial x_i} - g\frac{\rho(\eta)}{\rho_0}\frac{\partial \eta}{\partial x_i} - \frac{g}{\rho_0}\int_{x_3}^{\eta}\frac{\partial \rho'}{\partial x_i} dx_3 \\ &+ \frac{\partial}{\partial x_j}(\upsilon\frac{\partial u_i}{\partial x_j}) - 2\varepsilon_{ijk}\Omega_j u_k\end{aligned} \tag{4.4}$$

where u_i are the velocity vector components in the Cartesian x_i directions, υ is the turbulent viscosity and p_{atm} is the atmospheric pressure. ρ is the density, ρ' is its anomaly, ρ_0 is the reference density, $\rho(\eta)$ represents the density at the free surface, g is the acceleration of gravity, t is the time, Ω is the Earth's velocity of rotation and ε is the alternate tensor.

The mass balance equation (continuity) is:

$$\frac{\partial u_i}{\partial x_i} = 0 \tag{4.5}$$

The density ρ is calculated as a function of temperature and salinity by the equation of state [Leendertse and Liu, 1978]:

$$\begin{aligned}\rho &= (5890 + 38T - 0.375T^2 + 3S)/((1779.5 + 11.25T - 0.0745T^2) - (3.8 + 0.01T)S \\ &+ 0.698(5890 + 38T - 0.375T^2 + 3S)) \end{aligned} \tag{4.6}$$

This equation is an approximation for shallow water of the most widely used UNESCO equation [UNESCO, 1981].

The vertical velocity is calculated from the continuity equation by integrating between the bottom and the depth z where u_3 is to be calculated:

$$u_3(x_3) = \frac{\partial}{\partial x_1}\int_{-h}^{x_3} u_1 dx_3 - \frac{\partial}{\partial x_2}\int_{-h}^{x_3} u_2 dx_3 \tag{4.7}$$

The free surface equation is obtained by integrating the continuity equation over the whole water column:

$$\frac{\partial \eta}{\partial t} = \frac{\partial}{\partial x_1}\int_{-h}^{\eta} u_1 dx_3 - \frac{\partial}{\partial x_2}\int_{-h}^{\eta} u_2 dx_3 \tag{4.8}$$

The model also solves a transport equation for salinity, water temperature or any other tracer:

$$\frac{\partial \alpha}{\partial t} + u_j\frac{\partial \alpha}{\partial x_j} = \frac{\partial}{\partial x_j}(K\frac{\partial \alpha}{\partial x_j}) + FP \tag{4.9}$$

where α is the transported property, K is the diffusion coefficient and FP is a possible source or sink term.

4.3 Equations discretization

4.3.1 Spatial discretization

Mohid uses a finite volume approach [Chippada et al., 1998; Martins et al., 2001] to discretize the equations. Using this approach, the discrete form of the governing equations is applied macroscopically to a cell control volume. This approach uses the conservation equations in an integral form. A general conservation law for a generic quantity ϕ with sources (and sinks) s in a control volume Ω is then written as:

$$\underbrace{\frac{\partial}{\partial t}\int_\Omega \phi d\Omega}_{time derivative} + \underbrace{\int_S \phi v.n dS}_{advection} + \underbrace{\int_\Omega s d\Omega}_{sources-sinks} = 0 \tag{4.10}$$

After discretizing this expression in a cell control volume Ω_j where ϕ_j is defined, is obtained:

$$\frac{\partial}{\partial t}(\phi_j \Omega_j) + \sum_{faces} \phi v.n.\vec{S} = Q_j \Omega_j \tag{4.11}$$

This way, the procedure for solving the equations is independent of the cell geometry. According

to Martins [2000] and Montero [1999] the cell can have any shape with only some constraints since only fluxes among cell faces are required. Therefore, it is achieved a complete separation between physical variables and geometry [Hiersch, 1980]. The geometry is updated in every time step after computing the physical variables since the volumes can vary in the course of the calculus. Moreover, the spatial coordinates are independent, and any geometry can be chosen for every dimension. Cartesian and curvilinear coordinates are used in the horizontal and in the vertical a generic vertical coordinate with different sub-domains can be used. In is study Martins et al. [2001] pointed that this generic vertical coordinate minimizes the errors of some of the classical vertical coordinates (cartesian, isopycnal, sigma). Along the vertical direction the cell vertices have only a degree of freedom, being fixed in the horizontal plane. In the horizontal, the grid is staggered in an Arakawa C manner [Arakawa and Lamb, 1977], i.e. horizontal velocities are located in the center of the cell faces and elevation, turbulent magnitudes and any tracer are placed in the element center. Also in the vertical a staggering is used, with the vertical velocity, tracers and turbulent magnitudes placed in the top and bottom faces and horizontal velocities and elevation in the center.

4.3.2 Temporal discretization: the ADI algorithm

The temporal discretization is carried out using a semi-implicit algorithm: the ADI - Alternate Direction Implicit (see Abbott and Basco [1994]). This algorithm calculates alternatively one component of horizontal velocity implicitly while the other is calculated explicitly, avoiding the computation of the internal and external modes with different time steps (mode splitting approach). The resulting equation system is tridiagonal, and can be solved using the Thomas algorithm. This allows the preservation of the stability advantages of implicit methods without increasing the computational effort and associate phase errors. Also, this method allows the use of a longer time-step. The model has two discretization schemes coded: a 4 equations with two time level per iteration, the S21 scheme [Abbott et al., 1973], and the 6 equation algorithm by Leendertse [1967] (see Equation 4.12), more convenient when modelling systems with intertidal areas, since velocities are updated every half time step. In this study, only the 6 equation scheme is used.

$$\begin{aligned} u_2^{t+1/2} \longrightarrow \eta^{t+1/2}(u_1^{t+1/2}, u_2^{t}) \longrightarrow u_1^{t+1/2} \longrightarrow u_3^{*t+1/2} \overset{GeometryUpdate}{\longrightarrow} u_3^{t+1/2} \\ \longrightarrow S^{t+1/2}, T^{t+1/2} \longrightarrow \cdots \longrightarrow u_1^{t+1} \longrightarrow \eta^{t+1}(u_1^{t+1/2}, u_2^{t+1}) \longrightarrow u_2^{t+1} \\ \longrightarrow u_3^{*t+1} \overset{GeometryUpdate}{\longrightarrow} w_3^{t+1} \longrightarrow S^{t+1}, T^{t+1} \end{aligned} \tag{4.12}$$

In this case, the ADI scheme is applied to Equation 4.5 in order to calculate the free surface elevation. Basically, all the velocity integral in one direction is substituted by a momentum conservation equation keeping, in the orthogonal direction, the velocity explicit. A full description of the discretization can be found in several studies like Martins [2000], Montero [1999], Leitão [2003] or Theias [2005].

4.4 Boundary conditions

4.4.1 Free surface

At the free surface boundary all advective fluxes across the surface are assumed null, i.e. imposing a null W vertical flux:

$$Wflux\mid_{surface}= 0 \tag{4.13}$$

Diffusive flux of momentum is imposed assuming explicitly a wind surface stress, $\vec{\tau}_W$:

$$\upsilon_3 \frac{\partial u_i}{\partial x_3} \mid_{surface}= \vec{\tau}_W, i = 1, 2 \tag{4.14}$$

where υ_3 is the vertical eddy viscosity. The wind stress is calculated according to a quadratic friction law:

$$\vec{\tau}_W = C_D \rho_a \vec{W} \mid \vec{W} \mid \tag{4.15}$$

where C_D is a drag coefficient that is a function of the wind speed, ρ_a is the air density and $\vec{W}$ is the wind speed measured 10 m above the sea surface. In this study, the wind stress was not considered.

Temperature and salinity advective fluxes are imposed null. Other fluxes of heat and freshwater are introduced as a source (or a sink) term in the transport equation 4.9

4.4.2 Bottom boundary

At the bottom, the water flux is also assumed to be null and the bottom stress is calculated using a non-slip method with a quadratic law that depends on the near bottom velocity. This condition can be expressed by:

$$\upsilon_3 \frac{\partial u_i}{\partial x_3} \mid_{bottom}= C_D u_i \sqrt{u_1^2 + u_2^2},\ i = 1,\ 2 \tag{4.16}$$

where C_D is the bottom drag coefficient, which is calculated for 2D (Equation 4.17) and 3D (Equation 4.18) flows by:

$$C_D = g n^2 H^{-1/3} \tag{4.17}$$

$$C_D = \left(\frac{\kappa}{\lg \frac{z+z_0^b}{z_0^b}} \right) \tag{4.18}$$

where g is the gravity, n is the Manning coefficient, H is the depth of the water column, κ is the von Karman constant and z_0^b is the bottom roughness length. For stability reasons, this term is calculated implicitly in the momentum equation of the bottom cell, using a procedure described in Backhaus [1983]. No salinity and temperature fluxes are considered at the bottom.

4.4.3 Lateral closed boundaries

The closed boundaries of the domain corresponds to land. A free slip condition is used to resolve this lateral boundary:

$$\frac{\partial u_1}{\partial x_2} = \frac{\partial u_2}{\partial x_1} \tag{4.19}$$

$$u_i.n_i = 0,\ i = 1,\ 2 \tag{4.20}$$

Using the finite volume approach, this conditions are implemented specifying zero water fluxes and zero momentum diffusive fluxes for the cell faces in contact with land.

4.4.4 Open boundaries

These boundaries are necessary to confine the domain to the study area. The information imposed there must (or should) guarantee that what is happen outside the study area enter in order that the solution inside the domain is not corrupted. Also, waves inside the domain should be allowed to go out. Perfect open boundary conditions does not exist, being the most suitable ones those depending on the phenomena to be modelled. Review papers by Palma and Matano [1998, 2000] compare open boundary conditions in test cases. Some different boundary conditions were introduced in Mohid [Santos, 1995; Montero, 1999; Leitão, 2003]. Flow relaxation schemes applied to several variables, like temperature, salinity and velocities are also available [Leitão, 2003].

4.4.5 Moving boundaries

Moving boundaries are closed boundaries whose positions change in time. These arises in domains with intertidal areas where some points can be covered or uncovered depending on the tidal elevation. In this case the uncovered cells must be tracked. The criterium used in Mohid is well described in Martins [2000], Martins et al. [2001], Leitão [2003] and can be found in the assessment of Mohid-2D to the Ria de Aveiro chapter.

4.5 Surface heat fluxes parameterizations

Estuaries and costal lagoons are by nature highly subject to air-water interactive processes. The relative shallowness of these areas result in a significant temporal variability (daily, monthly or seasonal) which may exceed that of open oceanic waters. Furthermore, the relative importance of the individual terms of the heat budget equation could be quite different. The water-air heat changes are influenced by five distinct processes: solar shortwave radiation, atmospheric longwave radiation, water longwave radiation, sensible and latent heat flux. In Mohid, the total heat surface flux is obtained summing the three last processes referred above. The solar end atmospheric radiation penetrating in

the water column are converted in heat. The radiation entering in the water column is parameterized as a exponential function of depth by the law proposed by Kraus [1972]:

$$I(z) = F_{sol}\left(I_1 e^{-z/\lambda_1} + I_2 e^{-z/\lambda_2}\right),\ I_2 = 1 - I_1 \tag{4.21}$$

Indices 1 and 2 refer to the long and shortwave radiation components, respectively. z is positive downward, being $z = 0$ the sea surface. Values of I_1, λ_1 and λ_2 where published by Paulson and Simpson [1977] according to the classification found in Jerlov [1968]. These coefficients depend on the type of water of the study area.

In order to quantify the incoming solar radiation in the water surface, Mohid uses the formulation found in Brock [1981] which depends on the sun height, atmospheric absorption and albedo. The formulation is given by:

$$R_s = (1 - albedo) \times QS_0 \times AT \times neb \tag{4.22}$$

where R_s is the incoming solar radiation [$\mathrm{Wm^{-2}}$], QS_0 is the Solar Constant [$\mathrm{Wm^{-2}}$], AT is the atmospheric transference, *neb* is the nebulosity (% of cloud cover). QS_0 varies with the latitude, time of the year and day hour.

The net longwave radiation R_a [$\mathrm{Wm^{-2}}$] is calculated using [Swinbank, 1963]:

$$R_a = 0.937 \times 10^{-5} \sigma (273.15 + T_a)^6 (1 + 0.17 neb^2)(1 - R_e) \tag{4.23}$$

where σ is the Stefan-Boltzman constant ($5.6697{\times}10^{-8}$ $\mathrm{Wm^{-2}K^{-4}}$) and R_e is the radiation reflected by the sea surface (%).

The infrared radiation R_{br} [$\mathrm{Wm^{-2}}$] is calculated applying the Stefan-Boltzman law:

$$R_{br} = \varepsilon \times \sigma \times (273.15 + T_w)^4 \tag{4.24}$$

here ε is the water emissivity (~ 0.97) and T_w is the water temperature [K].

The latent H_L and sensible H_s heat fluxes (in [$\mathrm{Wm^{-2}}$]) are calculated using the Dalton and Bowen laws, respectively (adopted from [Chapra, 1997]):

$$H_L = (19.0 + 0.95 U_w^2) \times (e_{s,w} - r_h \times e_{s,a}) \tag{4.25}$$

$$H_s = C_b \times (19.0 + 0.95 \times U_w^2) \times (T_w - T_a) \tag{4.26}$$

where U_w is the wind speed [$\mathrm{ms^{-1}}$], $e_{s,w}$ is the saturated water pressure [mmHg], r_h is the relative humidity [values between 0 and 1], $e_{s,a}$ is the air saturation pressure [mmHg], C_b is the Bowen coefficient [$\sim$0.47 $\mathrm{mmHGK^{-1}}$], T_w and T_a is the water and air temperature [K]. The latent heat flux is directly related to the pressure vapor deficit and the sensible heat is related to the water-air temperature difference.

Chapter 5

Application of the Mohid-2D model to a mesotidal temperate coastal lagoon

The Ria de Aveiro is a mesotidal temperate complex shallow lagoon, located in the Northwest coast of the Iberian Peninsula. The assessment of the Mohid-2D model is performed through its calibration and validation for the Ria de Aveiro lagoon. The hydrodynamic model calibration was performed, adjusting the bottom friction coefficient, through the comparison between measured and computed time series of sea surface elevation (SSE) for 24 stations within the lagoon. Harmonic analysis of these data was performed in order to evaluate model's accuracy. For the M_2 constituent, that has the major amplitude, the average phase difference of both amplitude and phase, for all 24 stations, is 3 cm and 3°, respectively. The model performance was also evaluated computing the RMS errors between measurements and computed values of SSE and current velocity. To validate the hydrodynamic model, measured and computed SSE and current velocity data were compared for 11 stations. In addition, it was performed a comparison between water flow data (between the lagoon and the ocean) computed by the model and inferred from electric potential difference data obtained using a submarine electric cable crossing the entrance channel of the lagoon. A good calibration and validation was achieved revealing that the model can reproduce the barotropic flows in such a complex system like Ria de Aveiro.

5.1 Introduction

Coastal lagoons are saline water bodies separated or partially isolated from the sea. They may be linked to the sea by one or more channels which are small relative to the lagoon. Ria de Aveiro is a very complex system in terms of hydrodynamics and biogeochemical characteristics [Trancoso et al., 2005]. To understand its behavior it is necessary a prior knowledge of its physical processes. The most important of these is hydrodynamics.

Nowadays, numerical models are used as sophisticated techniques of interpolation and extrapolation of field data in both spatial and temporal domains. On the other hand, realistic model results

cannot be obtained without adequate supporting data [Cheng et al., 1991]. Thus, numerical and field data are complementary elements of one integrated research program. Nowadays, two-dimensional vertically integrated (2DH) models can be considered as reliable tools for the study of shallow coastal waters [Neves, 1985; Cheng et al., 1993; Inoue and Wiseman JR., 2000; Dias et al., 2003; Umgiesser et al., 2003].

A mathematical model can be considered as an approximate reconstruction of a real phenomenon. All parameterizations and approximations used in the models lead to deviations of the model results from nature. It is an accepted requirement that a numerical model of estuarine hydrodynamics should be verified, calibrated and validated before used in a practical application. However the procedures to perform these tasks are not widely accepted [Cheng et al., 1991]. Calibration and validation methods appear in several forms, depending on data availability, water body characteristics and researchers opinion [Hsu et al., 1999].

In the case of hydrodynamic modelling, the calibration is frequently made by qualitative comparison of short time series of predicted and measured data for the same location and period of time [Cheng et al., 1993]. Another method used consists in comparing the harmonic constituents generated from predicted and observed data. In some studies, the harmonic constants are not considered as time independent [Smith, 1977], although authors like Cheng et al. [1993]; Martins et al. [2002] considered harmonic constants as an invariant characteristic of the astronomic tide. In the case of Ria de Aveiro, Tomás and Dias [2004] shown, in a long term analysis of the harmonic constants at the lagoon's inlet, that meaningful changes are only observed in a scale of years. These changes may be related to dredging operations performed at the inlet or natural changes in the lagoon's bed which produces some hydrodynamic changes. Since harmonic constants can be considered independent of time and if they are available, concurrent field data is not required for model calibration and validation. This method has a major limitation since for its application a large amount of data is needed. Therefore, this method requires the use of a robust and efficient numerical model to generate long time series.

To quantify the model performance it is commonly accepted to determine the Root Mean Square Error (RMS) between model and field data [Hsu et al., 1999], as well as the relative mean absolute error (RMAE) [Walstra et al., 2001; van Rijn et al., 2003]. One aspects to point out on using RMAE is that this error is less susceptibly to outliers. However, this evaluation method is mainly used to qualify wave heights and current velocity data [Walstra et al., 2001; van Rijn et al., 2003], and it was not found any work presenting reference values to sea surface elevation (SSE). In this work the evaluation of the model will be performed through the use of RMS errors since this method could be considered as a general method to evaluate the accuracy of numerical models reproducing any variable.

In this work, the Mohid-2D model implementation for the Ria de Aveiro lagoon is presented, describing its assessment through calibration and validation against different sets of measured data. Due to the lagoon complex geometry and to the large number of calibration stations used, this goal

constitutes a very challenge task. It is also purpose of this work to give a contribution to define a complete methodology to perform numerical models calibration and validation.

The model is calibrated using as a first approach a qualitative comparison of the temporal evolution of SSE data measured in 1987/1988 at several locations. When a good match is obtained for all the stations, the model's accuracy is evaluated through the determination of the RMS and also through the comparison between amplitude and phase of the main tidal constituents determined from harmonic analysis of the observed and computed data. The validation procedure is performed using two independent data sets, which include observations of current velocities and SSE values (1997 data) and measured water fluxes at the lagoon's inlet for the period of October 2002.

Once the hydrodynamic model is fully implemented and its results are considered reliable it will be used to study the lagoon hydrodynamics and evaluate its evolution. A transport model is also being coupled to the hydrodynamic model in order to study the thermohaline structure within the lagoon, with a closer look to its central area, where occurs the mixing between fresh and salt water, and to the study of water exchange between the lagoon and the near ocean.

5.2 The study area

Ria de Aveiro is a shallow mesotidal lagoon located in the Northwest coast of Portugal (40°38'N, 8°44'W). It has a very irregular geometry (see Figure 5.1) being characterized by narrow channels and by the existence of intertidal areas, namely mud flats and salt marshes. The lagoon has a maximum width and length of 10 and 45 km, respectively. In spring tide covers an area of 83 km^2 at high tide reducing to 66 km^2 at low tide [Dias et al., 2000]. The averaged depth of the lagoon is 1 m, except in its navigation channels where dredging operations are often carried out. One single inlet at the western boundary allows the water exchange between the Atlantic Ocean and the lagoon. This inlet has about 20 m deep, 1.3 km long and 350 m wide.

Ria de Aveiro receives freshwater mainly from two rivers, the Antuã (5 m^3s^{-1} average flow) and the Vouga (50 m^3s^{-1} average flow) [Moreira et al., 1993; Dias et al., 1999]. Vouga River is responsible by approximately 2/3 of the freshwater input into the lagoon [Dias et al., 1999]. The other rivers have negligible flow, except the freshwater source in the south end of the Mira channel, which consists of a small system of ponds and rivers that have a flow which is not well known. Tides, which are semidiurnal, are the main forcing of circulation in the lagoon and conjugated with freshwater inflow they controls the water mass dynamics inside Ria de Aveiro. The minimum tidal range at the lagoon's mouth was referred as 0.6 m (neap tides) and the maximum tidal range as 3.2 m (spring tides) [Dias et al., 1999]. Extreme conditions of wind (values higher than 20 kmh^{-1}) may induce particular circulation patterns, mainly in shallow areas and wide channels [Dias, 2001].

The estimated tidal prism of the lagoon is 136.7×10^6 m^3 for maximum spring tide and 34.9×10^6 m^3 for maximum neap tide [Dias, 2001]. The total estimated freshwater input is very small (about 1.8×10^6 m^3 during a tidal cycle) [Moreira et al., 1993] when compared with the mean tidal prism at

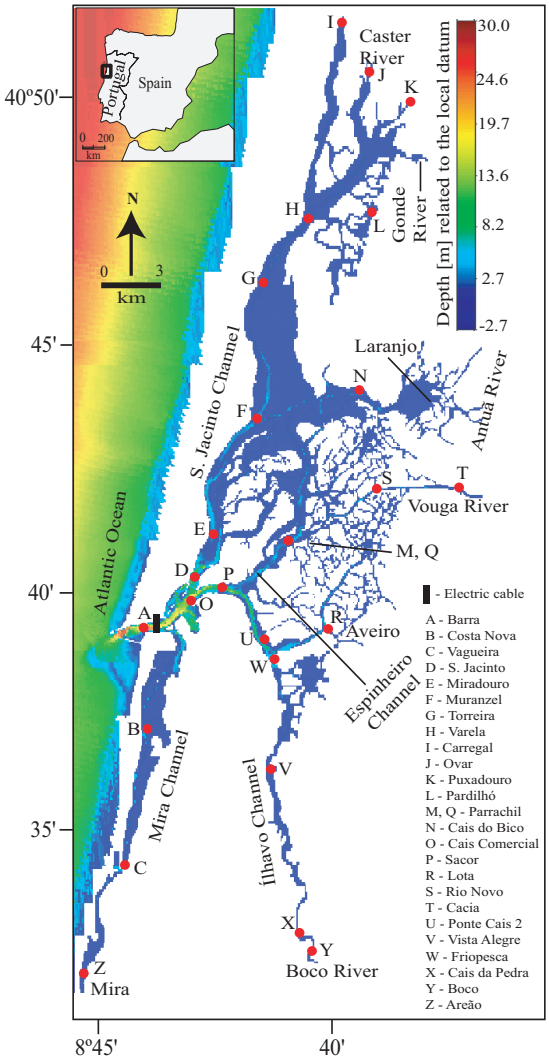

Figure 5.1: Ria de Aveiro lagoon, with the locations of the stations used in the calibration and validation of the numerical model and of the electric cable used to measure water flows (the water depth relative to the local datum).

the mouth of the lagoon (about 70×10^6 m^3), indicating that the lagoon may be vertically homogeneous in terms of salinity.

A prior hydrological characterization led to the conclusion that Ria de Aveiro can be considered vertical homogeneous during dry seasons. However, after important rainfall the stratification becomes important near the freshwater inflow locations [Dias et al., 1999].

5.3 The numerical model

The numerical model used in this study is Mohid, originally developed by the MARETEC - Marine and Environmental Technology Center group of the Instituto Superior Técnico [Martins et al., 1998,

2001]. This model was previously used successfully to simulate coastal and estuarine flows in several estuarine and coastal environments [Cancino and Neves, 1999; Martins et al., 2001; Neves et al., 1998; Coelho et al., 2001]. Mohid is a three-dimensional finite volume model with the ability to simulate flows in well and partially mixed systems. Due to the Ria de Aveiro characteristics it was considered the use of Mohid in a horizontal two-dimensional (depth integrated) mode as the right choice to simulate the lagoon's hydrodynamic.

5.3.1 The governing equations

The model solves the three-dimensional incompressible primitive equations. Hydrostatic equilibrium is assumed as well as Boussinesq approximation. The momentum and mass balance equations are:

$$\begin{aligned}\frac{\partial u_i}{\partial t} + \frac{\partial (u_i u_j)}{\partial x_j} &= -\frac{1}{\rho_0}\frac{\partial p_{atm}}{\partial x_i} - g\frac{\rho(\eta)}{\rho_0}\frac{\partial \eta}{\partial x_i} - \frac{g}{\rho_0}\int_{x_3}^{\eta}\frac{\partial \rho'}{\partial x_i}dx_3 \\ &+ \frac{\partial}{\partial x_j}(\upsilon\frac{\partial u_i}{\partial x_j}) - 2\varepsilon_{ijk}\Omega_j u_k \end{aligned} \tag{5.1}$$

$$\frac{\partial u_1}{\partial x_1} + \frac{\partial u_2}{\partial x_2} + \frac{\partial u_3}{\partial x_3} = 0 \tag{5.2}$$

The horizontal velocity components are calculated using Equation 5.1, where u_i are the velocity vector components in the horizontal cartesian x_i directions ($i = 1, 2$), u_j are the velocity vector components in the three cartesian directions x_j ($j = 1, 2, 3$), υ is the turbulent viscosity and p_{atm} is the atmospheric pressure. ρ is the specific mass, ρ' is its anomaly, ρ_0 is the reference specific mass, $\rho(\eta)$ represents the specific mass at the free surface, g is the acceleration of gravity, t is the time, Ω is the Earth's velocity of rotation and ε is the alternate tensor.

If the Continuity Equation (5.2) is integrated over the whole water column (between the free surface elevation $\eta(x, y)$ and the bottom $-h$, the free surface equation is obtained:

$$\frac{\partial \eta}{\partial t} = -\frac{\partial}{\partial x_1}\int_{-h}^{\eta} u_1 dx_3 - \frac{\partial}{\partial x_2}\int_{-h}^{\eta} u_2 dx_3 \tag{5.3}$$

where h is the depth. The hydrostatic approximation gives:

$$p(z) = p_{atm} + \rho_0 g(\eta - z) + g\int_{z}^{\eta}\rho' dz \tag{5.4}$$

Equation (5.4) relates pressure at any depth with the atmospheric pressure at the sea surface, the sea level and the pressure anomaly integrated between that level and the surface.

The bottom shear stress, $\vec{\tau}$, is represented as a quadratic function of velocity using the formulation proposed by Antoine Chézy [Dronkers, 1964] where $\vec{\tau}$ is proportional to the square velocity (5) and the drag coefficient (C_D) can be parameterized in terms of Manning friction coefficient (n), by applying Equation (5.6):

$$\vec{\tau} = C_D|\vec{V}|V \tag{5.5}$$

$$C_D = gn^2H^{1/3} \tag{5.6}$$

where $\vec{V}$ is the horizontal velocity vector and H ($H = h + \eta$) is the depth of the water column.

The model discretization is fully described in Martins et al. [2001].

5.3.2 Boundary conditions

Several types of boundaries were used in this application: free surface, bottom, lateral closed boundary, lateral opened boundary and moving boundary.

At the ocean open boundary the free surface elevation is specified and at the river boundaries the water flow is imposed. The lateral boundary condition at coastal boundaries is a free slip condition, imposed by specifying a zero normal component of mass and momentum diffusive fluxes at cell faces in contact with land. No mass fluxes at the surface and bottom were considered. Moving boundaries are closed boundaries whose position varies with time. This situation appears in domains with intertidal zones that are very common in Ria de Aveiro. In this case the uncovered cells must be tracked and with this purpose a criterion based in Figure 5.2 is used. $HMIN$ is the depth bellow which the cell is considered uncovered. In this case a thin volume of water above the uncovered cell is conserved. The cells of position i, j are considered uncovered when one of the two following situations is true:

$$H_{ij} < HMIN \wedge \eta_{ij-1} < -h_{ij} + HMIN \tag{5.7}$$

$$H_{ij-1} < HMIN \wedge \eta_{ij} < -h_{ij-1} + HMIN \tag{5.8}$$

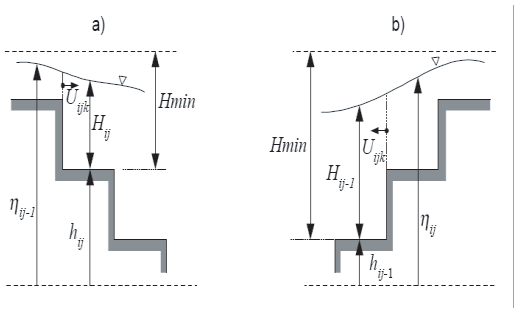

Figure 5.2: Conditions for a point to be considered uncovered (moving boundaries).

The second condition of (5.7) assures that the cell is not being covered by the tidal wave propagating from left to right and the second condition of (5.8) assures that the cell is not being covered by the tidal wave propagating from right to left. The noise formed by the abrupt change in velocity at the dry cells is controlled with a careful choice of $HMIN$ (in this case $HMIN = 0.10$ m) [Leendertse and Liu, 1978].

5.4 Application to the Ria de Aveiro

Bathymetry is probably the most important among many factors that affects the flow in shallow systems like Ria de Aveiro. The bathymetry controls the spatial variability of the current magnitude and direction, constituting a factor which assures the realism of the numerical model. The numerical grid must be sufficiently refined to resolve all the variations of depth and geometry, but as the grid resolution is refined the total number of grid points and the computation time increase excessively. Due to the lagoon complex geometry a grid with variable spatial step was developed. This grid has 429 by 568 cells, with dimensions of 40 by 40 meters in the central area of the lagoon (between 40°38' and 40°41' and 8°35' and 8°45') (Figure 5.1) and 40 by 100 meters in the north and south areas of the lagoon. The numerical bathymetry used in this study was developed from data concerning depth obtained from a general survey carried out in 1987/88 by the Hydrographic Institute of Portuguese Navy (IH). More recent bathymetric data is also available. In fact, recent dredging operations performed in 1998 in Mira and S. Jacinto channels and in 2002 close to the mouth of the lagoon supplied new bathymetric data that was used to actualize the numerical bathymetry. For these regions the original values of water depth were replaced by the recent ones. The water depth at each grid point was determined from the water volume of the cell, calculated using a Monte Carlo cubature method [Dias, 2001].

At the sea open boundary, located ~5200 m westward station A, the free surface elevation was specified from 38 tidal constituents obtained after harmonic analysis [Pawlowicz et al., 2002] of data measured at a tide gauge located close to the mouth of the lagoon (40°38'N and 8°44'W - station A). The tide was imposed in the ocean open boundary with a phase and amplitude correction factor for the major harmonic constants in a way that the model results reproduce the tidal elevation at the mouth tidal gauge.

5.5 Hydrodynamic model calibration

A number of tests were carried out to evaluate the hydrodynamic model sensitivity to changes in the parameters, such as time step, initial water level and horizontal eddy viscosity coefficient.The values adopted in this study were time step (Δt) of 10 s and horizontal eddy viscosity (υ) of 5 m^2s^{-1}. Initial conditions for the hydrodynamic model are null free surface elevation and null velocity in all grid points. These variables become independent on the initial conditions in all the computational domain after 48 hours of simulation (~4 tidal cycles). The model was spun up from rest over 2 days in order to guarantee the stability and independence from the initial conditions of the results.

The model calibration is defined as an operation in which specific values, or distributions, or a range of variation are given to the floating free model parameters, so that the model results fit best to a set of field observations [Koutitas, 1994]. The model calibration is subsequently based on the determination and the adjustment of the parameters to which the model is most sensitive.

The calibration of the hydrodynamic model was carried out comparing model results with values

of SSE measured in the years of 1987/1988 at 24 stations covering the entire area of the lagoon (Figure 5.1) [IH, 1991]. From the SSE observations data it is concluded that there is tidal energy damping, due to friction, as the tidal wave propagates from the mouth of the lagoon towards the end of the channels. This behavior is common in estuarine ecosystems [Hsu et al., 1999] and was analyzed, in the case of Ria de Aveiro, by Dias and Fernandes [2006]. The magnitude of the bottom friction coefficient determines changes in the tidal wave propagation within the lagoon. Therefore, the model parameter subjected to adjustments in the calibration process is the Manning bottom friction coefficient (n) (eq. 5.6).

In this study the procedure adopted to calibrate the model consisted in spatially varying the bottom roughness coefficient, by assigning Manning's values to specific regions of the numerical domain. This procedure was successfully tested by Smith and Cheng [1987] and Cheng et al. [1993] in numerical studies performed at Suisun and S. Francisco Bay areas, California. The model results are not, usually, very sensitive to the absolute values of n. However, it is known that the water depth strongly influences the bottom stress. This "influence" is introduced into the calculations by allowing Manning's coefficient values to vary as a function of water depth. Therefore, the introduction of this parameter is necessary to achieve a better reproduction of the observed data. It can be affirmed that the bottom friction should change according to the nature of the bed [Aldridge and Davies, 1993] and that an increase in the bottom friction will produce a decrease in the tidal wave in that zone of the channel and in the channel's upstream. Other assumption is that an increase in the bottom roughness will produce an increase in the phase lag for high tide and decrease for low tide [Fry and Aubrey, 1990].

Using these guiding principles the Manning coefficient was adjusted locally until the model results fits satisfactorily with the measurements. In the case of this study the best adjustment between model results and field observations was achieved through bottom roughness parameterized from Manning coefficients ranging between 0.022 and 0.045.

5.5.1 Results

Figure 5.3 shows the comparison between the computed and observed SSE time series for nine of the stations used in the model calibration (this procedure involved 24 stations). In this work the model performance in the reproduction of the SSE was measured by means of RMS error between computed and observed data:

$$RMS = \left\{ \frac{1}{N} \sum_{i=1}^{N} [\zeta_o(t_i) - \zeta_m(t_{t_i}]^2 \right\}^{1/2} \tag{5.9}$$

where $\zeta_o(t)$ and $\zeta_m(t)$ are the observed and computed SSE, respectively and N is the number of measurements in the time series. The RMS values were computed for each station and are shown in each plot.

In the whole, it was achieved a good agreement between computed and observed SSE for all the

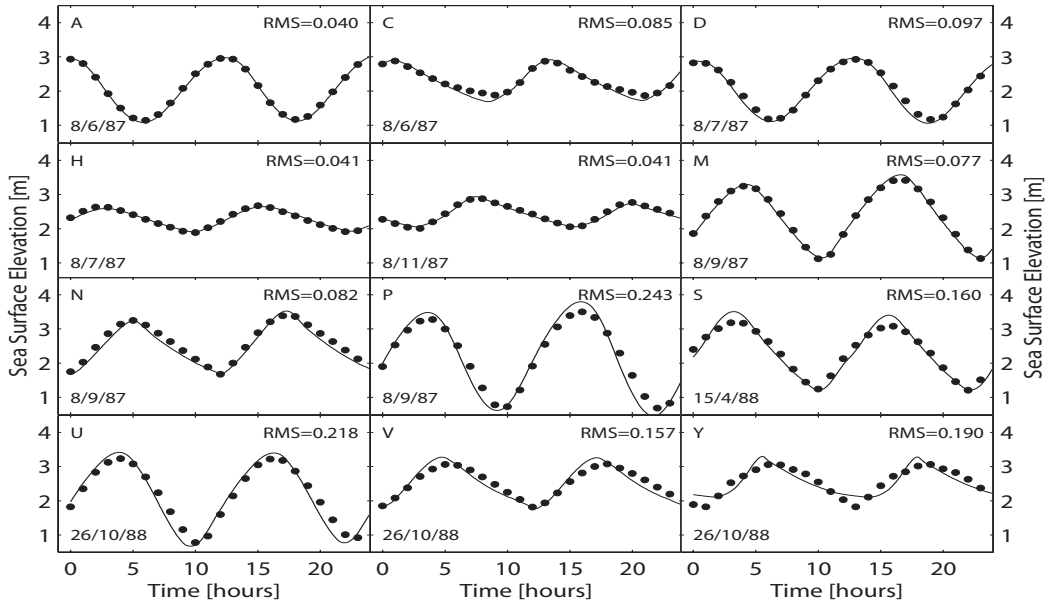

Figure 5.3: Comparison between SSE time series for stations A, C, D, H, I, M, N, S and V, used in the hydrodynamic model calibration procedure (•: data; solid line: model).

stations (Figure 5.3), revealing an accurate reproduction of the SSE in a system like Ria de Aveiro. Nevertheless, there are some aspects that should be addressed. At station A the agreement between computed and observed data should be perfect, however this is not the case. In fact, a RMS error of ∼4 cm was found for the station located at the lagoon mouth. This difference represents less than 2% of the mean tidal range near the mouth of the lagoon and may be justified by an inaccurate phase and amplitude correction factor for the major tidal constituents imposed at the open ocean boundary. This small error may partially explain the errors found in the other stations. In general the disagreement between computed and observed SSE is low with values lower than 5% of the local tidal range. The highest disagreement was found for stations P, T and U, with RMS errors around 10% of the tidal range. The errors occurred at station P and U (RMS = 0.243 m and RMS = 0.218 m, respectively) are difficult to explain, they are probably due to an integrated effect of bathymetry errors in terms of the water volume arrested in the tidal flats during the flood. However, it was not possible to improve the agreement between computed and observed data in these stations adjusting the Manning coefficient. At station T a RMS error of 0.234 m was computed. This difference between the computed and measured values may be due to several factors, such as the distance to the lagoon mouth (∼12 km), the fact that this station is placed close to the Vouga River mouth or the small width and depth of the channel (∼40 m and ∼2 m, respectively). At the end of Ílhavo channel (stations X and Y) the RMS error is about 7% of the local tidal range. These disagreements may be explained by some inaccurate definitions of the bathymetry at those areas. In fact, at Ílhavo channel there is a very narrow section, with a width of about 10 m, where strong currents occur. This region is very difficult to represent in

the numerical bathymetry, even with cells of 40 m wide. Therefore it is difficult to improve the model results in this channel without increasing to much the computational effort.

The importance of the proper simulation of the times for high and low tide in the modelling of tidal flows inside domains with large intertidal areas such as Ria de Aveiro, was demonstrated by Kuo and Park [1985]. In fact, if the side storage area is not properly taken into account, the model can reproduce the mean tidal range but the phase cannot be properly computed. The analysis of Figure 5.3 shows that the time lag between computed and observed data is very low for both high and low tide in almost all the stations. In this study the time lag is quantified through harmonic analysis.

Harmonic analysis [Pawlowicz et al., 2002] was performed on one month length time series for both observed and computed SSE for all the stations. Results for the three major semi-diurnal tidal constituents (M_2 - 12.42 h; S_2 - 12 h; N_2 - 12.9 h) determined for all the stations are presented in Figure 5.4 and reveal a rather good agreement both in amplitude and phase for these constituents (which represents ~90% of the tidal energy in Ria de Aveiro [Dias et al., 1999]).

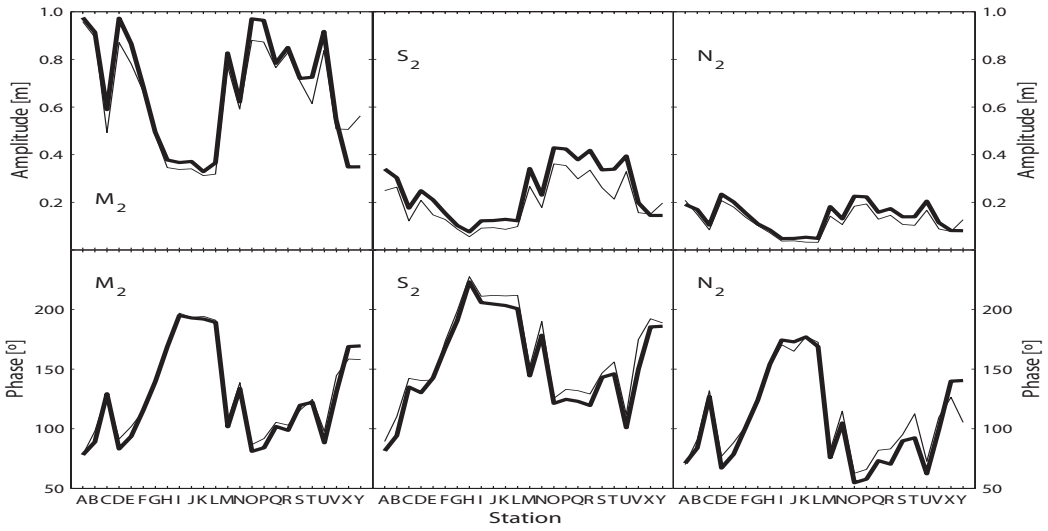

Figure 5.4: Comparison between amplitude and phase of the three major semi-diurnal tidal constituents (M_2, S_2, N_2) determined in all stations used in the calibration procedure (solid line: measurements; thick solid line: model).

For the M_2 constituent, which has the major amplitude, the mean difference of the amplitudes is about 3 cm and the standard deviation is ~7 cm. The mean phase difference for all the 24 stations is about 3° and the standard deviation is ~6°. One error of 1° corresponds to about 2 minutes departure in the arrival of high tide for a semi-diurnal constituent, which means that the average difference between field and model data is about 6 minutes for the M_2. Results for the other semi-diurnal constituents as well for the diurnal ones (not shown), are not so accurate as for the M_2 constituent. However, they reveal a good agreement between the computed and observed constants. The comparison between these values reveals that the amplitude of the major semi-diurnal constituents is

well reproduced by the model for the entire lagoon, with averaged differences lower than 5 cm. The predicted phase is also well reproduced by the model.

According to these results the model can be considered successfully calibrated.

5.6 Hydrodynamic model validation

The validation of a model is the procedure of comparing the model output with available field or laboratory data to prove the model efficiency. The measurements used to perform the validation have to be independent from the data set used for calibration.

Considering that in this work the model calibration was performed through comparison of harmonic constants of model results and field data, the model validation may not be relevant if the harmonic constants are considered independent of time. However, the data set used in the calibration process of this model is from 1987/1988, and according to Tomás and Dias [2004] in a large temporal scale the harmonic constants have slightly change at the lagoon inlet. Also considering that Ria de Aveiro is a very dynamic system in terms of its morphology, the validation of the model using a more recent data set is considered fundamental.

Taking into account the availability of recent field data two different periods were simulated to validate the model. The first simulation corresponds to a period during June 1997 where the model performance was evaluated by comparing the RMS error between computed and observed data of SSE and of current velocity for eleven and ten stations, respectively, distributed along the main channels of the lagoon.

The second simulation corresponds to a period during October 2002. In this case computed and observed data of the water fluxes between the lagoon and the ocean in a monthly time scale were compared. In the case of Ria de Aveiro, this comparison is particularly relevant, since the lagoon has a single inlet that allows the water exchange with the ocean. The observed water fluxes were determined using measurements of electrical potential difference between the shores as described in Nolasco et al. [2006].

5.6.1 Results

The validation procedure was carried out without changing the friction coefficients used during the calibration. In the ocean open boundary the tide synthesized for the considered period of measurements was imposed considering the same correction factor referred in Section 5.4. The remaining inputs were left unchanged.

When comparing current velocity values it is important to remember that this variable varies rapidly in space, both in magnitude and direction, from point to point. This behavior reflects the irregular geometry of the region and it produces higher discrepancies between field and computed results. Moreover, the model results are related to the mean value over the vertical and over the

horizontal spatial domain corresponding to the grid size, while the field data corresponds to a single point or, at best, an average over various points.

Considering that most of the lagoon's channels are aligned through a main direction, in order to compare the velocities the main flow directions were found for both measured and computed velocities at each station. These directions resulted almost coincident and the computed and measured current velocities were projected along these directions.

Figures 5.5 and 5.6 show the comparison between the computed and measured SSE and along flow direction velocities, respectively. The perpendicular flow direction velocities are residual and were not considered.

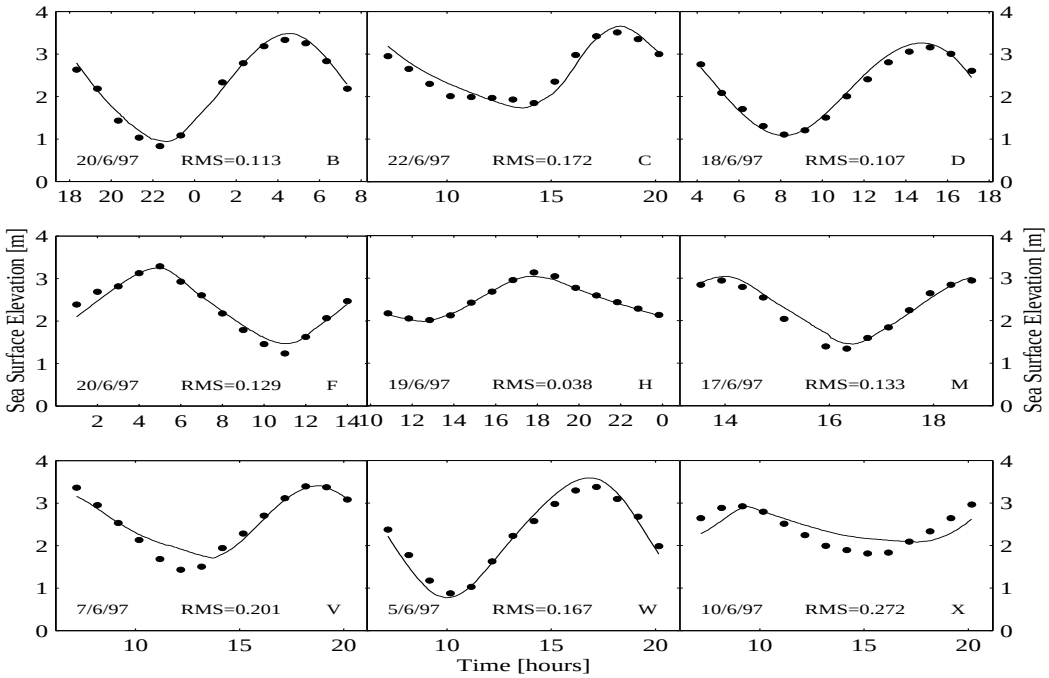

Figure 5.5: Comparison between SSE time series for stations B, C, D, F, H, M, V, W and X, used in the hydrodynamic model validation procedure (•: data; solid line: model).

The RMS errors of the SSE values are around 5%, for all the stations, except stations V (∼10%) and X (∼18%). As in the calibration procedure, the results for the far end of Ílhavo Channel are not so accurate, due to very narrow channel areas where the currents are to high. Except for these stations the agreement between values is rather good, revealing that a general agreement was achieved between computed and measured SSE.

From Figure 5.6 it is verified that there are discrepancies between the model and the field data when assessing velocities point by point. The *RMS* errors are very high, ranging from about 6% of the current amplitude in the case of the better adjustment (station D) to more than 50% for the worse case (station F). At stations B, C and D (near the lagoon's mouth), the phase errors are lower than 10 minutes, revealing a good reproduction of the observations. At stations F, H and M the model

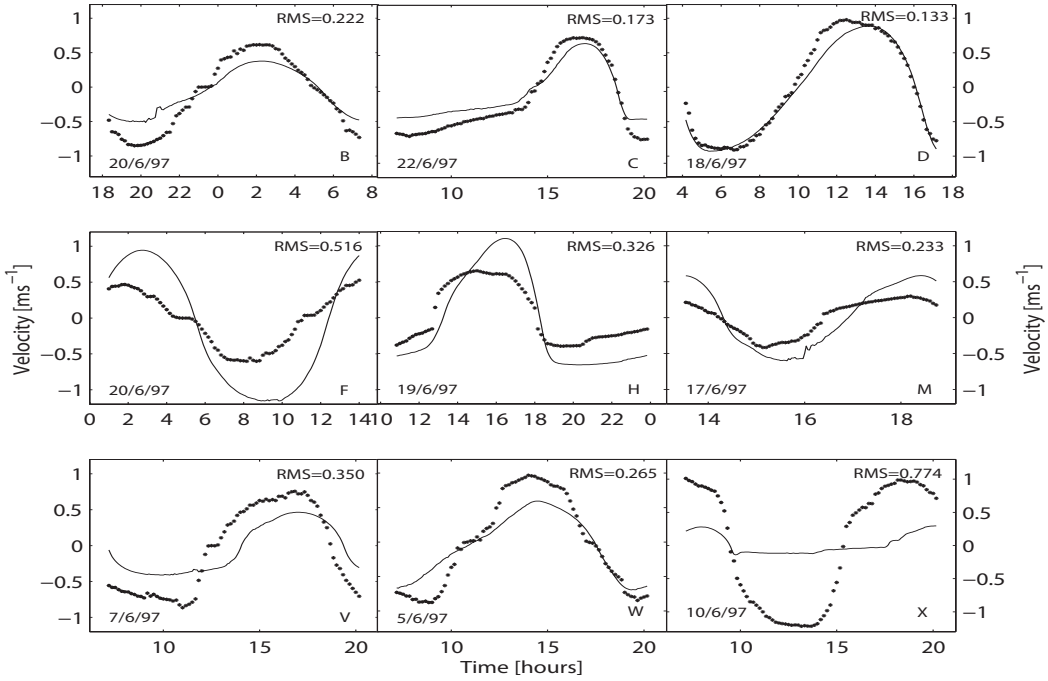

Figure 5.6: Comparison between time series of along flow direction velocities for stations B, C, D, F, H, M, V, W and X, used in the hydrodynamic model validation procedure (• data; solid line: model).

results are not so accurate, the phase difference between predicted and measured values is about 1 h, revealing a degradation of the predicted velocity values. The comparison is rather good for stations B, C and D. These stations are located at the center of wide channels and therefore it can be considered that the measured velocities are representative of the current speed in an area correspondent to a grid cell. For all the other stations, except stations V and X, the phase may be considered well reproduced. These two stations are located at the end of Ílhavo channel, which is characterized by very narrow areas that are not well resolved by a model using grid cells 40 meters wide.

The hydrodynamic model was also validated by comparing water flow data inferred through the use of MIV technique and computed by the model. The tidal evolution in the Ria de Aveiro is essentially determined by the lunar constituents. They represent more than 90% of the tidal energy. Therefore, only the observed and computed water flow induced by the lunar constituents (M_2 and O_1) and by M_4 (essentially generated inside the lagoon) will be compared.

Figure 5.7 shows the water flow induced by the referred constituents for both MIV (5.7A) and computed values (5.7B). The spectral analysis results of these time series are presented in Figure 5.8A and 5.8B, respectively. The higher energy peaks correspond to M_2, the major tidal constituent in the Ria de Aveiro, but M_4 and O_1 are also present in the spectra of MIV and model results. The direct comparison (for a short period) between the water flow computed by the model and obtained from MIV measurements is shown in Figure 5.9. The agreement between the two series is rather good.

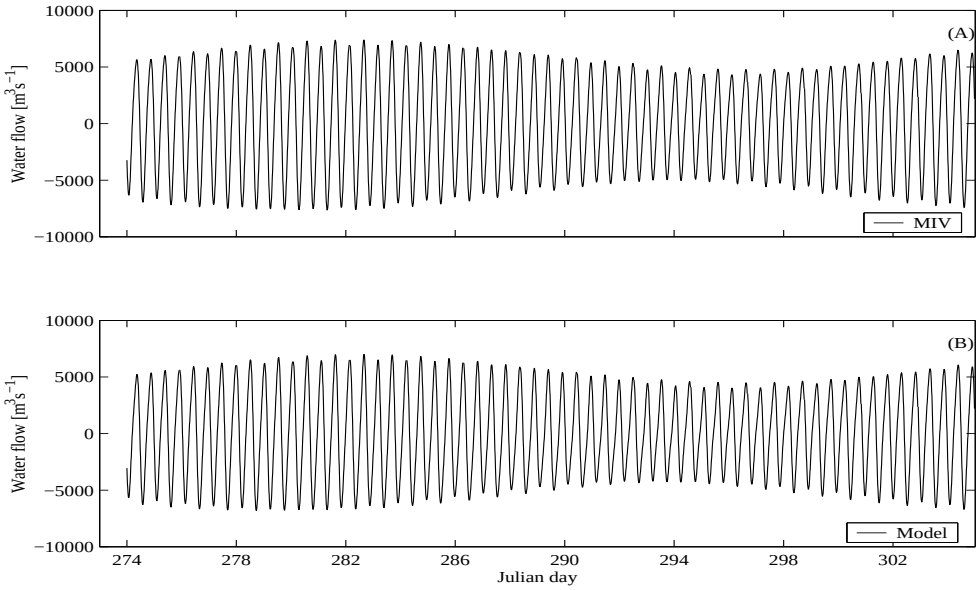

Figure 5.7: Tidal lunar water flow measured by the MIV technique (A) and computed by the hydrodynamic model (B).

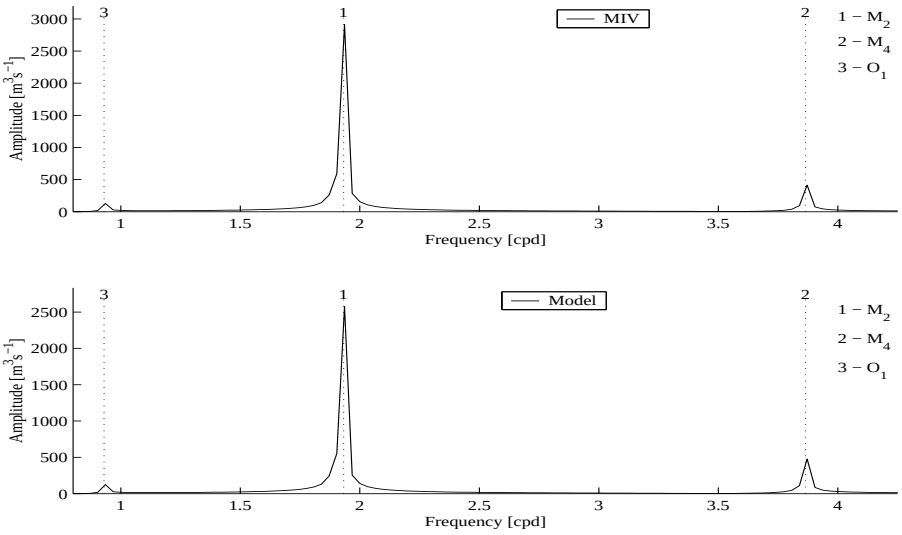

Figure 5.8: Amplitude spectra of the water flow obtained from the MIV technique and the hydrodynamic model.

The average values of total flow through the inlet during flood and ebb for spring and neap tide were computed. During spring tide, the average value of water flow passing across the bar during the flood period is 4124.8 (model) and 4586.1 m^3s^{-1} (MIV), and during the ebb period is -4136.3 (model) and -4696.2 m^3s^{-1} (MIV). During neaps, the average values during the flood is 2320.5 (model) and 2659.7 m^3s^{-1} (MIV), and during the ebb is -2721.2 (model) and -3170.3 m^3s^{-1} (MIV). The relative

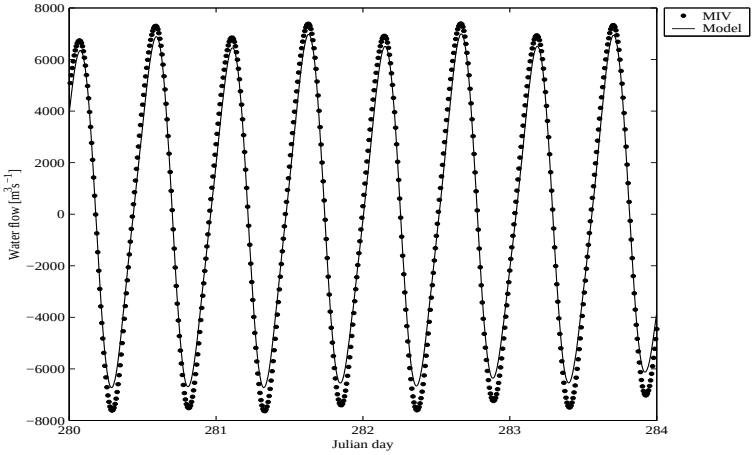

Figure 5.9: Comparison between tidal lunar water flow computed by the numerical model and obtained using the submarine cable (MIV technique).

errors of the average values computed by the model related to the average values inferred from the MIV results are about 10-12%.

From these results it may be concluded that the hydrodynamic model reproduces accurately the hydrodynamics of Ria de Aveiro in new and independent conditions, and therefore it may be considered validated.

5.7 Conclusions

The hydrodynamic model was successfully implemented for a very complex system as Ria de Aveiro. The results show that its calibration and validation were successfully carried out, revealing a good general agreement between computed and measured data. The validation also showed the ability of this hydrodynamic model to reproduces different sets of data in independent new conditions.

However, differences between model and field data exist. These differences are due to several factors, such as an inaccurate definition of the bathymetry for some particular regions of the domain, very narrow channels that are not well resolved by the horizontal grid and some uncertainties in the field data.

The results reveal that Mohid can accurately reproduce the barotropic flows in Ria de Aveiro, and therefore be considered as a valuable tool for future hydrodynamic and transport mstudies within the lagoon.

The procedures described here takes modelers through the basic steps on the implementation of hydrodynamic models. Moreover, this work pretend to present general and simple methods which may be used in the calibration and validation of these models by researchers or consultant professionals.

Chapter 6

Calibration and validation of the transport model

6.1 Introduction

As a natural tracer, salinity is used for the calibration of mixing processes within estuarine areas where a significant freshwater discharge exists. In these systems, mixing processes are mainly driven by the freshwater discharge and by the barotropic and baroclinic components of the pressure gradient due to tides and longitudinal salinity, respectively [Miranda and Castro Filho, 1996]. Therefore, the salinity distributions reflect the interaction effects between these processes. Assuming that the barotropic flows (tidal flows) have been calibrated and validated (see Chapter 5), the procedure used to calibrate the salt transport model is to compare measured and computed salinity time series. Once the transport model is considered calibrated, the mixing processes inside the channel may be considered well represented by the numerical model. On the other hand, the heat transport model calibration is only related to the heat and radiative fluxes parameterizations (Section 4.5 in Chapter 4). In the next section, a simple sensitivity analysis is presented on how heat surface fluxes (exchanges between the water and the atmosphere) influences the water temperature patterns within Ria de Aveiro. In this chapter the results of the the transport model calibration and validation are presented. Due to the structure of this dissertation, further details about the transport model equations and heat fluxes parameterizations are described in Chapter 4. Details about the implementation of the transport model are presented in Chapter 7.

6.2 On the influence of heat surface fluxes in the lagoon's water temperature horizontal patterns

In shallow systems as the Ria de Aveiro, the horizontal patterns of water temperature is strongly influenced by the exchanges between the water and the atmosphere (see Figure 6.1 for reference).

These patterns adjust dynamically to different sea and fluvial water temperature conditions, and also to meteorological forcing. In order to illustrate how the meteorological forcing affects the water temperature a simple test was carried out: two model simulations were performed using the same oceanic and landward boundary conditions, in one, surface heat fluxes were imposed (simulation 2) and, in the other, no heat fluxes were imposed (simulation 1).

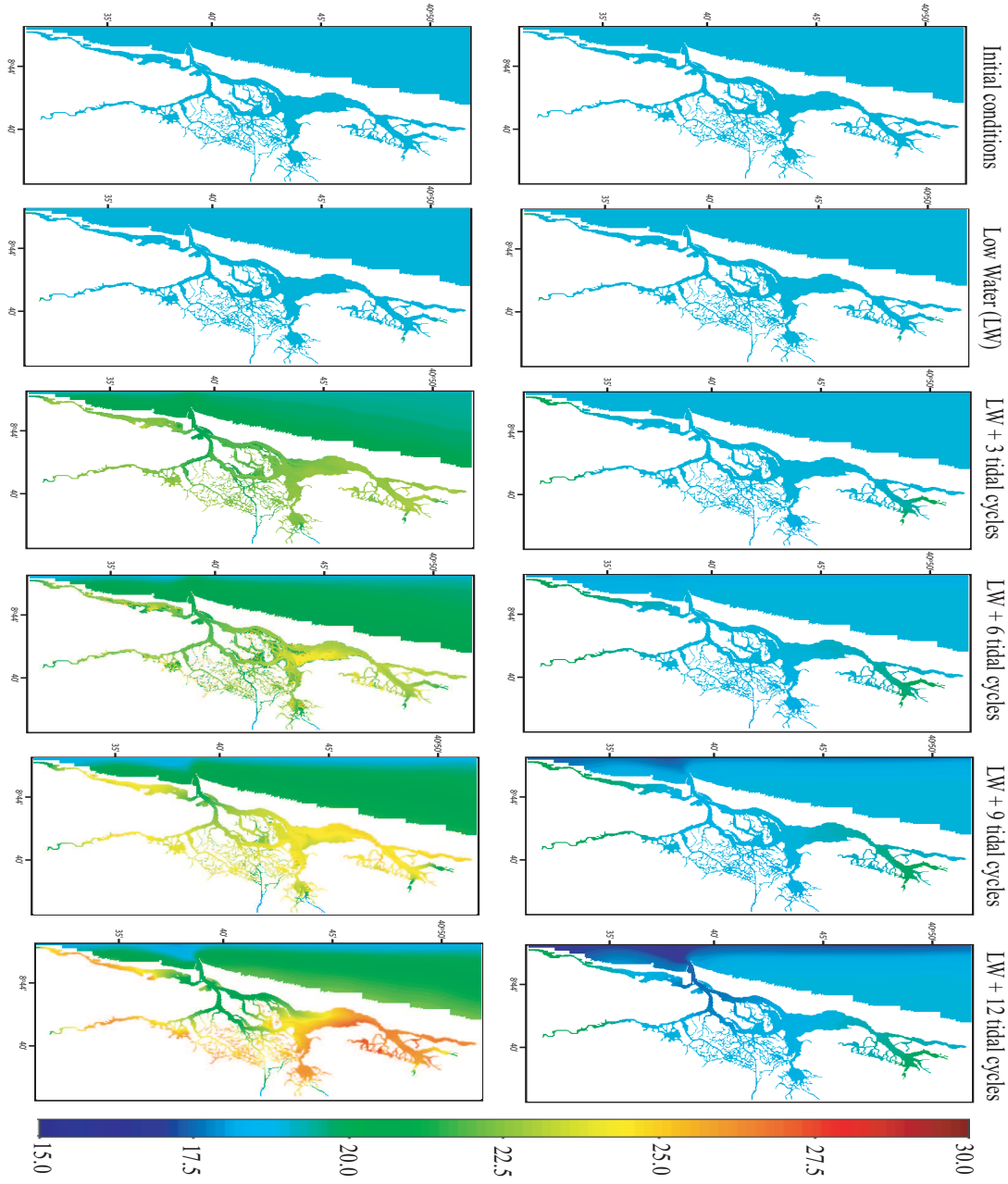

Figure 6.1: Ria de Aveiro water temperature horizontal structure without meteorological forcing (top row) and with meteorological forcing (bottom row). The water temperature units are °C.

At the open ocean boundary, the model was forced with tides and a water temperature constant value of 15°C (on both simulations) and, at the landward boundaries, different river flow and water temperature constant values were imposed: Vouga River - 20 m^3s^{-1} and 18°C; Antuã River and Mira River - 9 m^3s^{-1} and 18 and 20°C, respectively; rivers Boco, Caster and Gonde - 5, 7 and 6 m^3s^{-1}, respectively and 20°C. At the surface meteorological data, concurrent with the simulation periods (10 to 17 July 1996), from the NCEP database (nearest grid point: 40.952°N, -9.375°W), were imposed (simulation 2).

In Figure 6.1 are depicted the results for both simulations. At the top panel, are shown the water temperature horizontal patterns for the simulation where no heat fluxes were imposed. The bottom panel shows the water temperature patterns affected by heat fluxes.

When no heat fluxes are imposed (top row), the water temperature patterns are only determined by sea and fluvial water temperature. The rivers play a key role on the establishment of the temperature pattern at the north and south areas of the lagoon within its area of influence. The major changes in the temperature horizontal patterns are visible after 12 tidal cycles, when the rivers extend their influence at the north and south areas of the lagoon with water temperatures of ~20°C. At this time, the water temperature in the central area of the lagoon presents values of ~17°C, which are also visible in the near ocean. When meteorological forcing is used (bottom row), the water temperature structure changes after three tidal cycles, presenting values rounding 20°C within the lagoon. After 9 tidal cycles, the temperature structure is completely different with an increase of about 5°C in the shallow areas of the lagoon. After 12 tidal cycles, the water temperature within the lagoon present a maximum of ~28°C in the shallow areas of the lagoon and an increase of ~1-1.5°C near the lagoon's mouth in the navigation channel (deepest area).

In spite of the tidal and river flow influence on the water temperature horizontal structure, these results reveal the influence of variables like air temperature, relative humidity or incoming solar radiation in the shallow regions of the lagoon. Thus, in order to achieve a good implementation of heat transport models, it is necessary not only an accurate prescription of sea and river boundary conditions, but also the use of meteorological data for the model's implementation.

6.3 Calibration of salt and heat transport models

A set of salinity and water temperature data measured between 09/07/1996 and 28/07/1996 is available for comparison with model results. The data include long time series of salinity and water temperature measured near the lagoon's mouth. It also include 25 hours time series of hourly data measured at 7 different stations distributed along the lagoon channels (see Figure 7.1 in Section 7.2). These data were measured after a long dry period, a typical Summer season situation, where the freshwater inputs are expected to be low.

At the sea open boundary was specified salinity and water temperature time series (Figure 6.2). The freshwater discharge imposed at the upstream boundaries are not known, and in this study they are used as a calibration parameter. The values used were: Vouga river - 2 m^3s^{-1}; Antuã river - 0.5

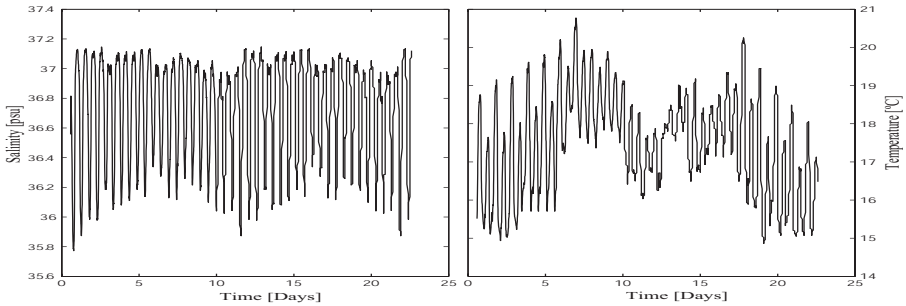

Figure 6.2: Time series of salinity and water temperature measured at the lagoon's mouth, and used as boundary conditions for the sea open boundary

m^3s^{-1}; Boco river - 2 m^3s^{-1}; Valas do Mira - 2 m^3s^{-1}; Caster and Gonde rivers - 0.5 m^3s^{-1}. The freshwater salinity values were specified as 0 psu, and a river's water temperature of 18 °C (Vouga river), 23 °C (Antuã River), 18 °C (Boco and Mira rivers) and 25 °C (Caster and Gonde rivers). In the calibration of the heat transport model it was imposed meteorological data (relative humidity, air temperature incoming solar radiation, wind modulus and direction), from the NCEP's data base, concurrent with the simulation periods. The initial conditions for the transport model are salinity and water temperature fields obtained by interpolation of typical values for each simulation period (see Figures 6.3a and 6.3b), because the time to dynamic equilibrium for these variables is much longer than for tides or tidal currents. Both heat and salt diffusion coefficients were set to 5 m^2s^{-1}.

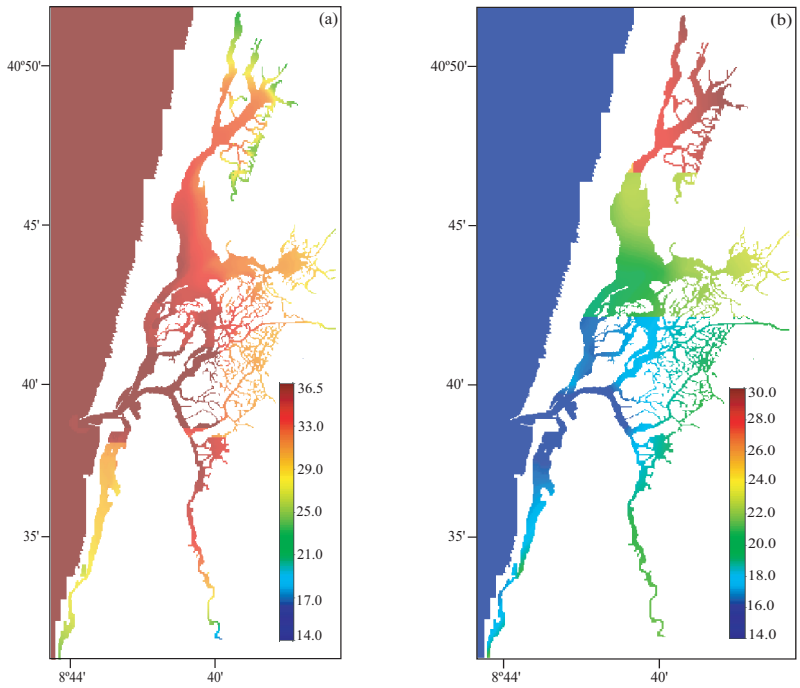

Figure 6.3: (a) Salinity [psu] and (b) water temperature [°C] fields used as model initial conditions for the calibration of the transport model

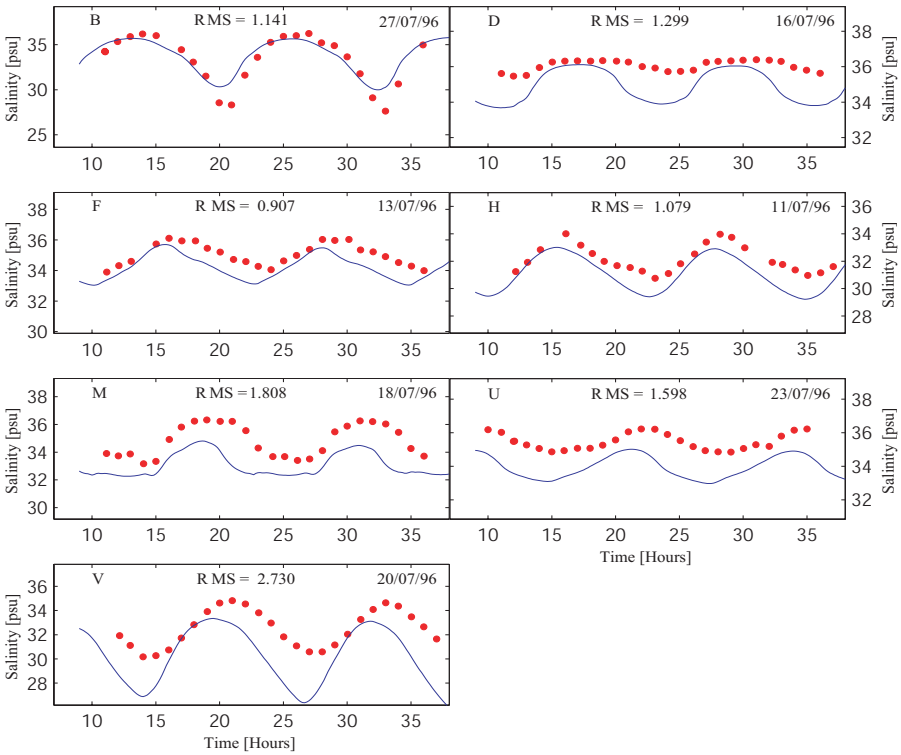

Figure 6.4: Comparison of salinity time series for the stations used during the calibration procedure. The measured data are plotted in red circles and the model's outputs are plotted in blue lines

The comparison between model and observed salinity values is depicted in Figure 6.4. The Root Mean Square Error (RMS) values were computed for all the stations and are displayed in each plot.

In general, a good agreement between computed and observed salinity data is achieved, revealing a good representation of the salinity time evolution and amplitude variation. The RMS values are about 5% of the mean salinity value (during two tidal cycles) for all stations, except at station V where the RMS value is 2.730 ($\sim$ 10% of the mean salinity value). At this point it is observed a delay of about 1.5 hours between computed and observed salinity values. Except at station B where the difference between computed and observed values is lower than 1 psu (during high water), the model seems to underpredict the salinity value with differences of about 2 psu during high water.

The comparison between predicted and observed water temperature values is depicted in Figure 6.5. It was achieved a good agreement between computed and observed water temperature values for all the stations. The lowest disagreement is obtained at station B, with a RMS of 0.998 between computed and observed time series. This value is about 5% of the mean water temperature value. At the other stations the RMS values oscillate between 10 and 15% of the mean water temperature value. From the figure, it can be seen that the model reproduces well the temporal evolution and underestimates the the amplitude variation, except at station D. During the low tide the maximum differences are reached (1-3°). These discrepancies may be due to errors when imposing the river water temperature values at the upstream boundaries. Probably, the freshwater temperature assumed

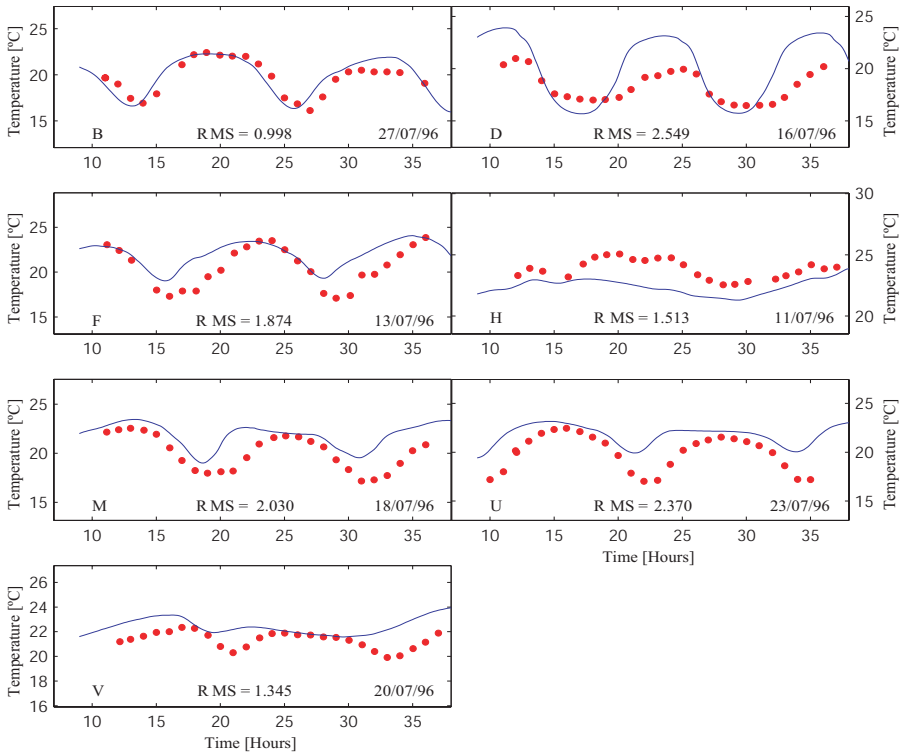

Figure 6.5: Comparison of water temperature time series for the stations used during the calibration procedure. The measured data are plotted in red circles and the model's outputs are plotted in blue lines

as a boundary condition may be not completely adequate. Another reason that could affect the model results could be related to cloud cover variations (a constant value was imposed, representing the mean value during the simulation periods), which affect the radiation absorbed by the water, and hence the water temperature.

Despite these factors, according to the results presented, it may be considered that the mixing processes are well reproduced by the model, and the water temperature distributions may also be considered well resolved by the numerical model.

6.4 Validation of the salt and heat transport models

The transport models were validated through the comparison of model results with an independent field data set. As in the validation of the hydrodynamic model (see Chapter 5) the salinity and water temperature values measured during June 1997 at 11 stations throughout the lagoon are used. These stations are presented in Figure 7.1 in Section 7.2. These data correspond to a wet period in which higher river runoffs than during the period used for the calibration are expected. Therefore, the transport modes are validated in different conditions than those observed during the calibration

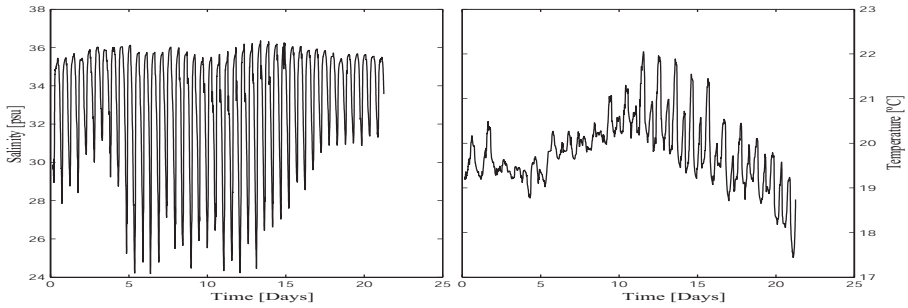

Figure 6.6: Time series of salinity and water temperature measured at the lagoon's mouth, and used as boundary conditions for the sea open boundary

period. As sea open boundary model inputs were used salinity and water temperature values measured every 10 minutes near the mouth of the lagoon (Figure 6.6).

The freshwater inflows used were: 7 m^3s^{-1} (Vouga river), 6 m^3s^{-1} (Antuã river), 1 m^3s^{-1} (Boco river), 5 m^3s^{-1} (Valas do Mira) and 1 m^3s^{-1} (Caster and Gonde rivers). The freshwater salinity was set to 0 psu and the water temperature of the fluvial waters was set to 24 °C. Once more, meteorological data from the NCEP's database were used. The initial conditions for the transport model are salinity and water temperature fields obtained by interpolation of typical values of each simulation period (see Figures 6.7a and 6.7b), and both heat and salt diffusion coefficients were set to 5 m^2s^{-1}.

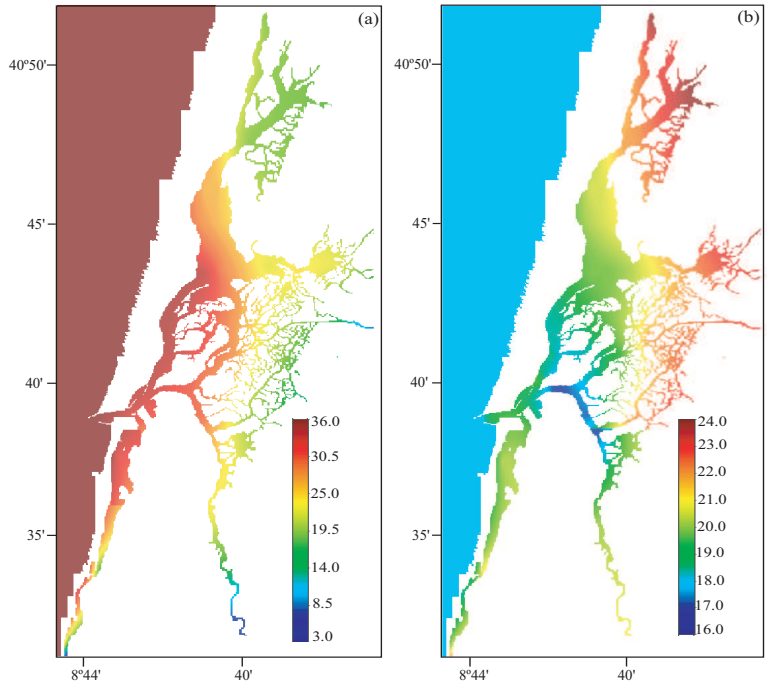

Figure 6.7: (a) Salinity [psu] and (b) water temperature [°C] fields used as model initial conditions for the validation of the transport model

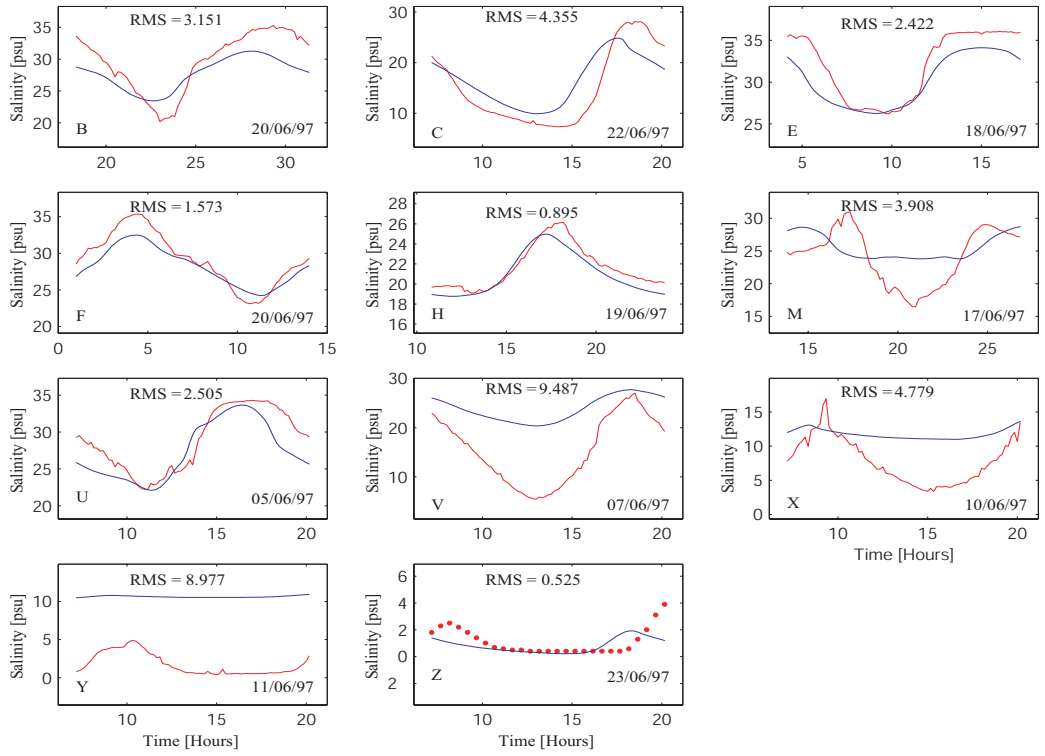

Figure 6.8: Comparison of salinity time series for the stations used during the validation procedure. The measured data are plotted in red and the model's outputs are plotted in blue.

The comparison between computed and observed salinity and water temperature data is depicted in figures 6.8 and 6.9, respectively.

The results reveal a good agreement between computed and observed data. The salinity results reveal that the model reproduces well the temporal evolution and the amplitude variation of the salinity, except for the stations M, V, X and Y where the amplitude variation is not well reproduced. The RMS errors ranged from 10 to 25% of the mean salinity value (obtained during one tidal cycle). The best results are obtained at stations F, H and U with values lower than 10% of the mean salinity value. Station M, V, X and Y results reveal that the model reproduces well the salinity temporal variation but not its amplitude variation. The RMS values are higher than 25% of the mean salinity value. These stations are located near the far end of Mira and Ílhavo channels, near freshwater sources, being strongly influenced by the boundary conditions that were chosen (freshwater discharge and freshwater salinity and water temperature values). The results at station Z reflect the river runoff that were imposed (5 m^3s^{-1}) with values close to the freshwater ones (0 psu). The river runoff imposed at Boco river (1 m^3s^{-1}) is very low and does not affect the salinity signal at stations V, X and Y.

The water temperature results reveal that the model reproduces well the temporal evolution of the water temperature but reveal some discrepancies in the amplitude variation. The RMS error values are lower than 10% of the mean water temperature value, except at stations V, X, Y and Z. In these stations, the discrepancy between computed and observed values may be explained by the

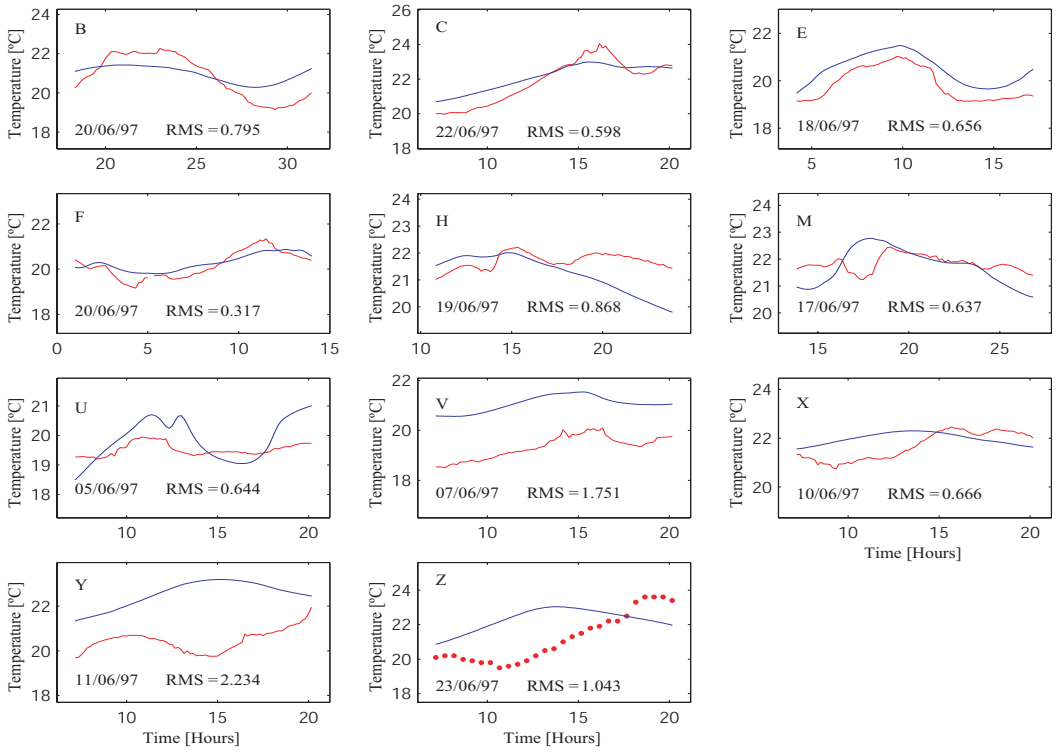

Figure 6.9: Comparison of water temperature time series for the stations used during the validation procedure. The measured data are plotted in red and the model's outputs are plotted in blue.

boundary conditions chosen for Mira and Ílhavo channels, because these stations are very close to the far end of these channels where the boundary conditions are imposed. At stations X, Y and Z the water temperature signal does not reflect the tidal variation at these locations. Instead, the results reflect a diurnal signal, i. e. the water temperature follows the air temperature temporal evolution with increasing between 8:00 h and 15:00 h and then decreasing until the end of the day. This may be explained by the morphological characteristics of the channels, which are very narrow and very shallow increasing the importance of the meteorological input.

However, from these results the salt and heat transport models may be considered validated, reproducing well the salinity and heat transfer processes in Ria de Aveiro.

6.5 Conclusions

The model used in this study - Mohid - seem to make use of an accurate bathymetry. In general, the horizontal grid resolves well the transport processes. The discrepancies revealed may be due to some uncertainties of the field data or the inadequacy in the use of a 2D depth-average model. In fact, as Dias [2001] pointed out, the field data used to calibrate and validate the transport models have some uncertainties related to the accuracy and resolution of the measuring instruments that were used, as well as with instruments failures and incorrect measuring procedures. The first are normally $\sim 0.1\%$

of the observed data and therefore may be neglected. The others may lead to large uncertainties and are very difficult to quantify. Therefore, a good quality of the field data should be guaranteed in order to achieve good model results.

Running a 2D depth-integrated model may be enough for studies of tidal time scale processes in a coastal lagoon like Ria de Aveiro. However, in deeper regions, such as the region from the mouth of the lagoon to the end of the Espinheiro channel, where stratification occurs, large vertical velocity shear is expected and a simple quadratic formulation for the bottom stress may be insufficient [Jenter and Madsen, 1989]. Therefore, a 2D depth averaged model may not be considered a good approximation, being a three-dimensional application the best modelling option.

Chapter 7

Horizontal patterns of water temperature and salinity in an estuarine tidal channel

This work presents results from two complementary and interconnected approaches to study water temperature and salinity patterns in an estuarine tidal channel. This channel is one of the four main branches of the Ria de Aveiro, a shallow lagoon located in the Northwest coast of the Iberian Peninsula. Longitudinal and cross-sectional fields of water temperature and salinity were determined by spatial interpolation of field measurements. A numerical model (Mohid) was used in a two-dimensional depth-integrated mode in order to compute water temperature and salinity patterns. The main purpose of this work was to determine the horizontal patterns of water temperature and salinity in the study area, evaluating the effects of the main forcing factors. The field results were depth-integrated and compared to numerical model results. These results obtained using extreme tidal and river runoff forcing, are also presented. The field results reveal that, when the river flow is weak, the tidal intrusion is the main forcing mechanism, generating saline and thermal fronts which migrate with the neap/spring tidal cycle. When the river flow increases, the influence of the freshwater extends almost as far as the mouth of the lagoon, and vertical stratification is established. Results of numerical modelling reveal that the implemented model reproduces quite well the observed horizontal patterns. The model was also used to study the hydrology of the study area under extreme forcing conditions. When the model is forced with a low river flow (1 $m^3 s^{-1}$) the results confirm that the hydrology is tidally dominated. When the model is forced with a high river flow (1000 $m^3 s^{-1}$) the hydrology is dominated by freshwater, as would be expected in such an area.

7.1 Introduction

Coastal lagoons are saline water bodies separated or partially isolated from the sea. They may be enclosed by one or more barrier islands, like Ria Formosa located in Algarve (in southern Portugal), as well as sand spits, and linked to the sea by one or more channels, which are small relative to the lagoon [Barnes, 1977, 1980], like Ria de Aveiro (in northern Portugal).

The main driving forces of circulation in a large number of estuaries and coastal lagoons are river flow at the head of the estuary, and changes in the sea level at the mouth of the estuary, which in turn determine the distribution of water properties like salinity and temperature, as well as the distribution of any other tracer. In coastal lagoons there are other forcing actions like precipitation to evaporation balance, wind stress and surface heat balance [Kjerfve, 1994] and they respond differently to these forcing actions.

Ria de Aveiro is the largest coastal lagoon in Portugal and the most dynamic in terms of physical and biogeochemical processes. It is a very important ecosystem in the region where it is situated due to the intense human activity in its waters and along its margins. In the last 20/30 years the lagoon was studied mainly from a biological and chemical point of view. There are not many studies or publications regarding the hydrology and physical processes of the lagoon. Despite this fact, a prior hydrologic study [Dias et al., 1999] reveals some of the main features of Ria de Aveiro. Records of water level, current velocity and thermohaline properties were performed at several stations in the lagoon during the summer seasons of 1996 and 1997. It was determined that the type of tide at the mouth of the lagoon is semi-diurnal and was observed that the astronomical tide is the main forcing driving water circulation in Ria de Aveiro. The tidal wave propagation in the lagoon has the characteristics of a damped progressive wave. According to this study Ria de Aveiro was found as a vertically homogeneous coastal lagoon. Nevertheless, some channels may reveal characteristics of a partially mixed estuary, depending on the freshwater input. The importance of the freshwater sources in the lagoon dynamics and of its seasonal effects remained to study until this work. The lagoon has been also studied through numerical modelling. These studies were performed to investigate topics as the tidal propagation in the lagoon [Dias et al., 2000], the lagrangian transport of particles [Dias et al., 2001] and studies of sediment particles [Lopes et al., 2001; Dias et al., 2003].

The lagoon has several freshwater sources, Vouga River being the most important one. This freshwater source is connected to the Atlantic through a channel located in the central area of the lagoon, Espinheiro channel. The major driving force is the tide, which together with the river runoff, determines the water mass behaviour in the channel. This channel is poorly known in terms of salt and heat transport processes, even though it is ideal to perform this kind of studies in Ria de Aveiro. The description of salinity patterns provides a basis for predicting the behaviour of other soluble substances, being suitable to study since the salt is a natural tracer. This study pretends to be a first step to better comprehend the interaction between the seawater and the freshwater within this system and to the understanding of its dynamics.

These studies require an enormous amount of field data, of salinity, water temperature and current speed, as well as the implementation of numerical models that combine hydrodynamic and transport modules. This contribution uses two complementary and interconnected approaches to study the water temperature and salinity patterns in Ria de Aveiro, combining field measurements with numerical modelling results. The main purpose of this paper is to determine the horizontal patterns of salt and water temperature in the Espinheiro channel and evaluating the importance of the main forcing mechanisms: tides and incoming river flow. To achieve this intention, a short description of the first annual

observational program of the hydrological properties in Ria de Aveiro will be given. Vertical profiles of salinity and water temperature were measured along the channel. These measurements were taken at spring and neap tides and the data obtained were used to interpolate longitudinal fields of these variables. An estimation of the river flow for the survey periods was also performed. Results will be presented and discussed, that reflect the influence of river flow and spring and neap tide conditions in the spatial distribution of the referred hydrological properties. Another aim of this work is to implement a transport model in a two-dimensional mode for the lagoon's entire area, with a closer look at its central area. The model used was Mohid - Water Modelling System, a finite volume model that combines hydrodynamic and transport modules.

7.2 The study area

The study area is situated in the very complex central area of Ria de Aveiro, a mesotidal and shallow (mean depth ~1 m) coastal lagoon located in the northwest Atlantic coast of the Iberian Peninsula. It includes two distinct regions: the first extending from the mouth of the lagoon to near section 5 (see fig. 7.1 for reference) and the second is the Espinheiro channel, extending from section 5 to near section 10. The study area is approximately 11 km long, has an average width of about 200 m and a mean depth, along its longitudinal axis, of about 10 m. The tides are semi-diurnal and they represent the major driving force of circulation in the lagoon [Dias et al., 1999].

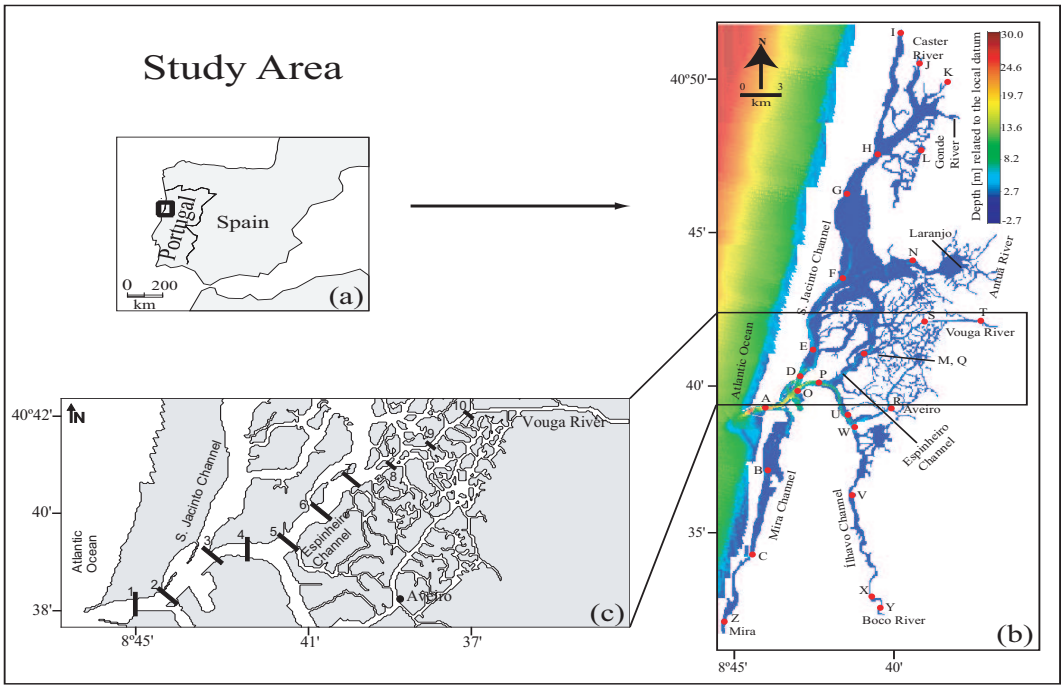

Figure 7.1: Study area, with reference to the location of the stations used to calibrate the hydrodynamic and transport model and the location of the ten cross-sections.

The estimated tidal prism for the lagoon at extreme spring and extreme neap tide is 136.7×10^6 and 34.9×10^6 m^3, respectively (tidal range of about 2 m) [Dias, 2001]. For the Espinheiro channel is about 40×10^6 at extreme spring tide and 15×10^6 m^3 at extreme neap tide [Dias, 2001]. The total estimated freshwater input for the lagoon is very small (about 1.8×10^6 m^3 during a tidal cycle) [Moreira et al., 1993] when compared with the tidal prism at the mouth or at the beginning of Espinheiro channel. Despite the fact that rivers have a small contribution in terms of water input, when compared to the tidal prism, they may have a long term-influence in the residual transport [Dias et al., 2003]. Dias et al. [2000] and Dias [2001] showed that the tide is strongly distorted as it progresses from the mouth toward the end of each channel of the lagoon, due to the channels geometry and bathymetry. The general characteristics of the tidal wave are those of a damped progressive wave. In shallow areas the tidal wave assumes the main characteristics of a standing wave. From a dynamical point of view the study area may be considered the most important in Ria de Aveiro, because here the strongest currents are observed, reaching values higher than 2 ms^{-1}. The lagoon's other channels are mainly shallow and tidal flat areas, contributing to a strong damping of currents.

7.3 Numerical models

7.3.1 The hydrodynamical and transport models

The numerical model adopted in this study was Mohid - Water Modelling System [Martins et al., 2001] developed by Maretec - Marine and Environmental Technology Center, IST, Lisbon. Mohid is a three-dimensional finite volumes model [Chippada et al., 1998], which uses an Arakawa-C grid [Arakawa and Lamb, 1977] to perform the computations. In this approach the discrete form of the governing equations are applied macroscopically to the cell control volume. The grid is therefore defined explicitly and the equations are solved using the same procedures, irrespectively of the cell geometry. Since the equations are solved in the form of flux divergences, this method guarantees the conservation of transported properties [Ferziger and Peric, 1995; Vinokur, 1989]. It uses an ADI - Alternate Direction Implicit scheme for the resolution of the equations. Two numerical schemes are implemented: the four equations S21 scheme [Abbott et al., 1973] and the six equations Leendertse scheme [Leendertse, 1967]. This model assumes the hydrostatic equilibrium, as well as the Boussinesq approximation and uses a vertical double sigma coordinate with a staggered grid.

The hydrodynamic governing equations are the momentum and the continuity equations. The hydrodynamic model solves the primitive equations in Cartesian coordinates for incompressible flows. The momentum and mass evolution equations are:

$$\begin{aligned}\frac{\partial u_i}{\partial t}+\frac{\partial (u_i u_j)}{\partial x_j} &= -\frac{1}{\rho_0}\frac{\partial p_{atm}}{\partial x_i}-g\frac{\rho(\eta)}{\rho_0}\frac{\partial \eta}{\partial x_i}-\frac{g}{\rho_0}\int_{x_3}^{\eta}\frac{\partial \rho'}{\partial x_i}dx_3 \\ &+ \frac{\partial}{\partial x_j}(\upsilon\frac{\partial u_i}{\partial x_j})-2\varepsilon_{ijk}\Omega_j u_k \end{aligned} \quad (7.1)$$

$$\frac{\partial \eta}{\partial t} = \frac{\partial}{\partial x_1}\int_{-h}^{\eta} u_1 dx_3 - \frac{\partial}{\partial x_2}\int_{-h}^{\eta} u_2 dx_3 \tag{7.2}$$

where u_i are the velocity vector components in the Cartesian x_i directions, η is the free surface elevation, υ is the turbulent viscosity and p_{atm} is the atmospheric pressure. ρ is the density and ρ' its anomaly, ρ_0 is the reference density, g is the acceleration of gravity, t is the time, h is the depth, Ω is the Earth's velocity of rotation and ε is the alternate tensor.

The model also solves a transport equation for salinity and temperature or any tracer. The advection-diffusion equation reads:

$$\frac{\partial \alpha}{\partial t} + u_j \frac{\partial \alpha}{\partial x_j} = \frac{\partial}{\partial x_j}(K \frac{\partial \alpha}{\partial x_j}) + FP \tag{7.3}$$

where α is the transported property, K is the diffusion coefficient and FP is a possible source or sink term.

The bottom shear stress ($\vec{\tau}$) is imposed using the formulation proposed by Chézy [Dronkers, 1964], where ($\vec{\tau}$) is proportional to the velocity squared (7.4) and the drag coefficient (C_D) can be parameterized in terms of the Manning friction coefficient (n) (7.5):

$$\vec{\tau} = C_D \mid \vec{V} \mid \vec{V} \tag{7.4}$$

$$C_D = g n^2 H^{-1/3} \tag{7.5}$$

where $\vec{V}$ is the horizontal velocity vector, n is the Manning coefficient and H is the depth of the water column.

7.3.2 Boundary conditions

Five types of boundaries were used in this study: free surface, bottom, lateral closed boundary, lateral opened boundary and moving boundary.

Elevation at the open boundary is specified from the tidal constituents obtained using measurements of sea surface elevation from a tidal gauge located at the mouth of the lagoon. Salinity and water temperature are also imposed at the ocean open boundary, and are considered constant in this work. At the river boundaries the river flow is imposed and salinity and water temperature are assumed constant in each simulation (varying in each case study). The lateral boundary condition at coastal boundaries is a free slip condition, imposed by specifying a zero normal component of mass and null momentum diffusive fluxes at cell faces in contact with land. No fluxes at the bottom and surface were considered. Moving boundaries are closed boundaries whose position varies in time. This situation occurs in domains with intertidal zones like Ria de Aveiro. In this case the uncovered cell must be tracked. A criterion based on Figure 7.2 is used.

$HMIN$ is a minimum depth below which the cell is deemed to be dry, thus, conserving a thin volume of water above the uncovered cell. The cells in position i, j are considered uncovered when

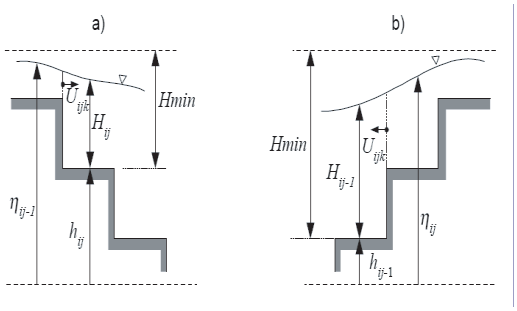

Figure 7.2: Conditions for a point to be considered uncovered (moving boundaries).

one of the two following conditions occurs:

$$H_{ij} < HMIN \text{ and } \eta_{ij-1} < -h_{ij} + HMIN \tag{7.6}$$

$$H_{ij-1} < HMIN \text{ and } \eta_{ij} < -h_{ij-1} + HMIN \tag{7.7}$$

where $H = h + \eta$ is the total depth. The second condition of 7.6 assures that the cell is not being covered by waves propagating from left to right and the second condition of 7.7 assures that the cell is not being covered by waves propagating from right to left. The model performs the same test in the i direction. The noise resulted from the abrupt variation in the velocity of the dry cells is controlled by a careful choice of $HMIN$ (in this case $HMIN = 0.1$ m) [Leendertse and Liu, 1978].

7.3.3 Application to the Ria de Aveiro

Due to the lagoon complex geometry and in order to decrease the computational effort a variable spatial grid step was developed. This grid has 429 by 568 cells, with dimensions ranging from 40 by 40 m (to obtain a higher resolution) in the central area of the lagoon where the channels are very narrow (represented in Figure 7.1c), to 40 by 100 m in the northern and southern areas, due to the orientation of the channels (north-south). The numerical bathymetry used was developed from data concerning depth obtained from a general survey carried out by the Hydrographic Institute of the Portuguese Navy in 1987/88. More recent bathymetric data, obtained from recent dredging operations in several channels (1998) and close to the lagoon's mouth (2002), were also used. The water depth at each grid point was computed, from the water volume of the cell, using a Monte Carlo cubature method [Dias, 2001].

The model was forced imposing at the oceanic open boundary the sea surface elevation determined from 38 tidal constituents, obtained through harmonic analysis [Pawlowicz et al., 2002] of values, measured during 2002 in a tidal gauge located at the mouth of the lagoon. At this open boundary the water temperature and salinity were considered fixed in each simulation, with values of 15 °C and 36 practical salinity units (psu), respectively. At the channel's head river flow values estimated for the survey periods, with values between 2 m^3s^{-1} and 116 m^3s^{-1} were imposed. The

water temperature and salinity of Vouga River were fixed for each simulation, with values ranging between 22 °C (September) and 11 °C (December) for the water temperature and a fixed value of 1 psu for the salinity. The time step is 10 s and the horizontal viscosity is 5 m^2s^{-1}. Initial conditions for the hydrodynamic model are null free surface gradients and null velocity in all grid points. For the transport model these are salinity and water temperature fields, obtained by interpolation of data collected in the study area on the autumn of 2003. For the transport model more realistic initial values were adopted because the time to reach dynamic equilibrium for these variables is much longer than that for tides and tidal currents. A value of 5 m^2s^{-1} was adopted for both salt and heat diffusion coefficients.

The numerical model was implemented in a 2D horizontal mode for the entire area of the lagoon. The goal was to reproduce the distribution patterns of salinity and water temperature in the entire lagoon, with a closer look at the study area described in section 7.2. Several simulations were performed in order to reproduce various field survey periods and to determine the horizontal patterns of salinity and water temperature under extreme tidal and river flow forcing conditions.

The hydrodynamic model was previously calibrated [Vaz et al., 2004] and validated for Ria de Aveiro. From the observation of sea surface elevation data it is concluded that there is tidal energy damping, due to friction, as the tidal wave propagated toward the end of the channels. In the case of Ria de Aveiro this behavior was analyzed by Dias and Fernandes [2006]. The magnitude of the bottom friction coefficient determines changes in the tidal wave propagation within the lagoon. The bottom roughness was parameterized from Manning coefficients; therefore the model parameter subjected to adjustments in the calibration process is the bottom friction coefficient. The procedure used to calibrate the model consisted in the spatially varying the bottom roughness by assigning Manning values to specific regions of the numerical domain.

The calibration procedure was performed comparing the harmonic constituents of the main tidal constituents determined from computed time series of sea surface elevation to those obtained from observed data for 24 stations located throughout the main channels of the lagoon. The data available was 1987 and 1988 data obtained from a field survey carried out by the Portuguese Navy. The better adjustment between computed and observed data was obtained for Manning coefficients ranging between 0.022 $m^{1/3}s^{-1}$ and 0.045 $m^{1/3}s^{-1}$. Figure 7.3 shows the comparison for the M_2 constituent, which is the most important tidal constituent in this lagoon. It represents about 90% of the tidal energy in Ria de Aveiro. For this constituent the mean phase and amplitude difference, for all 24 stations, is 3° and 3 cm, respectively. One error of 1° corresponds to about 2 minutes departure in the arrival of high tide for a semi-diurnal constituent, which means that the average difference between field and model data is about 6 minutes for the M_2. The validation procedure consisted in comparing simulated sea level and current velocities with observed data for 11 stations obtained in the summer of 1997. The Root Mean Squared Errors (RMS) of the sea level values are typically around 5% of the local tidal amplitude.

A current velocities comparison for three stations is presented in Figure 7.4.

Regarding current velocity there are some discrepancies between the field and model data when

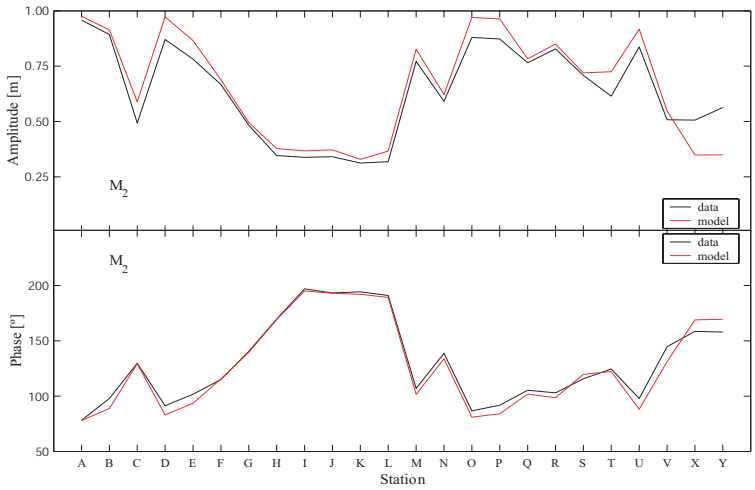

Figure 7.3: Comparison between tidal amplitude and phase for M_2 constituent for data and model results, plotted on each station used in the model calibration.

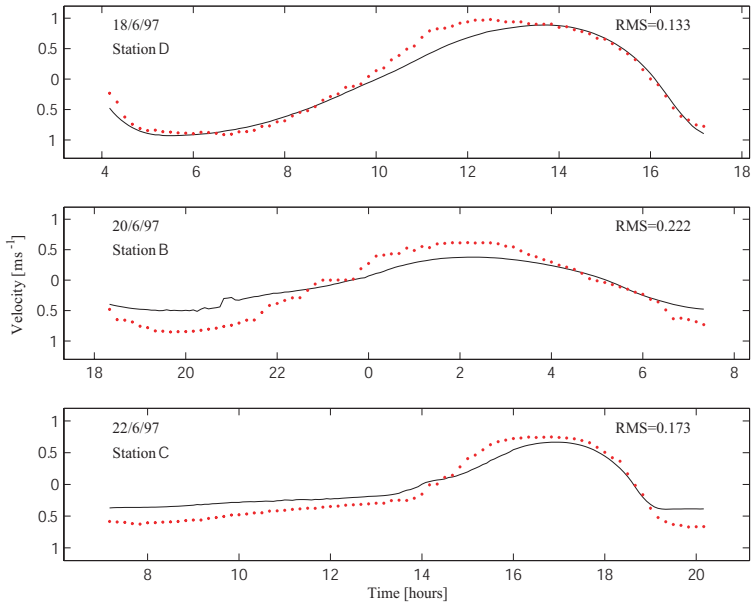

Figure 7.4: Comparison between time series of main flow directions velocities of data (dots) and model results (line), plotted for some of the stations used in the model validation.

assessing point by point. The RMS error for these three stations is lower than 30% of the current amplitude (the better adjustment is for station D with a RMS error of 6%). Nevertheless, the model does properly simulate the temporal variation of the current velocity considered in terms of the current phase.

Results of the calibration and validation processes indicate that a good implementation of the hydrodynamic model was achieved. The agreement between computed and observed time series of sea surface elevation rounds a RMS of 5% of the local tidal amplitude for almost all the stations.

Also, a good agreement for current velocities was achieved as shown in Figure 7.4. When comparing current velocities values it is important to remember that this variable varies rapidly in space, both in magnitude and direction, from point to point. This behavior reflects the irregular area geometry and it produces higher discrepancies between field and model results. Besides, the model results are related to the mean value over the vertical and horizontal spatial domain corresponding to the grid size, while the field data corresponds to a single point or, at best, an average over various points.

The transport model was also calibrated. This procedure was achieved by comparing computed and observed short time series of salinity and water temperature for 7 stations in the lagoon. The available data were from July 1996, representing a typical summer situation. A salinity and water temperature comparison for station B is depicted in Figure 7.5, showing a good agreement between computed and observed data of salinity and water temperature.

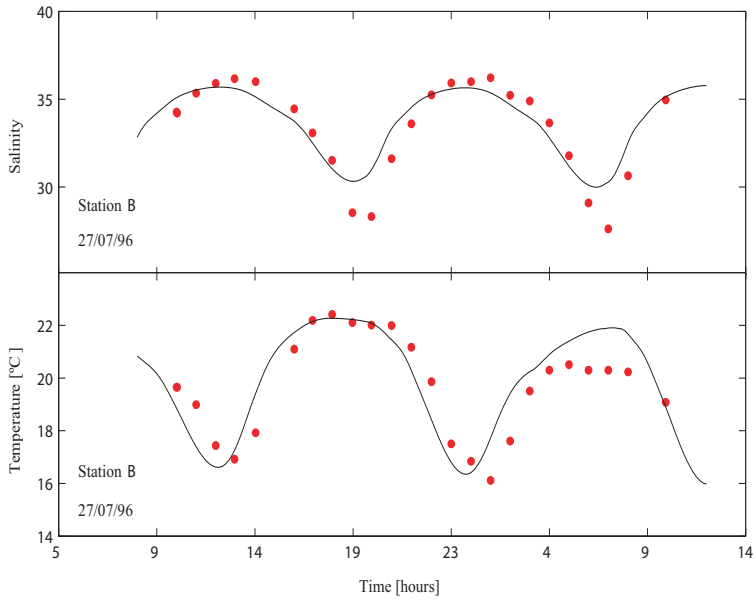

Figure 7.5: Comparison between data (dots) and model results (line) time series of salinity and water temperature, for one station used in the calibration of the transport model

During low tide were found differences of about 1 and 3 psu between the model and field salinity data for all the stations used in the transport calibration. At high tide, the differences are lower than 1 psu. Regarding the water temperature, were found differences, at low tide, of about 3 °C in some of the stations. In shallow systems like Ria de Aveiro the water temperature is ruled not only by the tidal propagation and the incoming river flow but also by meteorological factors. The air temperature, relative humidity, cloud cover and incoming solar radiation are very important due to the small depth of the water column. In the future, to improve the water temperature results, the exchanges between the water and the air will be included in the runs. Despite this fact, after these results both the hydrodynamical and transport models can be considered calibrated.

7.4 Field surveys

7.4.1 Materials and methods

In situ vertical profiles of hydrological properties, such as water temperature and salinity were measured in ten cross-sections (Figure 7.1) separated by 1000 meters using a mini STD model SD204. The survey period lasts from September 2003 until September 2004, but for the purpose of this study only the autumn results are analyzed (see Table 7.1).

Table 7.1: Autumn sample periods

Date	Tide	Tidal height [m^3s^{-1}]	River flow [m^3s^{-1}]
29/09/2003	spring	2.7	2.06
02/10/2003	neap	1.6	6.11
28/10/2003	spring	2.8	5.44
06/11/2003	neap	2.0	52.62
25/11/2003	spring	2.8	72.74
05/12/2003	neap	1.7	115.97

The first cross-section is located near the mouth of the lagoon and the last one is located near the channel's head, close to the mouth of the Vouga River. The *in situ* measurements were performed two times per month at spring tides (maximum of tidal amplitude) and at the following neap tide (minimum of tidal amplitude), and started approximately 1h 40min after the low tide hour predicted for section 1, during the flood stream. The profiles of salinity and water temperature were obtained at three points in every section: near the margins of the channel and in its axis.

In order to obtain the incoming freshwater flow from Vouga River, concurrent with the survey periods, measurements of current speed were also performed. These measurements were obtained using a Valeport current meter model 105 and were performed several kilometers upstream from the river mouth, 3 hours after the low tide hour predicted for the lagoon mouth. This procedure guarantees that the measurements of current speed were made outside the region of tidal flood influence.

Longitudinal and cross-sectional fields of water temperature and salinity were determined by spatial interpolation of the measured data using an ordinary Point-Krigging method [Cressie, 1993]. The longitudinal fields were computed for three different depths: near surface, half water column and near the channel's bed. Depth integrated longitudinal fields of water temperature and salinity were also computed. These last results were compared to the results of the 2D depth-integrated model used in this study. These longitudinal fields act like synoptic snapshots of the channel in terms of water temperature and salinity.

7.5 Results and discussion

After being calibrated the hydrodynamic and transport models have been used to study the hydrodynamics and transport of salt and heat in Ria de Aveiro. Several runs were performed to characterize

the dynamics of the lagoon, with a closer look at its central area, in terms of the water temperature and salinity behavior, considering different tidal and river runoff forcings.

Short runs of the model were carried out, covering the field survey periods for several spring/neap cycles in the autumn of 2003. The results of the model simulations were compared to the field results to prove the ability of the implemented model to reproduce the salinity and water temperature patterns in the study area.

In order to analyze the behavior of the study area under extreme conditions several runs of the model were also performed under conditions of high/low river runoff and astronomical tide forcing (neap/spring tidal forcing).

For the entire study area and for extreme conditions of river runoff and tidal forcing the fractional freshwater concentration [Dyer, 1997] was also computed:

$$f = 1 - \frac{S_n}{S_s} \tag{7.8}$$

where S_s is the salinity of the undiluted sea water and S_n is the mean salinity in a given segment of the estuary. The goal was to determine the relative importance of spring or neap tide forcing and of high or low river runoff forcing in the establishment of salinity and water temperature patterns in the study area.

7.5.1 Field surveys

The mean Vouga River runoff estimated for the period from September to December was about 42.5 m^3s^{-1}, with a minimum value of 2.06 m^3s^{-1} (September) and a maximum of 115.97 m^3s^{-1} (December). The autumn of 2003 may be considered a dry season when compared to previous years [Dias, 2001]. Results of salinity and water temperature for these extreme cases will be analyzed and discussed. In this period the tidal amplitude ranges from a minimum of 1.6 m on October 2^{nd} and a maximum of 2.8 m in all the spring's dates.

Figure 7.6 illustrates the differences in the distribution patterns of salinity in the case of two neap tide periods (tidal amplitudes of 1.6 and 1.7 m) and in conditions of low and high river flow (6.11 and 115.97 m^3s^{-1}) for three different depths: surface, mid water and near the bed. In the case of the low river flow, the channel can be considered nearly vertically homogeneous and highly saline, almost as far as section 8, where a saline front is observed. Close to the channel's head, the relative effect of the freshwater inflow increases and values of salinity between 6 (surface) and 11 psu (bottom) are observed. For the high river flow, the effect of the freshwater extends to the mouth of the lagoon, mainly in the surface layer, leading to vertical stratification (near the surface, the salinity is about 22.5 psu and near the bottom is about 32.5).

The longitudinal gradients of water temperature are less perceptible (weaker) than those of salinity, both in spring and neap tide conditions. As an example, the water temperature values ranges between 11 and 14 °C in the neap tide period of December 5^{th}, while the salinity gradient ranges

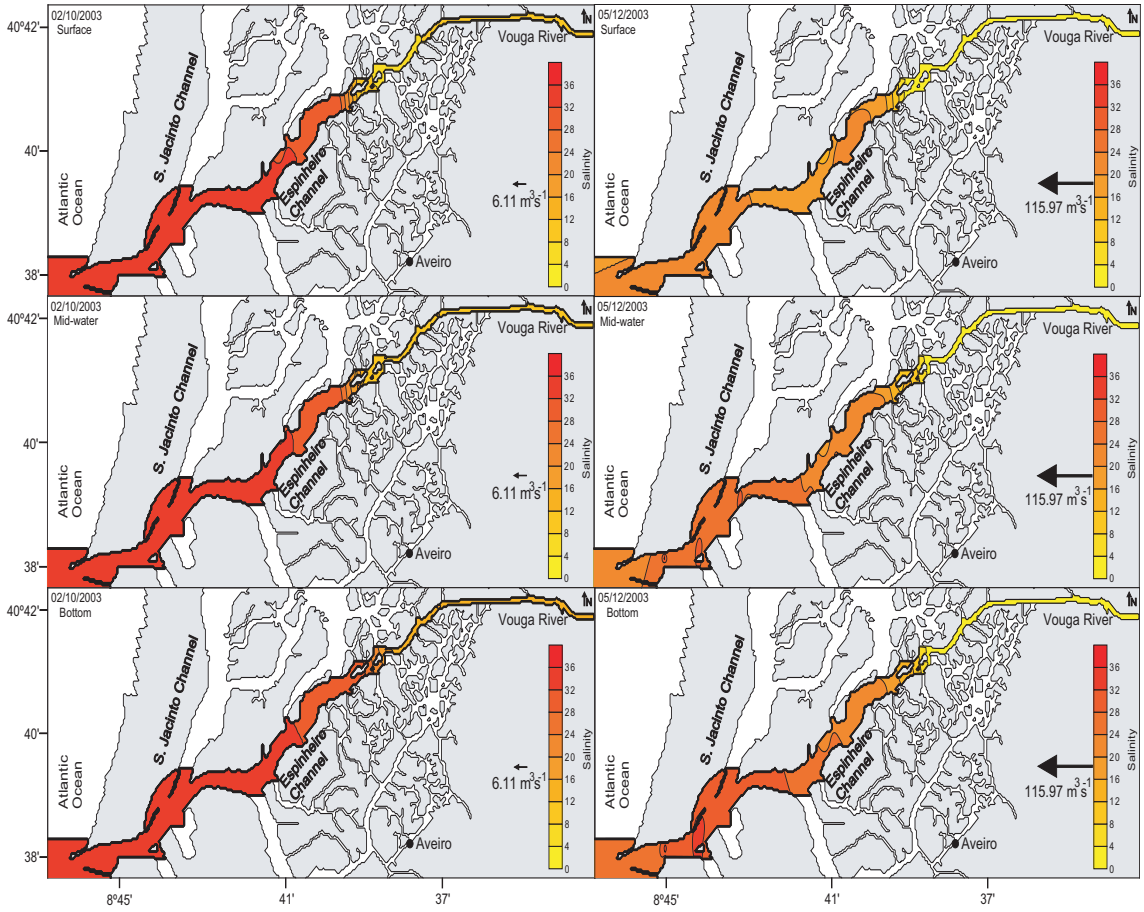

Figure 7.6: Surface, mid-water and bottom salinity distributions. Neap tide periods of 2/10/2003 and 5/12/2003. River flow of 6.11 m^3s^{-1} and 115.97 m^3s^{-1}.

between 0 and 28 psu (depth average values). However, the temperature patterns are similar to those discussed for the salinity.

The effect of the river runoff increase at the mouth of the lagoon is shown in the cross-sectional distribution of salinity at section 1 for the cases presented in Figure 7.6. These results (see Figure 7.7) reveal the influence of the low and high river flow at section 1. When the river flow is weak, the cross-sectional distribution of salinity is almost vertically homogeneous and the water column is mainly saline. When the river runoff is high, the freshwater influence is felt even at the lagoon's mouth, being established a vertical gradient of salinity, ranging from ~20 at the surface to ~35 psu at the bottom. At the channel's head the river flow induces an opposite effect. When the river flow is high the cross-sectional salinity distribution is almost vertically homogeneous (water column characterized by freshwater) and when the river flow is weak a vertical stratification is established.

The field results show that when the river flow is weak (with values ranging between 2 and 6 m^3s^{-1}), the saline intrusion goes further along the channel than under strong freshwater runoff. Even in the case of low river flow, the channel's head is mainly filled by freshwater and as the saline

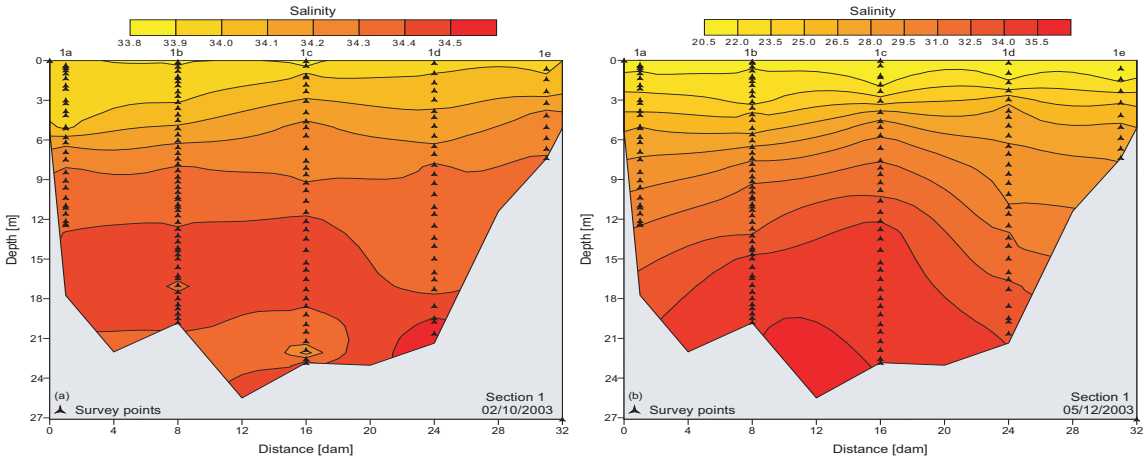

Figure 7.7: Salinity cross-sections at section 1. Survey days: Neap tide periods of (a) 2/10/2003 and (b) 5/12/2003. River flow of: (a) 6.11 m^3s^{-1} and (b) 115.97 m^3s^{-1}.

intrusion goes further along the channel's bed than along the surface, the vertical stratification is higher near the channel's head than in the rest of the channel. In these cases the hydrodynamics of the study area are determined mainly by the tide. In the opposite case, when the river flow is high, the freshwater extends its influence toward the lagoon's mouth leading to vertical stratification along most of the channel.

Saline and thermal fronts are generated between sections 8 and 9 in spring tide periods. These fronts are probably generated as a response to bathymetric features and river runoff variability. In this region, the channel's depth changes abruptly (from 10 m to ~2 m) and the tidal excursion reaches the region of freshwater influence, where the salty water (more dense) mixes with the incoming freshwater leading to a pronounced horizontal gradient of salinity and water temperature. These fronts could migrate with the spring/neap tidal cycle and with changes in the river flow. In fact, these fronts are the boundary between two distinct areas of this channel: the first one extends from the mouth of the lagoon until near section 7 and it is dominated by the tidal flux; the other is one area that could be considered as the fluvial estuary of the Vouga River, being characterized by freshwater inputs but still subjected to tidal effects.

At neap tides, these strong horizontal gradients are observed between sections 7 and 8, about 1 km closer to the mouth of the lagoon, because the saline intrusion does not extend so far in this case due to smaller tidal prisms and current velocities.

For similar freshwater inputs the salinity difference between the mouth of the lagoon and the channel's head is larger at neaps than at springs, when the tidal currents are stronger and the oceanic water intrusion goes further within the channel. The relative effect of the river flow in the horizontal patterns of salinity and water temperature is stronger at neaps, when the tidal currents are weaker.

In Figure 7.8 are depicted the along channel depth averaged salinity (7.8a and 7.8b) and water temperature (7.8c and 7.8d) values. From 7.8a and 7.8b is perceptible that when the river flow is similar (September and October data) the tidal excursion goes further upstream in spring than in neap

tide (~1 km), due to the higher velocity currents. When the end of the autumn is closer, the river flow increases and its effect become more important in the establishment of the salinity patterns than the tidal effect. The freshwater influence extends itself until section 6. When the river flow is 115.97 m^3s^{-1}, the influence of the freshwater extends almost section 3 (1 km from the mouth of the lagoon) with salinities lower than 30 psu.

Figures 7.8c and 7.8d show the autumn variation of the water temperature along the channel. It can be observed that the water temperature values decay along the season and that exists an inversion of the temperature gradients between the beginning of the autumn and its end. In fact, in September and October the oceanic temperatures values are lower than the river ones, and in November and December it is noticeable the opposite. The figures previously depicted show that the sample strategy is correct and the data are reliable.

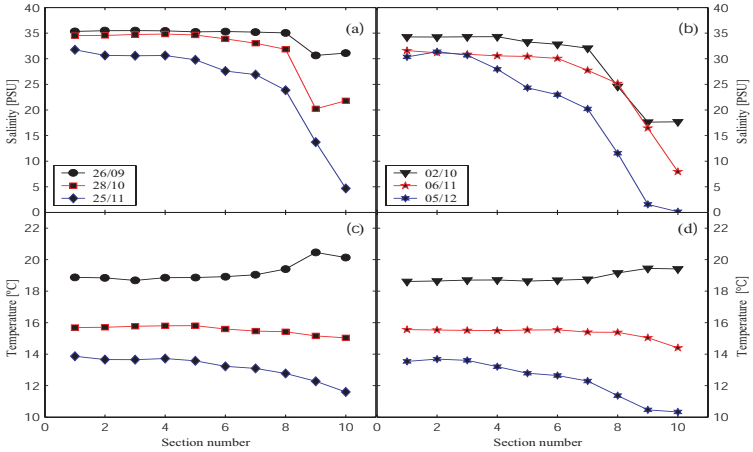

Figure 7.8: Depth-averaged along channel salinity and water temperature values. Springs (7.8a and 7.8c): 26/09 (river flow = 2.06 m^3s^{-1}), 28/10 (river flow = 5.44 m^3s^{-1}) and 25/11 (river flow = m^3s^{-1}). Neaps (7.8b and 7.8d): 02/10 (river flow = 6.11 m^3s^{-1}), 06/11 (river flow = 52.62 m^3s^{-1}) and 05/12 (river flow = 115.97 m^3s^{-1}).

7.5.2 Observed data / model data

Model simulations were performed for the periods corresponding to the field surveys, forcing the model with the freshwater inputs determined in the field work. The purpose of these short simulations was to find out if the numerical model is able to reproduce the measured saline and thermal fronts in such a complex area.

Figure 7.9 shows the numerically computed and observed depth integrated fields of water temperature for the neap tide period of October 2^{nd} (low river flow - 6.11 m^3s^{-1}) and December 5^{th} (high river flow - 115.97 m^3s^{-1}). The results of the 2D depth integrated model are consistent with the measurements, as shown in the figure. The model results and the measurements reveal similar patterns in the longitudinal distribution of salinity (not shown) and water temperature. The thermal and saline (not shown) fronts are well reproduced by the model as shown in Figures 7.9a and 7.9b. The model

results show the thermal front placed in the exactly same area as revealed by the measurements. When the river flow increases, the effect of the freshwater inflow in the channel is well reproduced by the transport model. The numerical results reproduce the observed longitudinal gradient of water temperature, which extends from the channel's head until the lagoon's mouth, where values of 14 °C are observed in both situations. Therefore, it can be considered that a 2D depth integrated model is a reliable tool to study transport processes in shallow areas like Ria de Aveiro.

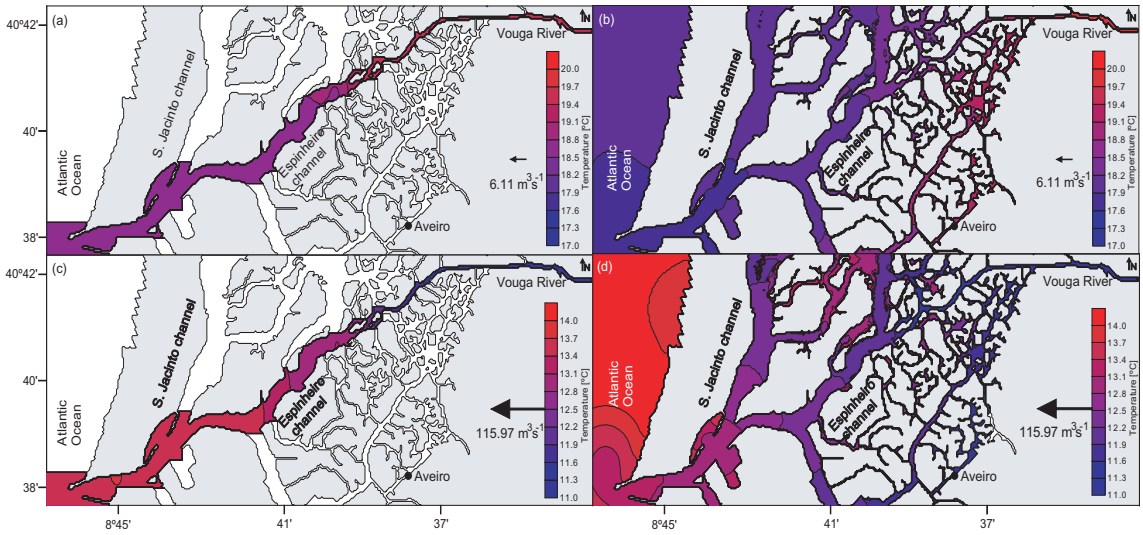

Figure 7.9: Depth-integrated water temperature fields. (a) and (c) field data, (b) and (d) computed data. (a) and (b) neap tide period of 02/10/2003, river flow of 6.11 m^3s^{-1} and (c) and (d) neap tide period of 05/12/2003, river flow of 115.97 m^3s^{-1}.

7.5.3 Salinity and water temperature distributions under extreme forcing conditions

Once the numerical model is considered able to reproduce the reality it can be used to perform several other studies. One of these studies is to evaluate how the study area responds to changes in the forcing factors and determine the establishment of salinity and water temperature longitudinal patterns under different forcing conditions. As previously proved these studies can be performed using the model in a horizontal two-dimensional mode. In this case the simulations were performed under extreme forcing conditions of astronomical tidal forcing and high and low river flow.

Vicente [1985] presents values correspondent to flood flows for periods of 25 and 100 years of 3400 and 4100 m^3s^{-1}, respectively. Another study by Castanho et al. [1968] presents values for the maximum daily flow, for return periods of 1, 5, 10 and 25 years, of 505, 875, 960 and 1020 m^3s^{-1}. Meanwhile, Castanho et al. [1968], present values of minimum flow of the order of 1 m^3s^{-1}. The model simulations were performed using river flows of 1 m^3s^{-1} and 1000 m^3s^{-1}. These values can be considered extreme taking into account the values presented in this paragraph.

Figure 7.10 shows results of the longitudinal salinity fields for 2 different situations: (a) spring tide combined with river flow of 1000 m^3s^{-1} during high tide and (b) neap tide with river flow of

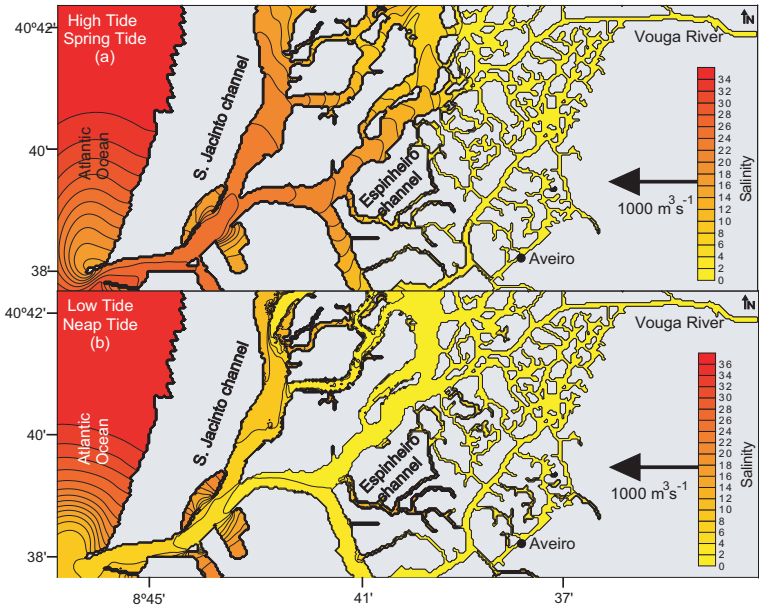

Figure 7.10: Depth integrated salinity fields (model results). (a) High tide, spring tide, river flow of 1000 m^3s^{-1}. (b) Low tide, neap tide, river flow of 1000 m^3s^{-1}.

1000 m^3s^{-1} during low tide. The 2D depth integrated results using a river flow of 1 m^3s^{-1} are not shown because they are almost redundant concerning the results shown in section 7.5.1.

When the low tide is reached, the model results are in agreement with the expected pattern of salinity both in spring (not shown) and neap tide periods. In fact, these results reveal that, in this case, the freshwater extends throughout all the study area (including the coastal zone) revealing that the Vouga River influence is very important in the establishment of the hydrology of the study area during flood periods. Therefore, due to the relatively small channel dimensions very low salinity values are obtained for the outside of the lagoon both at neap tide (between 7 and 9 psu) and at spring tide (between 5 to 8 psu) when the currents are higher.

During flood periods, the tide pushes the freshwater upstream revealing that, even in this extreme situation of river flow, the salinity intrusion is very significant along the length of the study area. When the high tide is reached, a longitudinal salinity gradient is established both at neaps (not shown) and springs. However, even at high tide, salinity at the lagoon's entrance is lower than the typical ocean values (around 36 psu), as found in the previous cases of low river flow. The freshwater that leaves the lagoon during the ebb dilutes the oceanic water in the coastal region near the lagoon's mouth. During the flood this freshwater enters the lagoon and mixes with the freshwater incoming from Vouga. The values of salinity in the mouth of the lagoon are between 22 and 25 psu in spring and neap tide, respectively. The patterns of water temperature are the same as the discussed for salinity.

The fractional freshwater concentration [Dyer, 1997] was also computed for two of the studied situations: minimum freshwater and maximum freshwater within the estuary. The results are depicted in Figure 7.11 and show that the minimum amount of water within the channel occurred in spring

tide conditions with a low river flow of 1 m^3s^{-1} when the high tide is reached (Figure 7.11a). In this case, values lower than 0.1 were found almost up to the channel's head, revealing that in the study area, there is almost no dilution of the salt water coming from the ocean. The saline intrusion goes further upstream than in any other case and the channels are filled with salt water. In this situation the hydrology is completely tidally dominated. The maximum freshwater within the channel occurred in the case of neap tide conjugated with an extreme river flow of 1000 m^3s^{-1}, when the low tide is reached (Figure 7.11b). Values ranging between 0.7 and 0.8 were found from the channel's head up to the lagoon's mouth. In this case the hydrology of the channels is strongly dependent on the Vouga River forcing and the study area is filled with freshwater.

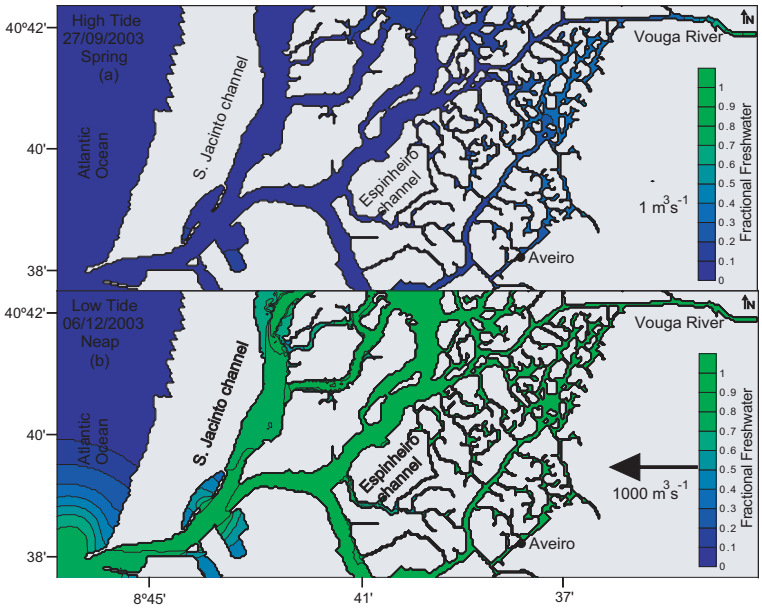

Figure 7.11: Fractional freshwater concentrations. (a) minimum quantity of water within the channel (high tide, spring tide period of 26/09/2003) and (b) maximum quantity of water within the channel (low tide, neap tide period of 06/12/2003).

7.6 Conclusions

The spatial and temporal distribution of hydrological properties, like salinity and water temperature, in a system like the one studied in this work, is strongly dependent on the balance between the spring/neap tidal cycle and the river flow. Observations reveal the existence of vertical stratification in the study area when the river runoff is high. The salty water, more dense, develops within the channel through the bottom layer, near the channel's bed, and the freshwater through the top layer, revealing a typical estuarine behavior.

Results obtained using field data show a strong horizontal gradient of salinity and water temperature which migrates with the spring /neap cycle. This strong horizontal gradient seems to mark the

boundary between two distinguished sectors: a marine estuary, in close connection with the sea and an upper fluvial estuary characterized by the freshwater from the river but still subject to a semi-diurnal tidal effect. In this channel, for low river flow, these estuarine fronts migrate from between section 7 and 8 to between section 8 and 9 (about 1 km), depending if the tide is a neap or a spring one, respectively.

The model used in a two-dimensional horizontal depth integrated mode reproduces the main features found from the field data. When the river flow is weak, the saline and thermal fronts are well reproduced by the model as previously showed. When the river flow is high, even thought the model results are consistent with the expected patterns, it would be more adequate to study the transport processes using the model in a three-dimensional mode, in order to reproduce the vertical stratification found from the measurements. Due to the complexity of the study area, this is a very difficult task, which is presently being performed. It can be considered that Mohid was successfully implemented and that it is a useful tool to study transport processes in complex estuarine environment.

Results obtained with a Lagrangian approach by Dias et al. [2003] are in agreement with the present conclusions confirming the importance of these channels from the hydrodynamic and transport perspective. Trajectories of passive tracers released along the channel revealed that the transport was towards the lagoon's mouth. These results indicate the low residence time of the central area of the lagoon and the importance of the water exchanged between the channel and the ocean.

In the future results from the three-dimensional model will be studied in order to perform better hydrodynamic and transport studies in this area.

Chapter 8

Three-dimensional modelling of the Espinheiro Channel

A 3D baroclinic model (Mohid) is used to perform hindcast simulations in a tidal channel: Espinheiro Channel (Portugal). These simulations are conducted for four distinct periods where markedly different river discharges and tides occurred, and the outputs are compared with time series measurements and synoptic thermohaline data. The model reveals its ability in reproducing observed temporal variability in sea level height and along channel velocity, presenting skill coefficients higher than 0.85. The model qualitatively reproduces along-channel thermohaline distributions at three different vertical levels, during low-to-medium river inflow, underestimating the salinity stratification when the river flow is high (higher than 100 $m^3 s^{-1}$). In general, the trends inferred from the observation are reproduced by the numerical model.

The residual currents were calculated revealing an ebb-dominated channel, with more intense ebb current near the surface, due to the freshwater incoming from the landward boundary, and less intense ebb current near the channel's bed. The cross-sectional tidally-averaged structure of salinity and longitudinal velocity analyzed near the channel's mouth and ~4 km upstream reveal ebb residual currents near the south shore and flood residual currents near the north shore under low-to-medium river discharge. When the river discharge is high (higher than 100 $m^3 s^{-1}$), the channel is nearly laterally homogeneous in terms of salinity and residual velocity presenting a two-layer structure with flood currents near the bottom and ebb currents at the top layer. The salt transport was also analyzed and follows the same patterns found in the cross-sectional residual velocity.

The cross-sectional vertical structure of the channel, near its mouth, presents well mixed characteristics during high water, turning to partially stratified at low water. At mid channel the vertical cross-sectional structure turn from weakly-to-strongly stratified during the tidal cycle. Near the channel's mouth, the water exchange is mainly driven by the tidal forcing, except under high river flow events when the freshwater extends its influence from the channel's head to its mouth.

8.1 Introduction

Espinheiro channel is a tidal channel located in the central area of Ria de Aveiro, a mesotidal coastal lagoon located in the north coast of Portugal. This channel is located in the very complex central area of the lagoon and it includes two distinct regions: the first extending from the mouth of the lagoon to about 1 km upstream station C (Figure 8.1) and the second is the Espinheiro channel itself, extending from that point to the east boundary of the channel (a few kilometers upstream). For simplicity, the study area from the mouth of the lagoon until the Vouga River will be hereinafter referred as Espinheiro channel.

This channel connects the major source of freshwater of the lagoon (Vouga River), responsible for more than 2/3 of the freshwater input [Dias et al., 1999], and the Atlantic Ocean and receives contributions from several other channels (see Figure 8.1). The main stem stretches for approximately 11 km long, having an average width of about 200 m and a mean depth along its longitudinal axis of about 10 m. The tides are mixed semidiurnal, with M_2 being the most important constituent,

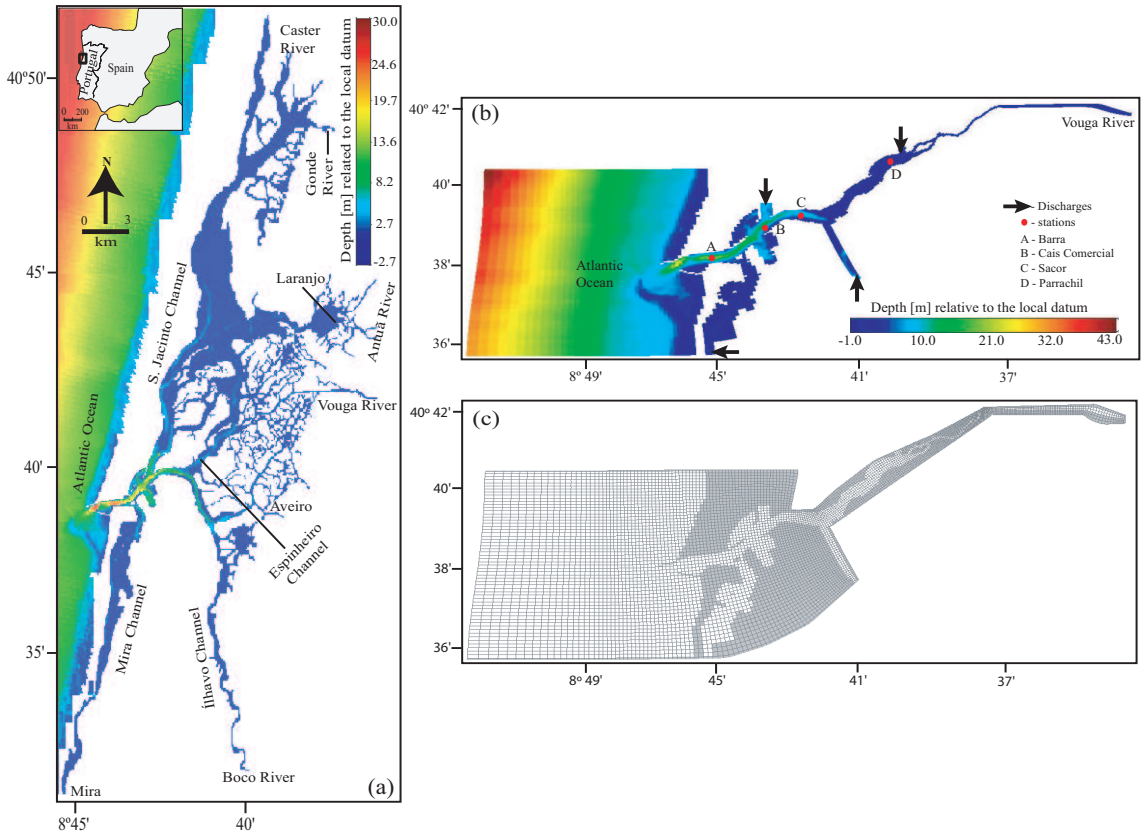

Figure 8.1: (a) Bathymetry of the Ria de Aveiro lagoon and adjacent coastal area. Major tributaries are marked. (b) Bathymetry of the Espinheiro Channel with the discharge points (marked with arrows) and its major freshwater tributary. The location of the stations used in the hydrodynamic calibration procedure is marked. Depths are in meters (over the local datum). (c) Horizontal curvilinear coordinate system.

representing ~90% of the tidal energy [Dias et al., 1999]. The tidal forcing is important with a range at the lagoon's mouth higher than 3 m during spring tides [Dias et al., 1999]. The channel's dynamics is mainly controlled by the interaction of tides and incoming river flow. However, it is also influenced by water exchanges with other channels. The channel's vertical structure is strongly dependent on the tidal strength and river inflow, changing from well mixed to partially stratified. For example, during the flood some regions may present salt wedge or partially stratified characteristics becoming well mixed by the end of the ebb. Thus, the channel's behavior adjusts dynamically to changes in the river flow and tidal mixing, as revealed by MacCready [1999] in his theoretical study in an idealized channel. The lack of continuous (or periodic) observational programs, which allow the characterization of the vertical structure of the channel, become necessary the implementation of numerical models to perform detailed physical studies.

Ria de Aveiro has four main channels, and due to their unique characteristics each one of them may be considered as an independent estuary connected to a common inlet. The hydrography of each channel is determined by different tidal prisms and freshwater inputs. The estimated tidal prism for the lagoon's mouth at extreme spring and extreme neap is according to Dias [2001] 136.7×10^6 and 34.9×10^6 m^3, respectively. Near station C (~1 km upstream) it is about 40×10^6 at extreme spring and 15×10^6 m^3 at extreme neap tide [Dias, 2001]. The total estimated freshwater input for the lagoon is very small (about 1.8×10^6 m^3 during a complete tidal cycle) [Moreira et al., 1993] when compared to the tidal prism, both at the mouth and at the beginning of Espinheiro channel. The small ratio between the freshwater input and the tidal prisms indicate the circulation is mainly induced by tides. However, the combination of these two factors (tidal regime and freshwater inflow) highly influences the thermohaline horizontal patterns [Vaz et al., 2005a].

Espinheiro channel has a low ratio between tidal amplitude and depth, revealing an ebb dominated channel [Dias, 2001]. The channel is very dynamic, presenting current velocity maximums higher than 2 ms^{-1} [Dias, 2001]. Generally, the longitudinal salinity differences lie between 20 and over than 30 psu, depending on the freshwater inputs [Dias, 2001; Vaz et al., 2005a]. The channel can be divided into three distinct regions: (a) a marine or lower estuary dominated by ocean waters, (b) a middle estuary where the mixing between the fresh and salt water occurs and (c) an upper or fluvial estuary characterized by freshwater, but subject to a daily tidal action. This delimitation is dynamic and can change seasonally (or in lower time scales) due to the tide, winds or the freshwater inflow. This dynamic delimitation has been referred by Kjerfve [1990] and Miranda et al. [2002] in their studies. The advection plays a major role on the salt transport in the Espinheiro Channel. However, diffusion processes may also be relevant contributors for the salt transport [Vaz and Dias, submitted]. Dias et al. [2003] computed residence times lower than 2 days for the whole study area, revealing a good water renewal.

In the past, due to the general shallowness of the lagoon (averaged depth of 1 m over the local datum) the lagoon was modelled using a 2D depth-integrated model [Dias et al., 2000; Dias, 2001; Dias et al., 2003]. The hydrodynamic and transport model results were compared to measurements

at monitoring stations throughout the lagoon, and this comparison revealed a good fit between model results and observations.

The model used in this study is Mohid, a 3D baroclinic modelling system which has been used to simulate several estuaries and coastal systems. In the Ria de Aveiro, Mohid has been used to perform water quality studies [Trancoso et al., 2005; Saraiva, 2005] in which macroalgae productivity has been studied. The horizontal patterns of water temperature and salinity were modelled using Mohid [Vaz et al., 2005a] implemented in a 2D depth-integrated mode. The model results have been compared with a field data set, and the results reveal that the model reproduces qualitatively the observed longitudinal thermohaline distributions.

Nowadays, a major motivation to implement and improve hydrodynamic models is the importance of 3D localized processes in the scope of the hydrodynamic influence on the water quality of estuarine areas. Observational programs often do not cover the entire study area. Therefore 3D hydrodynamic models may be used to complement observations. The narrow and complex morphology of the channel with its several contributors makes this area a challenging place to develop, for the first time, a predictive three-dimensional model.

This work describes the implementation of Mohid in a 3D mode for the Espinheiro channel, providing a comparison of several short hindcast simulations to a set of time series and spatial thermohaline distributions of the Espinheiro channel. The general circulation within the channel is studied using different forcing conditions: spring and neap tides and low-to-high river inflow. Issues like the cross-sectional tidal and tidally-average structure are analyzed and the channel vertical structure is examined using estuarine parameters as the Richardson number and the buoyancy frequency. The available measured data are sparse in time. The data used in this work were obtained during 1987 (sea level height), 1997 (water velocity), 2003 and 2004 (thermohaline distributions). Model/data comparison provides a qualitative/quantitative evaluation of the model's predictive skill and may point out several aspects on the model's parameterizations or the forcing data that require some improvement.

The transport model simulations cover four periods correspondent to spring and neap tide and low-to-high river inflow and the hydrodynamic is validated using the sea level height and current velocity referred above. The paper structure is as follows. Section 8.2 describes the model's physics and configuration for the Espinheiro Channel and in the next sections the results and conclusions are presented.

8.2 Model

8.2.1 Model physics

The Espinheiro Channel's predictive model is an implementation of Mohid - Water Modelling System. Mohid is a baroclinic finite volume model, designed for coastal and estuarine shallow water applications, like Ria de Aveiro, where flow over complex topography, flooding and drying of inter-

tidal areas, changing stratification or mixing conditions are all important. Mohid allows an integrated modelling approach of physical and biogeochemical processes.

Mohid has been used to model hydrodynamic and thermohaline transport in several estuaries and coastal areas of the Iberian Peninsula. Martins et al. [2001] simulate the flow features of a mesotidal well mixed estuary, bringing to evidence the advantages of the finite-volume method to implement the generic vertical coordinate; the circulation pattern driven by tide and horizontal density gradient between river and shelf waters was established for the Ria of Pontevedra (NW Spain), and the variability of tidal velocities and salinity was studied [Villarreal et al., 2002]; a methodology, based on the computation of the residence time and integrated water fraction, to understand the transport patterns in the Tagus estuary (Portugal) was proposed by Braunschweig et al. [2003]; and the horizontal patterns of thermohaline properties under extreme forcing events were studied in Ria de Aveiro [Vaz et al., 2005a]. Mohid is a modelling system continuously under development, and the home page can be found at http://www. mohid.com. Some of the key features of the model are highlighted below. A complete description of the model can be found in Martins et al. [2001], Leitão [2003] or Theias [2005].

Mohid solves the equations of motion using an orthogonal (or curvilinear) Arakawa-C grid [Arakawa and Lamb, 1977]. The temporal discretization is carried out using a semi-implicit algorithm: the ADI - Alternate Direction Implicit [Abbott and Basco, 1994]. This algorithm is applied in the computation of the water level. This hydrodynamic property is computed from the divergence of the horizontal water fluxes. The ADI algorithm assumes alternatively one component of the horizontal velocity implicitly while the other is calculated explicitly, avoiding the computation of the internal and external modes with different time steps (mode splitting approach). The model has a simple method for handling the flooding/drying of intertidal areas, in which the uncovered cells are tracked. This method consists on defining one depth below which the cell is considered uncovered ($HMIN$), conserving a thin layer of water above the uncovered cell. The cells are considered uncovered if the total depth ($H = \eta + h$) is lower than $HMIN$ and if the sea level height (η) is lower than the local depth (h) plus $HMIN$ [Martins et al., 2001].

Mohid has several high order advection schemes. In this work, the horizontal and vertical advection of momentum and mass are computed using a TVD-Superbee method (total variation diminishing) [Roe, 1985]. Lately, this method is being recommended for coastal and estuarine simulations [Gross et al., 1999; Stips et al., 2004; Banas and Hickey, 2005]. This method is free from numerical oscillations and guaranteed to be stable and less computationally expensive.

Mohid also allows the choice between several turbulence closures. It has coupled the one-dimensional General Ocean Turbulence Model (GOTM) [Burchard et al., 1999], a water-column model which allows the use of different turbulent closure schemes. Here, two different closure schemes were used for the calculation of the turbulent viscosity/diffusivity coefficients: the $\kappa - \varepsilon$ and the Mellor-Yamada schemes [Burchard and Bolding, 2001; Mellor and Yamada, 1982] using the stability function parameterization proposed by Canuto et al. [2001]. Warner et al. [2005] tested a number of two-equation schemes ($\kappa - \varepsilon$, $\kappa - \omega$, $\kappa - \kappa l$) and found minor differences in their ability to

reproduce estuarine salinity fields. A review of these two-equation schemes can be found in Burchard [2002].

8.2.2 Model's configuration for the Espinheiro Channel

Mohid has been configured to be applied in the Espinheiro Channel. Bathymetry in the channel is extracted from data obtained by the Hydrographic Institute of the Portuguese Navy in 1987/1988. More recent bathymetric data, obtained from recent dredging operations in several channels (1998) and close to the lagoon's mouth (2002), were also used. Figure 8.1 shows the model's bathymetry and grid. An orthogonal curvilinear coordinate system [Driscoll and Vavasis, 1998] was designed to follow the general orientation of the channel including its major tributaries and the near coastal ocean. The grid spacing is less than 100 m in the longitudinal and about 50 m in the cross-channel direction. High resolution is used in order to properly resolve the physical features of the channel. The total number of grid points is 200 by 200 and, in the vertical direction, the model uses 10 sigma layers. The domain was designed to resolve the channel's dynamic, and not the dynamics of the near coastal ocean. Although the near shelf bathymetry is realistic (limiting the computational time), there are no measurements of physical variables that allow a full implementation (calibration/validation) of the model, permitting the coupling between the channel's internal dynamic and shelf processes. This coupling process remains a future goal.

Ria de Aveiro is a branched coastal lagoon in which the shelf waters that enter spread toward the main channels. Thus, the amount of water at upstream locations is lower than at the lagoon's inlet. This affects the dynamics of the study area. The arrow marked boundaries depicted in Figure 8.1b were included in the curvilinear grid in order to simulate the inflow/outflow of water between the Espinheiro Channel and the neighborhood channels. Thus, in order to simulate this inflow/outflow at these locations, the model use as boundary conditions water flow, salinity and water temperature time series computed using a two-dimensional (depth-integrated) application of the model for all the area of the lagoon.

The 2D application uses a variable spatial step cartesian grid with higher resolution in the central area of the lagoon (40×40 m), calculating time-varying discharge, salinity and water temperature time series at the arrow marked locations. At the open ocean boundary the model was forced using tides and at the landward boundary the forcing was river inflow values typical for each run. At the oceanic and landward boundaries, the water temperature and salinity are considered fixed in each simulation, typical values being imposed for each period. At the surface, heat fluxes were imposed. The model uses the heat fluxes parameterizations described by Chapra [1997] (see Section 4.5). The meteorological data used are from the University of Aveiro automatic station and are concurrent with the simulated periods. The time step is 10 s and the horizontal eddy viscosity is 5 m^2s^{-1}. The initial conditions for the hydrodynamic model are null free surface gradients and null velocity in all grid points. For the transport model the initial conditions are salinity and water temperature fields, obtained by interpolation of data collected in the study area. More realistic conditions are needed

for the transport model, since the time to reach dynamic equilibrium is much longer than for tides and tidal currents. A value of 5 m^2s^{-1} was adopted for both salt and heat diffusion coefficients. The two-dimensional application is fully described in Vaz et al. [2005a] and in the submitted paper Vaz et al. [Submitted] (see Chapters 5 and 7).

The 3D model uses, at the bottom, the shear friction stress imposed assuming a velocity logarithmic profile. The vertical eddy viscosity and diffusivity are computed by the model using GOTM (coupled to Mohid) [Burchard et al., 1999]. Coefficients of horizontal viscosity and diffusivity are set to 2 m^2s^{-1}. Initial conditions for the hydrodynamic model are the same of the 2D application. Initial conditions for the 3D transport model are constant values of salinity and water temperature (typical values for each run). At the ocean open boundary the model is forced by tide determined from 38 tidal constituents obtained after harmonic analysis [Pawlowicz et al., 2002] of data measured at a tidal gauge located close to the lagoon's mouth in 2002. At the landward boundary freshwater inflow was imposed, and at the arrow marked boundaries water inflow/outflow, salinity and temperature fluxes were also prescribed (Figure 8.1b). On the offshore open boundary and at the river boundary constant values of salinity and water temperature were prescribed (S_{sea} = 36.5 and S_{river} = 0, water temperature varies from run to run).

The hydrodynamic was spun up from rest over 2 days (~ 4 tidal cycles). This is considered a fair adjustment period for the hydrodynamic model. For the transport model, the spin up period is of the order of the lagoon's residence time. For the Espinheiro Channel, Dias [2001] found a residence time of 2 days (near the channel's head), and about 14 days at the northern area of the lagoon. The spin-up period is not included in the results, and the initial state of a run refers to the end of the spin-up period.

8.3 Results

8.3.1 Evaluation of the model results: model skill

The model results are evaluated using the Skill parameter, a statistical method presented by Wilmott [1981]. This method has been used recently by Li et al. [2005] and Warner et al. [2005] to assess the model results in their simulations of the Hudson River and Chesapeake Bay. The Skill parameter is given by,

$$Skill = 1 - \frac{\sum_{i=1}^{N} |X_{mod} - X_{obs}|^2}{\sum_{i=1}^{N} (|X_{mod} - \overline{X}_{obs}| + |X_{obs} - \overline{X}_{obs}|)^2} \tag{8.1}$$

where X is the variable being compared, $\overline{X}$ its time mean and N is the number of measurements. This parameter describes the degree to which the observed deviation about the observed mean correspond to the modelled deviation about the observed mean. A Skill of 1.0 means a perfect agreement between model results and observations (complete disagreement yields a Skill of 0.). Model skill is evaluated for all prognostic quantities.

8.3.2 Sea level height

The semidiurnal tidal constituents -M_2 and S_2- explain more than 90% of the sea level variability in Ria de Aveiro [Dias et al., 1999], being the remaining variations caused by tidal interactions, lower frequency tidal and other meteorological forcings. Thus, the tidal propagation in the channel is dominated by the semidiurnal tide and exhibits a spring neap variation. Figure 8.2 shows the comparison between observed and modelled time series of sea level height for four stations of the Espinheiro Channel (see Figure 8.1b). The observed sea level height was obtained in a general survey of the Hydrographic Institute of the Portuguese Navy in 1987 [IH, 1991].

In general, the sea level height results reveal a good qualitative agreement between model and observations. At station A, the Skill is 0.93, a high value which show a good agreement near the mouth of the channel. As the tidal wave travels upstream the model Skill remain high with values of 0.90 (station B) and 0.87 (stations C and D).

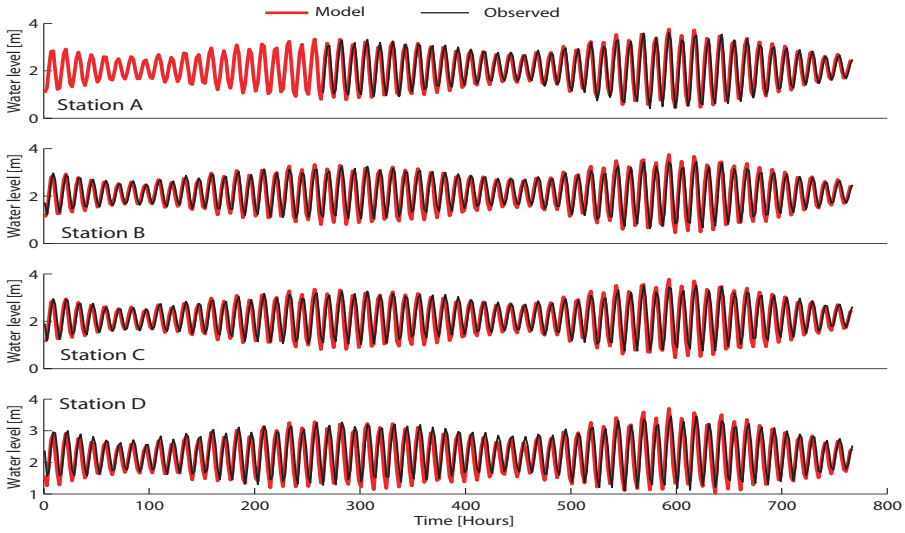

Figure 8.2: Comparison between modelled and observed time series at stations A, B, C and D throughout the channel. The simulation period is from August 16^{th} to September 16^{th} 1987.

At Table 8.1 the results of the harmonic analysis [Pawlowicz et al., 2002] performed to the time series depicted in Figure 8.2 are shown.

Phase differences between model results and observations are low. For the M_2 constituent the differences increase from 2.20° at station A to 10.08° at station D. The average phase difference for the four stations is ~7.0°, which corresponds to an average delay between measured and computed data of about 14 minutes. The averaged amplitude difference is about 5 cm (for the four stations). The results presented here are confirmed by the correlation coefficient values (between observed and model data) which decreases upstream revealing some degradation of the results. At station A, this coefficient is ~0.86 decreasing to ~0.77 at station D. The results for the other two semidiurnal

Table 8.1: Harmonic analysis results comparison of field and model generated water level data. Results for the more energetic tidal constituents in the Espinheiro Channel (M_2, S_2, N_2)

	Station	A	B	C	D
M_2 Amplitude [m]	Field	0.954	0.873	0.867	0.770
	Model	0.966	0.954	0.958	0.803
	Difference	-0.012	-0.082	-0.091	-0.033
M_2 Phase [°]	Field	78.99	85.98	90.68	105.50
	Model	76.79	80.22	81.33	95.42
	Difference	2.20	5.76	9.35	10.08
S_2 Amplitude [m]	Field	0.449	0.370	0.366	0.282
	Model	0.444	0.436	0.436	0.337
	Difference	0.005	-0.066	-0.071	-0.054
S_2 Phase [°]	Field	113.35	123.87	131.24	149.54
	Model	116.32	120.31	121.68	138.75
	Difference	-2.97	3.56	9.56	10.79
N_2 Amplitude [m]	Field	0.214	0.177	0.183	0.130
	Model	0.219	0.215	0.215	0.163
	Difference	-0.005	-0.038	-0.033	-0.033
N_2 Phase [°]	Field	47.04	62.56	65.76	80.12
	Model	51.18	55.12	56.37	71.11
	Difference	-4.14	7.44	9.39	9.01

constituents (S_2 and N_2) are as accurate as for the M_2 both in amplitude and phase (see Table 8.1 for reference).

For the M_2 constituent, the results obtained using the 3D model are so accurate as the results obtained using the 2D application of the model. In fact, at station A the amplitude difference between measured and computed (using the 2D model) data is about 2.2 cm and the phase difference is lower than 1°. This means that using the 3D model a lower amplitude difference (~1 cm) and a higher phase difference (~1.3°) are obtained. These differences in the sea level are not significantly reduced by changing the bottom drag coefficient, and it is not clear why they occur. The tide was imposed at the ocean open boundary affected by a phase and amplitude correction factor for the major harmonic constants (see Section 5.4). This has been done in order to assure that the model reproduces the tidal elevation measured at the lagoon's mouth tidal gauge. This correction was made using the 2D numerical model previously implemented for the entire area of the lagoon and maintained for this study, and could be an error source, since the curvilinear grid has high resolution and does not constitute an error source. In spite these differences, the 3D model qualitatively and quantitatively reproduces sea level height variations within the Channel.

8.3.3 Velocity

In Figure 8.3 are depicted the measured and computed time series of along flow direction velocity at station D which represent the only current velocity data available in the Espinheiro Channel. The observed data were taken ~50 cm below surface and are compared with the velocities computed at the top layer. The measurements were taken during the Summer of 1997. The along channel velocity results reveal a semidiurnal variation. In spite of the high Skill score (0.84), the model

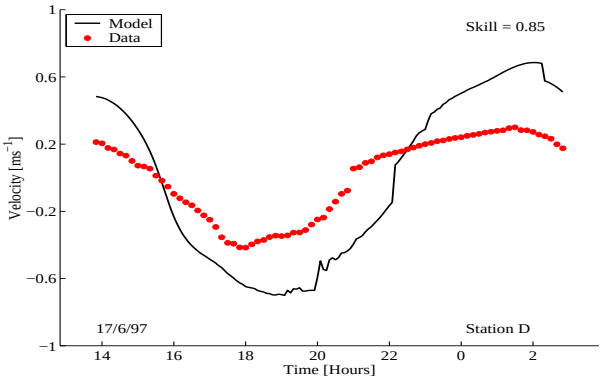

Figure 8.3: Time series of along flow direction velocity used in the hydrodynamic validation

results overestimate the observed velocity, revealing a velocity amplitude of ~1.1 ms^{-1} (model) and ~0.7 ms^{-1} (observations).

The current velocity changes rapidly both in magnitude and direction from point to point. The model results are the averaged value for one grid cell, while the field data is a value measured at a single point. Another factor that could explain some of the difference between computed and measured velocity is some inaccuracy of the numerical bathymetry that affects the results. These facts originate intrinsic differences between model results and observations and may explain some of the differences observed.

8.3.4 Thermohaline longitudinal structure

The simulations include two spring tide periods with low and high river inflow (26/09 and 25/11/2003) and two neaps also with high and low river inflow conditions (29/01 and 25/07/2004). The tidal amplitude during spring tide was 2.8 m and during neaps was 1.3 and 1.6 m. The river inflow imposed at the landward boundary was 2.06 (September 2003) and 72.74 m^{3}s^{-1} (November 2003), and for the neap simulations was 2.0 (July 2004) and 143.16 m^{3}s^{-1} (January 2004). The model results were compared to the thermohaline observation taken during the flood period representing synoptic snapshots of the along channel salinity and water temperature distribution. These thermohaline data were taken under the scope of a one year survey in which vertical profiles of thermohaline variables were sampled twice a month during spring and neap tide (see Chapter 2).

Figure 8.4 shows the longitudinal salinity structure through the channel longitudinal axis. In general, the trends inferred from the observations are reproduced by the model. When the river flow is weak (~2 m^{3}s^{-1}), the salinity values near the channel's head (8 to 10 km from the mouth) are not well reproduce (Figures 8.4(a, b, c) and 8.4(j, k, l)). This discrepancy may be due to the salinity initial conditions imposed in the transport model (a constant value of 35 psu within the whole channel) and to the low river inflow at the landward boundary which is not high enough to flush out the saline water. Despite these discrepancies, the best overall results were achieved using these conditions. When this region's values are used, the model Skill present values between 0.44 (Figure 8.4a) and 0.86 (Figure

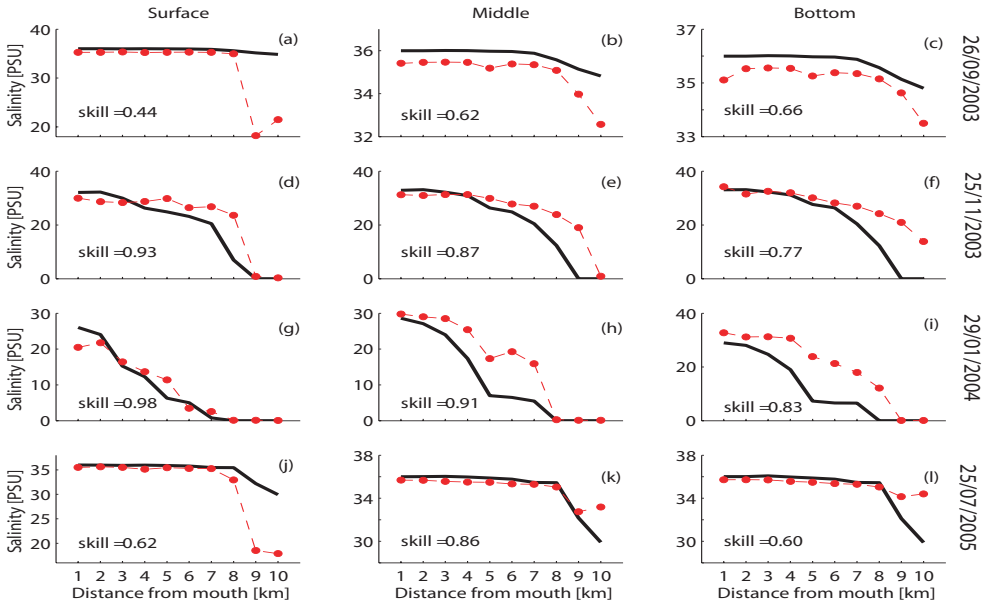

Figure 8.4: Comparison of longitudinal salinity distributions for observed (•) and model results (line) at three different vertical levels for (a, b, c) 26/09/2003, (d, e, f) 25/11/2003, (g, h, i) 29/01/2004, (j, k, l) 25/07/2004

8.4k). Using the results for the first 8 km, the model Skill increases to values near 0.9. Figures 8.4(a, b, c) and 8.4(j, k, l) were chosen to illustrate the difference between the tidal propagation under low river flow and spring and neap tidal conditions, respectively. As it can be seen, the oceanic water flows further upstream (~1 km) during spring tide, due to the higher tidal prism (volume of water entering the channel during a tidal cycle), and the higher tidal currents. When the river flow is high (November and January simulations), the longitudinal salinity structure is well reproduced by the model, with Skill values higher than 0.75. In the surface layers (surface and mid water column), the mixing between oceanic and riverine waters is well calculated by the model with Skill values higher than 0.85. Despite these high Skills, the longitudinal salinity distributions are underestimated by the model, mainly due to the constant freshwater inflow imposed at the landward boundary. Hence, the predicted vertical stratification is weaker than the observed stratification. The arrow marked boundary conditions (water fluxes, salinity and water temperature time series) are also very important for the Espinheiro Channel's results. In fact, Ria de Aveiro has several freshwater tributaries (marked in Figure 8.1a), and during the colder seasons, when the rainfall is higher, increasing the river inflow, they are very important in the establishment of the water temperature and salinity patterns within the lagoon, and hence to determine the boundary conditions that are prescribed to the baroclinic model.

In Figure 8.5 are depicted the water temperature longitudinal distributions during the periods referred above. The simulations were carried out imposing heat fluxes at the surface boundary. For these fluxes calculations, Mohid uses the parameterizations described by Chapra [1997] (see Section 4.5).

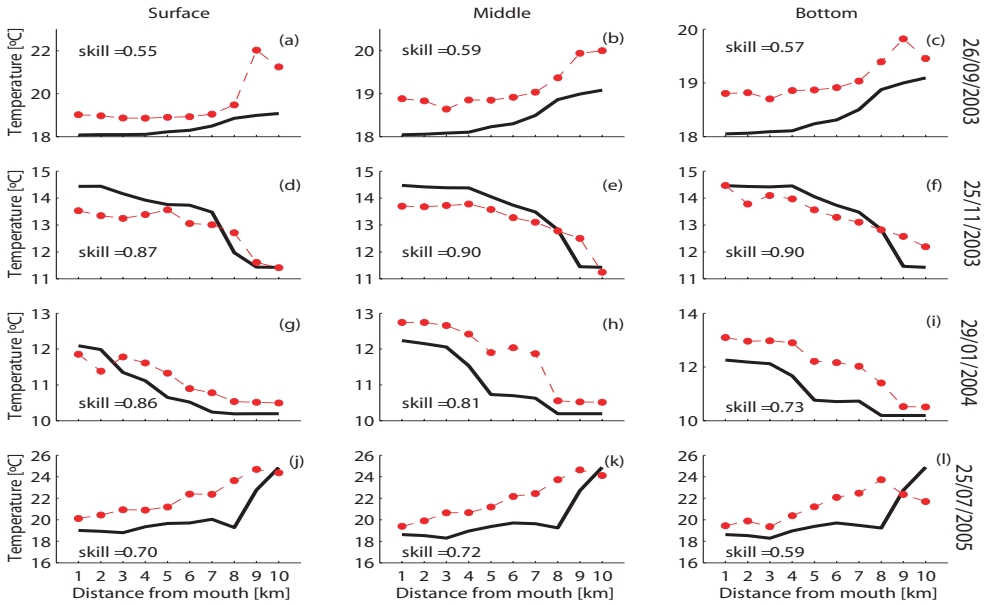

Figure 8.5: Comparison of longitudinal water temperature distributions for observed (•) and model results (line) at three different vertical levels for (a, b, c) 26/09/2003, (d, e, f) 25/11/2003, (g, h, i) 29/01/2004, (j, k, l) 25/07/2004

In general, the model reproduces well the trends inferred from the observations. When the river flow is weak (September and July simulations), the model underestimates the temperature distribution within the channel. The mean difference between predicted and observed values is, in general, lower than 2°C, except at the surface level during the September simulation. The higher water temperature values are observed near the surface due to the water/near atmosphere heat exchanges. Near the channel's head, the water temperature values is also controlled by the fluvial water temperature, which is higher during the Summer periods. When the river flow is high (November and January simulations), the water temperature distribution within the channel is mainly controlled by the mixing between oceanic and riverine waters, being the surface fluxes less important in the calculations. The general trends are well reproduced by the model, with a Skill around 0.9 and 0.8 during the November and January simulations, respectively. During the January simulation, the water temperature distribution is highly dominated by the freshwater inflow from the landward boundary, and the model underestimates the temperature distribution. As previously referred, the boundary conditions prescribed at the arrow marked locations (see Figure 8.1b) may also affect the amount of salt or brackish water that enters in Espinheiro Channel. In fact, during the Autumn and Winter, when the rainfall is high and the freshwater inflow increases at the Ria de Aveiro major tributaries, the thermohaline distributions are affected by water exchanges between Espinheiro and the other channels of the lagoon. The fresh and brackish water increases within the lagoon and hence in the Espinheiro Channel.

8.3.5 Characteristics of the residual circulation

Superimposed on the back-and-forth water flow there is an averaged steady water motion, known as residual circulation. This circulation has a time scale similar to the tidal cycle time scale, and an amplitude which is typically one or two orders of magnitude lower than that of the tidal currents. In spite of its small amplitude, the residual circulation can determine the long-term transport which is very important in the ecological systems. There are two different approaches to determine the residual circulation using numerical models: The first is filtering or time averaging the transient solution computed by the model, and the second is solving numerically the residual velocity evolution equations, which are obtained by time averaging the transient velocity evolution equations. Neves [1985] shows that both methods are physically equivalent and give the same results. In this study is used the first approach.

Residual circulation was calculated for each simulation period at two different levels: near the surface (Figures 8.6a and 8.7a) and near the bottom layer (Figures 8.6b and 8.7b). The results presented here represent the residual flow driven by tides and freshwater during the spring tides of September 26^{th} (river flow of 2.06 m^3s^{-1}) and November 25^{th} (river flow of 72.74 m^3s^{-1}). The residual values were calculated by tidally averaging the transient solution computed by the model and are about one order of magnitude lower than the tidal currents within Espinheiro Channel.

With no freshwater inflow, the tide induced residual currents is seaward at the surface and bottom

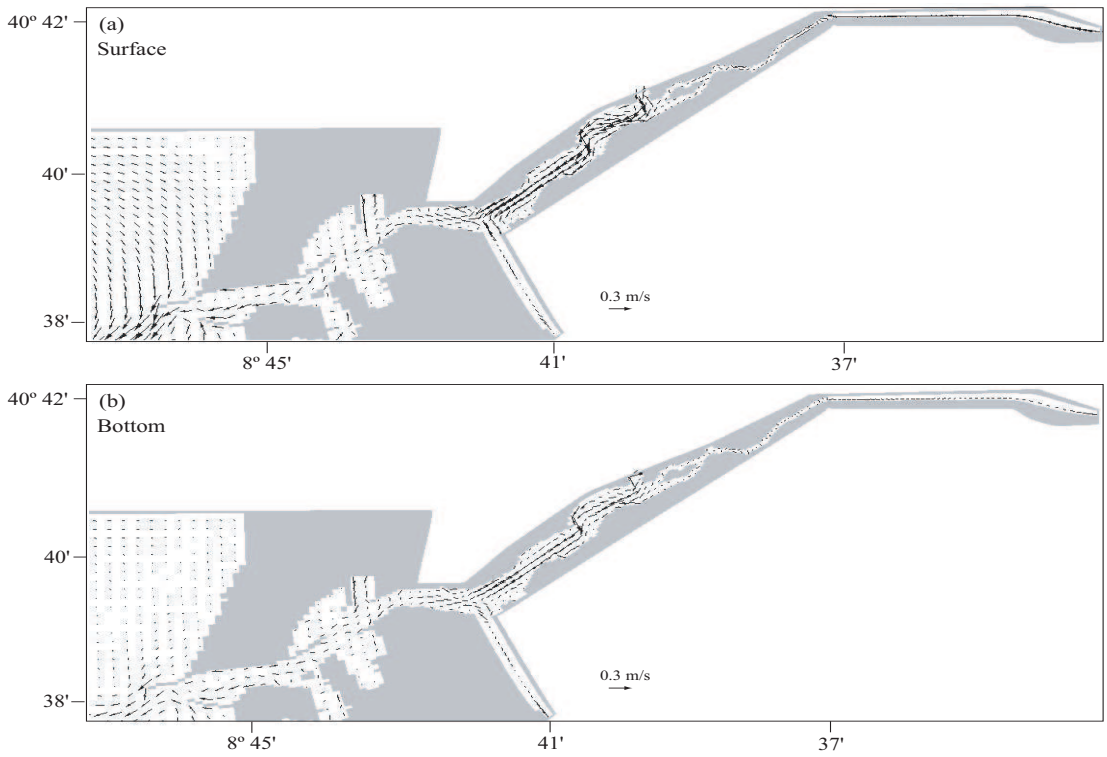

Figure 8.6: Tidally averaged (September simulation) residual flow (a) surface and (b) bottom layers.

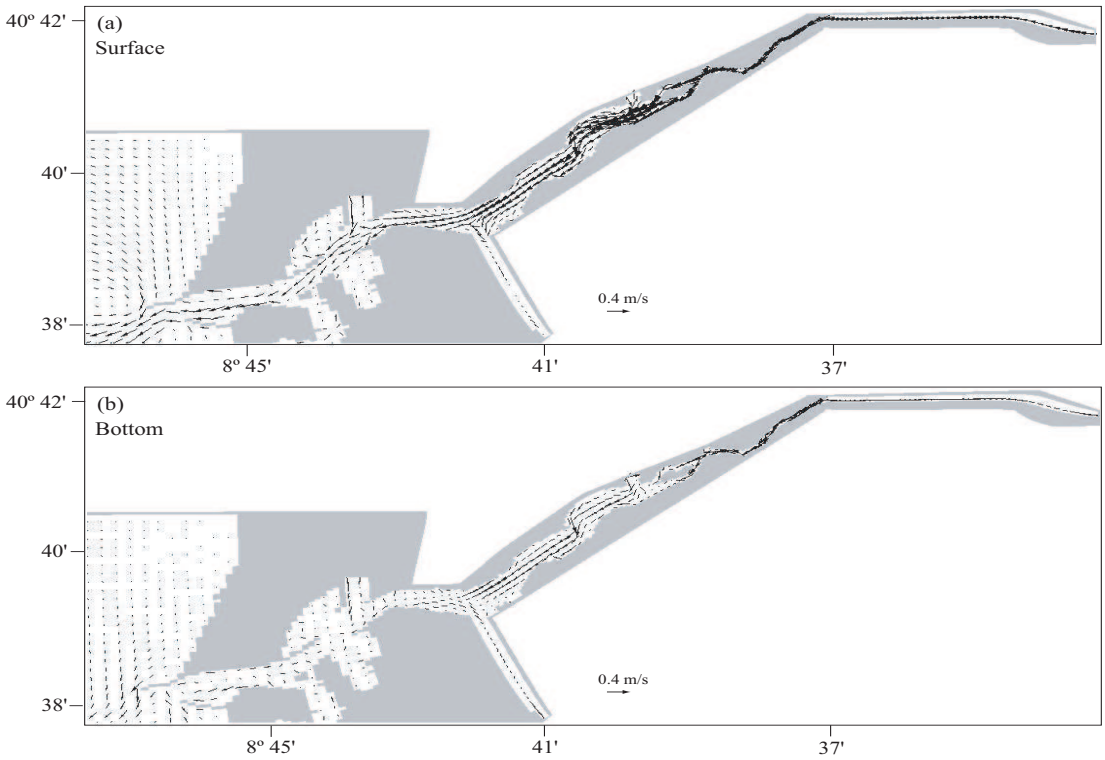

Figure 8.7: Tidally averaged (November simulation) residual flow (a) surface and (b) bottom layers.

layers, revealing an ebb-dominated channel (not shown). This channel feature was demonstrated by Dias [2001]. In that study, a depth-integrated numerical model was used to capture the barotropic residual circulation within Ria de Aveiro induced by tides, river inflow and winds. The results observed are consistent with an ebb-dominated channel, the surface and near bottom current are always directed seaward. However, currents show some spatial variability. The surface currents are visibly more intense flowing out the estuarine water (Figures 8.6a and 8.7a). This jet-like current spreads over the whole channel width in almost all the channel area. However, near the inlet it is more intense close to the south shore. The bottom current is also seaward but less intense. Near the mid-channel region, this current is somehow variable due to interaction with the topography, as shown in Figures 8.6b and 8.7b. The results presented in this section, have shown that the model can qualitatively capture some of the characteristics of the tidally-averaged estuarine circulation revealed in a prior study by Dias [2001].

Near the channel's inlet, the residual currents were found more intense close to the south shore than to the north shore. In order to confirm this feature, the longitudinal velocity component and salinity were tidally-averaged and the results for three longitudinal sections - north and south shore and channel axis - at the entrance channel are depicted in Figure 8.8. The results are from the November (25/11/2003) and January (29/01/2004) simulations.

The two simulation periods compared here correspond to a spring tide (November) and a neap

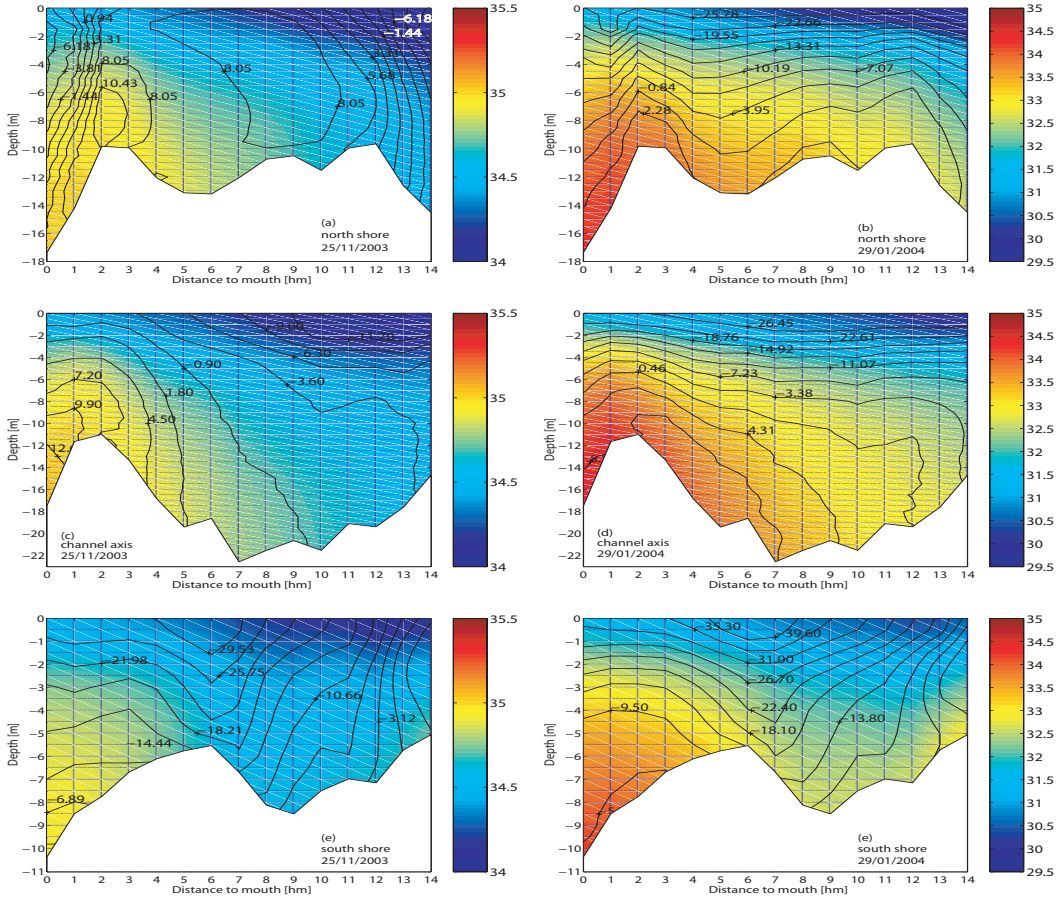

Figure 8.8: Tidally-averaged longitudinal velocity (contours, cms^{-1}) and salinity (colour, psu) longitudinal structure at the inlet of Ria de Aveiro. The longitudinal sections are from the November and January simulation results and were obtained at three locations: (a, b) north shore, (c, d) channel axis and (e, f) south shore.

tide (January). In general, the results from January 29^{th} (river flow of 143.16 m^3s^{-1}) show a stratified water column in terms of salinity and longitudinal velocity due to the intense river inflow and moderate tide. The results from November 25^{th} (river flow of 72.74 m^3s^{-1}) also reveal a stratified water column, but they present a more intense longitudinal gradient of longitudinal velocity due to a intense tide and a lower river inflow.

Near the north shore during November 25^{th} (Figure 8.8a), the longitudinal residual velocity structure presents positive (inward) values in a large portion of the longitudinal section. At this location, the residual velocity presents negative values (outward) near the surface at the end of the entrance channel (~1300 m from the mouth) and near the mouth. The negative residual currents near the mouth may be due to the river inflow and to the fact that these grid cells are close to the beginning of the north jettie, which may influence the results at this location. The positive residual velocity found at this location is due to a very weak recirculation that can be found close to the north shore. The

January 29^{th} results show ebb residual currents at this location. The exception is near the bottom at the mouth of the channel where is visible an inward residual velocity and more saline water. This structure is strongly influenced by the high river inflow, which produces more intense ebb currents at the entrance channel.

At the channel's axis, the model results show a more intense salinity gradient during the January simulation, resulting from the more intense river inflow and moderate tidal regime (neap tide). The residual currents show a two-layer structure during January 29^{th} (Figure 8.8d), presenting ebb currents at the top layers and flood currents near the bottom. During November 25^{th} (Figure 8.8c), the residual currents present a more visible longitudinal gradient, presenting flood (inward) values at the mouth and ebb (outward) values from the middle to the end of the entrance channel. The velocity structure, at the central axis of the channel, is strongly affected by the intense tidal regime on the November 25^{th} and by the high river inflow on the January 29^{th}.

At the south shore longitudinal section, the model results present ebb residual currents on both simulations. This negative values of the residual velocity are visible for all the water column, with higher values at the top layers and decreasing toward the bottom. The influence of the freshwater inflow in the velocity structure is visible in Figures 8.8c and 8.8f, with intense values at the surface, where the currents are enhanced by the freshwater flow from the river. On January 29^{th}, the residual currents near the surface are ~5 cms^{-1} higher than during the November 25^{th} simulation.

The results depicted in Figure 8.8, reveal and confirm some of the results presented in this study. In the performed simulations were found a preferential flow path near the south shore. During the ebb period, the estuarine waters flow preferentially closed to the south shore of the entrance channel, as the results from the residual circulation illustrate. A zoom of the residual currents for the November simulation is presente here (Figure 8.9).

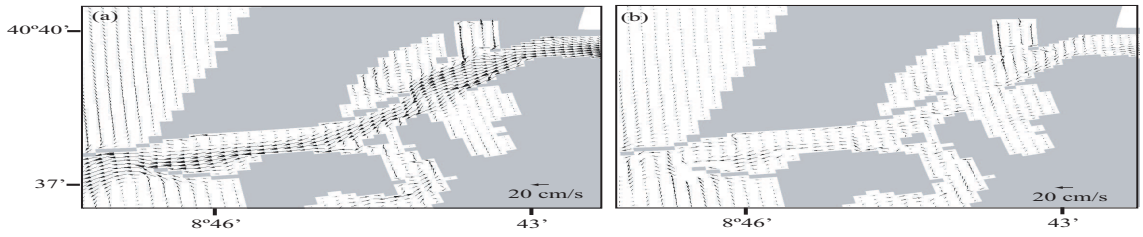

Figure 8.9: Averaged residual flow (a) surface layer and (b) at the bottom layer. Simulation period: 24/11 to 27/11/2003.

8.3.6 Cross-sectional tidally-averaged velocity and salt transport

The model was also applied to provide insight into transport of water and salt through two cross-sections: one near the channel's inlet (cross-section 1), near station A, and the other ~1 km upstream station C (cross-section 4, see Figure 8.1). The two cross-channel sections have a triangular shape (smooth slope from center to the shore) with a deeper zone near the center, and may be considered

representative of the lower and mid-channel region. The channel's width is about 350 m for both sections and they have a maximum depth of ∼25 (cross-section 1) and ∼13 m (cross-section 4). In this section the results obtained from the model simulations referred in Section 8.3.4 are displayed and discussed. The longitudinal velocity component and salinity were averaged over two complete tidal cycles in order to remove the tides and reveal the characteristic features of the estuarine circulation [Pritchard, 1952; Hansen and Rattray, 1965].

The lateral and vertical structure of the tidally-averaged (or residual) salinity and longitudinal velocity component is shown. Positive velocity values are referred as landward velocities and negative values as seaward values. Near the channel mouth, during low river flow periods (September and July simulations, river flow of ∼2 m^3s^{-1}), the salinity structure is almost homogeneous, revealing a well mixed section (see Figure 8.10a and 8.10d). However, the residual velocity pattern is different, with ebb current values near the south shore decreasing toward the middle of the section and flood current values near the north shore of the channel. During medium (Figure 8.10b) and high (Figure 8.10c) river inflow events, the salinity structure present stratification through the water column but the channel may be considered as laterally homogeneous in terms of salinity. During the November simulation, the residual velocity presents the same patterns as at the low river inflow periods, i. e. ebb currents near the south shore decreasing toward the center of the channel and flood currents near the north shore. During the January simulation, when the river inflow is high (143.16 m^3s^{-1}), the residual velocity pattern, at cross-section 1, reveals flood currents near the bottom and ebb currents at mid-column and near the surface, revealing a stratified water column and nearly flat isotachs through the cross-section.

Near the mouth of the channel, the predicted tidally-averaged salt transport corresponds to the same pattern observed in the velocity, with a net upstream salt flux (positive) close to the north shore of the section decreasing toward the center of the channel, and presenting a net downstream salt flux (negative) from the middle toward the south shore of the channel. This feature is visible in all simulations, except for the January simulation (Figure 8.10g), where following the same pattern of the residual velocity the cross-section present a net upstream salt flux close to the bottom and a downstream salt flux at the upper layers. During this period the gravitational circulation appears as an important mechanism for salt transport at cross-section 1. Another feature found during the analysis is that, in general, the salinity values are higher during the flood than during the ebb, leading to a landward transport. This is the tidal cycle correlation term of the salt transport and can be important in branching and curved estuaries [Fischer et al., 1979; Banas and Hickey, 2005]. The September and July simulations were carried out under similar river inflow (about 2 m^3s^{-1}), and show a higher down-channel salt transport during spring tide (Figure 8.10e) than during neap tide (Figure 8.10h). This result is expected since the residual currents are higher during the spring tide period that has been simulated.

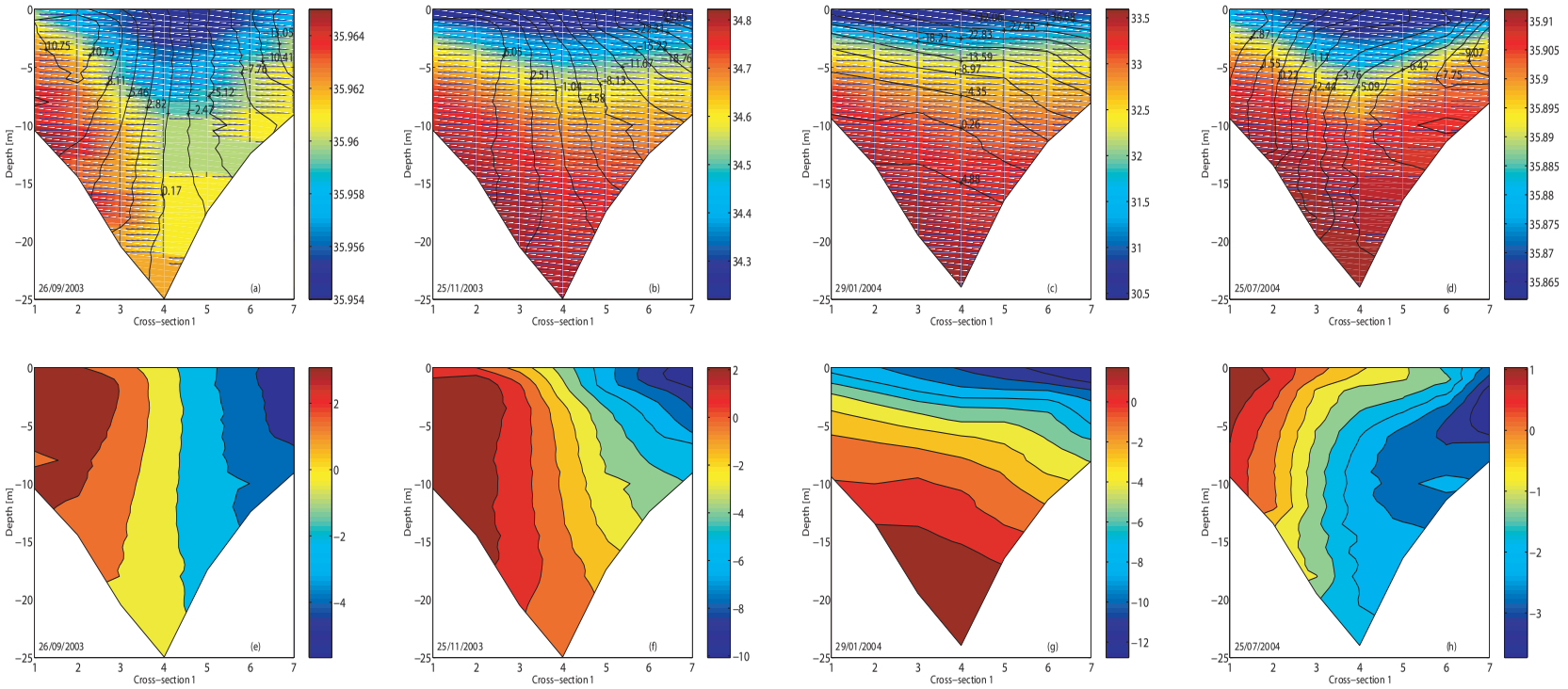

Figure 8.10: (a, b, c and d) Cross-sections of tidally-averaged salinity (color) and longitudinal velocity component (cms^{-1}) (upstream view); (e, f, g and h) predicted tidally-averaged salt transport ($psu.cms^{-1}$) for cross-section 1, near the mouth of the lagoon (upstream view).

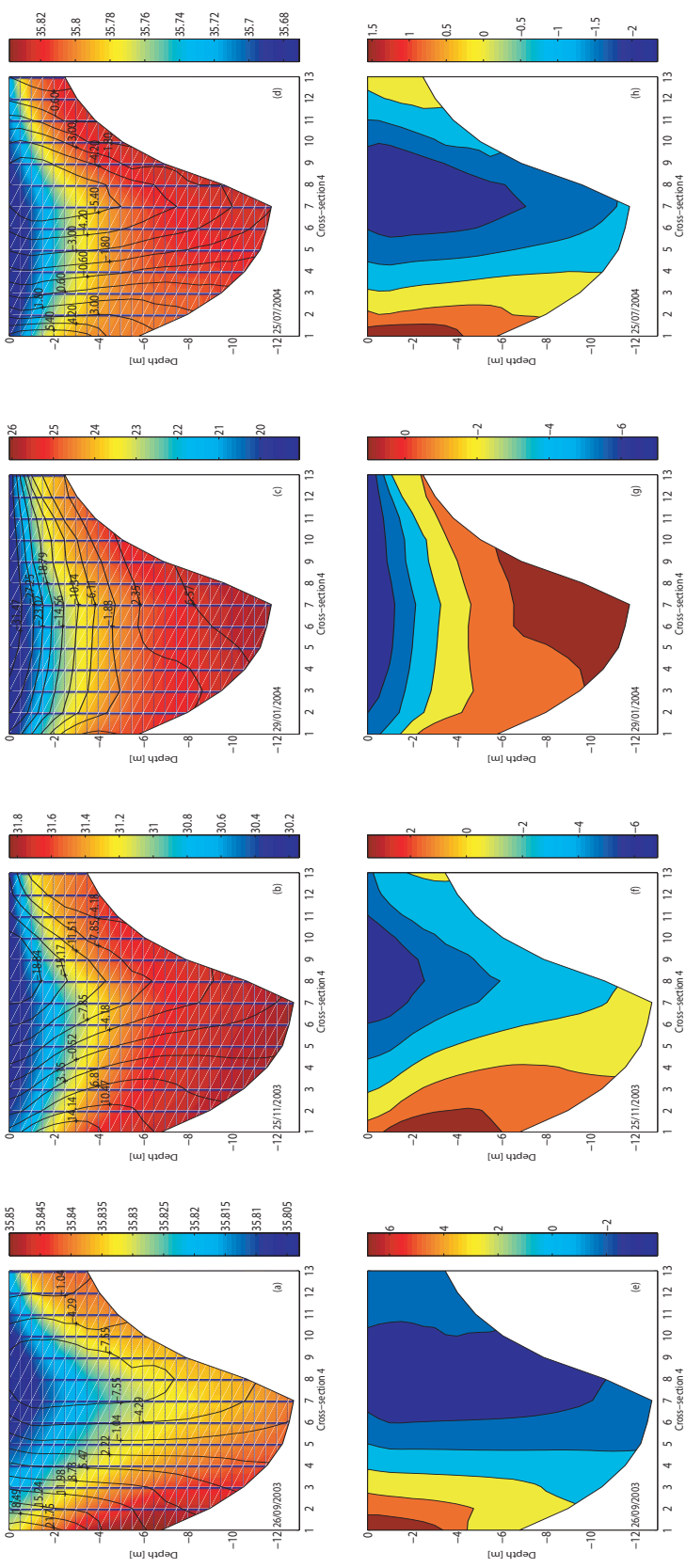

Figure 8.11: (a, b, c and d) Cross-sections of tidally-averaged salinity (color) and longitudinal velocity component (cms^{-1}) (upstream view); (e, f, g and h) predicted tidally-averaged salt transport ($psu.cms^{-1}$) for a cross-section ~4 km upstream of the channel mouth (upstream view).

At cross-section 4, located ~4 km upstream, the results reveal the same kind of patterns as near the channel's mouth at cross-section 1, as shown in Figure 8.11. During September (Figure 8.11a) and July (Figure 8.11d), the salinity structure is nearly laterally and vertically homogeneous, with salinity variations of the order of tenths of psu. During medium and high river inflow events (Figures 8.11b and 8.11c) the lateral structure is nearly homogeneous, but the vertical structure presents stratification with values ranging from 30 (surface) to 32 (bottom) on the November simulation and 19 (surface) to 26 (bottom) on the January simulation. The residual velocity structure is similar to the one found at cross-section 1 for all four simulations. Ebb currents are visible from the middle of the channel to the south shore and flood currents are visible near the north shore. During the January simulation (Figure 8.11c), when the river inflow is high, the channel may be considered laterally homogeneous in terms of residual salinity and velocity, but present stratification with flood currents near the bottom and ebb currents at the top layers.

The tidally averaged salt transport corresponds to the patterns found in the velocity with landward transport near the north shore and seaward transport near the south shore. During the January simulation (Figure 8.11g), the landward transport is found near the bottom and at the top layers the transport is seaward.

8.3.7 Cross-sectional tidal thermohaline structure

Once the model implemented, it may be used to characterize the cross-sectional thermohaline and velocity structure of the channel. In the following figures, are depicted the distributions of salinity, water temperature and longitudinal velocity (u component) at the two cross sections referred in Section 8.3.6. The cross-sectional fields were determined for a neap tidal period with a high freshwater inflow (143.16 m^3s^{-1}) representing a Winter situation (January 29, 2004). The cross-sectional distributions are representative of low water (a, b, c), mid flood (d, e, f), high water (g, h, i) and mid ebb (j, k, l) and are referred to the low and high water near the channel's inlet.

At cross-section 1 (Figures 8.12a, 8.12b and 8.12c, near the channel's mouth) at low water, the salinity structure reveals a stratified water column, with values ranging from 26 psu at the top layers to 30 psu near the bottom. From the bottom until mid water, the water column is almost well mixed. The water temperature structure presents values of 12.1 near the surface and 12.3 near the bed, showing a reasonably well mixed structure in terms of temperature. The along channel velocity component cross-sectional and vertical structures, reveal a stratified water column with more intense ebb currents at the top layers and less intense values from mid water until the bottom of the section. The u-velocity presents ebb values throughout the water column, ranging from -0.76 near the surface to ~ -0.03 near the channel's bed. At this time the estuarine water is still being flushed out from the channel, revealing a time lag between velocity and water level (this will be analyzed later).

At mid flood, three hours after the low water (Figure 8.12d, 8.12e and 8.12f), the water column remains highly stratified in terms of salinity, presenting lower values of 25 psu at the top layers and values of 35 psu near the channels bed. However, the salinity structure reveals some lateral

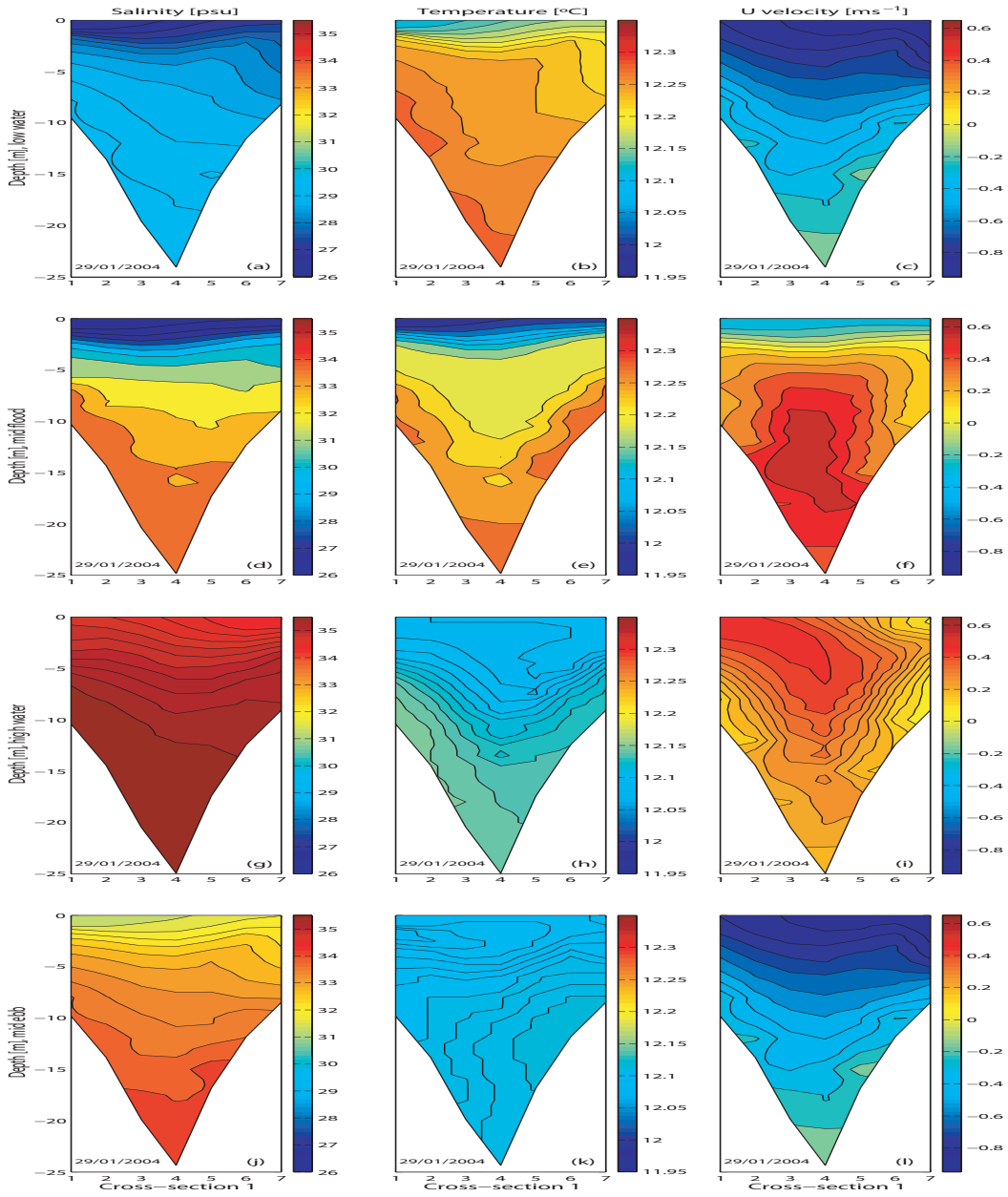

Figure 8.12: Cross-sectional distribution of salinity (a, d, g, j), water temperature (b, e, h, k) and longitudinal velocity (c, f, i, l) at a lower channel station located near the channel's mouth (upstream view). Simulation period: 29/01/2004. River inflow: 143.16 m^3s^{-1}

homogeneity. Close to the north shore, near the bed, the values found are higher (35 psu) than close to the south shore (~33-34 psu). This could be related to the jetties direction, which induces a flood main path near the north shore of the inlet. The water temperature cross-sectional structure reveals some stratification with lower values near the surface (11.9 to 12.1°C) and higher values near the channel's bed. At this time (three hours after low water), the u-velocity structure still presents ebb

velocities at the top layer (~ -0.3 ms^{-1}). At mid-water and close to the bottom the velocity is positive (inward velocity), presenting values ranging from ~0.2 to ~0.6 ms^{-1}.

At high water (Figures 8.12g, 8.12h and 8.12i), the salinity structure reveals some stratification, with a top-to-bottom salinity difference of 1 psu, and reveals also lateral homogeneity. The cross-sectional water temperature structure shows a well mixed section with values rounding 12.1°C. The u-velocity structure presents flood (positive) values, presenting a velocity maximum near the surface of ~0.6 ms^{-1}. Once more it is visible that at high water the water is still flowing upstream.

During the ebb period, about 3 hours after high water, the salinity structure shows a stratified water column with a top-to-bottom difference of about 3 psu. At this time, the salinity structure reveals an almost lateral homogeneity in terms of salinity. The section is well mixed in terms of water temperature, and at this time the u-velocity presents ebb values through all the cross-section. The higher values are found at the top layers enhanced by the landward water flowing from the Vouga River.

One last remark about the water temperature structure is that through all the tidal cycle lower values are found close to the surface than at the bottom layers. This is due to the colder water discharged from the river and also due to a decrease of the water temperature along the afternoon and evening of January 29^{th}.

At cross-section 4 (Figure 8.13), almost the same features are observed as the channel's mouth. However, at this location, the river effect is stronger than near the channel's mouth and several issues should be pointed out. At low water, the water column is highly stratified in terms of salinity. The maximum and minimum values are found close to the bed (19 psu) and the surface (13 psu), respectively. The cross-sectional water temperature structure is identical to the salinity structure with a top-to-bottom difference of ~0.5°C. At this time, the u-velocity structure shows ebb and more intense values at the top layers with a maximum near the surface of ~0.6 ms^{-1}. Near the channel's bed slightly flood (positive) values of 0.01 ms^{-1} are found.

During the flood (Figures 8.13d, 8.13e and 8.13f, ~3 hours after low water), the salinity cross-section show an highly stratified water column, with a top-to-bottom salinity difference of ~14 psu. Salinity values are lower near the surface than at low water, revealing the time lag between the minimum salinity value and water level. The cross-sectional structure of water temperature follows the salinity structure, showing a stratified water column. Lower water temperature values are found at the top layers (~10.8°C) increasing toward the bottom until a maximum of 12.2°C. The cross-sectional u-velocity structure shows a maximum flood (positive) velocity at mid water (0.44 ms^{-1}), and near the surface presents ebb values of -0.24 ms^{-1}. This shows that at this time, the flood is not fully developed, at almost 4 km upstream of the channel's inlet, revealing the river influence in this mid channel station.

At high water (Figures 8.13g, 8.13h and 8.13i), the water column is stratified with a top-to-bottom difference of ~6 psu. The water temperature structure follows the salinity structure, and also presents stratification, presenting lower values near the surface (11.9°C) and a maximum of 12.2° close to the channel's bed. The u-velocity cross-sectional structure present a maximum in the middle of the water

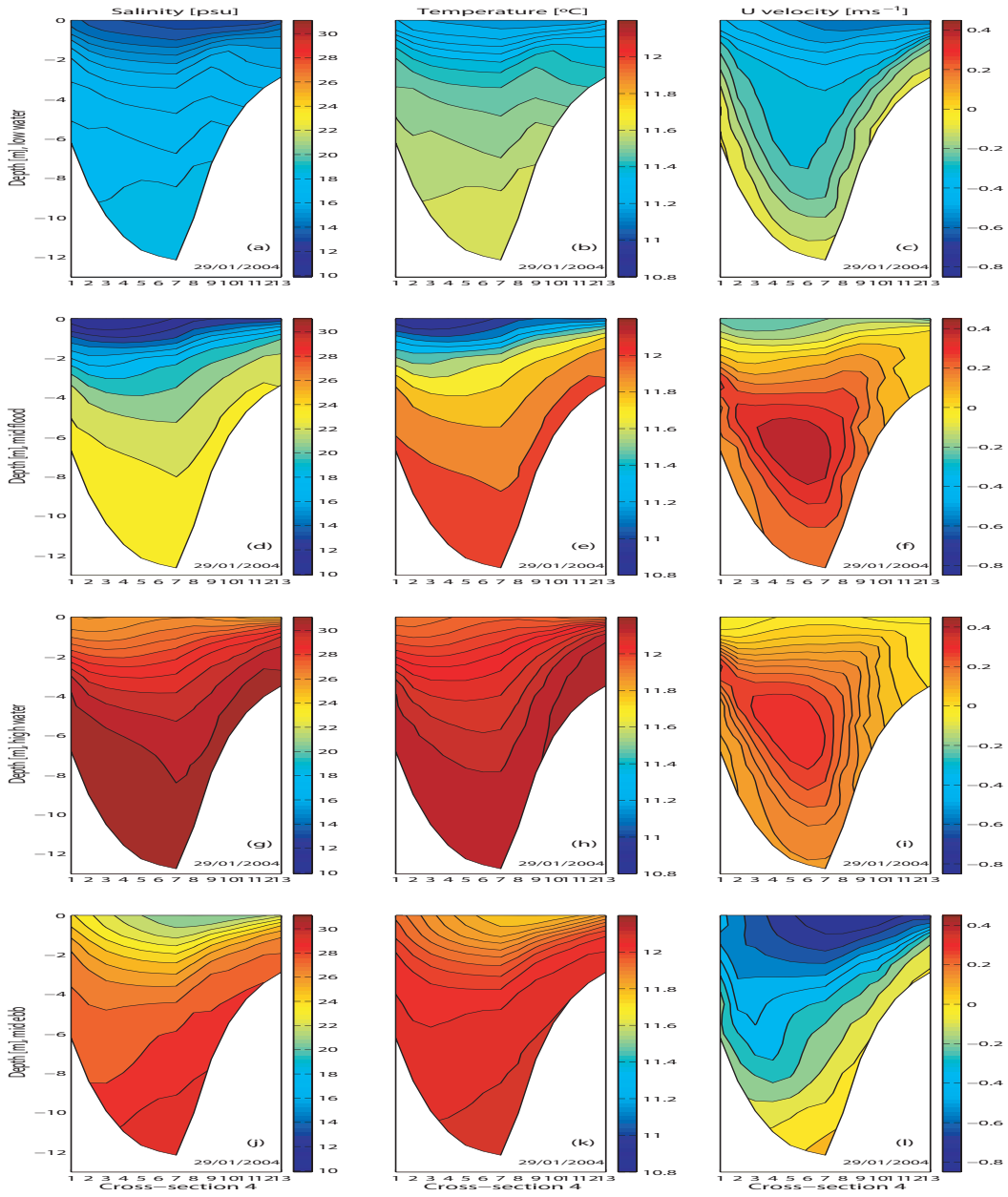

Figure 8.13: Cross-sectional distribution of salinity (a, d, g, j), water temperature (b, e, h, k) and longitudinal velocity (c, f, i, l) at a mid channel station located upstream of station C (upstream view). Simulation period: 29/01/2004. River inflow: 143.16 m^3s^{-1}

column (0.32 ms^{-1}). Near the surface, the u-velocity presents a slightly negative value of -0.04 ms^{-1}, meaning that the river flow is still dominant over tide at high water.

During the ebb period (Figures 8.13j, 8.13k and 8.13l), the cross-sectional salinity and water temperature structures show a stratified water column. The top-to-bottom salinity and water temperature difference are 9 psu and 0.41°C, respectively. At this time, u-velocity cross-sectional structure roughly follows the salinity structure. The higher u-velocity values are found from the middle of the

cross-section toward the south shore with values of ~ -0.8 ms^{-1}. Hypothetically, this may be related to the channel's curvature which induces a preferential flow path close to the south shore of the channel. At this time, the ebb is not fully developed and a u-velocity positive value is found at the central axis of the channel near its bed.

8.3.8 Evaluating the phase difference between water level, salinity and longitudinal velocity

The analysis of Figures 8.12 and 8.13, have revealed the existence of a phase difference between water level, u-velocity and the occurrence of the maximum and minimum of salinity. In this channel, as in other tidal channels and estuaries, tidal elevation and velocity are not in phase, and the maximum and minimum salinity occur before or after high and low water. The use of a tested numerical model is particularly useful, not only to know the three-dimensional or longitudinal structure of a domain, but also to understand how different forcing conditions affect the occurrence of maximums and minimums of estuarine variables and the phase difference between them. In order to examine this phase lag vertical profiles of u-velocity and salinity are used, obtained at the central axis of the channel (at the cross-sections previously referred), during a complete tidal cycle for the four simulation periods described in this study.

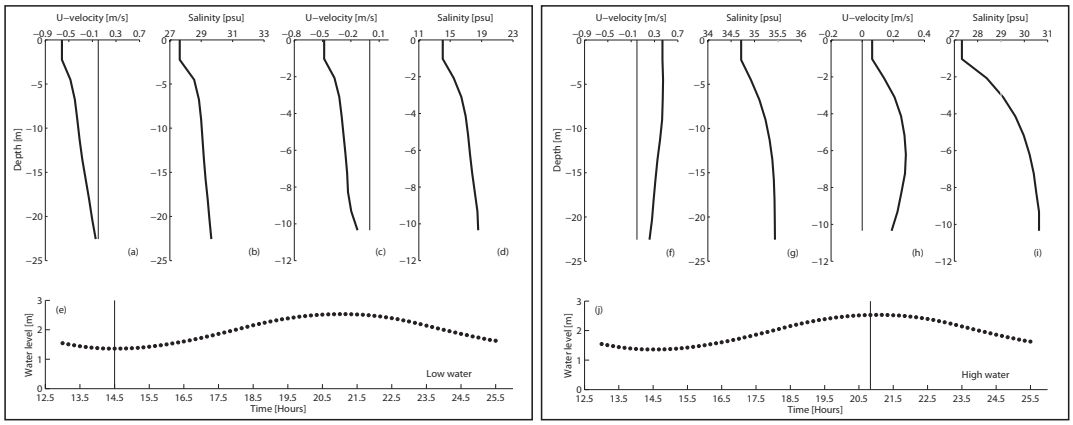

Figure 8.14: Computed vertical profiles of u-velocity and salinity at cross-section 1 (a, b, f, g) and cross-section 4 (c, d, h, i) central axis for January 29^{th} 2004. Left panel: low water; right panel: high water

A pronounced stratification and shear velocity at both locations at low (left panel) and high water (right panel) is noticeable from the salinity abd velocity profiles. At low water, ebb currents are visible at both cross-sections with a more pronounced shear at cross-section 1 (Figure 8.14a) and a similar stratification at both cross-sections. Near the surface, the longitudinal velocity present values of about -0.6 ms^{-1}, decreasing toward the channel's bed. At cross-section 4 ebb currents of about -0.5 ms^{-1} are found at the top layer, decreasing towards the bottom. The salinity profiles reveal some stratification, with top-to-bottom salinity differences of about 2 and 5 psu at cross-sections 1 and 4,

respectively. At high water (right panel), the water is still being pushed into the channel, presenting flood velocities at both cross-sections. Near the channel's mouth (cross-section 1, Figure 8.14f), a typical logarithmic velocity profile is visible, with more intense values near the surface (~0.4 ms^{-1}). At cross-section 4 (Figure 8.14h), the influence of the river discharge is visible in the velocity profile, with lower values at the surface, increasing up to the middle of the water column and then decreasing toward the bottom.

In Figure 8.15 are depicted the vertical profiles of u-velocity and salinity at cross-sections 1 and 4 at two different times: the beginning of the flood period and when the flood is fully developed in the entire water column.

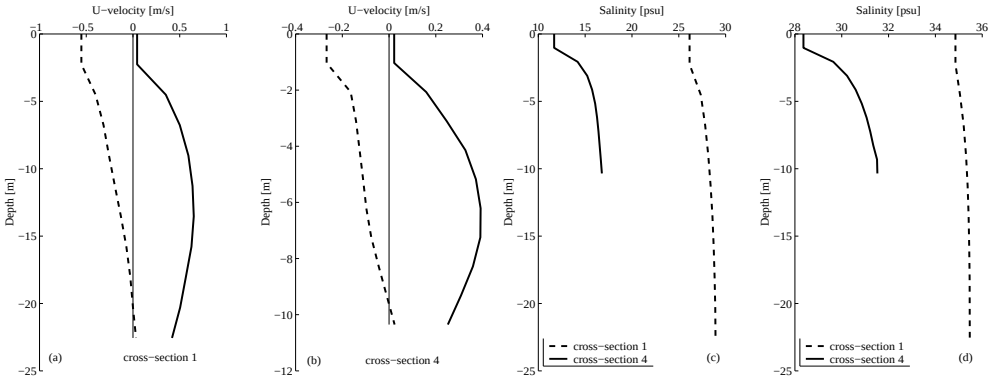

Figure 8.15: Vertical profiles of u-velocity at cross-sections 1 (a) and 4 (b). Dashed line: beginning of the flood and solid line: fully developed flood current. The velocity units are ms^{-1}. (c) and (d) represent the minimum and maximum salinity profiles during the tidal cycle.

At cross-sections 1 and 4 (Figures 8.15a and 8.15b), the flood period begins respectively 30 minutes and 1h 40 min after the low water. The water flow into the channel begins at the bottom layer and the flood is fully developed 3h 40 min after low water at both cross-sections (Figures 8.15a and 8.15b). This long time period necessary to achieve a fully developed flood, may be due to the intense freshwater inflow from the Vouga River which enhances the ebb currents at the surface and acts like a countercurrent in opposition to the tidal intrusion. The maximum flood velocity is reached 4h 50min after the beginning of the flood period at cross-section 1. At cross-section 4 the velocity maximum is reached after 3h 40 min after the beginning of the flood. The difference of about 1 hour, between the two maximums, is due to the influence of the high river discharge which decreases the flood velocity profile at the central area of the channel.

When the minimum (Figure 8.15c) and maximum (Figure 8.15d) salinity values are reached, the salinity profiles reveal lower values at cross-section 4 where the freshwater influence is higher. The salinity minimum occurs about 30 minutes after the beginning of the flood period at both cross-sections, revealing a time lag between the low water and the salinity minimum of ~1 hour. The salinity maximums occur 50 minutes and 1 hour after the high water at cross-section 1 and 4, respectively. From the figure is also visible that when the minimums and maximums salinities are

reached, there is stratification at both cross-sections. The top-to-bottom salinity difference is lower at the mouth of the lagoon. This fact may be related to the lower influence of the freshwater at this point and by the high velocity values, which increases turbulence and therefore increases mixing in the water column.

The Espinheiro Channel dynamic is mainly influenced by the interaction of tidal forcing and river inflow. From the four simulations described in this study, it is possible to characterize the phase difference between tidal elevation, longitudinal velocity and the occurrence of salinity minimums and maximums. In fact, changing the tidal forcing from neap to spring and imposing a low-to-high river inflow, slightly modifies the phase difference between these estuarine variables. For example, for the spring tide of November 26^{th} when the river inflow is weak (2.06 m^3s^{-1}), the time difference between the beginning of the flood and the low water is 1h 30min and less than 1h 40min at cross-sections 1 and 4, respectively. Increasing the river inflow (72.74 m^3s^{-1}) but keeping the tidal amplitude (spring tide simulation of November 25), this time difference is about 1h 40min at cross-section 1. When the river inflow changes from medium-to-high, the salinity minimum is reached after the beginning of the flood: 30 minutes under high river inflow and neap tide conditions (January 29^{th}) and 10 minutes under medium river inflow and spring tide conditions (November 25^{th}). The salinity maximums are reached, at both cross-sections, from 1 to 1h 20min after high water, at cross-sections 1 and 4, respectively. During the two periods of medium-to-high river inflow, the maximum flood current is reached typically, at both locations, 1 hour before high water.

8.3.9 Time evolution of tidal currents and thermohaline variables

Tidal currents and density (σ_t) time evolution were analyzed, both at the channel's inlet and at a mid channel station (located at the channel's axis at the two cross-sections previously examined), during two tidal cycles under a tidal range of about 1.3 and 1.6 m (moderate tidal regime) and high (143.16 m^3s^{-1}) and low (2.0 m^3s^{-1}) river inflow conditions (January 29 and July 25, 2004, respectively).

During this high river runoff event, the σ_t structure at the lower (Figure 8.16a) and mid channel station (Figure 8.16b) is similar. However, at the lower channel station (near the channel's inlet), σ_t values range from 20 kgm^{-3} close to the surface during low water to 26 kgm^{-3} during high water. The pycnocline is visible at mid-depth after the low water hour. The isopycnals are slightly downward tilted during the ebb and flood periods, presenting a constant value of 26 during the hours around high water. At the mid channel station, during the period from mid ebb tide to mid flood tide, the σ_t pattern reveal some stratification (revealed by the slightly tilted isolines). The pycnocline is visible during the low water at mid-depth. The σ_t patterns follow the tidal propagation increasing during the flood and decreasing during the ebb. The tidal velocity pattern is also similar at both stations, also following the tidal pattern: positive during flood tide and negative during ebb tide. At the lower channel station (Figure 8.16c), the isotachs are slightly downward tilted, presenting more intense values near the surface (-1.0 ms^{-1}) where the ebb currents are enhanced by the river discharge which transport less saline water through the channel until the shelf. The flood tidal currents present a

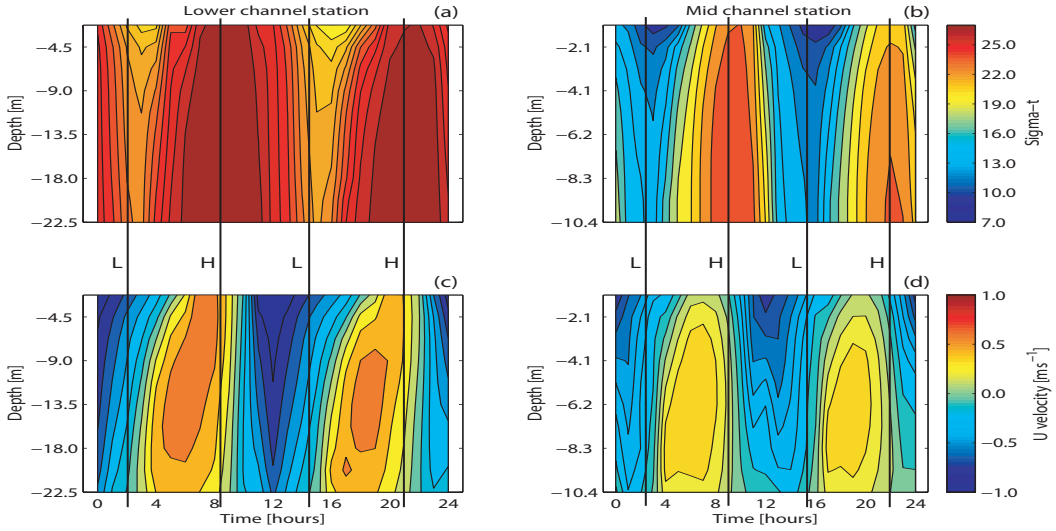

Figure 8.16: Time evolution of the isopycnals (σ_t) and tidal currents calculated at two stations under neap tide conditions on January 29, 2004: near the channel's inlet (a, c) and 1 km upstream of station C (b, d). The river inflow imposed at the landward boundary is 143.16 m^3s^{-1}. L and H are referred as low and high water.

maximum of 0.9 ms^{-1}. At the mid channel station (Figure 8.16d), the ebb currents are similar to the ones near channel's inlet (maximum of -1.0 ms^{-1}), but the flood tidal currents are lower (maximum of 0.5 ms^{-1}). At this location the river discharge effect is higher, filling the water column with brackish water (the exception is during high water), turning the flood currents lower.

In Figure 8.17 the density and tidal velocities patterns for the July 25 simulation are depicted.

During the low river flow period of July 25, at the lower channel station (Figure 8.17a), the σ_t patterns reveal an apparent stratification. However, at this location, σ_t range from 25.6 near the surface to 26 kgm^{-3} near the bottom, revealing a well mixed water column. At the mid channel station (Figure 8.17b), the water column reveal some stratification around the low water with σ_t values ranging from 25 to 26 kgm^{-3}. During the flood tide, the water column becomes well mixed with σ_t values of $\sim$ 26 kgm^{-3}. The current velocity structure is similar at both stations (Figures 8.17c and 8.17d). The isotachs are nearly vertical, following the tidal propagation pattern: negative during ebb tide turning positive during the flood tide. The ebb and flood maximums are lower at the mid channel station. Near the channel's inlet the tidal velocity range from -0.8 to 0.8 ms^{-1} during ebb and flood tide, respectively. At the mid channel station, the ebb currents present a maximum of -0.7 and the flood currents a maximum of 0.4 ms^{-1}.

In general, the tidal evolution of the thermohaline properties and of the tidal velocity reveal a slight partially mixed mixed water column. This can be due to the high tidal currents which increase the turbulence near the channel's bed, and, hence, the water column mixing. This is visible during the high river inflow event, when during the ebb tide the whole water column is progressively filled with freshwater, and conversely with salt water during the flood tide. These results reveal an asymmetry

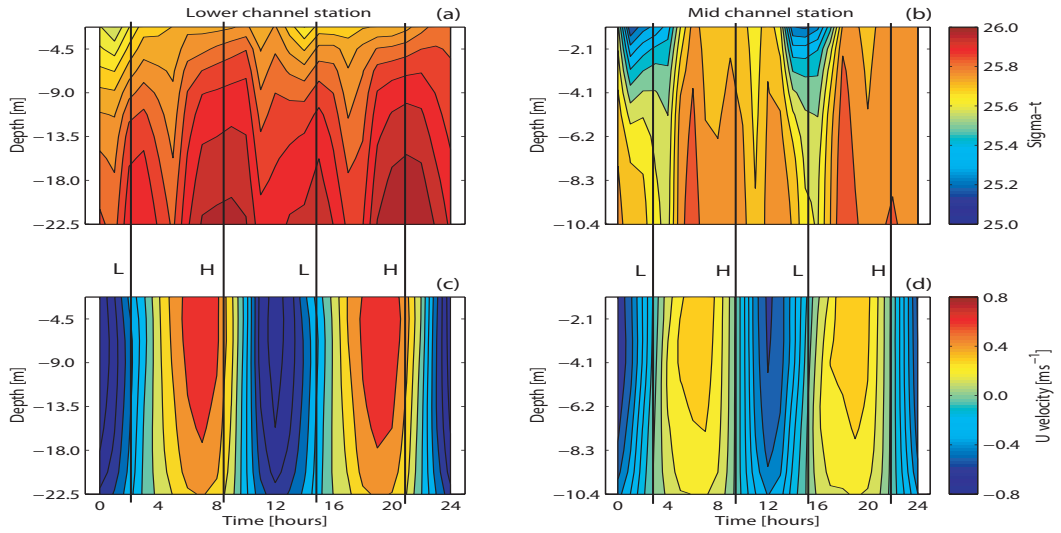

Figure 8.17: Tidal evolution of the isopycnals (σ_t) and tidal currents calculated at two stations under neap tide conditions on July 25, 2004: near the channel's inlet (a, c) and 1 km upstream of station C (b, d). The river inflow imposed at the landward boundary is 2.0 m^3s^{-1}. L and H are referred as low and high water.

between ebb and flood currents showing an ebb-dominated channel, where the ebb currents are more intense than the flood currents.

8.3.10 Estuarine stratification

In order to evaluate the estuarine stratification in the Espinheiro Channel under different conditions of tidal ranges and river inflow, the Estuarine Richardson number, Ri_E, [Fischer, 1972; Fischer et al., 1979; Dyer, 1997] was calculated at a lower channel and at a mid channel station. This number expresses the ratio of the gain of potential energy due to the freshwater discharge to the mixing power of tidal currents, and it is defined as

$$Ri_E = g\left(\frac{\Delta\rho}{\rho}\right)\left(\frac{Q_f}{bU_{rms}^3}\right) \tag{8.2}$$

where Q_f is the river inflow, b is the width of the section where the data were taken, $\Delta\rho$ is the density difference between sea and freshwater, ρ is the mean density and U_{rms} is the root-mean-square tidal velocity. According to Fischer [1972] and Fischer et al. [1979], if Ri_E is greater than 0.8 the estuary is considered highly stratified, if it is smaller than 0.08 the estuary is considered well mixed and finally, if $0.08 < Ri_E < 0.8$ the the estuary is considered partially mixed. Moreover, the water column stability was analyzed using the Brunt-Väisälä frequency (N) (or buoyancy frequency) [Pond and Pickard, 1983], calculated at the two locations previously referred. N is defined as

$$N = \left(\frac{g}{\rho}\frac{\Delta\sigma_t}{\Delta z}\right)^{1/2} \tag{8.3}$$

where ρ is the density, σ_t is the density at atmospheric pressure (1000 kgm^{-3}) and z is the depth measured from the surface. The results for the four simulations performed as well as the hydrographic conditions are presented in Table 8.2.

Table 8.2: Estuarine Richardson number (Ri_E) and maximum Brunt-Väisälä frequency (N_{max}) as a function of the tidal range and river inflow at the lower channel station (LC) and mid channel station (MD)

Date	Tidal range [m]	River inflow [m^{3}s^{-1}]	Station	Ri_E	N_{max} [min^{-1}]
26/09/2003	2.8	2.06	LC	0.001	0.56
			MD	0.005	0.72
25/11/2003	2.8	72.74	LC	0.050	0.93
			MD	0.180	1.87
29/01/2004	1.3	143.16	LC	0.950	1.71
			MD	2.597	3.84
25/07/2004	1.6	2.00	LC	0.010	0.69
			MD	0.054	0.97

According to the results presented in Table 8.2, when the river flow is weak, the Espinheiro Channel behaves as a well mixed estuary at the lower channel area (independently of the tidal regime), changing to highly stratified when the river flow is very high and during neap tide. Even during a high river inflow event (November, 25) but under spring tide conditions (tidal range of 2.8 m, and higher tidal velocities), this channel area behaves as a well mixed estuary. At the mid channel area, the Espinheiro Channel changes from well mixed to highly stratified depending on the river inflow. In fact, when the river inflow is weak this area is considered as a well mixed estuary independently on the tidal regime. When the river inflow increases, this area changes from partially stratified under spring tide conditions to highly stratified under neap and high river inflow. The characteristics of the whole flow have been analyzed using Ri_E. This information can be complemented by means of the Brunt-Väisälä frequency calculated at the two locations previously referred. Figure 8.18 depicts the Brunt-Väisälä values as a function of the layer's depth for both locations under high (Figure 8.18a) and low river inflow (Figure 8.18b).

Both figures show high values of N near the surface layers and low values near the channel's bed, indicating a more stratified water column near the surface and more homogeneous near the bed for the two channel locations analyzed. The overall N is higher at the mid channel station due to the freshwater effect at this location. Figure 8.18b reveals lower values of N than in Figure 8.18a both close to the surface and the bed. This is due to the almost negligible river inflow, which at this location make the water column well mixed. On both cases, the lower values of N were found at the lower channel station where the highest tidal velocities were found. In general, these model results do not illustrate the existence of a a visible pycnocline, being more visible a monotonic decrease of N toward the channel's bed. This fact may indicate an overestimated mixing of the water column. Only under a high river runoff event, a pycnocline is visible at a depth of $\sim$ 2.5 (lower channel station) and $\sim$ 1.04 m (mid channel station). In this case, the maximum Brunt-Väisälä frequency ranges from 1.71 to 3.84 min^{-1} at the lower and mid channel stations, respectively.

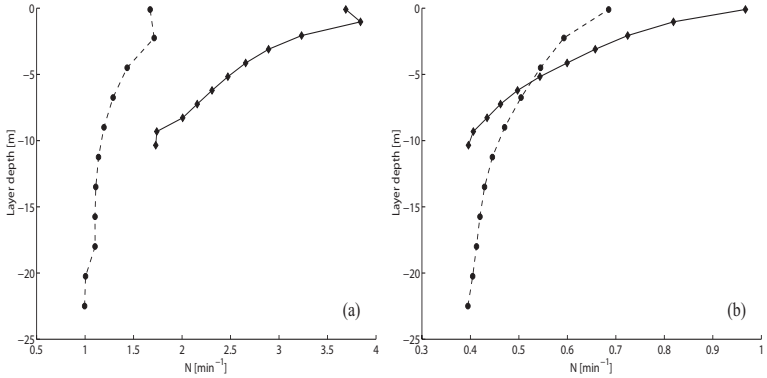

Figure 8.18: Brunt-Väisälä frequency (N [m^{-1}]) as a function of layer depth [m] on January 29 (a) and on July 25, 2004 (b). Black circles corresponds to the lower channel station, black diamonds to the mid channel station.

8.4 Discussion and conclusions

A 3D baroclinic numerical model (Mohid) was used to perform hindcast simulations of the Espinheiro Channel covering short periods of time in order to assess the channel's vertical structure under different tidal and river inflow conditions. The first part of this study show a comparison of model results with field measurements in order to check the model's capacity in reproducing hydrodynamic and thermohaline measurements. Then, it was tried to find some of the channel's features, as the residual circulation, cross-sectional vertical structure of the channel, the tidal evolution of thermohaline variables and the estuarine stratification. For that purpose four short periods of time (4 days) it were chosen during different tidal ranges (spring and neap tides) and freshwater inflow (low-to-high river runoff) in order to perform hindcast simulations.

The baroclinic model reproduces the observed temporal variability in sea level height and current velocity. For the sea level height, the Skill coefficient ranged from 0.93 at station A to 0.87 at station D. For the along channel velocity, this coefficient presents a value of 0.84. This Skill value may be due to the fact that model results are related to the averaged value over the horizontal spatial domain corresponding to a grid cell, while the field data is the value at a single point. In general, the baroclinic model reproduces the along-channel thermohaline distributions. Although the Skill coefficient presents higher values during high river runoff conditions, the model can also reproduce the thermohaline distributions when the river flow is weak (September and July simulations). The overall results were influenced by the thermohaline patterns near the channel's head. In fact, at this location, the model could not reproduce well the thermohaline distributions under low river runoff conditions (September and July simulations), presenting values different from those observed, especially when we took into account the salinity results. When the river inflow is high (November and January simulations), the model tends to underpredict the observed salinity pattern. This can be due to the high current velocity within the channel which tends to increase the turbulence and hence the vertical mixing and to the chosen landward boundary condition which presents a constant

value during the simulations. In general, the along-channel water temperature distributions were reproduced by the model, with differences in the order of 1-2 °C.

The residual currents were also examined. The general characteristics within the domain are those of an ebb-dominated channel, revealing a more intense current near the surface due to the freshwater inflow. Another feature found, from the analysis of the residual circulation at the entrance channel of Ria de Aveiro, is that near the north shore of the channel's inlet the residual currents present very weak positive (inward) values, revealing a residual recirculation at this location. Near the south shore the residual currents present negative (outward) values. This may suggest that, at the entrance channel of the lagoon, the water flow during ebb has a preferential path near the south shore of the channel's entrance. This preferential path during the ebb period may be related to the channel's curvature which induces a flow path close to the south shore of the lagoon's inlet.

The tidally-averaged cross-sectional and vertical structure of the channel were examined at two cross-sections separated by ∼4 km. They present similar salinity and residual velocity structures. Under low-to-medium river runoff the channel is laterally homogeneous in terms of salinity. However, the residual velocity structure is different, presenting landward velocities near the north shore of the channel and seaward velocities at the south shore. When the river inflow is high (higher than 100 m^3s^{-1}), the channel presents a typical estuarine behavior, with landward residual currents near the bottom and seaward currents at the top layers. The tidally-averaged salt transport follows the same patterns found in the residual currents results, presenting landward salt transport near the north shore and seaward salt transport near the south shore under low-to-medium river runoff. When the river flow is high, the landward salt transport was found near the channel's bed, being seaward at the top layers.

The model was used to characterize the cross-sectional vertical structure of the channel at two locations, represented by a lower channel station (near the channel's mouth) and a mid channel station (∼ 1 km upstream of station C). Near the mouth, the results reveal a well mixed structure during high water turning to partially stratified during the low water. The maximum current velocities are reached during the ebb, near the surface and south shore. At mid channel, the cross-sectional structure varies from weakly-to-strongly stratified from high to low water. The current velocities are lower than those calculated for the channel's mouth. The model results reveal a phase difference between sea level height, current velocity and the occurrence of maximums and minimums of salinity. Near the channel's mouth, and under spring tides with low-to-medium river discharge (September and November 2003 simulations), the time difference between low water (sea level minimum) and the beginning of the flood is ∼1h 40 min. This value changes on the neap tide of January 29^{th} when the time difference between low water and the beginning of the flood is ∼30 minutes. This may be due to the moderate tidal currents (lower than 1 ms^{-1} near the inlet) which reverses more rapidly than during spring tide.

The Espinheiro channel is an energetic tidal channel in which, the water mass dynamics is essentially driven by tides and river runoff. It is well known that the river flow, which causes an inflow of buoyancy, tends to maintain stratification, and that the tidal flow due to the friction causes mixing.

So, within the channel, at locations where the tidal currents are lower, the river flow can extend its influence producing stratification. This fact is illustrated by the results of the mid channel station. Near the channel's mouth, tidal currents are higher activating turbulent mixing, and generating well mixed conditions, except during high river runoff events when this area is partially stratified. In this channel, the high tidal currents are frequently able to homogenize the water column. Near the channel's mouth, the water exchange is mainly due to the tide, except under high river flow events when the freshwater extends its influence from the channel's head to its mouth.

For simulations of an estuarine environment, the prescription of boundary conditions is critical. These boundaries include the free surface, the bottom closed surface and the lateral open boundaries. Although, the density is more affected by salinity differences, in this work, it was imposed, at the free surface boundary, surface fluxes in order to proper simulate the water temperature within the channel. The surface wind stress was not considered, since its importance as a main driving force is not relevant in a narrow branched tidal channel as the Espinheiro Channel. The bottom surface requires a drag coefficient that may vary spatially or temporally. In these simulations a constat value was used, chosen from previous efforts. Scalar quantities along an open boundary are critical and challenging since they involve processes beyond the study domain. As an example, in some estuaries, the response of the river plume on the continental shelf to changes in freshwater inflow and wind conditions could be relevant.

The implementation and use of numerical models is a valuable tool that provides the spatial and temporal resolution of the velocity and scalar fields not accessible by observation only. In this domain, future applications should be able to model the near-ocean salinity accurately in order to improve the results within the channel. The model skill should be improved using a better prescription of boundary conditions in order to satisfy scalar and momentum fluxes across the boundaries. The boundary condition for bottom stress and open boundary conditions for salinity are crucial to increase the model skill. Although the horizontal grid presents a high resolution, results may be improved by increasing the vertical layers, especially in the region from the channel's mouth to the mid channel station previously referred.

The results presented in this chapter reveal that the baroclinic model (Mohid) used to reproduce the Espinheiro Channel dynamics was successfully implemented. To put in operation a three-dimensional model in such a complex area was a fascinating challenge. Due to the complex morphology and shallowness of the channel there were several difficulties to overcome. For each of the baroclinic model simulations of the Espinheiro Channel it was necessary to run first the model in a 2D (depth-integrated) mode for the entire lagoon, in order to compute the landward boundary conditions to impose at the landward open boundaries. This type of nesting is computationally very expensive and brings some limitations to long term simulations, since the computational time is very high in these cases. Other limitation is the high resolution of the horizontal grids, necessary to accurately resolve the physical processes within the channel. This high resolution limits the use of larger time steps in order to reduce the computational time. Moreover, the shallowness of the study area does not allow the use of a higher number of vertical layers in order to improve the results at the deeper

locations. Nevertheless, in spite all the difficulties and limitations, the approach used during this work is considered suitable to produce good results on modelling studies of the Espinheiro Channel.

Chapter 9

Conclusions

The Ria de Aveiro has four main channels, and due to their unique characteristics they behave as independent estuaries connected to a common inlet. The main purpose of this work was to study the thermohaline dynamics of one of these estuarine areas: the Espinheiro Channel, which is located in the complex central area of the lagoon. To achieve this main goal two interconnected approaches were used: field work and numerical modelling studies.

The field work may be considered well succeeded, since the measurements of physical parameters in the Espinheiro Channel increased the existent data base of hydrodynamic and hydrologic variables, contributing to a better characterization of the channel's dynamic. The numerical model used in this work (Mohid) reproduces adequately the major hydrodynamic features of Ria de Aveiro and of Espinheiro Channel in 2D depth-integrated and 3D modes, respectively. The numerical bathymetries of Ria de Aveiro and Espinheiro Channel were well represented by the model, which treated with accuracy flooding and drying of intertidal areas in such a complex study area.

The main results presented in this work reveal that the thermohaline dynamic both in Ria de Aveiro and Espinheiro Channel is a delicate balance between tides, river inflow and meteorological forcings.

The one year sampling campaign of thermohaline variables in the Espinheiro Channel has provided a major insight into its hydrographic features, revealing that the channel's hydrodynamics is largely dependent on the tidal wave characteristics and freshwater inputs variability. The analysis of the measured data revealed that when the river flow is low - less than 10 m^3s^{-1} - the water column is filled with salt water from the ocean until almost 8 km from the channel's mouth. When the river flow is higher than 100 m^3s^{-1} vertical stratification is established along the channel, and the freshwater from Vouga River extends its influence up to the channel's mouth. When the river flow lies between 30 and 50 m^3s^{-1}, the channel can be divided into three different regions: a lower marine region where the thermohaline variables present oceanic values; an intermediate inner region where mixing between ocean and river water occurs and a upper fluvial region which is dominated by freshwater but is still subject to a semidiurnal tidal action.

The formation of strong salinity gradients (commonly related to estuarine fronts) was observed

during the sampling period in a region between 7 and 8 km from the channel's mouth. The generation of these gradients is related to the interaction between salt and freshwater as well as to changes in the morphology (width and depth) of the channel. It was observed that these fronts migrate within a region of about 1 km, depending on the tidal regime: neap or spring tides. The estuarine fronts observed are mainly salinity fronts. The longitudinal water temperature variation within Espinheiro Channel is smoother than the salinity gradient. Apart from the dependence on the water temperature variations at the channel's boundaries (ocean and river), and due to the shallowness of the several regions of the channel, the water temperature pattern within Espinheiro is closely related to meteorological variations in air temperature, incoming solar radiation or relative humidity.

The 25 hour surveys performed near the channel's head, originated changes in the classification of the upper fluvial region of the Espinheiro Channel. During the cold season surveys (January and December 2004), this region presents salt wedge characteristics, with the occurrence of stratification/destratification events during the flood and ebb periods. On the other hand, this region presents partially mixed characteristics during June and August survey periods when the freshwater inflow is lower.

The balance between the seaward salt transport induced by the river discharge and the landward dispersion induced by various mixing mechanisms was assessed using measurements of velocity and salinity, sampled during two tidal cycles, near the mouth and head of the Espinheiro Channel. The total salt transport was decomposed into 7 terms: one advective due to the freshwater discharge (or residual circulation) and 6 dispersive terms which acts to transport salt upstream. From this approach, it was found that the major contributions to the salt transport near the channel's mouth are the transport due to the freshwater discharge and the tidal correlation terms, which may be correlated to topographic trapping. Near the channel's head, the major contributions are due to the freshwater discharge and the gravitational circulation terms. In these areas, where the gravitational circulation term is important, a compensating bottom current is originated to transport salt upstream, balancing the salt flushed out by the river. Eventhough the short term surveys performed were too small in order to give insight on meteorological effects influencing salt transport, they can produce valuable results regarding processes on tidal and subtidal time scales as the presented in this work.

The modelling task performed throughout this work began by assessing the hydrodynamic module of Mohid in a two-dimensional mode for all the lagoon. The model results were evaluated against several data sets of seal level height, current velocity and water flow. A good calibration and validation of the hydrodynamic model was achieved, revealing its ability in reproducing the barotropic flows in such a complex system as Ria de Aveiro. The transport module of Mohid was also implemented in a two-dimensional mode for all the lagoon. When no meteorological forcing is imposed, the longitudinal structure of water temperature in Ria de Aveiro is only affected by the sea and riverine water temperature, and the initial conditions suffer a major change after 12 tidal cycles (~6 days). Imposing meteorological forcing, the water temperature pattern begins to change after 3 tidal cycles, revealing the cooling effect due to exchanges between the water and the near atmosphere. The model results show the Mohid's ability in reproducing field results of temporal evolution of salinity and

water temperature. The major discrepancies were found in the water temperature results and may be related to the freshwater temperature assumed as boundary condition both at the oceanic open boundary and at the landward boundaries. The model seems to make use of an accurate bathymetry, and in general, the horizontal grid resolves well the transport processes.

The water temperature and salinity horizontal patterns and their dependence on the tidal and river inflow forcing were also studied for the central area of Ria de Aveiro under extreme conditions of tide and river inflow. When the river flow is high (1000 m^3s^{-1}), the freshwater extends to the entire central area of Ria de Aveiro (including the coastal zone) being determinant on the establishment of the thermohaline patterns in the central area of the lagoon. Despite this river discharge influence, during the flood the tide pushes the freshwater upstream revealing, even under extreme river flow discharge, a salinity intrusion of almost 8 km. When the river inflow is weak (lower than 10 m^3s^{-1}), the salinity and water temperature horizontal structure is mainly influenced by mixing due to turbulence caused by the tidal propagation within the lagoon.

The three-dimensional baroclinic model of Espinheiro Channel was used to cover topics like the residual circulation within the channel, with a closer look to its inlet; the cross-sectional tidally-averaged structure and salt transport; the cross-sectional thermohaline and tidal velocity structure of the channel; the temporal evolution of density and tidal currents. The vertical structure of the channel was also examined using estuarine parameters as the Richardson Number and buoyancy frequency, which are calculated from the model results.

The baroclinic model reveals its ability to qualitatively and quantitatively reproduce observations of sea level height, velocity and thermohaline variables. The overall results present a high skill score, when compared with observations, for almost all the channel's area. The exception is the region between 1 km upstream station D and the channel's head, a very narrow and shallow area of the channel, where the model was not able to reproduce accurately the thermohaline patterns. When the river flow changes from low-to-medium values, the model qualitatively reproduces the observed thermohaline patterns in the channel. When the river flow is higher than 100 m^3s^{-1}, the model tend to underpredict the observed salinity pattern. This may be due to the high current velocities within the channel, which increases turbulence and hence vertical mixing. Another factor that could limit the results is the constant value of river discharge imposed at the landward boundaries during the simulations.

The general characteristics of the residual circulation within the domain are those of an ebb-dominated channel, revealing more intense values near the surface due to the freshwater discharge. From the analysis of the residual circulation at the entrance channel of Ria de Aveiro, was found, in all simulations, that near the north shore of the Channel's inlet the residual currents are positive (inward) values, and near the south shore the residual currents are negative (outward) values. This may suggest a particular circulation pattern, with a preferential path during the flood and ebb near the north and south shore of the inlet.

The cross-sectional and vertical residual currents and salinity reveal that, under low-to-medium river runoff, the channel is laterally homogeneous in terms of salinity. However, the residual velocity

structure is different, presenting landward velocities near the north shore of the channel and seaward velocities at the south shore. When the river inflow is high (higher than 100 m^3s^{-1}), the channel presents a typical estuarine behavior, with landward residual currents near the bottom and seaward currents at the top layers. The tidally-averaged salt transport follows the same patterns found in the residual currents results, presenting landward salt transport near the north shore and seaward salt transport near the south shore under low-to-medium river runoff. When the river flow is high, the landward salt transport was found near the channel's bed, being seaward at the top layers.

Near the mouth, the cross-sectional thermohaline and longitudinal velocity patterns reveal a well mixed structure during high water turning to partially stratified during low water. The maximum current velocities are reached during the ebb, at the surface and south shore. At mid channel, the cross-sectional structure varies from weakly-to-strongly stratified from high to low water. The current velocities are lower than those calculated for the channel's mouth. The model results reveal a phase difference between sea level height, current velocity and the occurrence of maximums and minimums of salinity. Near the channel's mouth, and under spring tides with low-to-medium river discharge (September and November 2003 simulations), the time difference between low water (sea level minimum) and the beginning of the flood is ~1h 40 min. This value changes on the neap tide of January 29^{th} when the time difference between low water and the beginning of the flood is ~30 minutes.

Sampling strategies like the one followed in the data acquisition - synoptic and short term surveys - were chosen due to the limited instrumentation available and some logistic problems like human limitations and the impossibility of performing long term measurements along the channel. In fact, the measurement of salinity, water temperature and current velocity during several consecutive tidal cycles, and at several locations along the channel, would allow for a better assessment of the hydrography of the channel. Issues like the salt fluxes or the classification of the channel in terms of salinity and current structures would benefit of this long term data acquisition. One way to overcome the lack of measured data is the use of a numerical model for the Espinheiro Channel. However, this channel is sinuous and has a complex geometry (a common feature within Ria de Aveiro), and the implementation of the numerical model turn out to be very challenging.

An orthogonal curvilinear coordinate system was designed to follow the general orientation of the channel including its major tributaries and the near coastal ocean. High resolution was used in order to properly resolve the physical features of the channel. Due to its location and because its hydrology is influenced by the adjacent channel's contributions, time varying fluxes of water, salinity and water temperature were imposed at the boundaries between Espinheiro and the other main channels. The approach adopted consists on running the model in a two-dimensional mode for all the lagoon in order to obtain these fluxes, and then impose them as landward boundary conditions and run the three-dimensional model for the Espinheiro Channel. Due to the relative small size of the grid cells this approach is very time consuming, since the model is run twice (first in a 2D mode and then in a 3D mode). Nevertheless, this kind of nesting proved to be an adequate solution to overcome the difficulties on modelling the Espinheiro Channel.

In order to perform hydrodynamic and transport simulations within estuarine environments, the prescription of reliable boundary conditions is essential. Besides the forcings prescribed in this study, in future model applications the surface wind stress should be considered and its role as a major driving force assessed. Future simulations will also benefit from a bottom drag coefficient that may vary spatially or temporally. At the open lateral boundaries, momentum balances may be obtained from observations of river flow and tidal elevations. Scalar quantities along an open boundary are critical and challenging since they evolve processes beyond the study domain. Also, future model applications should be able to model the near-ocean salinity accurately in order to improve the results within the channel. Although the horizontal grid present a high resolution, it should be able to improve the results by increasing the vertical layers, especially in the region from the channel's mouth to the mid channel station previously referred.

It remains for the future several experimental studies in order to increase the knowledge about thermohaline dynamics in the Espinheiro Channel. It will be useful in the future to perform field surveys that cover an entire spring-neap cycle in order to evaluate the temporal variation of the salinity, water temperature and current velocity. A better spatial coverage of critical areas of the channel - its mouth and central area - would be a valuable contribution to better understand cross-sectional variation of these estuarine variables. These field surveys should, ideally, last for at least one year in order to characterize the seasonal cycle of thermohaline variables within the channel. Short term high resolution - spatial and temporal - surveys of salinity and velocity are needed in order to study the strong salinity gradients (estuarine fronts) identified in this work.

Bibliography

Abbott, M. B., Basco, D. R., 1994. Computational fluid dynmics: an introduction for engineers. Longman Scientific and Technical, London, 425 p.

Abbott, M. B., Damsgaardand, A., Rodenhuis, G. S., 1973. System s21, Jupiter a design system for two-dimensional nearly-horizontal flows. J. Hyd. Res., 1–28.

Abrantes, I., Dias, J. M., Rocha, F., 2005. Spatial and temporal variability of suspended sediments concentration in Ria de Aveiro lagoon and fluxes between the lagoon and the ocean. Journal of Coastal Research SI39, (In press).

Abrantes, M. I. R. R., 2005. Os sedimentos superficiais da margem continental, sector Espinho - Cabo Mondego: a utilização das fracções finas como traçadores de dinâmica sedimentar actual. Ph.D. thesis, Universidade de Aveiro, Aveiro, Portugal.

Aldridge, J. N., Davies, A. M., 1993. A high resolution three-dimensional hydrodynamical tidal model of the Eastern Irish Sea. Journal of Physical Oceanography 23, 207–224.

Almeida, M. A., Cunha, M., Alcantâra, F., 2001. Factors influencing bacterial production in a shallow estuarine system. Microbial Ecology 42 (3), 416–426.

Alvarez, I., deCastro, M., Gomez-Gesteira, M., Prego, R., 2005. Inter- and intra-annual analysis of the salinity and temperature evolution in the Galician Rias Baixas-ocean boundary (northwest Spain). Journal of Geophysical Research 110, doi: 10.1029/2004JC002504.

Alvarez, I., deCastro, M., Gomez-Gesteira, M., Prego, R., 2006. Hydrographic behavior of the Galician Rias Baixas (NW Spain) under the spring intrusion of the Miño River. Journal of Marine Systems 60, 144–152.

Álvarez, I., deCastro, M., Prego, R., Gómez-Gesteira, M., 2003. Hydrographic characterization of a winter-upwelling event in the ria of pontevedra (NW Spain). Estuarine Coastal and Shelf Science 56, 869–876.

Arakawa, A., Lamb, V., 1977. Computational design of the basic dynamical processes of the UCLA general circulation model. Meth. Comput. Phys. 17, 174–267.

Araújo, I. G. B., 2005. Sea Level Variability: Examples From the Atlantic Coast of Europe. Phd Thesis, School of the National Oceanography Centre, Southampton, UK.

Backhaus, J., 1983. A semi-implicit scheme for the shallow water equations for application to shelf sea modelling. Cont. Shelf Sea Res. 2, 243–254.

Banas, N. S., Hickey, B. M., 2005. Mapping exchange and residence time in a model of Willapa Bay, Washington, a branching, macrotidal estuary. Journal of Geophysical Research 110 (C11011), doi: 10.1029/2005JC002950.

Banas, N. S., Hickey, B. M., MacCready, P., Newton, J. A., November 2004. Dynamics of Willapa Bay, Washington: A highly unsteady, partially mixed estuary. Journal of Physical Oceanography 34, 2413–2427.

Barnes, R. S. K., 1977. The coastline (356 pp). Wiley, Chichester, UK.

Barnes, R. S. K., 1980. Coastal Lagoons (106 pp). Cambridge: Cambridge University Press.

Bérgamo, A. L., 2000. Características da hidrografia, circulação e transporte de sal: Barra de Cananéia, sul do mar de Cananéia e baía do Trapandé. Dissertação de mestrado, Instituto oceanográfico, Universidade de S. Paulo, S. Paulo.

Bobos, I., Rocha, F., 2006. Radiocaesium dispersion and fixation in the lagoons systems of ria de aveiro. Journal of Geochemical 88 (1-3), 367–372.

Borrego, C., Pinho, P., Costa, F., Cardoso da Silva, M., 1990. The Case Study of Ria de Aveiro. Draft report, GRIA, Aveiro, 61 pp.

Bowden, K. F., 1963. The mixing processes in a tidal estuary. Int. J. Air Pollut. 7, 343–356.

Bowden, K. F., 1967. Circulation and diffusion. In Estuaries. No. 85. AAAS Publ., Washington, D. C., pp 15-36.

Bowen, M. M., Geyer, W. R., 2003. Salt transport and the time-dependent salt balance of a partially stratified estuary. Journal of Geophysical Research 108 (C5), 3158, doi: 10.1029/2001JC001231.

Braunschweig, F., Martins, F., Chambel, P., Neves, R., 2003. A methodology to estimate renewal time scales in estuaries: the tagus estuary case. Ocean Dynamics 53, 137–145.

Brock, T. D., 1981. Calculating solar radiation for ecological studies. Ecological Modelling.

Burchard, H., 2002. Applied turbulence modelling in marine waters. Lect. Notes Earth Sci. 100, springer, New York.

Burchard, H., Bolding, K., 2001. Comparative analysis of four second-moment turbulence closure models for the oceanic mixed layer. Journal of Physical Oceanography 31, 1943–1968.

Burchard, H., Bolding, K., 2002. GETM, a general estuarine transport model: scientific documentation. tech. report, European Community, Ispra, Italy.

Burchard, H., Bolding, K., Villarreal, M. R., 1999. GOTM, a general ocean turbulence model: scientific documentation. tech. report, European Community, Ispra, Italy.

Burchard, H., Bolding, K., Villarreal, M. R., 2004. Three-dimensional modelling of estuarine turbidity maxima in a tidal estaury. Ocean Dynamics 54, 250–265.

Cameron, W. M., Pritchard, D. W., 1963. Estuaries. In: The Sea. ed. M. N. Hill, John Wiley & Sons, New York, pp. 306–324.

Cancino, L., Neves, R., 1999. Hydrodynamic and sediment suspension modelling in estuarine systems. Part II: Application to the Western Scheldt and Gironde estuaries. Journal of Marine Systems 22, 117–131.

Canuto, V. M., Howard, A., Cheng, Y., Dubovikov, M. S., 2001. Ocean turbulence I: One-point closure model. momentum and heat vertical diffusivities with and without rotation. Journal of Physical Oceanography 31, 1413–1426.

Castanho, J. P., Carvalho, R., Vera-Cruz, D., 1968. Barragem no Rio Vouga e desvio dos esgotos - anteprojecto (55 pp). Unpublished report, ii.

Chapra, S. C., 1997. Surface Water Quality Modeling. Civil engineering series. McGraw-Hill.

Cheng, R. T., Burau, J. R., Gartner, J. W., 1991. Interfacing data analysis and numerical modelling for tidal hydrodynamic phenomena. In: Parker, B. B. E. (Ed.), Tidal Hydrodynamics. John Wiley and Sons, New York, USA, pp. 201–219.

Cheng, R. T., Casulli, V., Gartner, J. W., 1993. Tidal, residual, intertidal mudflat (TRIM) model and its applications to San Francisco Bay, California. Estuarine, Coastal and Shelf Science 36, 235–280.

Chippada, S., Dawson, C., Wheeler, M., 1998. A Godonov-type finite volume method for the system of shallow water equations. Comput. Methods Appl. Mech. Eng 151, 105–130.

Coelho, H., Neves, R. J. J., White, M., Leitão, P. C., Santos, A. J., 2001. A circulation model for Western Iberia. Journal of Marine Systems 32, 153–179.

Coelho, H., Santos, A., Rosa, T. L., Neves, R., 1994. Modelling the wind drivem flow in the Iberian Peninsula. GAIA 8, 71–78.

Coelho, J. P., Rosa, M., Pereira, E., Duarte, A., Pardal, M. A., 26. Pattern and annual rates of scrobiculania plana mercury bioaccumulation in a human induced mercury gradient. Estuarine Coastal and Shelf Science 69 (3-4), 629–635.

Cressie, N. A. C., 1993. Statistics for Spatial Data. John Wiley and Sons, New York, 900 pp.

Cugier, P., Le Hir, P., 2002. Development of a 3d Hydrodynamic Model for Coastal Ecosystem Modelling. Application to the Plume of the Seine River. Estuarine Coastal and Shelf Science 55, 672–395, doi: 10.1006/ecss2001.0875.

Cunha, M. A., Almeida, M., Alcantâra, F., 2001. Short-time responses of the natural planktonic bacterial community to the changing water properties in an estuarine environment: ectoenzymatic activity, glucose incorporation and biomass production. Microbial Ecology 42 (1), 1–12.

Cunha, M. M. P. R., 1999. Peracaridan crustacea in Ria de Aveiro (NW Portugal): Taxonomic composition and spatial-temporal structure of the assemblages; life history and secondary production of corophium multisetosum stock, 1952 (amphipoda, corophiidae). Ph.D. thesis, University of Aveiro, 195 pp.

deCastro, M., Gomez-Gesteira, M., Alvarez, I., Prego, R., 2004. Negative estuarine circulation in the Ria of Pontevedra (NW Spain). Estuarine Coastal and Shelf Science 60, 301–312.

Dias, J. M., 2001. Contribution to the study of the Ria de Aveiro hydrodynamics. Ph.D. thesis, University of aveiro, Portugal, University of Aveiro, 288 p.

Dias, J. M., Fernandes, E. H., 2006. Tidal and subtidal propagation in two Atlantic estuaries: Patos Lagoon (Brazil) and Ria de Aveiro Lagoon (Portugal). Journal of Coastal Research (SI39), in press.

Dias, J. M., Lopes, J. F., 2006. Implementation and assessment of hydrodynamic, salt and heat transport models: The case of Ria de Aveiro Lagoon (Portugal). Environmental Modelling and Software 21, 1–15.

Dias, J. M., Lopes, J. F., Dekeyser, I., 1999. Hydrological characterisation of Ria de Aveiro, Portugal, in early summer. Oceanologica Acta 22 (5), 473–485.

Dias, J. M., Lopes, J. F., Dekeyser, I., 2000. Tidal propagation in Ria de Aveiro lagoon, Portugal. Phys Chem Earth (B) 25, 369–374.

Dias, J. M., Lopes, J. F., Dekeyser, I., 2001. Lagrangian transport of particles in Ria de Aveiro lagoon, Portugal. Phys Chem Earth (B) 26 (9), 721–727.

Dias, J. M., Lopes, J. F., Dekeyser, I., 2003. A numerical system to study the transport properties in the Ria de Aveiro lagoon. Ocean Dynamics 53, 220–231.

Driscoll, T. A., Vavasis, S. A., 1998. Numerical conformal mapping using cross-ratios and delaunay triangulation. SIAM J. Sci. Comput. 19 (6), 1783–1803.

Dronkers, J., van de Kreeke, J., 1986. Experimental determination of salt intrusion mechanisms in the Volkerak Estuary. Neth. J. Sea Res 20, 1–19.

Dronkers, J. J., 1964. Tidal Computations in Rivers and Coastal Waters. North-Holland Publishing Company.

Dyer, K. R., May 1974. The salt balance in stratified estuaries. Estuarine and Coastal Marine Science 2, 273–281.

Dyer, K. R., 1982. Mixing caused by lateral internal seiching within a partially mixed estuary. Estuarine, Coastal and Shelf Science 15 (4), 443–457.

Dyer, K. R., 1997. Estuaries. A Physical Introduction, 2^{nd} Edition. John Wiley and Sons, 195 pp.

Dyer, K. R., Gong, W. K., E., O. J., May 1992. The cross sectional salt balance in a tropical estuary during a lunar tide and discharge event. Estuarine, Coastal and Shelf Science 34, 579–591.

Dyer, K. R., New, A. L., 1986. Intermittency in estuarine mixing. Academic Press, New York.

Ferziger, J., Peric, M., 1995. Computational methods for fluid dynamics. Springer, New York.

Fischer, H. B., 1972. Mass transport mechanisms in partially stratified estuaries. J. Fluid Mech. 53 (4), 671–687.

Fischer, H. B., 1976. Mixing and dispersion in estuaries. Annual review of fluid mechanics. Annual Reviews 8, 107–133.

Fischer, H. B., List, J. E., Koh, R. C. Y., Imberger, J., Brooks, N. H., 1979. Mixing in Inland and Coastal Waters. Academic Press, New York.

Fry, V., Aubrey, D. G., 1990. Tidal velocity asymmetries and beload transport in shallow embayments. Estuarine, Coastal and Shelf Science 30, 453–473.

Geophysics Study Commitee, 1997. Overview and Recommendations. Estuaries, Geophysics and the Environment. Tech. rep., National Academy of Sciences, Washington, D. C., 1–10.

Gibson, J. R., Najjar, R. G., 2000. The response of Chesapeake Bay salinity to climate-induced changes in streamflow. Limnology and Oceanography 45, 1764–1772.

Granja, H. M., 1996. A laguna de Aveiro no contexto da evolução da zona costeira do noroeste de Portugal nos ultimos milhares de anos. In: Seminário Sobre Lagunas Costeiras e Ilhas-Barreira da Zona Costeira de Portugal. Associação Eurocoast-Portugal, pp. 107–123.

Gross, E. S., Koseff, J. R., Monismith, S. G., 1999. Evaluation of advective schemes for estuarine salinity simulations. Journal Hydraulic Engineering 125, 32–46.

Haidvogel, D. B., Arango, H. G., Hedstrom, K., Beckmann, A., Malanotte-Rizzoli, P., Shchepetkin, A. F., 2000. Model evaluation experiments in the North Atlantic Basin: Simulations in non-linear terrain following coordinates. Dyn. Atmos. Oceans 32, 239–281.

Hansen, D. V., Rattray, M., 1965. Gravitational circulation in straits and estuaries. Journal of Marine Research 23, 104–122.

Hansen, D. V., Rattray, M., 1966. New dimensions in estuarine classification. Limnology and Oceanography 11, 319–326.

Harcourt-Baldwin, J. L., Diedericks, G. P. J., 2006. Numerical modelling and analysis of temperature controlled density currents in Tomales Bay, California. Estuarine Coastal and Shelf Science 66, 417–428.

Hiersch, C., 1980. Numerical computation of internal and external flows. Vol I: Fundamentals of numerical discretization. Wiley Series in Numerical Methods in Engineering. John Wiley and Sons, Chichester.

Hsu, M. H., Kuo, A. Y., Kuo, J. T., Liu, W. C., 1999. Procedure to calibrate and verify numerical models of estuarine hydrodynamics. Journal of Hydraulic Engineering, 166–182.

Hunkins, K., May 1981. Salt dispersion in the Hudson estuary. Journal of Physical Oceanography 11 (5), 729–738.

IH, 1991. Instituto Hidrográfico, Recolha e processamento de dados de marés, correntes, temperaturas e salinidades na Ria de Aveiro. Tech. Rep. Relatório FT.MC. 5/87, Instituto Hidrográfico, Instituto Hidrográfico, Lisboa, Portugal.

Inoue, M., Wiseman JR., W. J., 2000. Transport, mixing and stirring processes in a Louisiana estuary: a model study. Estuarine, Coastal and Shelf Science (50), 449–466.

Jay, D. A., Geyer, W. R., Uncles, R. J., Vallino, J. Largier, J., Boynton, W. R., 1997. A review of recent developments in estuarine scalar fluxes estimation. Estuaries 20, 262–280.

Jay, D. A., Smith, J. D., 1990a. Residual circulation in shallow estuaries 1: Highly stratified, narrow estuaries. Journal of Geophysical Research 95, 711–731.

Jay, D. A., Smith, J. D., 1990b. Residual circulation in shallow estuaries 2: Weakly stratified and partially mixed, narrow estuaries. Journal of Geophysical Research 95, 733–748.

Jenter, H. L., Madsen, O. S., 1989. Bottom stress in wind-driven depth-averaged coastal flows. Journal of Physical Oceanography 19, 962–974.

Jerlov, N. G., 1968. Optical Oceanography. Elsevier, 194 p.

Kjerfve, B., 1975. Velocity averaging in stuaries characterized by a large tidal range to depth ratio. Estuarine and Coastal Marine Science 3.

Kjerfve, B., 1986. Circulation and salt flux in a well mixed estuary. In: Physics of Shallow Estuaries and Bays. J. van de Kreeke. Spring Verlag, pp. 22–29.

Kjerfve, B., 1989. Estuarine geomorphology and physical oceanography. In: Physics of Shallow Estuaries and Bays. J. van de Kreeke. Spring Verlag, pp. 22–29.

Kjerfve, B., 1990. Manual for investigation of hydrological processes in mangrove ecosystems. Tech. rep., UNESCO/UNDP, New Dehli, 79 pp.

Kjerfve, B., 1994. Coastal lagoon processes. In: Coastal Lagoon Processes. Vol. 60 of Elsevier Oceanographic Series. Kjerve, B. (Ed), Amsterdam, pp. 1–8.

Koutitas, C., 1994. Field and lab measurements for models verification-calibration-validation. MAST Advanced Course on Computational and Modelling Aspects of Oceanography. North-Holland Publishing Company.

Kranenburg, C., 1986. A timescale for long-term salt intrusion in well-mixed estuaries. Journal of Physical Oceanography 16, 1329–1331.

Kraus, E. B., 1972. Atmosphere-Ocean Interaction. Clarendon Press, Oxford.

Kuo, A., Park, K., 1985. A framework for coupling shoals and shallow embayments with main channels in numerical modelling of coastal plain estuaries. Estuaries 18, 341–350.

Lavelle, J. W., Mofjeld, H. O., Lempriere-Doggett, E., Cannon, G. A., Pashinski, D. J., Cokelet, E. D., Lytle, L., Gill, S., 1988. A multiply connected channel model of tides and tidal currents in Puget Sound, Washington, and a comparison with updated observations. Tech. Rep. ERL PMEL-84, NOAA Tech. Memo, Pacific Marine Environmental Laboratory, NOAA, 103 pp.

Leendertse, J., 1967. Aspects of a computational model for long water wave propagation. Memorandum rh-5299-rr, Rand Corporation, Santa Monica, 165 p.

Leendertse, J., Liu, S., 1978. A three-dimensional turbulent energy model for non-homogeneous estuaries and coastal sea systems. In: Nihoul, J. (Ed.), Hydrodynamics of estuaries and Fjords. Elsevier, Amsterdam, pp. 387–405.

Leitão, P. C., 1996. Modelo de dispersão lagrangeano tridimensional. Tese de Mestrado em Ecologia, Gestão e Modelação de Recursos Marinhos, Instituto Superior Técnico, Lisboa.

Leitão, P. C., 2003. Integração de Escalas e de Processos na Modelação do Ambiente Marinho. Tese de Doutoramento, Instituto Superior Técnico. Universidade Técnica de Lisboa, Lisboa, Portugal.

Lewis, R. F., Lewis, J. O., 1983. The principal factors contributing to the flux of salt in a narrow, partially stratified estuary. Estuarine and Coastal Marine science 16, 599–626.

Li, M., Zhong, L., Boicourt, W. C., 2005. Simulations of Chesapeake Bay estuary: Sensitivity to turbulence mixing parameterizations and comparison with observations. Journal of Geophysical Research 110 (C12004), doi: 10.1029/2004JC002585.

Lopes, J. F., Dias, J. M., Cardoso, A. C., Silva, C. I. V., 2005. The water quality of the Ria de Aveiro lagoon: From observations to the implementation of a numerical model. Marine Environmental Research 60, 594–628.

Lopes, J. F., Dias, J. M., Dekeyser, I., 2001. Influence of tides and river inputs on suspended sediment transport in the Ria de Aveiro lagoon, Portugal. Phys. Chem. Earth (B) 26 (9), 729–734.

Lopes, J. F., Dias, J. M., Dekeyser, I., 2006. Numerical modelling of cohesive sediments transport in the Ria de Aveiro lagoon, Portugal. Journal of Hydrology 319, 176–198.

MacCready, P., 1999. Estuarine adjustment to changes in river flow and tidal mixing. Journal of Physical Oceanography 29, 708–726.

MacCready, P., Geyer, W. R., 2001. Estuarine salt flux through an isohaline surface. Journal of Geophysical Research 106 (C6), 11629–11637, June 15, 2001.

MacCready, P., Hetland, R. D., Geyer, W. R., 2002. Long-term isohaline salt balance in an estuary. Continental Shelf Research 22.

Mantovanelli, A., 1999. Caracterização da dinâmica hídrica e do material particulado em suspensão na Baía de Paranaguá e em sua bacia de drenagem. Dissertação de mestrado, Universidade Federal do Paraná, Departamento de Geologia, 152pp.

Martins, F., 2000. Modelação matemática tridimensional de escoamentos costeiros e estuarinos usando uma abordagem de coordenada vertical genérica. Ph.D. thesis, Universidade Técnica de Lisboa, Instituto Superior ´Técnico, Portugal.

Martins, F., Leitão, P., Silva, A., Neves, R., 2001. 3D modelling in the Sado estuary using a new generic vertical discretization approach. Oceanologica Acta 24 (1), 1–12.

Martins, F., Neves, R., Leitão, P., 1998. A three-dimensional hydrodynamic model with generic vertical coordinate. In: Proceedings of Hydroinformaticś98. Vol. Vol. 2. Babovic, V. and Larsen, L. (Eds.), Balkema, Rotterdam, pp. 1403–1410.

Martins, R. P., Vilela, C. P. X., Rosso, T. C. A., 2002. Hydrodynamic numerical modelling of Guanabara Bay, Rio de Janeiro, Brazil - a preliminary calibration. In: Littoral 2002. pp. 329–335.

Mellor, G. L., Yamada, T., 1982. Development of a turbulence closure model for geophysical fluid problems. Rev. Geophys. 20, 851–875.

Miranda, L. B., Bérgamo, A. L., Mendes de Castro, B., 2005. Interactions of river discharge and tidal modulation in a tropical estuary, NE Brazil. Ocean Dynamics 55, 430–440, doi: 10.1007/s10236-005-0028-z.

Miranda, L. B., Bérgamo, A. L., Ramos e Silva, C. A., 2004. Dynamics of a tropical estuary: Curimataú River, NE Brazil. Journal of Coastal Research Special issue 39, (In press).

Miranda, L. B., Castro Filho, B. M., 1996. On the salt transport in the Cananéia sea during a spring tide experiment. Rev. bras. oceanogr. 44 (2), 123–133.

Miranda, L. B. d., Castro, B. M., Kjerfve, B., 2002. Princípios de Oceanografia Física de Estuários. Editora da Universidade de S. Paulo, S. Paulo, iSBN: 85-314-0675-7.

Monismith, S. G., Fong, D. A., 1996. A simple model of mixing in a stratified tidal flow. Journal of Geophysical Research 101, 28583–28595.

Monismith, S. G., Kimmerer, W., Burau, J. R., Stacey, M. T., 2002. Structure and flow-induced variability of the subtidal salinity field in northern San Francisco Bay. Journal of Physical Oceanography 32, 3003–3019.

Montero, P., 1999. Estudio de la hidrodinámica de la ría de vigo mediante un modelo de volúmenes finitos. Ph.D. thesis, Universidad de Santiago de Compostela, Spain.

Moreira, M. H., Queiroga, H., Machado, M. M., Cunha, M. R., 1993. Environmental gradients in a southern estuarine system: Ria de Aveiro, Portugal, implication for soft bottom macrofauna colonization. Neth. J. Aquat. Ecol. 27 (2-4), 465–482.

Morgado, F., Queiroga, H., Melo, F., Sorbe, J. C., 2003. Zooplankton abundance in a coastal station of the Ria de Aveiro inlet (north-western Portugal): relations with tidal and day/night cycles. Acta Oecologica 24, 175–181.

Neves, R., Coelho, H., Leitão, P., Martins, H., Santos, A., 1998. A numerical investigation of the slope current along the Western European margin. In: Computational Methods in Water Resources XII. Vol. 2. Burgano, V. and Karatzas, G. and Payatakas, A. and Brebbia, C. and Gray, W. and Pinder, J. (Eds), pp. 369–376.

Neves, R., Santos, A., Coelho, H., Martins, H., Leitão, P., Miranda, R., 1999. A circulation model for the European Ocean Margin. Deep Sea Research.

Neves, R. J. J., 1985. Étude Experimentale et Modélisation des Circulations Transitoire et Résiduelle dans l'estuaire du Sado. Ph.D. thesis, University of Liège, Liège, Belgium, 271 pp.

Newton, A., Mudge, S. M., 2003. Temperature and salinity regimes in a shallow, mesotidal lagoon, the Ria Formosa, Portugal. Estuarine, Coastal and Shelf Science (57), 73–85.

Nolasco, R., Soares, A., Dias, J. M., Monteiro Santos, F. A., Palshin, N. A., Represas, P., Vaz, N., 2006. Motionally induction voltage measurements at estuarine environments: the Ria de Aveiro Lagoon (Portugal). Geophysical Journal International. doi: 10.1111/j.1365-246x.2006.02936.x.

Nunes Vaz, R. A., Lenon, G. W., de Silva Samarasinghe, J. R., 1989. The negative role of turbulence in estuarine mass transport. Estuarine Coastal and Shelf Science 28, 361–377.

Nunes Vaz, R. A., Simpson, J. H., 1994. Turbulence closure modeling of estuarine stratification. Journal of Geophysical Research 99, 16143–16160.

Officer, C. B., Kester, D. R., 1991. On estimating the non-advective tidal exchanges and advective gravitational circulation exchanges in an estuary. Estuarine Coastal and Shelf Science 32, 99–103.

Palma, E. D., Matano, R. P., 1998. On the implementation of passive open boundary conditions for a general circulation model: The barotropic case. Journal of Geophysical Research 103, 1319–1342.

Palma, E. D., Matano, R. P., 2000. On the implementation of passive open boundary conditions for a general circulation model: The three-dimensional case. Journal of Geophysical Research 105, 8605–8627.

Paulson, C. A., Simpson, J. J., 1977. Irradiance measurements in the upper ocean. Journal of Physical Oceanography 7, 952–956.

Pawlowicz, R., Beardsley, B., Lentz, S., 2002. Classical tidal harmonic analysis including error estimates in MATLAB using T_TIDE. Computers and Geosciences 28, 929–937.

Perillo, G. M. E., 1995. Geomorphology and Sedimentology of Estuaries. Elsevier, Amsterdam.

Pond, S., Pickard, G. L., 1983. Introductory Dynamical Oceanography, 2nd Edition. Pergamon Press, Oxford, 329 pp.

Prandle, D., 2004. Saline intrusion in partially mixed estauries. Estuarine Coastal and Shelf Science 59, 385–397.

Prego, R., Dale, A. W., deCastro, M., Gómez-Gesteira, M., Taboada, J. J., Montero, P., Villareal, M. R., Pérez-Villar, V., 2001. Hydrography of the Pontevedra Ria: Intra-annual and temporal variability in a Galician coastal system (NW Spain). Journal of Geophysical Research 106 (C9), 19845–19857.

Pritchard, D. W., 1952. Salinity distribution and circulation in the Chesapeake Bay estuarine system. J. Mar. Res. 15, 33–42.

Pritchard, D. W., 1967. Observations and circulation in coastal plain estuaries. In Estuaries. No. 83. AAAS Publ., Washington, D. C., pp 37–44.

Queiroga, H., Costlow, J. D., Moreira, M. R., 1994. Larval abundance patterns of carcinus maenas (decapoda, brachyura) in Canal de Mira (Ria de Aveiro, Portugal). Mar. Ecol. Prog. Ser. 111, 63–72.

Ramalhosa, E., Segade, S. R., Pereira, E., Vale, C., Duarte, A., 2006. Mercury cycling between the water column and surface sediments in a contaminated area. Water Research 40 (15), 2893–2900.

Ré, M., Cruz, M., Quintaneiro, I., Rua, J., Borrego, C., 1991. Ambiente versus zonas costeiras: gestã e preservação de uma zona crítica. In: Actas do 2° Simpósio Sobre Protecção e Revalorização da Faixa Costeira do Minho ao Liz. pp. 118–127.

Rippeth, T. P., Fisher, N. R., Simpson, J. H., 2001. The cycle of turbulent dissipation in the presence of tidal straining. Journal of Physical Oceanography 31, 2458–2471.

Rocha, F., Silva, E., Bernardes, C., Vidinha, J., Patinha, C., 2005. Chemical and mineralogical characterization of the sediments from the mira, ilhavo and ovar channels of aveiro lagoon (portugal). Ciencias Marinas 31 (1B), 253–264.

Roe, P. L., 1985. Some contributions to the modeling of discontinuous flows. Lect. Notes Pure Appl. Math. 22, 163–193.

Santos, A. J. P., 1995. Modelo hidrodinâmico tridimensional de circulação oceânica e estuarina. Tese de Doutoramento, Universidade Técnica de Lisboa, Lisboa, 273 p.

Saraiva, A. S. C., 2005. Modelação Ecológica da Ria de Aveiro: O Papel das Macroalgas. Tese de Mestrado, Instituto Superior Técnico. Universidade Técnica de Lisboa, Lisboa, Portugal.

Simpson, J. H., Brown, J., Matthews, J., Allen, G., 1990. Tidal straining, density currents, and stirring in the control of estuarine stratification. Estuaries 13, 125–132.

Simpson, J. H., Sharples, J., 1991. Dynamically-active models in the prediction of estuarine stratification. In: Springer (Ed.), Dynamics and Exchanges in Estuaries and the Coastal Zone. ed. D. Prandle, New York, pp. 101–103.

Simpson, J. H., Sharples, J., Rippeth, T. P., 1991. A prescriptive model of stratification induced by freshwater runnof. Estuarine Coastal and Shelf Science 33, 23–35.

Simpson, J. H., Vennel, R., Souza, A. J., 2001. The salt fluxes in a tidally-energetic estuary. Estuarine, Coastal and Shelf Science 52, 131–142, doi: 10.1006/ecss.2000.0733.

Smith, L. W., Cheng, R. T., 1987. Tidal and tidally averaged circulation characteristics of Suisun Bay, California. Water Resources Research 23 (1), 143–155.

Smith, N. P., 1977. Meteorological and tidal exchange between Corpus-Christy Bay, Texas, and northwestern Gulf of Mexico. Estuarine Coastal Mar. Sci. (5), 511–520.

Stanev, E., Wolff, J. O., Burchard, H., Bolding, K., Floser, G., 2003. On the circulation in the East Frisian Wadden Sea: Numerical modelling and data analysis. Ocean Dynamics 53, 27–51.

Stips, A., Bolding, K., Pohlmann, T., Burchard, H., 2004. Simulating the temporal and spatial dynamics of the North Sea using the new model GETM (general estuarine transport model). Ocean Dynamics 54, 266–283.

Swinbank, W. C., 1963. Long-wave radiation from clear skies. Quarterly Journal of the Royal Meteorological Society 89, 339–348.

Taboada, J. J., November 1999. Aplicación de modelos numéricos al estudio de la hidrodinámica y del flujo de partículas en el Mar Mediterráneo. Ph.d Thesis, Universidad de Santiago de Compostela, Spain.

Taboada, J. J., Prego, R., Ruiz-Villarreal, M., Montero, P., Gómez-Gesteira, M., Santos, A., pérez Villar, V., 1998. Evaluation of the seasonal variation in the residual patterns in the ría de vigo (NW Spain) by means of a 3D baroclinic model. Estuarine, Coastal and Shelf Science 47, 661–670.

Theias, H., 2005. Numerical Modeling of Non-Hydrostatic Processes in Estuarine and Coastal Regions. Msc Thesis, Universidade Técnica de Lisboa, Instituto Superior ´Técnico, Portugal.

Tomás, L. M., Dias, J. M., 2004. Tidal characterization at the Ria de Aveiro inlet. In: Littoral 2004. pp. 676–677.

Trancoso, A. R., Saraiva, S., Fernandes, L., Pina, P., Leitão, P., Neves, R., 2005. Modelling macroalgae using a 3d hydrodynamic-ecological model in a shallow, temperate estuary. Ecological Modelling 187, 232–246.

Umgiesser, G., Canu, D. M., Solidoro, C., Ambrose, R., 2003. A finite element ecological model: a first application to the venice lagoon. Environmental Modelling and Software 18, 131–145.

UNESCO, 1981. Tech. report on the joint panel on oceanographic tables and standards. Technical papers in marine science 36, UNESCO, 24 pp.

van Rijn, L. C., Walstra, D. J. R., Grasmeijer, B., S. J., Pan, S., Sierra, J. P., 2003. The predictability of cross-shore bed evaluation of sandy beaches at the time scale of storms and season using process-based profiles models. Coastal Engineering 47, 295–327.

Vaz, N., Dias, J. M., submitted. Physical driving of salt fluxes in an estuarine tidal channel. Environmental Fluid Mechanics.

Vaz, N., Dias, J. M., Leitão, P., 2004. Hydrodynamical modelling of the Ria de Aveiro lagoon: Mohid's preliminary calibration. In: Proceedings of Littoral 2004. pp. 774–775.

Vaz, N., Dias, J. M., Leitão, P., Martins, I., 2005a. Horizontal patterns of water temperature and salinity in an estuarine tidal channel: Ria de Aveiro. Ocean Dynamics 55, 416–429, doi: 10.1007/s10236-005-0015-4.

Vaz, N., Dias, J. M., Leitão, P., Nolasco, R., Soares, A., Submitted. Application of the mohid-2d model to a mesotidal temperate coastal lagoon. Computers and Geosciences.

Vaz, N., Dias, J. M., Martins, I., 2005b. Dynamics of a temperate fluvial estuary in early Winter. Global NEST Journal 7 (3), 237–243.

Vicente, C. M., 1985. Caracterização hidráulica e aluvionar da Ria de Aveiro, utilização de modelos hidráulicos no estudo de problemas da Ria. Jornadas da Ria de Aveiro, III, Edição da Câmara Municipal de Aveiro, Portugal, 41–58.

Villarreal, M. R., Montero, P., Taboada, J. J., Prego, R., Leitão, P. C., Péres-Villar, V., 2002. Hydrodynamic model study of the ria de pontevedra under estuarine conditions. Estuarine, Coastal and Shelf Science 54 (1), 101–113.

Vinokur, M., 1989. An analysis of finite-difference and finite-volume formulations of conservation laws. J. Comput. Phys. 81, 1–52.

Walstra, D. J. R., van Rijn, L. C., Blogg, H., van Ormondt, M., 2001. Evaluation of a hydrodynamic area model based on the COAST3D data at Teignmouth 1999. Report TR121 - EC MAST project No MAS3-CT97-0086. Tech. rep., HR Wallingford, UK, D4.1-D4.4.

Warner, J. C., Geyer, W. R., Lerczak, J. A., 2005. Numerical modeling of an estuary: A comprehensive skill assessment. Journal of Geophysical Research 110 (C05001), doi: 10.1029/2004JC002691.

Wilmott, C. J., 1981. On the validation of models. Phys. Geogr. 2, 184–194.

Zhong, L., Li, M., 2006. Tidal energy fluxes in the Chesapeake Bay. Continental Shelf Research 26, 752–770.

Zhou, M., 1998. Influence of bottom stress on the two-layer flow induced by gravity currents in estuaries. Estuarine Coastal and Shelf Science 46, 811–825.